

UNCLASSIFIED



AD NUMBER

AD-479 205

NEW LIMITATION CHANGE

TO

DISTRIBUTION STATEMENT - A

Approved for public release;  
distribution is unlimited

LIMITATION CODE: 1

FROM

No Prior DoD Distr Scty Cntrl St'mt Assigned

AUTHORITY

SAMSO, VIA USAF LTR; Feb 28, 1972.

19990303146

THIS PAGE IS UNCLASSIFIED

479205

9

**SYSTEM SUPPORT STUDIES UNDER  
PRODUCTION SUPPORT PROGRAM**

**(Part Two of Two Parts)**

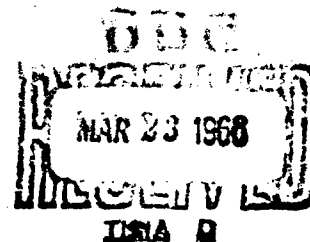
**Report 0162-06TDR-9-Vol 2  
(Tasks 41-011, -014, -016, -017, -018,  
-019, -020, -022, -023, and -025)**

**by**

**H. E. Childres**

**Contract AF 04(694)-308  
(CCN 41 and SA 33)**

**Prepared for**



**Headquarters Air Force Ballistics Systems Division  
Air Force Systems Command, USAF  
Norton Air Force Base, California  
BSRPA**

**Reproduced From  
Best Available Copy**

19990303146

Report 0162-06TDR-9-Vol 2

This document is subject to special export controls  
and each transmittal to foreign governments or foreign  
nations may be made only with prior approval of the  
Air Force Ballistic Systems Division.

SYSTEM SUPPORT STUDIES UNDER  
PRODUCTION SUPPORT PROGRAM

Report 0162-06TDR-9-Vol 2  
(Tasks 41-011, -014, -016, -017, -018,  
-019, -020, -022, -023, and -025)

by

H. E. Childres

Contract AF 04(694)-308  
(CCN 41 and SA 33)

Prepared for

Headquarters, Air Force Ballistic Systems Division  
Air Force Systems Command, USAF  
Norton Air Force Base, California

BSRPA

**AEROJET-GENERAL CORPORATION**  
A SUBSIDIARY OF THE GENERAL TIRE & RUBBER COMPANY

9032T



FOREWORD

This final report, which consists of two volumes, describes the results of studies and tests made by Aerojet-General under the System Support portion of the Production Support program, which was conducted under Supplemental Agreement 33 to Contract AF 04(694)-308.

The following list defines contents of the two volumes and relates the various tasks to the project directive numbers that were used for task definition in the Production Support Program Plan.\*

<u>Volume</u>	<u>Task</u>	<u>Project Directive</u>
1	Variability Analyses, Materials and Production	41-001
	Resolve Propellant and Liner Production Problems	41-002
	Analyses of Potential Production Problems	41-003
	Production Support for LITVC Gas Generators	41-008
1	LITVC and RC Packaging Design Study	41-010
2	Study of TVC System Pressurization Methods	41-011
	Nozzle-Motor Configuration Optimization Study	41-014
	Motor Development Programs, Layout and Analysis	41-016
	Bladder Improvement Study	41-017
	LITVC Manifold-and-Joint Design Study	41-018
	Investigation of Exit-Cone Material Behavior	41-019
	Igniter Initiator, Materials-and-Performance Evaluation	41-020
	Characterization of Pyrotechnic Ignition Properties	41-022
	Evaluation of Alternative Insulation Materials	41-023
2	Roll-Control Valve Transducer Testing	41-025

This final report supersedes the preliminary final reports that were submitted in accordance with program requirements and which are listed below.

<u>Report No.</u>	<u>Tasks Covered</u>	<u>Date of Issue</u>
0162-06TDR-1	FDs 41-003, -010, -011, -016, and -018	15 Jul 1965
0162-06TDR-3	FDs 41-001, -002, -008, -014, and -020	30 Jul 1965
0162-06TDR-5	FDs 41-017, -019, -022, -023, and -025	24 Sep 1965

\*Minuteman Production Support Program Plan, Report 0162-06PS-2, dated 15 January 1965.

Report 0162-06TDR-9-Vol 2

APPROVAL STATEMENT

This final report summarizes the results of System Support studies of the Production Support program, which was conducted from 18 August 1964 through 31 September 1965 by the Aerojet-General Corporation for the Air Force Ballistic Systems Division. The program was authorized by Contract Change Notification 41 and Supplement Agreement 33 to Contract AF 04(694)-308. The report consists of Volumes 1 and 2 and Supplement 1 to Volume 2; the supplement contains classified (CONFIDENTIAL) material applicable to one section of Volume 2. Report format is based on AFSC Regulation No. 80-20, dated 3 August 1964, and AFSC Regulation No. 80-20A (Change), dated 25 September 1964.

This report has been reviewed and is approved.



R. D. Miller, Captain, USAF  
Project Officer

ABSTRACT

A series of studies was made wherein evaluations, investigations, and analyses were conducted in support of production programs for Wing VI Minuteman second-stage motors, WS-133B. Summaries of effort and accomplishments for the ten areas of program effort discussed in this volume of the final report are presented below:

1. Studies were made of injectant-type thrust vector control systems that could be considered feasible for potential application with the Wing VI Minuteman second stage and other solid-propellant motors. The systems investigated include: stored gas, blow down, solid- and liquid-propellant generators, primary and secondary VaPAK, differential piston decomposition, and auxiliary and main-tank injection.

2. Toward deriving range increase, investigations were made to increase motor propellant loading by increasing nozzle submergence. Studies indicated potential savings in the weight of inert components such as the liquid injection thrust vector control (LITVC) system, nozzle housing, and insulation. In conjunction with glass-case studies, investigations were made to determine the value of analytical methods in the design of bosses.

3. Investigations were made to evaluate the physical and mechanical properties of composite materials for the expulsion bladder of the LITVC system. Bladder materials investigated were Viton A-HV with Dacron (currently used in the Wing VI second-stage motor), Viton A-HV with Nomex HT 2-41, and Viton A-HV with Dacron and a nylon barrier.

4. Program studies were directed toward improvement of the LITVC and roll control (RC) system by development of leak-proof joints and by replacing various joints through welding.

5. Laboratory tests were made to establish the performance of tape-wrapped exit cone materials (graphite- and silica-phenolic tapes) and to determine the behavior of these materials and interface bonds when considering various material and processing variables.

6. A series of igniter assemblies was tested to determine the adequacy of an igniter initiator having an unbonded, solid polyurethane-foam spacer in place of the bonded, perforated spacer.

7. Ignition properties were characterized for advanced propellants, propellant blends, and pelleted-form pyrotechnics. Of primary interest were pyrotechnics having wide temperature- and altitude-range capabilities.

8. Evaluations were made of recently developed elastomeric compounds. Included were ethylene propylene terpolymers and butyl acrylics.

9. An intensive study was conducted to resolve discrepancies for roll-control valve and position-transducer inspection data between manufacturing facilities and between various government facilities.

TABLE OF CONTENTS

	<u>Page</u>
I. Study of TWC System Pressurization Methods, Project Directive 41-011	I-1
A. Introduction	I-1
B. Objectives and Scope of Work	I-2
C. Summary of Work Performed	I-3
D. Technical Discussion	I-3
II. Nozzle-Motor Configuration Optimization--Project Directive 41-014	II-1
A. Objectives	II-1
B. Discussion	II-1
Appendix II-A Subsonic Particle-Trajectory Solution	II-A-1
Appendix II-B Nozzle Performance Evaluation Program	II-B-1
III. Motor Development, Layout, and Analysis-Project Directive 41-016	III-1
IV. Bladder Improvement Study--Project Directive 41-017	IV-1
A. Objective	IV-1
B. Summary	IV-1
C. Test Methods	IV-2
D. Test Results	IV-5
E. Literature Survey	IV-8
F. List of References	IV-19
V. LITVC Manifold and Joint Design Study--Project Directive 41-018	V-1
A. Design of Leak-Proof Joints	V-1
B. Preassembly Feasibility Study	V-2
C. Stress Analysis	V-2
D. Thermal Analysis	V-4
E. Laboratory Evaluation of Viton O-Ring	V-5
F. Weld Evaluation Laboratory Tests	V-7
G. Literature Survey	V-7
VI. Investigation of Exit Cone Material Behavior--Project Directive 41-019	VI-1
A. Objective	VI-1
B. Laboratory Studies	VI-1
C. The Partial Release of the Exit Cone-Housing Bond Line	VI-6
D. Alternative Methods of Exit Cone Retention	VI-7
E. Proof Test Procedures, Tooling, and Pressure Levels	VI-8
F. X-Ray Inspection of Nozzle Assemblies	VI-9

Report 0162-06TDR-9-Vol 2

TABLE OF CONTENTS (cont.)

	<u>Page</u>
Appendix VI-A Testing of Specimens from Full-Scale Exit Cones, Results and Observations	VI-A-1
Appendix VI-B Testing of Specimens from Subscale Exit Cones, Results and Observations	VI-B-1
Appendix VI-C Stress Analysis of the Wing VI Minuteman Nozzle Support Structure and Sea-Level Exit cone	VI-C-1
VII. Igniter Initiator Materials-and-Performance Evaluation--Project Directive 41-020	VII-1
A. Task Description	VII-1
B. Conclusions and Recommendations	VII-1
VIII. Characterization of Pyrotechnic Ignition Properties--Project Directive 41-022	VIII-1
A. Summary	VIII-1
B. Technical Discussion	VIII-1
IX. Evaluation of Alternative Insulation Materials--Project Directive 41-023	IX-1
A. Program Objective	IX-1
B. Materials	IX-1
C. Test Methods and Results	IX-1
D. Conclusions	IX-2
X. Roll-Control Valve Transducer Testing--Project Directive 41-025	X-1
A. Introduction	X-1
B. Conclusions and Recommendations	X-1
C. Program	X-2
D. Analysis	X-3
E. Interim Actions Taken	X-7
F. Roll Valve Assembly and Test Sequence	X-8
G. Voltage Calibration of the Square Wave Excitation	X-9

LIST OF ILLUSTRATIONS

	<u>Figure</u>
Summary of TVC Pressurization Systems Considered	I-1
Pressurization System Requirements and Characteristics	I-2
Pressurization System Analysis	I-3
Stored-Gas Feed-System Design Calculations	I-4
Stored-Gas System Schematic	I-5
Pressure Decay of $N_2O$ VāPaK System	I-6
VāPaK System Design Calculations	I-7
Secondary VāPaK System Schematic	I-8
Improved Minuteman Submerged Nozzle, Layout No. 1	II-1
Improved Minuteman Submerged Nozzle, Layout No. 2	II-2
Improved Minuteman Submerged Nozzle, Layout No. 3	II-3
Curve of Propellant Weight vs Nozzle Submergence Depth	II-4
Curve of Inert Weight vs Nozzle Submergence Depth	II-5
Curves of Preliminary and Corrected Missile Ranges vs Nozzle Submergence	II-6
Improved Minuteman Motor	II-7
Interface Areas Affected by Design Changes	II-8
Injector Boss, Minuteman Optimization Study	II-9
Injector Boss, Minuteman Optimization Study	II-10
Injector Boss, Minuteman Optimization Study	II-11
LITVC System Gain Curves for Various Nozzle-Submergence Depths	II-12
LITVC System Performance vs Injector Location	II-13
Aluminum Nozzle Shell	II-14
Titanium Nozzle Shell	II-15
Steel Nozzle Shell	II-16
Ti/Al Honeycomb Nozzle Shell	II-17
Improved Minuteman Glass Case	II-18
Glass-Fiber Case Weight vs Flexural Stiffness	II-19
Typical Submerged Nozzle Configuration	II-20
Typical Boss-Ring and Shell Configuration	II-21

Report 0162-06TDR-9, Volume 2

List of Illustrations (cont.)

	<u>Figure</u>
Polaris B-3 Nozzle-Support Ring	II-22
Deformation of Ring and Shell	II-23
Recommended Ring Area for In-Plane-Wrapped, Filament-Wound Pressure Vessel	II-24
Minuteman Aft Closure Particle Stream Lines--1 Micron Particles	II-25
Minuteman Aft Closure Particle Stream Lines--5 Micron Particles	II-26
LITVC Permeation Storage Configuration	IV-1
LITVC Freon 114B-2 Permeation Test Specimen	IV-2
Permeation Rate of Freon 114B-2 through Three LITVC Bladder Composition Construction at 80°F	IV-3
Permeation Rate of Freon 114B-2 through Three LITVC Bladder Composites at 110°F	IV-4
Permeation Rate of Freon 114B-2 through Three LITVC Expulsion Bladder Composites	IV-5
Biaxial Burst-Test Fixture	IV-6
Uniaxial Stress-Strain Data	IV-7
Effects of Freon 114B-2 on the Tensile Strength of Three LITVC Bladder Composites at 110°F	IV-8
Effect of Freon 114B-2 on the Elongation of Three LITVC Bladder Composites at 110°F	IV-9
Peel Strength of Viton A-HV to Fabric Reinforcement for Three Expulsion Bladder Composites after Exposure to Freon 114B-2 at 110°F	IV-10
The Effect of Freon 114B-2 on the Peel Strength of Viton A-HV to Fabric Reinforcement at 110°F	IV-11
Allowable Loads for Three LITVC Composites Exposed to Freon at 80°F	IV-12
Allowable Loads for Three LITVC Bladder Composites Exposed to Freon at 125°F	IV-13
Allowable Loads for Three LITVC Bladder Composites Exposed to Freon at 170°F	IV-14
Weight and Length Change of Materials Immersed in Freon 114B2 at Room Temperature	IV-15
Results of Freon Immersion of Bladder Materials (Acidity and Appearance Changes)	IV-16
Average Specific Permeability of Several Candidate Bladder Materials	IV-17

Report 0162-06TDR-9, Volume 2

List of Illustrations (cont.)

	<u>Figure</u>
Permeability Tests on Fluoroelastomers	IV-18
Results of Permeability Tests on 6-in. Viton A-HV Test Bottles (United States Rubber Company Test Procedures)	IV-19
Average Permeability for Each Triplicate Set of 6-in. Viton Test Bottles at Eight Intervals	IV-20
Materials Demonstrating Satisfactory Impermeability to Freon 114B-2	IV-21
Permeability Testing	IV-22
Torch Test of Samples at 1950°F Heat-Flux Estimated to Be 15 btu/sec/ft <sup>2</sup>	IV-23
Torch Test of Polyester Lined Viton A-HV at 1950°F with Heat Flux Approximately 15 btu/sec/ft <sup>2</sup>	IV-24
Torch Test of Reduced Thickness Viton A-HV at 1950°F with Heat Flux Approximately 15 btu/sec/ft <sup>2</sup>	IV-25
Torch Test of Viton B Samples at 1950°F with Heat Flux Approximately 15 btu/sec/ft <sup>2</sup>	IV-26
Torch Test of Viton B Samples at 1950°F with Heat Flux Approximately 15 btu/sec/ft <sup>2</sup>	IV-27
Tensile Strength and Elongation of Viton A-HV Dacron and Low Molecular Weight Polyethylene as Currently Used in Arc-LMSC Design	IV-28
Average Tear Strength (Five Samples Each) (1b/in.)	IV-29
Mechanical Properties Viton B-Nylon-Viton B Laminate Arrowhead Products	IV-30
Freon Compatibility Tests--Mechanical Properties	IV-31
Effect of Freon 114B-2 on Viton A-HV	IV-32
RC Subsystem Joint Used in Stress Analysis	V-1
TVC Subsystem Joints Used in Stress Analysis	V-2
RC System Components	V-3
TVC System Components	V-4
Minimum Margins of Safety	V-5
Thermal Properties Used in Analysis	V-6
Thermal Analysis, RC Valve Temperature	V-7
Thermal Analysis, Tank-Inlet Temperature Distribution	V-8
Thermal Analysis, RC Gas-Generator Flange Temperatures	V-9



Report 0162-06TDR-9, Volume 2

List of Illustrations (cont.)

	<u>Figure</u>
Thermal Analysis, Elbow Dump Line Temperature	V-10
Test Setup for Evaluation of O-Rings at 1150 to 1200°F	V-11
Results of Viton O-Ring Tests	V-12
Thermal Profile of Sea-Level Cone at Expansion Ratio of 2.5:1	VI-1
Thermal Profile of Sea-Level Cone at Expansion Ratio of 6.75:1	VI-2
Slab Specimen from Full-Scale Cone	VI-3
Shear-Test Specimens	VI-4
First-Hole Pattern for Slabs	VI-5
Second-Hole Pattern for Slabs	VI-6
Configuration of Subscale Cones	VI-7
Material Data for Subscale Cones	VI-8
Debulk and Cure Cycles for Cones Code 92-1 and -2 and 94-1 and -2	VI-9
Test Data from Full-Scale and Subscale Cones	VI-10
Cross Section of Sea-Level Cone and Titanium Housing	VI-11
Sketch of Metal Ring for Sea-Level Cone Retention	VI-12
Sketch of Silica Laminate Ring for Sea-Level Cone Retention	VI-13
Sketch of Steel Sleeve for Sea-Level Cone Retention	VI-14
Sketch of Revised Proof Test Fixture	VI-15
Temperature- and Pressure-vs-Time Curves for Specimen O-1 (As Received) from Full-Size Cone 2168016	VI-A-1
Temperature- and Pressure-vs-Time Curves for Specimen O-2 (As Received) from Full-Size Cone 2168016	VI-A-2
Temperature- and Pressure-vs-Time Curves for Specimen P-1 (Post-Cured) from Full-Size Cone 2168016	VI-A-3
Temperature- and Pressure-vs-Time Curves for Specimen O-1 (As Received) from Full-Size Cone 2168017	VI-A-4
Temperature- and Pressure-vs-Time Curves for Specimen O-2 (As Received) from Full-Size Cone 2168017	VI-A-5
Temperature- and Pressure-vs-Time Curves for Specimen P-1 (Post-Cured) from Full-Size Cone 2168017	VI-A-6
Temperature- and Pressure-vs-Time Curves for Specimen P-2 (Post-Cured) from Full-Size Cone 2168017	VI-A-7

Report 0162-06TDR-9, Volume 2

List of Illustrations (cont.)

	<u>Figure</u>
Temperature- and Pressure-vs-Time Curves for Specimen 0-1 (As Received) from Full-Size Cone 2168018	VI-A-8
Temperature- and Pressure-vs-Time Curves for Specimen 0-2 (As Received) from Full-Size Cone 2168018	VI-A-9
Temperature- and Pressure-vs-Time Curves for Specimen P-1 (Post-Cured) from Full-Size Cone 2168018	VI-A-10
Temperature- and Pressure-vs-Time Curves for Specimen P-1 (Post-Cured) from Full-Size Cone 2168018	VI-A-11
Temperature- and Pressure-vs-Time Curves for Specimen FSC-1 from Low-Volatile Content, Snap-Cured Subscale Cone	VI-B-1
Temperature- and Pressure-vs-Time Curves for Specimen FSC-2 from Low-Volatile Content, Snap-Cured Subscale Cone	VI-B-2
Temperature- and Pressure-vs-Time Curves for Specimen 96-1 from Subscale Cone (Water Added During Cure)	VI-B-3
Temperature- and Pressure-vs-Time Curves for Specimen 96-2 from Subscale Cone (Water Added During Cure)	VI-B-4
Temperature- and Pressure-vs-Time Curves for Specimen 99-1 from Low IRPI Subscale Cone	VI-B-5
Temperature- and Pressure-vs-Time Curves for Specimen 99-2 from Low IRPI Subscale Cone	VI-B-6
Temperature- and Pressure-vs-Time Curves for Specimen 02-1 from Medium IRPI Subscale Cone	VI-B-7
Temperature- and Pressure-vs-Time Curves for Specimen 02-2 from Medium IRPI Subscale Cone	VI-B-8
Temperature- and Pressure-vs-Time Curves for Specimen 03-1 from High IRPI Subscale Cone	VI-B-9
Temperature- and Pressure-vs-Time Curves for Specimen 03-2 from High IRPI Subscale Cone	VI-B-10
Temperature- and Pressure-vs-Time Curves for Specimen 92-1 from Special Debulk Subscale Cone	VI-B-11
Temperature- and Pressure-vs-Time Curves for Specimen 92-2 from Special Debulk Subscale Cone	VI-B-12
Temperature- and Pressure-vs-Time Curves for Specimen 94-1 from Special Debulk Subscale Cone	VI-B-13
Temperature- and Pressure-vs-Time Curves for Specimen 94-2 from Special Debulk Subscale Cone	VI-B-14

Report 0162-06TDR-9, Volume 2

List of Illustrations (cont.)

	<u>Figure</u>
Epon 2216 Stress vs Strain-Test Results	VI-C-1
Meridional Stress along Inner Surface of FM 5014	VI-C-2
Hoop Stress in FM 5014	VI-C-3
Meridional Stress along Outer Surface of FM 5020	VI-C-4
Hoop Stress in FM 5020	VI-C-5
Maximum Bond Normal Stress Epon 2216	VI-C-6
Maximum Bond Shear Epon 2216	VI-C-7
Maximum Interlaminar Shear between FM 5020 and FM 5014	VI-C-8
Hoop Stress in 6AL-4V Titanium Housing	VI-C-9
Meridional Stresses along Inner and Outer Surfaces of 6AL-4V	VI-C-10
Deflection of Titanium Sea-Level Exit Cone Interface	VI-C-11
Meridional Stress along Surface of FM 5014 Sea-Level Exit-Cone, 6.04-in. Bond Release	VI-C-12
Meridional Stress along FM 5020 Sea-Level Exit-Cone Liner, 6.04-in. Bond Release	VI-C-13
Maximum Hoop Stress in Cone Liner	VI-C-14
Maximum Bond Shear Housing--Sea Level Exit Cone Interface	VI-C-15
Bond Tensile Stress Titanium--Sea Level Exit Cone Interface	VI-C-16
Comparison of Deflection Curves along Titanium--Exit-Cone Liner Interface at 627 psi Proof, 6.04-in. Bond Release	VI-C-17
Comparison of the Deflection Curves along the Titanium and Sea-Level Exit-Cone Liner Interface for Firing Conditions, 6.04-in. Bond Released	VI-C-18
Deflection Curves for Various Proof Conditions, 6.04-in. Bond Release	VI-C-19
Igniter-Initiator Pressure-vs-Time Curves	VII-1
Propellant Blending and Properties Variations	VIII-1
Effect of Pressure on Threshold Ignition Time	VIII-2
Arc-Image Furnace Test Results	VIII-3
Beryllium Propellant Arc-Image Furnace Test Results	VIII-4
Heat-Loss Determination, JFN Charge in JANAF Bomb	VIII-5

Report 0162-06TDR-9, Volume 2

List of Illustrations (cont.)

	<u>Figure</u>
Ballistic Properties of BPN Ignition Pellets	VIII-6
Ballistic Properties of Mg-TFE Ignition Pellets	VIII-7
Volumetric Loading Density of BPN and Mg-TFE Ignition Pellets	VIII-8
Burning Rate vs Pressure of BPN Ignition Pellets in JANAF Closed Bomb	VIII-9
Burning Rate vs Pressure of Mg-TFE Ignition Pellets in JANAF Closed Bomb	VIII-10
Prospective Insulation Materials	IX-1
Metal Adhesion Test Results	IX-2
Heat Flux, Btu/ft <sup>2</sup> -sec Ablation Rate vs Cold-Wall Heat Flux	IX-3
Overall Variance Analysis of Parameters Affecting Null-position Output	X-1
Output Voltage Readings for Task 25 Valves, CW Position	X-2
Output Voltage Readings for Task 25 Valves, CCW Position	X-3
Histograms of Output Voltages for Task 25 Valves, CW Position	X-4
Histograms of Output Voltages for Task 25 Valves, CCW Position	X-5
Histograms of Differential Voltage Readings, RC Position Transducer, CW Position	X-6
Histograms of Differential Voltage Readings, RC Position Transducer, CCW Position	X-7
Correlation Diagram, Transducer Excitation Voltage vs Output Voltage for Task 25 Valves, CW Position	X-8
Correlation Diagram, Transducer Excitation Voltage vs Output Voltage for Task 25 Valves, CCW Position	X-9
Correlation Diagram, Transducer Excitation Voltage vs Output Voltage for Production Valves, CW Position	X-10
Correlation Diagram, Transducer Excitation Voltage vs Output Voltage for Production Valves, CCW Position	X-11
Correlation Diagram, Solenoid Voltage vs Transducer Output Voltage for Task 25 Valves	X-12
Correlation Diagrams, Temperature vs Output Voltage for Task 25 Valves, CW Position	X-13

Report 0162-06TDR-9, Volume 2

List of Illustrations (cont.)

	<u>Figure</u>
Correlation Diagram, Temperature vs Output Voltage for Task 25 Valves, CCW Position	X-14
Histograms of Differential Voltage Readings between AGE and ETR Equipment, Task 25 Valves, CW Position	X-15
Histograms of Differential Voltage Readings between AGE and ETR Equipment, Task 25 Valves, CCW Position	X-16
Correlation Diagram, Differential Output Voltage vs Energization Time, Task 25 Valves, CW Position	X-17
Correlation Diagram, Differential Output Voltage vs Energization Time, Task 25 Valves, CCW Position	X-18
R.C. Transducer, Output Voltage Checks at ETR on 52FTM-454, CW Position	X-19
R.C. Transducer, Output Voltage Checks at ETR on 52 FTM-454, CCW Position	X-20
Overall Variance Analysis of Parameters Affecting CW Output Voltages	X-21
Overall Variance Analysis of Parameters Affecting CCW Output Voltages	X-22
Normalized Regression Line Diagram for Preliminary Normalized Output Voltages vs Excitation, Solenoid Voltage, and Energization Time, CW Position	X-23
Normalized Regression Line Diagram for Preliminary Normalized Output Voltages vs Excitation, Solenoid Voltage, and Energization Time, CCW Position	X-24
Recalibration Values of Six Kavlico Equipped Valves	X-25
Calibration of New Kavlico Equipped Valves	X-26

V.

LITVC MANIFOLD AND JOINT DESIGN STUDY--PROJECT DIRECTIVE 41-018

The following data summarize the progress made prior to cancellation of the effort in the LITVC manifold and joint design study. The objectives of this study were to design leak-proof joints for the Mod 4B LITVC and RC system and to conduct subsystem tests to demonstrate the adequacy of the redesigned joints.

Program results include design data for leak-proof joints, preassembly feasibility data, thermal analyses, detailed stress analyses, O-ring evaluation test data, weld evaluation laboratory test data, and literature survey data to justify the evaluation of dissimilar metal combinations.

A. DESIGN OF LEAK-PROOF JOINTS

The roll-control subsystem joints involved in this study are shown in Figure V-1; the TVC subsystem joints are shown in Figure V-2.

1. Roll-Control Joint Discussion

The roll-control generator joint is identical to the existing design except that the Flexitallic gasket has been replaced by a Viton O-ring, and the mean seal diameter has been increased from 1.58 to 1.84 in.

The roll-control valve joint flanges were enlarged to accommodate an insulation insert which prevents overheating of the O-ring sealing area. The neck of the roll control valve was extended to eliminate envelope problems between the tank support and the handling ring which would have required a change to the Aeronautronics casting drawing of the valve body.

The bolted joints of the roll-control nozzle were replaced by welded joints. This requires that a change be made to the Space General nozzle elbow drawing and to the Aeronautronics valve casting drawing.

2. TVC Joint Discussion

The TVC generator joint is identical to the existing design except that the Flexitallic gasket has been replaced by a Viton O-ring, and the mean seal diameter has been increased from 1.76 to 1.88 in.

The TVC T-joint to the relief-valve bolted joint was replaced by a welded joint. As a result, the relief-valve casting would have to be changed and the valve seat would have to be assembled from the opposite direction.

The relief valve-to-dump line joint was redesigned by moving the bolted joint away from the heat sink of the relief valve housing and by adding an insulation insert of Fiberite MX-2600 to prevent overheating of the sealing area. This would require a change to the Vickers' housing so that an elbow could be welded to the housing.

V, A, Design of Leak-Proof Joints (cont.)

The TVC manifold to the TVC tank insert was redesigned by removing the bolted joint and welding directly to the TVC tank insert. The tank insert would be redesigned so that the burst diaphragm could be assembled from the inside. In an alternative design considered an MX-2600 insulation insert would be added to the enlarged bolted joint.

B. PREASSEMBLY FEASIBILITY STUDY

Preliminary studies were made of the Mod 4B LITVC and RC system assembly to determine the feasibility of preassembly. Results indicate that preassembly of the following joints could be made: (1) RC nozzle to RC valve, (2) relief valve to TVC manifold, and (3) tank insert to TVC manifold.

C. STRESS ANALYSIS

A stress analysis was conducted to determine the structural adequacy of the redesigned hot-gas joints (Section VI, A, Figures V-1 and -2). The results indicate that the applied stresses are within the structural design criteria, which are based on a factor of safety of 1.25. Detailed stress calculations are available to substantiate the results of this study.

1. Redesigned Hardware

The RC hardware (Figure V-3) consists of a gas generator and two valve-nozzle assemblies bolted, 180 degrees apart, to the motor aft skirt. Externally insulated hot-gas lines run from a flow divider at the gas generator to each valve. In the redesigned RC hardware, the flanged joint of the nozzle attachment was replaced by a welded joint. The gas-generator joint and RC valve joint were modified to accommodate insulated rubber O-ring seals.

The TVC hardware (Figure V-4) consists of a gas generator with a pressure relief valve and a hot-gas line leading to the toroidal Freon tank. The two dump lines terminating at the motor aft skirt, 180 degrees apart, enable the excess hot gas to escape from the pressure relief valve. In the redesigned TVC hardware, the flanged joints of the tank-inlet and pressure-relief-valve were replaced by welded joints. The dump-line joint at the pressure relief valve and the gas-generator joint were modified to accommodate insulated rubber O-ring seals.

2. Structural Analysis

All redesigned components and the effects of these components on the existing structures to which they are attached were analyzed on the basis of the following design criteria.

V, C, Stress Analysis (cont.)

a. Roll Control System

Ultimate pressure,  $P_{ult}$  = 1.25 (MEOP)  
= 1.25 (2400)  
= 3000 psi

Maximum temperature,  $T_{max}$  = 2200°F or as determined by thermal analysis.

b. TVC System

Ultimate pressure,  $P_{ult}$  = 1.25 (MEOP)  
= 1.25 (680)  
= 850 psi

Maximum temperature,  $T_{max}$  = 2200°F or as determined by thermal analysis.

c. TVC Exhaust Manifold

Ultimate Pressure,  $P_{ult}$  = 1.25 (MEOP)  
= 1.25 (75)  
= 94 psi

Maximum temperature,  $T_{max}$  = 2200°F

d. Manifold Thermal Growth

An analytical evaluation of the loads developed as a result of manifold thermal growth was beyond the scope of this analysis. These loads are relatively small and do not significantly change the minimum margins of safety.

3. Margins of Safety

The minimum margins of safety computed for all components are shown in Figure V-5.



V, LITVC Manifold and Joints Design Study--Project Directive 41-018 (cont.)

D. THERMAL ANALYSIS

To eliminate any possible gas leakage from the LITVC and RC system, all hot-gas joints in the base area were re-examined. A Viton seal and an insulating material to protect the seal were incorporated in those joints that could not be welded. The joints analyzed include those at the RC inlet, the alternative injectant tank inlet, the RC gas-generator outlet, and the elbow dump line.

A thermal analysis was conducted to determine the temperatures in the new joint designs. All network elements for the two-dimensional method of electrical analogy are generated by the 278B computer program. The highest temperature in the seal area of the four joints analyzed was 1000 to 1075°F at the RC gas generator.

The following assumptions were made in order to use a computer solution:

- (1) gas temperature of 2200°F, (2) perfect thermal contact between all interfaces, (3) no loss of heat by radiation or convection, (4) material properties remain constant (Figure V-6), (5) the diameter of the flanges was increased to account for the corners, and (6) convection coefficients were calculated from the following formula.

$$h = 0.023 \frac{K}{D} (N_{RE})^{0.8} (N_{PR})^{0.4}$$

1. Roll Control Inlet Flange

Results of the thermal analysis of the RC inlet flange are shown in Figure V-7. An insulator was required to protect the seal from extreme temperatures. Rubber and plastic insulators were eliminated because a material was required that ablates clean or does not ablate at all since no foreign material is allowed in the gas stream. Teflon was inadequate because its low ablation temperature would require too much material. The required thermal protection was provided by Pyrolytic graphite, which has low conductivity direction (C direction) normal to the gas flow. Zirconium oxide, although not used in the computer program, was expected to also provide the thermal protection required without ablating. Although the Pyrolytic graphite and the small conduction paths on each side of this graphite protect the seal, these small conduction paths set up some high temperature gradients which may cause some stress problems.

2. Tank Insert

Results of the thermal analysis of the tank inlet are shown in Figure V-8. The temperature in the seal area after 74 sec is 550°F; MX-2600 insulation was used.

V, D, Thermal Analysis (cont.)

3. Roll Control Gas Generator

Results of the thermal analysis of the roll control gas generator are shown in Figure V-9. Test data indicate that the average temperature observed in the RC generator T-flange was 560°F, with one temperature of 720°F being observed. Temperatures in the seal should be much higher; however, analysis of the existing design indicated that the seal temperature was 485°F. The higher temperature observed in the subsystem test (SST) could be attributed to the gap between the insulator and the T flange, which was not considered in the SST analysis. The thermal analysis was therefore conducted using convective heating in the gap, and a film coefficient of 115 Btu/ft<sup>2</sup>°F for the gap heating. The latter value was determined by running different film coefficients in the computer program until the average temperature obtained from test data on the T flange (560°F) was obtained at 70 sec. The redesigned T-flange was analyzed applying these conditions. The added heat sink (Figure V-9) to the T-flange, however, merely enlarged the heat path, and the seal temperature was higher than in the existing design. The present RC gas generator design, therefore, is recommended for use.

4. Area of the Dump Line Elbow

Analysis of the temperature in the area of the seal for the dump line elbow (Figure V-10) indicates that after 74 sec the temperature near the seal is 460°F.

5. Conclusions

Although the highest temperature in the seal was 1000 to 1075°F, this could be reduced by about 100°F by moving the seal outward as shown in Figure V-9. In addition, the heating in the RC gas generator could be greatly reduced if heating in the existing gap were eliminated.

E. LABORATORY EVALUATION OF VITON O-RING

The objective of these laboratory tests was to determine the sealing capabilities of Viton O-rings at a maximum pressure and temperature of 1800 psi and 1155°F, respectively, when used on the new gas seal joints of the Minuteman Wing VI Mod 4B LITVC and RC system.

A schematic diagram of the test setup is shown in Figure V-11. The sealing faces of the fixture were checked for flatness to + 0.002 in. after each test, and the O-ring and fixture groove were coated with DC-4 silicone grease before each test. The threads of the six assembly bolts were coated with molybdenum disulfide lubricant before a torque of 40 to 50 in.-lb was applied. The fixture was pressurized to 1850 to 1900 psi and held for 1 to 3 minutes while it was leak tested with a soap solution. The pressure was then reduced to 1800 psi, and the fixture was immersed in the molten tin bath at 1150 to 1200°F. A thermocouple in the fixture is located within 0.030 in. of the sealing O-ring. As the temperature of the

Report C162-06TDR-9-Vol 2

V, E, Laboratory Evaluation of Viton O Ring (cont.)

fixture rose past 700°F, the pressure was reduced from 1800 to 1250 psi and held there for the remainder of the 10 minute test. Following the test, the fixture was removed from the bath, depressurized, cleaned of residue, and checked for flatness. The strip-chart recorders were calibrated before testing began to provide full-scale readings of 2000 psi for pressure and 2230°F for temperature.

Twelve O-rings were tested, three each from four batches, and the results in Figure V-12 show no leaks or pressure losses during any of the tests. A pressure increase of 50 to 100 psi was observed as the fixture was placed in the bath. The pressure was then reduced to 1800 psi. Within 20 to 30 sec after immersion, the temperature rose to over 700°F, and the pressure was manually reduced to between 1200 and 1250 psi. No further valve adjustments were made, and the pressure curves generally showed a slight increase from 1220 to 1280 psi. The condition of the O-rings was the same in all cases following the tests.

The O-rings were reduced to a brittle black residue which crumbled readily into a powder or granules. Slight pitting of the stainless steel (T-347), which was observed after two tests, grew more pronounced after the sixth test when the fixture was removed from service for refac ng. The pitting appeared to be about 0.0005 in. deep.

The results in Figure V-12 show that the 0.006-in. shim and three of the four 0.004-in. shims caused failure or initial leakage within about 1 minute. The fixture normally provides for about 0.025 to 0.030-in. compression of the O-ring section diameter so the effect of the shim is to reduce this compression by the thickness of the shim.

The tests conducted with 0.002-in. shims indicate that this amount of nonparallel structure may be tolerable. Tests without DC-4 silicone grease on the O-ring indicate that the grease had little effect on the sealing efficiency of the O-ring.

Of the tests which had no pressure loss, the pressure and temperatures listed are those observed after 10 minutes in the tin bath. The fixture generally reached a temperature of over 1100°F within 50 to 70 sec. Most of the tests in which no leakage occurred had a pressure increase from 1240 to between 1280 to 1320 psi, corresponding to an average gas temperature of about 32°F. In the test to determine the pressure rise that would occur if no manual pressure bleed-off were used, the fixture was pressurized to 1600 psi and immersed in the tin bath for 10 minutes. The resulting pressure was 1700 psi, corresponding to an increase in gas temperature of only 40°F, assuming the nitrogen was at ambient temperature (70°F) before immersion of the fixture.

The condition of the O-rings was the same after all tests; the decomposition temperature of the Viton material is considered to be between 600 and 675°F; and the Viton material could perform satisfactorily as a static pressure seal at temperatures above its decomposition temperature if it is properly seated and compressed.

## V, LITVC Manifold and Joints Design Study--Project Directive 41-018 (cont.)

## F. WELD EVALUATION LABORATORY TESTS

The materials for the weld evaluation laboratory test program were procured. Three different material combinations were to be studied in this investigation to evaluate the conditions that will exist in the redesigned LITVC and RC system. Specimens of 17-7PH welded to Haynes 25 alloy were prepared for a crack-sensitivity test and a longitudinal bend test, but an analysis of the results was not completed.

## G. LITERATURE SURVEY

A literature survey was conducted to justify the evaluation of dissimilar metal combinations, and the results of this survey are summarized below.

1. Current Design

Many of the joints in the hot-gas lines of the LITVC and RC system are bolted joints which have periodically caused leakage problems. The alloys used in these fittings include T-347 stainless steel, N-155, a chromium-cobalt-nickel-iron alloy, and Haynes 25. The thickness of the joints does not exceed 0.250 in.

2. Survey Data

Considerable data<sup>(1)</sup> were found on the welding of T-347 stainless steel. This grade of steel is commonly used where welding is required during fabrication. No difficulty was encountered in welding this type steel to Haynes 25 and N-155, and relatively thin-walled sections (3/16 to 1/4 in. thick), such as those proposed for the hot-gas joints should be readily welded. The strengths of welds in these alloys are listed below:

<u>Alloy</u>	<u>Thickness</u>	<u>Ultimate Tensile Strength, psi</u>	<u>Yield Strength, psi</u>	<u>Elongation in 2 in., %</u>
Haynes 25 <sup>(2)</sup>	0.094	130,000	73,000	30
	0.125	133,000	70,000	34
N-155 <sup>(3)</sup>	0.125	108,000	60,000	22
	0.250	111,000	65,000	21
T-347 <sup>(1)</sup>	0.250	93,000	65,000	35

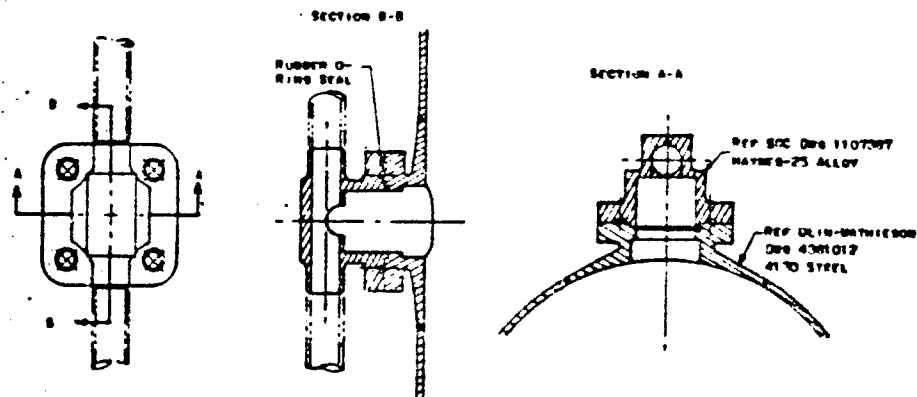
(1) Welding Research Council Bulletin No. 43, October 1958, Welding Type 347 Stainless Steel Piping and Tubing by George E. Linnert.

(2) Union Carbide Stellite Co., Data Sheet for Haynes-25

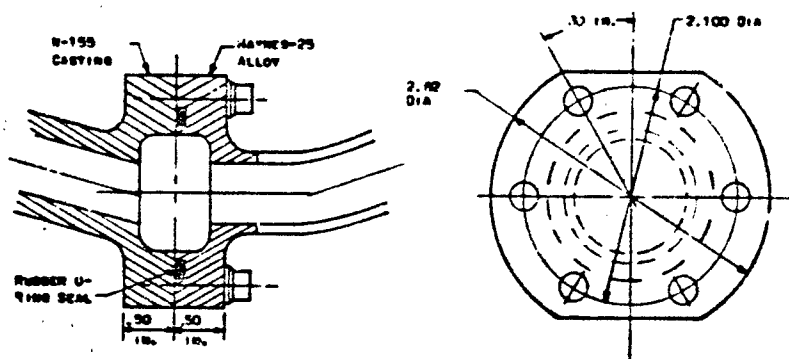
(3) Union Carbide Stellite Co., Data Sheet for Multimet (N-155)

V, G, Literature Survey (cont.)

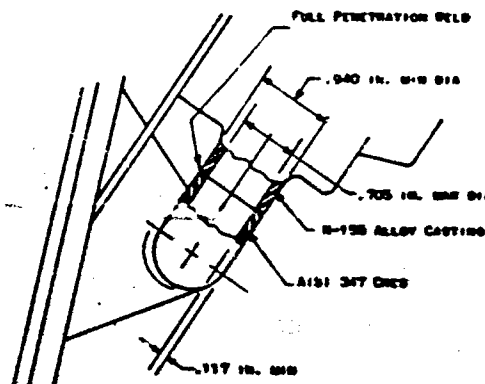
Welding experience using these metal alloys by the liquid rocket operations at Aerojet, Sacramento, indicates that in wrought or cast form neither of these alloys has ever been a source of special difficulty as long as proper procedures were followed. These alloys were welded in various components of the Titan II, M-1, and Nerva motors.



ROLL CONTROL GENERATOR JOINT



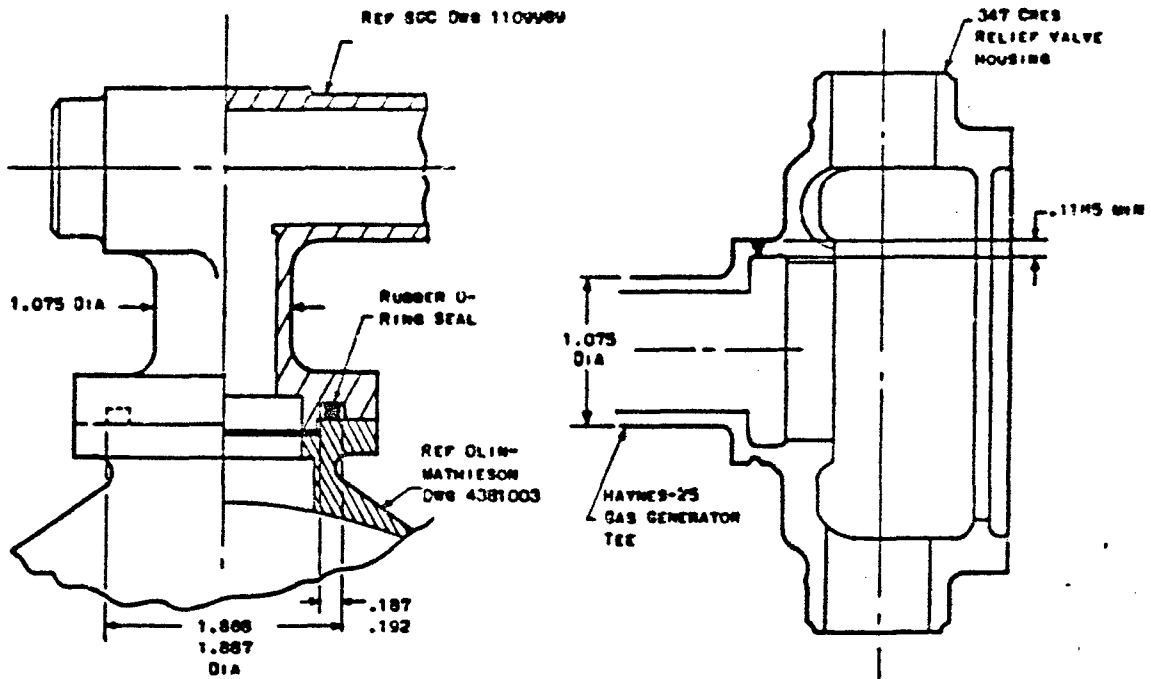
ROLL CONTROL VALVE JOINT



ROLL CONTROL NOZZLE JOINT

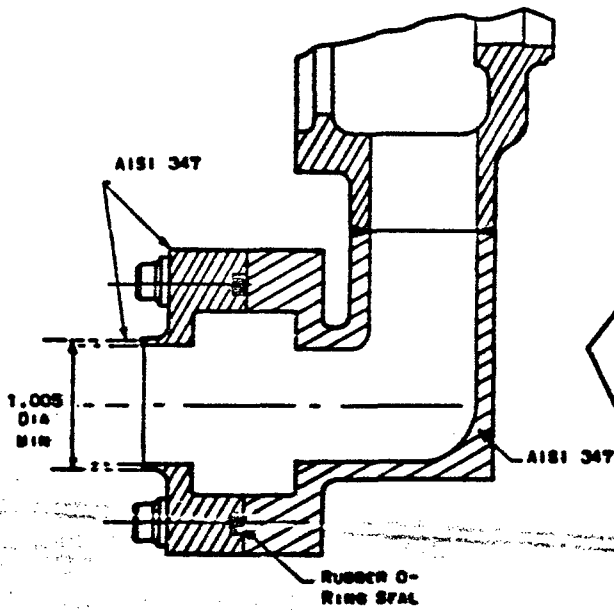
RC Subsystem Joint Used in Stress Analysis

Figure V-1

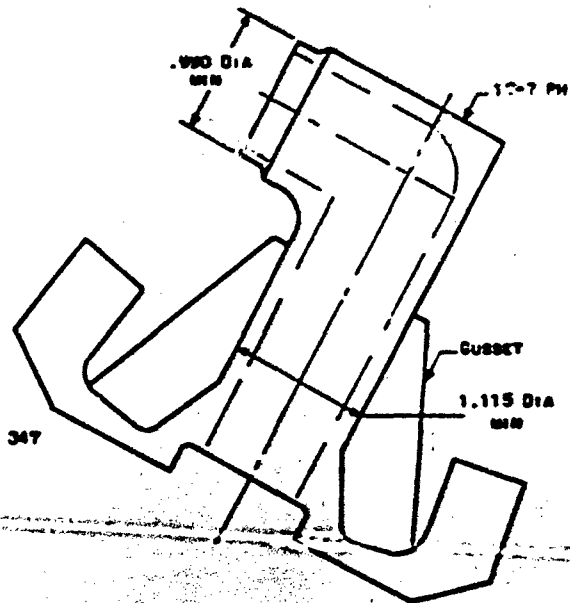


TVC GAS GENERATOR JOINT

RELIEF VALVE HOUSING WELDED JOINT



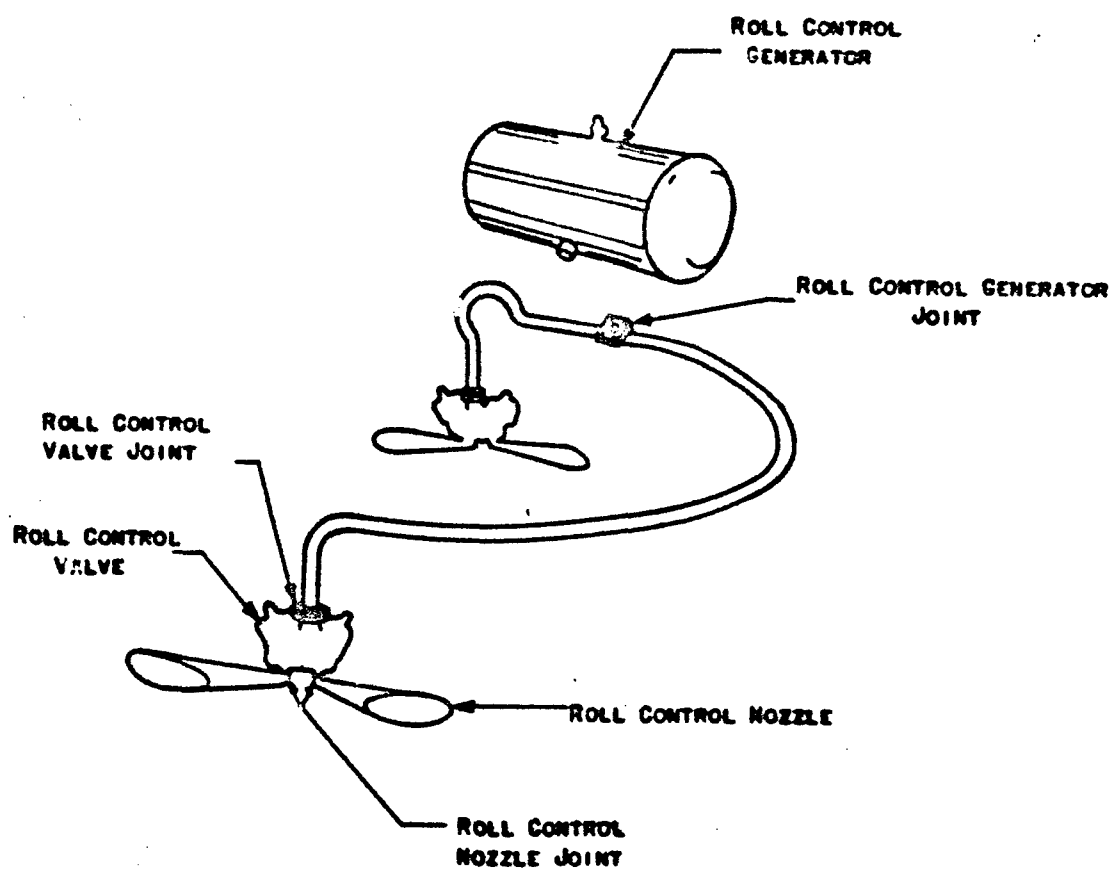
DUMP LINE JOINT



TVC TANK INLET WELDED JOINT

TVC Subsystem Joints Used in Stress Analysis

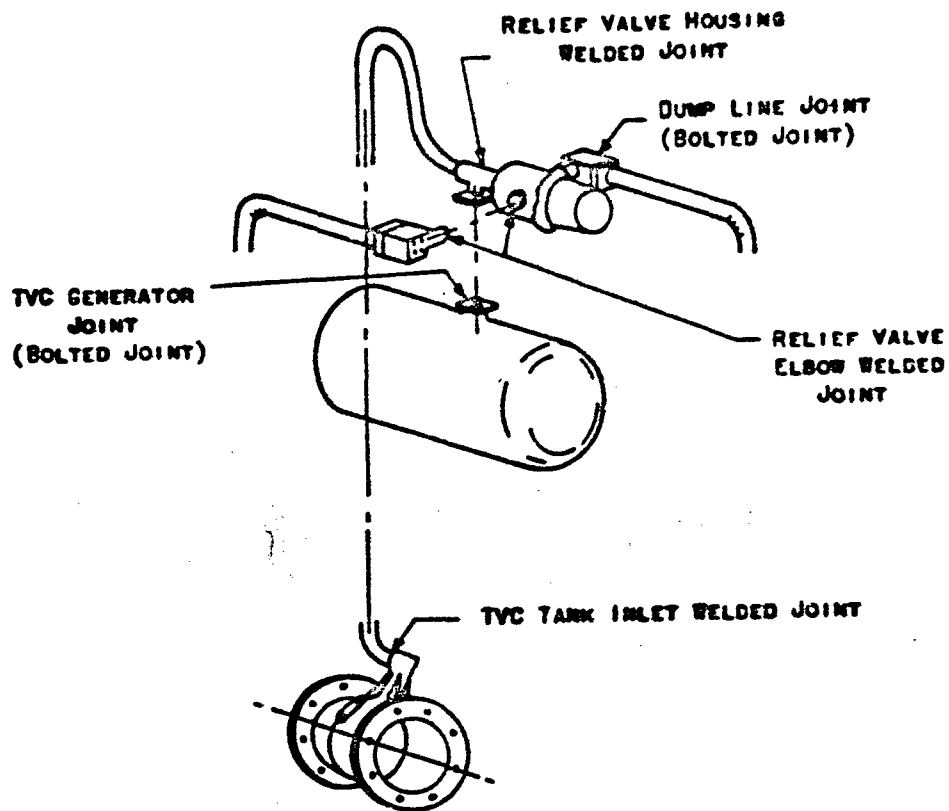
Figure V-2



RC System Components

Figure V-3





TVC System Components

Figure V-4

<u>Component</u>	<u>Material</u>	<u>Type Stress</u>	<u>Design Condition</u>	<u>MS*</u>	<u>MS Type</u>
RC generator joint	Haynes-25	--	--	**	--
RC valve joint	Haynes-25 and N-155 alloy	Bolt pre-tension	MEOP at 10 sec	.33	Yield
RC nozzle joint	N-155 alloy and AISI 347	Hoop stress at weld	MEOP and thrust loads at 10 sec	1.10	Ult.
TVC generator joint	Haynes-25	--	--	**	--
TVC relief valve housing; welded joint	Haynes-25 and AISI 347	Meridional stress at weld	MEOP at maximum temperature	.18	Ult.
Dump line joint	AISI 347	Hoop stress at weld	MEOP at maximum temperature	.75	Ult.
TVC tank inlet welded joint	Haynes-25 and 17-7 PH	Hoop stress at weld	MEOP at maximum temperature	1.10	Ult.

\* Margin of Safety

\*\* No detailed analysis was performed because the modifications to these joints were minor and resulted in less severe loading.

Minimum Margins of Safety

Figure V-5

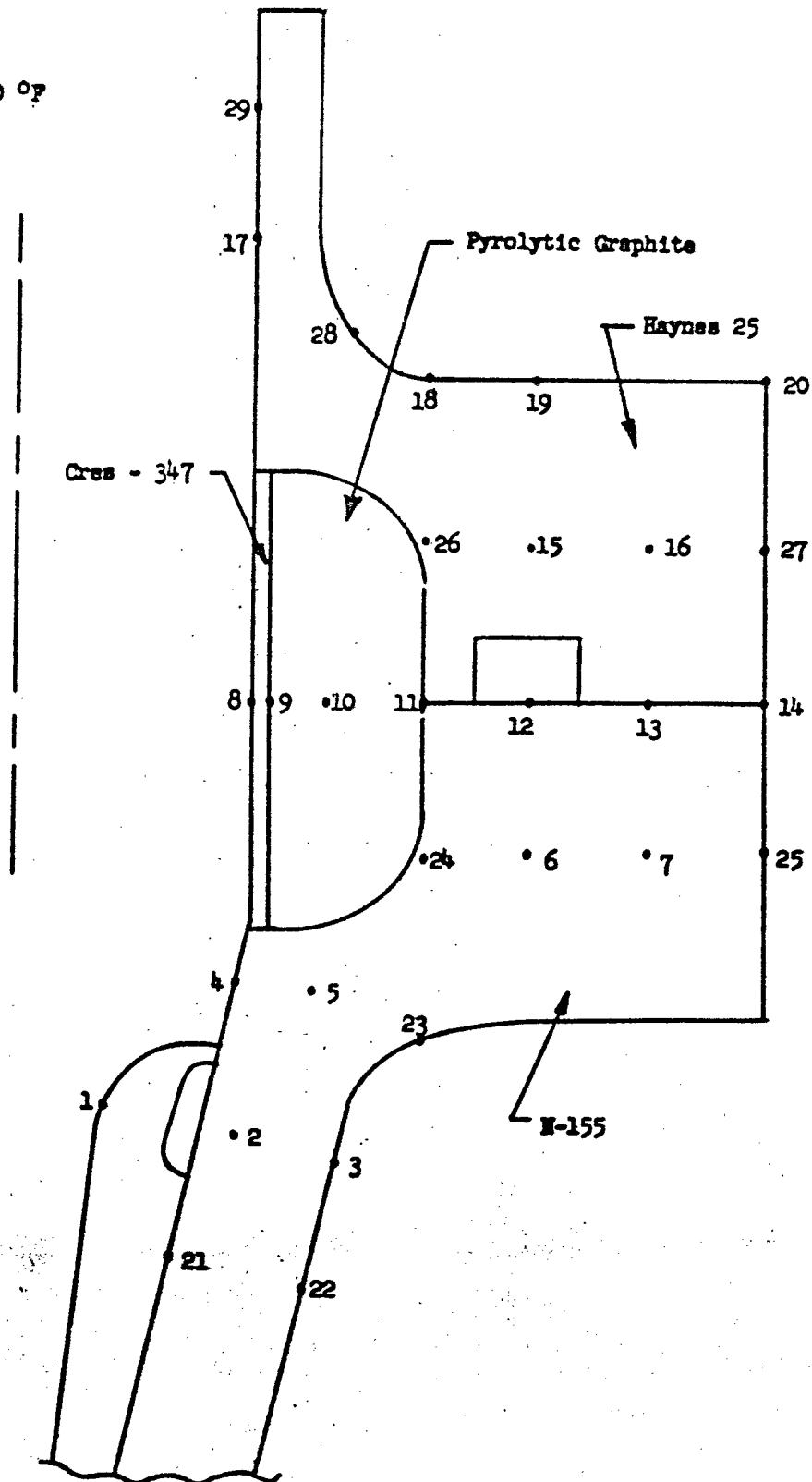
<u>Material</u>	<u>Thermal Conductivity, Btu/hr/ft/°F</u>	<u>Specific Heat Btu/lb-°F</u>	<u>Density, lb/ft<sup>3</sup></u>
17-7PH	10.6	0.10	483
Cres 347	9.25	0.118	495
Haynes	10	0.092	570
Cres 316	12.4	0.12	501
4130 Steel	24.7	0.107	489
Refrasil	0.08	0.23	60
MX 2600	0.157	0.19	114
N-155	10	0.11	512
Pyrolytic Graphite	Variable	Variable	137
RPD 150	0.124	0.27	112

Thermal Properties Used in Analysis

Figure V-6

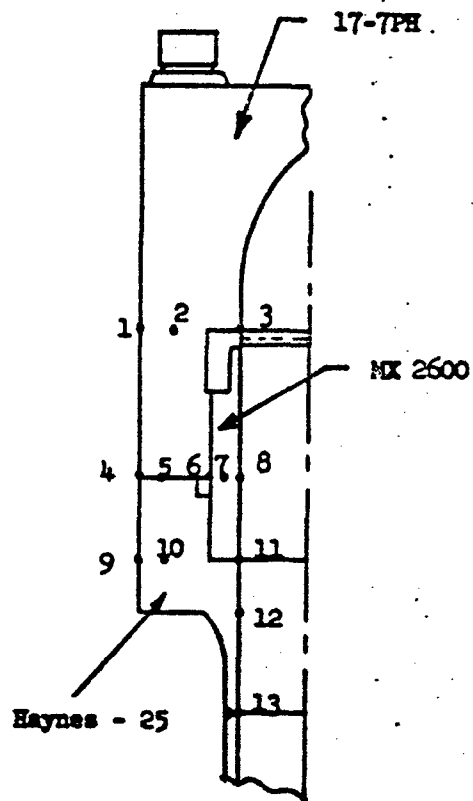
Gas Temp = 2200 °F

Node	Temp, °F, at 74 sec
1	2140
2	1970
3	1850
4	1930
5	1890
6	920
7	800
8	2130
9	2120
10	1570
11	1020
12	900
13	795
14	745
15	860
16	780
17	1880
18	1130
19	930
20	750
21	2020
22	1990
23	1560
24	1120
25	750
26	930
27	740
28	1430
29	2100



Thermal Analysis, RC Valve Temperature

Figure V-7

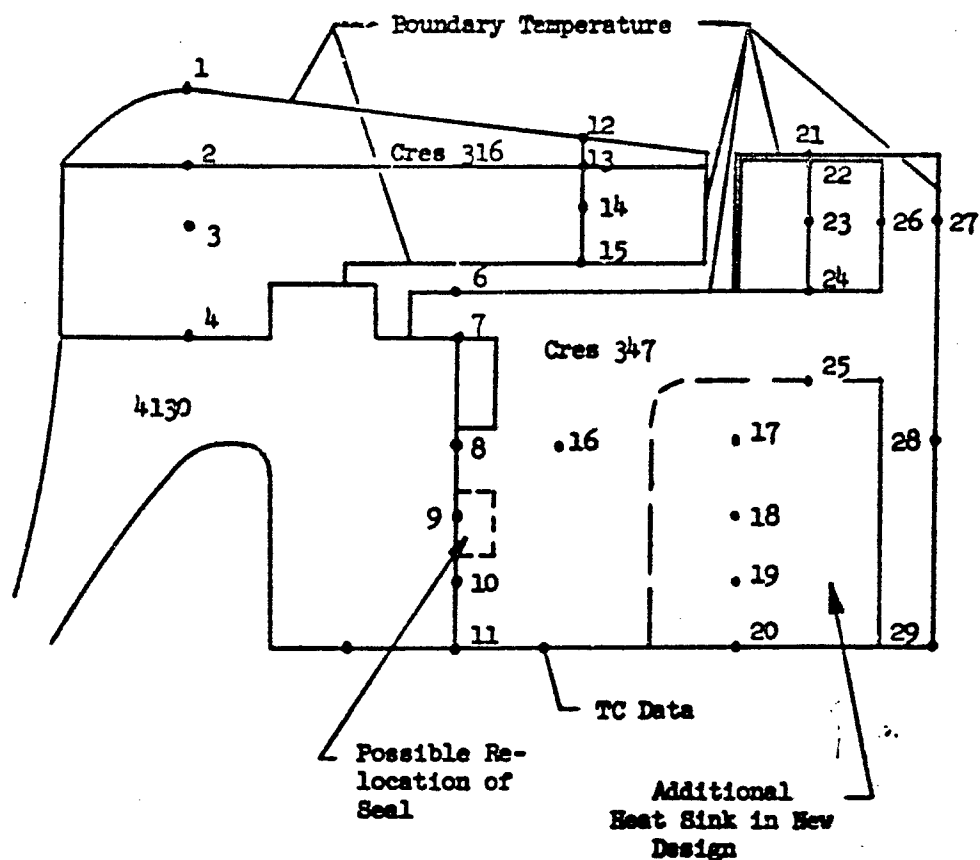


Node	Time, sec	
	10	74
1	190	640
2	220	670
3	600	940
4	95	530
5	97	530
6	110	550
7	980	1500
8	1900	2035
9	130	615
10	150	625
11	1880	1965
12	750	1120
13	1480	1690

Thermal Analysis, Tank-Inlet Temperature Distribution

Figure V-8

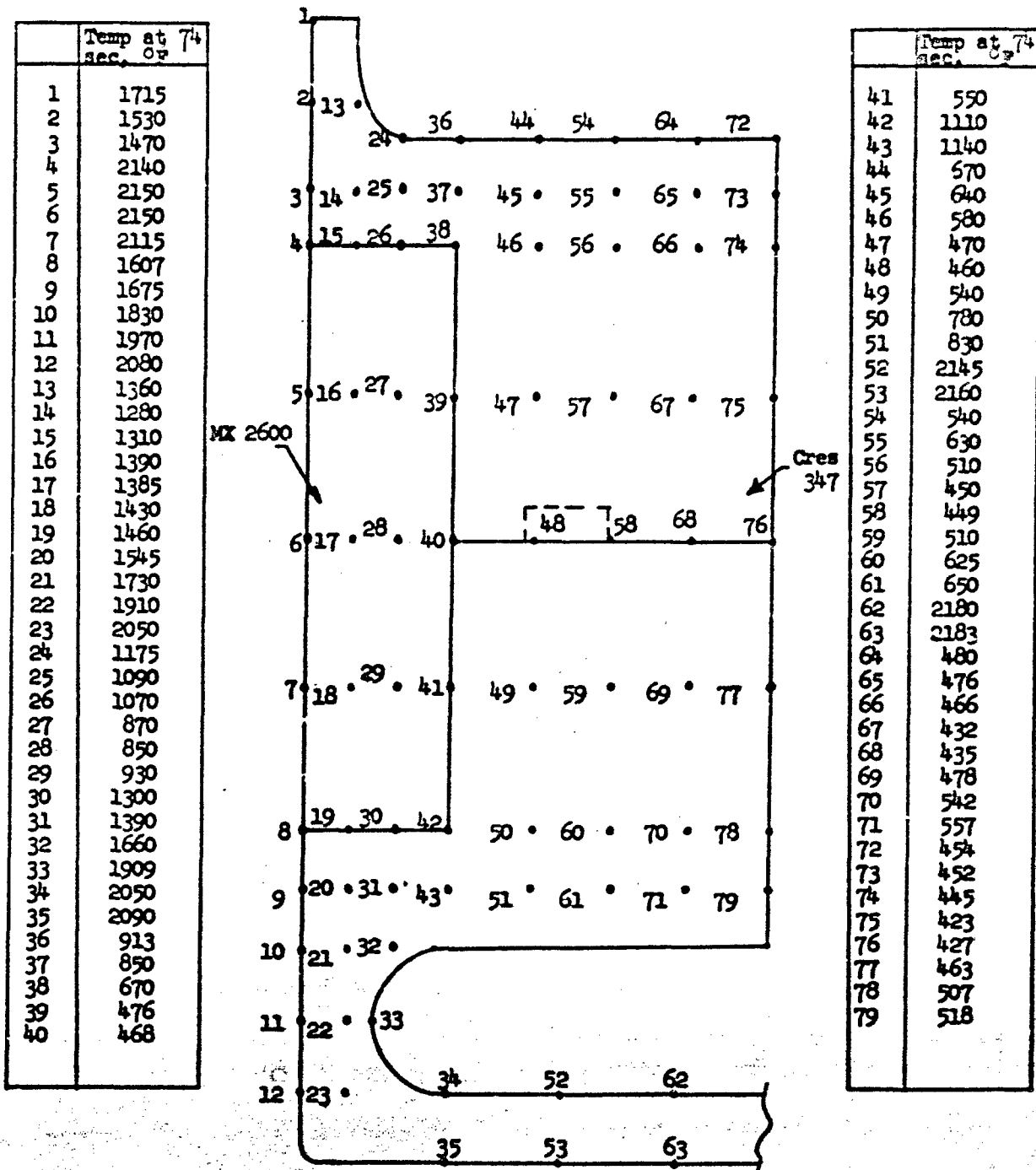
Node	Present Design	New Design
	Time, sec	Time, sec
	74	74
1	2155	2135
2	2110	2110
3	1090	1090
4	750	1065
5	615	1080
6	1075	1380
7	1000	1320
8	820	1190
9	710	1140
10	640	1110
11	610	1100
12	2080	2080
13	2080	2080
14	2010	1985
15	2165	2170
16	850	1355
17	-	1575
18	-	1510
19	-	1475
20	-	1460
21	2075	2075
22	2075	2075
23	1850	1860
24	1720	1790
25	1700	1740
26	2070	2060
27	2070	2065
28	2140	1990
29	2080	1970



--- Present Design  
 — New Design

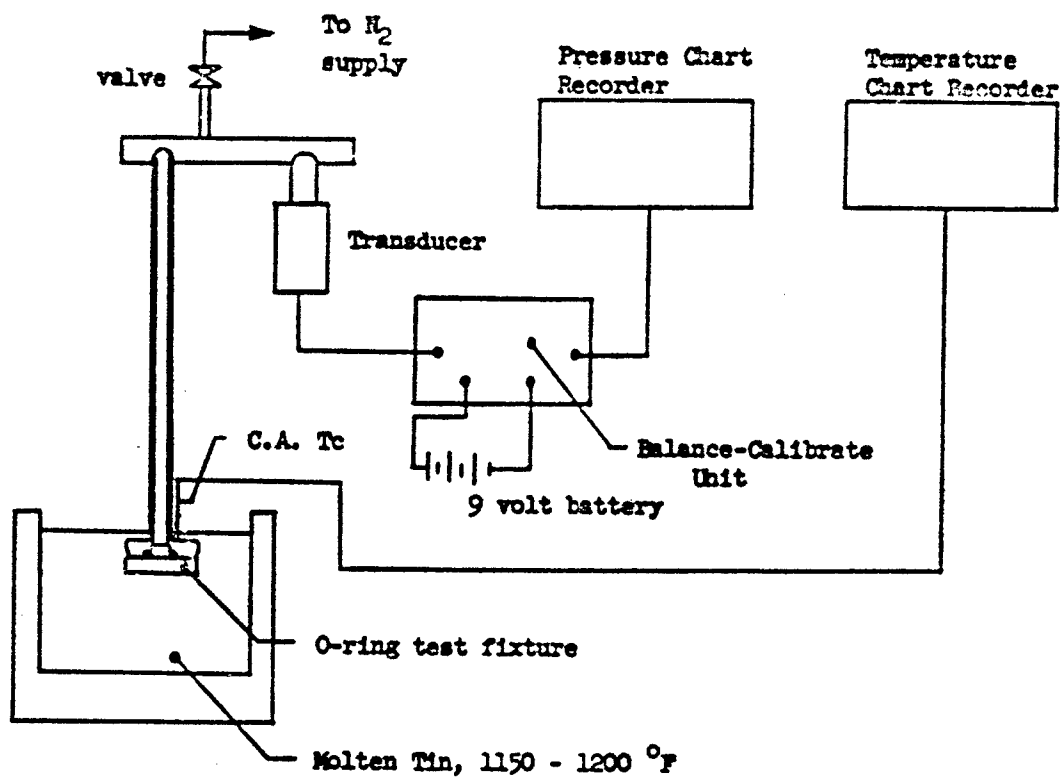
Thermal Analysis, RC Gas-Generator Flange Temperatures

Figure V-9



Thermal Analysis, Elbow Dump Line Temperature

Figure V-10



Test Setup for Evaluation of O-Rings at 1150 to 1200°F

Figure V-11



Test*	Batch	Induced Cap, in.	Duration, min	Pressure, in.	Temp, °F	Remarks
1	0-58	None	10	1285	1180	No failure.
2	0-58	↓	↓	1240	1180	↓
3	0-58			1280	1180	
4	0-908			1280	1180	
5	0-908			1260	1116	
6	0-908			1260	1180	
7	0-3660			1245	1180	
8	0-3660			1260	1116**	
9	0-3660			1285	1180	
10	0-4576			1260	1200	
11	0-4576			1200	1137	
12	0-4576			1270	1160	
25	0-58	0.006	50 sec	1250	1010	Sudden failure.
13	0-58	0.004	45 sec	1830	710	Slow leak/640 psi/in 10 min.
16	0-908	0.004	70 sec	1240	990	Slow leak/880 psi/in 10 min.
19	0-3660	0.004	50 sec	1800	895	Sudden failure.
22	0-4576	0.004	10	1280	1200	No failure.
14	0-58	↓	↓	1310	1158	↓
17	0-908			1320	1179	
20	0-3660			1280	1158	
23	0-4576			1300	1158	
15	0-58			1290	1179	
18	0-908			1240	1158	
40	0-3660			1280	1179	No failure.***
41	0-4576			1260	1158	No failure.***
42	0-58			1280	1158	No failure.***
43	0-908			1270	1158	No failure.***
44	0-3660		45 sec	1240	1116	Slow leak/800 psi/in 10 min***
45	0-4576		10	1320	1158	No failure.***
46	0-3660		10	1290	1179	No failure.***
47	0-4576	None	10	1720	1179	No failure. Initial pressure 1600 psi. No bleed-off.

\* Test numbers do not indicate chronological order.

\*\* Thermocouple failure

\*\*\* No DC-4 grease used on O-ring.

#### Results of Viton O-Ring Tests

Figure V-12

VI.

INVESTIGATION OF EXIT CONE MATERIAL BEHAVIOR--PROJECT DIRECTIVE 41-019

A. OBJECTIVE

The objective of this program was to establish the performance of tape-wrapped exit-cone materials during motor firing by laboratory testing of exit-cone samples and to obtain data relating to the behavior of these materials and interface bonds when considering various material and process variables.

To further understand the problem the following additional areas were investigated:

1. The effect of char on the nozzle-interface bond strength and on nozzle strength.
2. The partial release of the exit-cone-housing bond line.
3. Proof-test procedures, tooling, and pressure levels.
4. Alternative methods of exit-cone retention.
5. X-ray inspection of nozzle assemblies.

B. LABORATORY STUDIES

For the initial phase of this program, plasma-arc testing was performed on exit-cone samples to study the behavior of the material and the interface bond between materials when considering volatile content, resin advancement, cure cycles, and gas-release openings. As the basis for the testing, a temperature-vs-time history during firing was theoretically computed for an existing nozzle at various expansion ratios. These data were compared with actual firing histories of cones that performed abnormally during motor firings. In the Minuteman Wing VI program, graphite liners had been ejected from six sea-level exit cones. Four of these were ejected at tailoff, when the interface line between the graphite and the silica-phenolic tape was charred and at a maximum/minimum temperature of 1880°F and 960°F (Figures VI-1 and -2). The remaining two liners were ejected at approximately 40 sec after ignition at a maximum/minimum interface temperature of 1170°F and 360°F (Figures VI-1 and -2). A combination of temperature and time based on the above data was used in the test program outlined below.

1. Materials and Specimen Preparation for Laboratory Studies

Plasma-arc tests were performed on samples of three Wing VI sea-level cones and seven subscale cones having various volatile contents to determine if abnormalities encountered could be duplicated and to observe the change in material behavior. Interface pressures and temperatures were recorded during testing. Additional plasma-arc testing was performed on specimens to determine if drilling holes in the liner or post-curing the part improved the performance.

VI, B, Laboratory Studies (cont.)

a. Full-Size Cones

The three full-scale cones (FN 369937) were made of FM-5014/FM-5020 by Cleveland Pneumatic Industries. Removal of the cones from nozzle assemblies was achieved by heating the assemblies to approximately 400°F and applying sufficient force to break the bond between the cone and the titanium housing. The nozzle assemblies had been proof-pressure tested. Two of these cones showed cracks prior to testing; one was cracked in the graphite wrap, and one in the silica wrap.

Eight 10-in. by 10-in. slabs and four interface shear-test specimens were cut from each cone as shown in Figures VI-3 and -4. The volatile content in both wraps was determined for each slab. The slabs from each cone were prepared for testing as follows:

- (1) Two slabs were left in their original state.
- (2) Two slabs were post-cured at 300°F for 48 hr.
- (3) Two slabs were prepared with holes drilled through the graphite liners (see Figure VI-5).
- (4) Two slabs were prepared with holes drilled through the liner (see Figure VI-6).

b. Subscale Cones

Seven cones were made to the configuration shown in Figure VI-7. Two 10-by 10-in. slabs and four interface shear specimens were cut from each of the seven cones as shown in Figures VI-3 and -4. The volatile content in both wraps were determined for each slab.

To obtain a part with minimum volatile content for comparison, a small-scale part was made by the snap-cure method. This cone (Specimen Code FSC-1 and -2) was made by Fiberite from MX-4500/MX-2600. The MX-4500 liner was wrapped at 220°F with a roller pressure of 200 lb/in. and cured in an autoclave for 2 hr at 150 psi and 300°F. The autoclave temperature was increased from room temperature to cure temperature at a rate of three degrees/minute. The cured liner was machined on the outside diameter and overwrapped with silica tape with a mandrel temperature of 290°F, tape temperature of 300°F, roller pressure of 300 lb/in., and a mandrel speed of 4 rpm. The surface of the MX-4500 liner was covered with an epoxy-phenolic modified resin prior to adding the silica tape.

To obtain test specimens with extremely high volatile content, a small-scale cone was made with water added during the cure cycle. This cone (Specimen Code 96-1 and -2) was made of FM-5014/FM-5020 in accordance with Specification AGC-34311, Types II and IV; material data are shown in Figure VI-8. The cone was manufactured like a Wing VI cone in accordance with Drawing 369937, with the following exceptions:

VI, B, Laboratory Studies (cont.)

- (1) Only two wraps were used.
- (2) Only two debulk cycles were used.
- (3) Water was introduced between the silica overwrap and the vacuum bag prior to the last debulk and cure cycles. Debulk and cure cycles were in accordance with Drawing 382123.

Small-scale cones were made of material with high, medium, and low resin advancement. These cones (Specimen Codes 03-1 and -2, 02-1 and -2, and 99-1 and -2) were made of FM-5014/FM-5020 in accordance with Specification AGC-34311, Types II and IV; material data are shown in Figure VI-8. The cones were manufactured like a Wing VI cone in accordance with Drawing 369937, except that only two wraps and two debulk cycles were used. Debulk and cure cycles were in accordance with Drawing 382123.

Two cones were made from material of normal advancement and volatile content, and a debulk and cure cycle as shown in Figure VI-9. These cones (Specimen Codes 92-1 and -2 and 94-1 and -2) were made of FM-5014/FM-5020 in accordance with Specification AGC-34311, Types II and IV; material data are shown in Figure VI-8. The cones were manufactured like a Wing VI cone in accordance with Drawing 369937, except that only two wraps and one short debulk cycle were used.

2. Test Procedures

A pressure gage and a thermocouple were installed through the silica liner at the interface between the two materials on all slab specimens that did not have holes drilled through the graphite phenolic liner. Only a thermocouple was installed at the interface of the slab specimens with drilled holes. The slabs were suspended on a wire with the thermocouple and the pressure gage (when applicable) was attached to a continuous recording instrument. Two oxyacetylene torches were placed 6-1/2 in. from the graphite phenolic liner. The flame was set to give approximately 225 Btu/ft<sup>2</sup>/hr and covered approximately a 5-in.-dia area at the center of the slab. The test was stopped when the specimens were obviously separated at the interface or had cracked through the liner. After testing the slabs were sectioned through the center, and visually inspected.

Of the four interface shear specimens from each cone, two were charred in an Argon atmosphere for 30 minutes at 1500°F. The uncharred and charred interface shear specimens were tested in a Tinius Olsen testing machine at room temperature.

3. Summary of Test Results

a. Full-Size Cones

Test results for specimens from the full-scale exit cones (SN 2168016, 2168017, and 2168018) are summarized in Figure VI-10.\* Detailed

\*Figure VI-10 includes test results for specimens from subscale cones.

VI, B, Laboratory Studies (cont.)

descriptions and results of observations of the tests are presented in Appendix VI-A. Temperature- and pressure-vs-time curves are given in the figures in Appendix VI-A.

Except for one drilled specimen from Cone SN 2168018, some cracks were detected in the graphite phenolic wrap of all the specimens tested. Only three specimens did not crack at the silica-graphite interface; these were one post-cured slab specimen and two drilled specimens from Cone SN 2168018. Except for the post-cured and drilled specimens of the same cone, the silica wrap of all specimens cracked during testing.

The following observations were made based on the test results:

(1) No relationship was detected between interface cracking and volatile content, although the volatile content did vary from cone to cone.

(2) Post-curing did not significantly improve performance.

(3) Drilling 1/16-in.-dia holes, 1/4 or 1/2 in. apart, in the graphite liner to the silica interface did improve to some degree the post-fired interface condition, but did not eliminate cracking. The two materials generally remained in closer contact than the undrilled specimens.

(4) Only one as-received specimen, from Cone SN 2168016, developed a blister that was similar to those noted on the cones of fired Wing VI motors.

b. Subscale Cones

Test results for specimens from the subscale exit cones are included in Figure VI-10. Results of analyses of test data and curves of temperature and pressure vs time are presented in Appendix VI-B.

On the basis of results of testing the subscale exit cones, the following observations were made:

(1) As was noted with the full-scale cone specimens, a variance in volatile content did not influence interface performance.

(2) By increasing the tape material advancement, B staging or IRPI, some degree of improvement was noted at the interface.

(3) A shorter debulk cycle did not improve interface performance.

4. Evaluation and Discussion of Test Results

a. General

In evaluating the results given in Figure VI-10 and Appendixes VI-A and -B; it should be noted that the laboratory test conditions do not precisely

VI, B, Laboratory Studies (cont.)

simulate those experienced during actual firings; slab specimens tested in the laboratory are subjected to more severe and uneven loading conditions. When the cone is heated during firing, the graphite wrap expands into the silica overwrap and creates a compressive stress at the interface that aids mechanical locking and friction between the materials. Shear forces develop at the interface only in the longitudinal direction.

When a slab specimen is tested in the laboratory, the compressive forces are eliminated and shear forces are developed in all directions at the interface. Peel forces from curving of the parts caused by uneven heat distribution also tend to develop. Since the laboratory test is more severe, the results do not truly represent actual firing conditions. Because most of the laboratory specimens cracked to some degree, it becomes difficult to quantitatively compare results for the various specimens tested. However, by visual observations of the testing and analysis of the test results, trends of performance can be determined.

For future programs of this type, ring specimens instead of slab sections will be used to obtain data of a more discriminate nature; ring specimens could be made to more accurately simulate firing conditions.

b. Shear Testing

The results for shear testing (Figure VI-10) show generally higher shear values for the specimens taken from the small cones as compared to those taken from the full-scale cones. While this may be a result of the fact that the small cones had less debulk time, delaminations were noted on two test specimens from a full-scale cone prior to testing, and it is probable that other small undetected cracks were present which influenced the test results. Photomicrographs of phenolic graphite and silica-wrapped parts that were subjected to high stresses showed numerous small cracks in the phenolic resin.

Too few shear specimens were tested to quantitatively evaluate the small cones. The appreciable variance in data for specimens from the same cone, noted in some instances, negate any possibility of making a valid comparison.

Because the interface shear specimens all curved during charring and were concave on the graphite-wrap side during tensile testing, the actual shear strength of the interface bond is greater than measured. In addition, the moment introduced because of the curvature is not accounted for in the calculations.

The length of the test specimens appeared to be reduced after charring; graphite shrinking was greater than that of the silica. Since the coefficient of thermal expansion of silica at char temperature is several times as great as for the graphite wrap and since the silica is the better insulator, it charred slower and retained a high modulus of elasticity longer than did the graphite. All these effects tended to curve the charred test specimens and resulted in fictitiously low shear values..

VI, B, Laboratory Studies (cont.)

While the charred specimens taken from the small cones indicate greater interface shear strength than those taken from the full-scale cones, the results are considered inconclusive because of the interface separation which occurred during the charring of many of the full-scale cone samples.

c. Conclusions

Results of this study indicate that changes in volatile content, debulk cycle time, and adding a post-cure treatment do not influence the performance at the interface. However, drilling holes in the graphite liner and increasing the tape material advancement, B staging or IRPI does appear to improve performance at the interface bond. Because of the severity of the laboratory test, all specimens cracked to some degree, making it difficult to evaluate accurately the effects of material and processing variables on material behavior.

On the basis of these tests it can be stated that interface bond cracking is initiated at relatively low interface temperatures. Fracture is caused by a combination of thermal stresses, pressure from expanding air entrapped at the interface, and the boiling off of volatiles from interface materials. While this indicates that the interface line should be maintained at the lowest possible temperature to ensure maximum reliability, the exact temperature limitations on the interface line are unknown. Although this indicates that the requirement for a low interface temperature minimizes the insulation benefits obtained from the silica wrap, the silica wrap does provide an extra margin of safety if the graphite liner is ejected.

C. THE PARTIAL RELEASE OF THE EXIT CONE-HOUSING BOND LINE

The objective of this analysis was to study the effect of releasing the bond between the sea-level plastic exit cone and the titanium housing at the T-joint. A complete stress analysis, presented in Appendix VI-C, was performed for all parts affected by this change.

The stress analysis included investigations of the nozzle in the area affected by the bond release for proof-pressure testing without a bond release and with bond releases of 6, 6.5, and 7.5 in. Investigations were also made for conditions at the start and end of firing with bond releases of 6, 6.5, and 7.5 in.

Results of the analysis show that an optimum stress condition exists for a bond release of approximately 7.5 in. This change in the Wing VI nozzle would reduce the stresses in the plastic cone and the bond line to a level with definite positive margin of safety. The cracks now experienced in some cones at proof pressure testing would be eliminated, and the possibilities of losing the graphite phenolic liner and of blistering of the liner during firing would be greatly reduced.

VI, Investigation of Exit Cone Material Behavior--Project Directive 41-019 (cont.)

D. ALTERNATIVE METHODS OF EXIT CONE RETENTION

1. Objective

The objective of this program was to investigate alternative means of retaining the sea-level exit cone in the housing.

2. Summary of Requirements

The cone is presently held in place by a snap ring at the forward end and by the bond between the housing and the cone.

The following forces are acting on the cone during firing:

- a. Chamber pressure on the OD of the submerged portion if acting through the housing to eject the cone.
- b. Nozzle gas pressure at the split line between the graphite insert and the forward face of the cone is acting to eject the cone.
- c. Nozzle gas pressure on the ID of the cone and at the split line adjacent to the altitude cone is acting to retain the cone.
- d. Thermal expansion forces on the cone, which expand it into the housing, are acting to eject the cone.

These forces together have a resultant ejection force of 61,500 lb at the end of firing at a chamber pressure of 570 psi. The highest ejection force, however, occurs during proof pressure testing at 627 psi, when the chamber pressure acting to eject the cone results in a force of 85,000 lb.

If the bondline and the friction forces between the housing and the cone are ignored, the present snap ring alone is capable of providing a retention force of 80,500 psi, based on an interlaminar shear strength of 1500 psi in the plastic. This retention force is satisfactory under firing conditions but not for proof pressure testing.

The bond between the housing and the cone is capable of providing a retention force of 2,000,000 lb or approximately 23 times the ejection force with an evenly distributed shear stress of 1250 psi.

3. Alternative Methods Investigated

The sea-level cone is made of a graphite-phenolic tape inner liner and a silica-phenolic tape overwrap; both tapes are wrapped parallel to the centerline. During firing, all the graphite and part of the silica cloth become charred.



VI, E. Alternative Methods of Exit Cone Retention (cont.)

The charred portion of the cone has shown some signs of interlaminar cracking in all Wing VI motor firings. Approximately 20% (0.20 in.) of the silica material remains uncharred. Assuming an interlaminar shear strength of 1500 psi for the uncharred silica and none for the charred material, the maximum obtainable retention force in one plane on the cone is  $F = D \frac{0.20}{\sin}$  (see Figure VI-11). At the aft end, where the diameter is the greatest, the retention force is equal to 92,000 lb at the end of firing. Figures VI-12 and -13 show two alternative methods that would retain the cone at the aft end but that do not offer any improvement over the current design.

Figure VI-12 shows the incorporation of a metal retaining ring, which is held and locked in place by the altitude exit cone. This metal ring extends in between the cones far enough to take advantage of the shear strength of the uncharred material in the sea-level cone, but still stays below the heat-affected zone to prevent the conduction of heat into the cones.

Figure VI-13 shows an all-silica laminate insert at the aft of the sea-level cone. This insert, like the metal retaining ring, would be held in place by the altitude exit cone. This design would provide a retention force of 256,250 lb, including the retention of the snap ring. Gaps for thermal expansion are left between both the insert and the sea-level cone, and the insert and the altitude exit cone. The laminate-insert design would provide a desired increase in shear area over the present design and would also help to keep the inner wrap from being ejected.

Other methods of retaining the cone with plastic and metal inserts at the injector ports (Figure VI-14) are unsatisfactory because of the small shear area reached in the plastic cone. Inserts or pins through the housing are also unsatisfactory because of the number required to obtain a satisfactory shear area in the plastic and because of sealing problems.

If the silica overwrap was wrapped at an angle with the nozzle center line in such a way that the ejection force could be taken up in cross laminar shear in the plastic, a much smaller shear area would be required, since the cross-laminar shear allowable is approximately seven times greater than the interlaminar. Other methods of retention might then be practiced.

E. PROOF TEST PROCEDURES, TOOLING, AND PRESSURE LEVELS

The objective of this investigation was to compare the severity of the proof-pressure test now used with the conditions actually encountered during firing, and to establish a proof pressure test method closely duplicating firing conditions.

VI, E, Proof Test Procedures, Tooling, and Pressure Levels (cont.)

The structural analysis (Appendix VI-C) shows that with the liner released at the T-joint the present proof-pressure test method is satisfactory. The test method duplicates the stresses at start of firing fairly closely in the high stress areas and will not overstress any part of the nozzle. Without a bond release, the proof pressure should be dropped to 470 psi to obtain a closer relationship between the stresses at proof testing and start of firing. It is possible that an even closer simulation of the maximum stresses could be obtained if a back pressure was used in the titanium exit cone flange to achieve the same ejection force in the nozzle at proof test as during firing (see Figure VI-15). Because of time limitations, this analysis was not conducted. However, the proof-test analysis for a released liner condition was performed and showed a reduction in critical liner stresses. The present proof-pressure test tooling seems adequate for testing a nozzle with a released liner.

F. X-RAY INSPECTION OF NOZZLE ASSEMBLIES

The objective of this investigation was to determine by X-ray examination if cracks exist in the plastic sea-level exit cone in the T-joint area.

To date seven Wing VI motor nozzle assemblies have been X-rayed to evaluate discontinuities on the inner surface of the graphite inner wrap. Each of these assemblies showed evidence of discontinuities on the inner surface of the assembly from 6 to 12 in. aft of the entrance cap. The suspect areas varied in length from about 4 in. to the entire circumference of the cone. Width and depth of the suspect areas could not be determined by visual inspection.

Tangential radiographs were made at 15-degree intervals on each assembly using the 10 MEV Linac. The Linac was aligned with the nozzles to place the suspect areas at the center of the radiation field, and exposures were made on Ansco type-B film. Satisfactory visualization of the inner and outer wraps of the exit cone was obtained, but on none of the assemblies was it possible to demonstrate any discontinuity in the graphite.

Nozzle assembly SN 2168037 contained a delamination in the silica outer wrap which extended from the outside diameter of the cone through a wrap and along the interface between the silica and graphite for a distance of about 2 in. The delamination occurred along the interface between two plies except at 240 degrees where it involved an additional ply, resulting in a double image at that point. The delamination between wraps appears to have involved only the interface without appreciable damage to either cone. Although a surface discontinuity was present in the graphite at this level, there was no radiographic evidence of damage to this portion of the assembly.

VI, F, X-Ray Inspection of Nozzle Assemblies (cont.)

Tangential and radial radiography with the Linac do not lend to evaluation of the quality of the bond between the silica cone and the titanium housing. There is evidence, however, that radial projections made with equipment in the 150 to 300 kvp range may offer some information as to the uniformity of the adhesive between these two structures. Radial views received from the Downey Plant on nozzles SN 2168028 and 2168029 exhibit density changes that may be caused by voids in the adhesive. Similar density changes are present on the radiographs of nozzle SN 637655. On the radiographs of this nozzle, however, the density changes are present only in the area forward of the bolt ring on the housing. This area was covered by a rubber insulator at the time of X-ray, and the density changes may be arising at the insulator-housing interface. On the basis of this very limited sample, it appears that significant voids in the adhesive between cone and housing may be detected by radial X-ray. X-ray should be performed prior to application of the rubber insulator forward of the nozzle bolt ring.

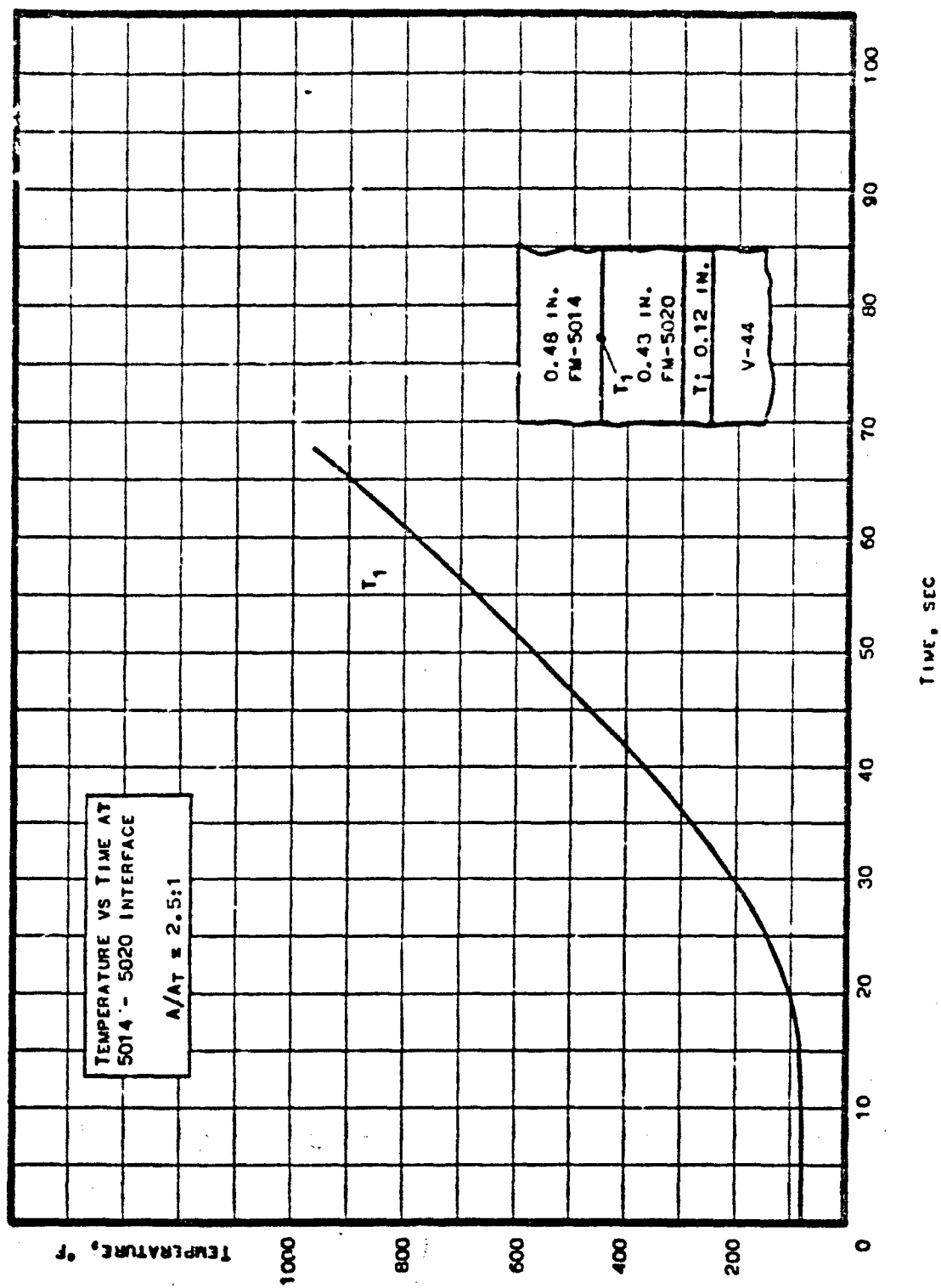
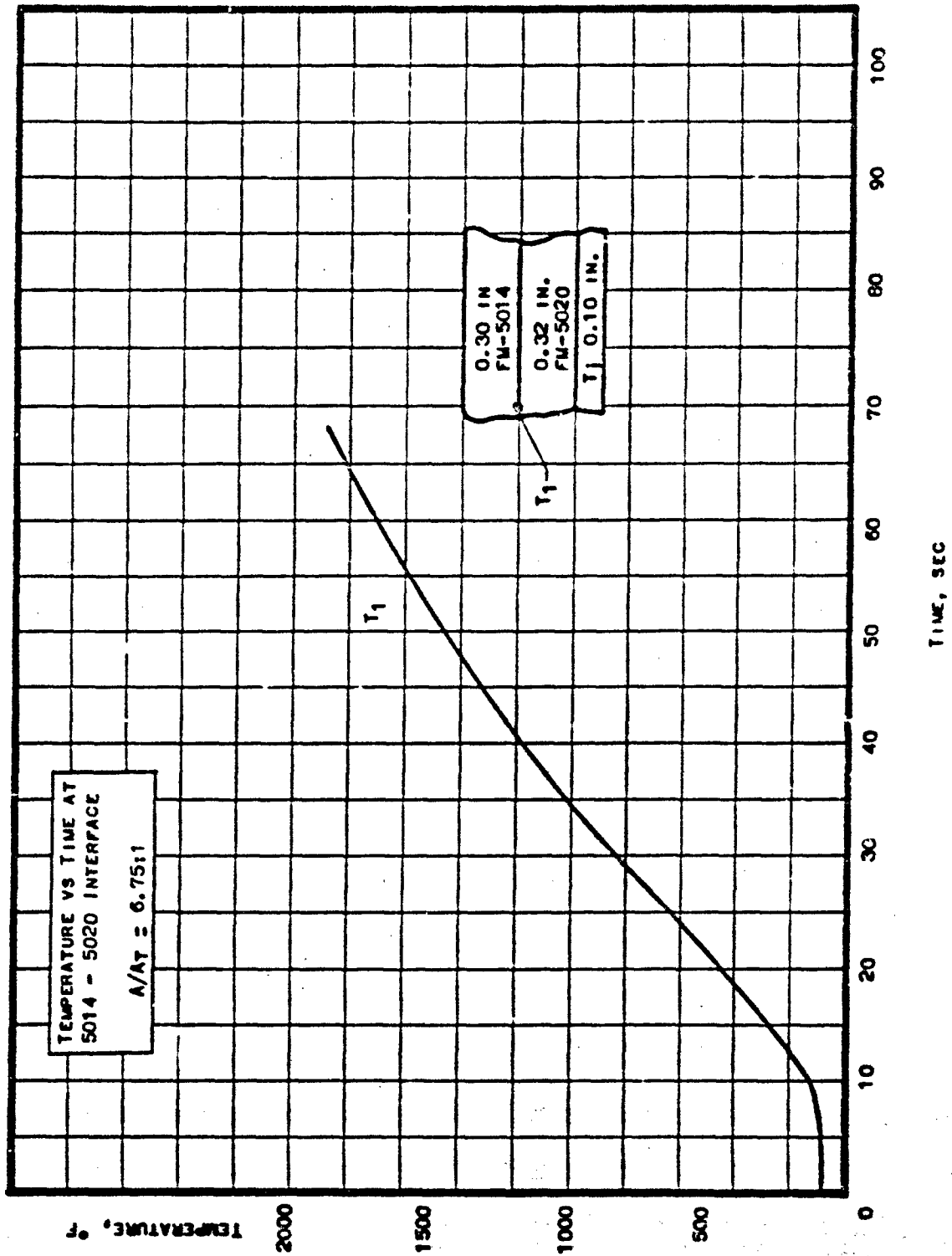


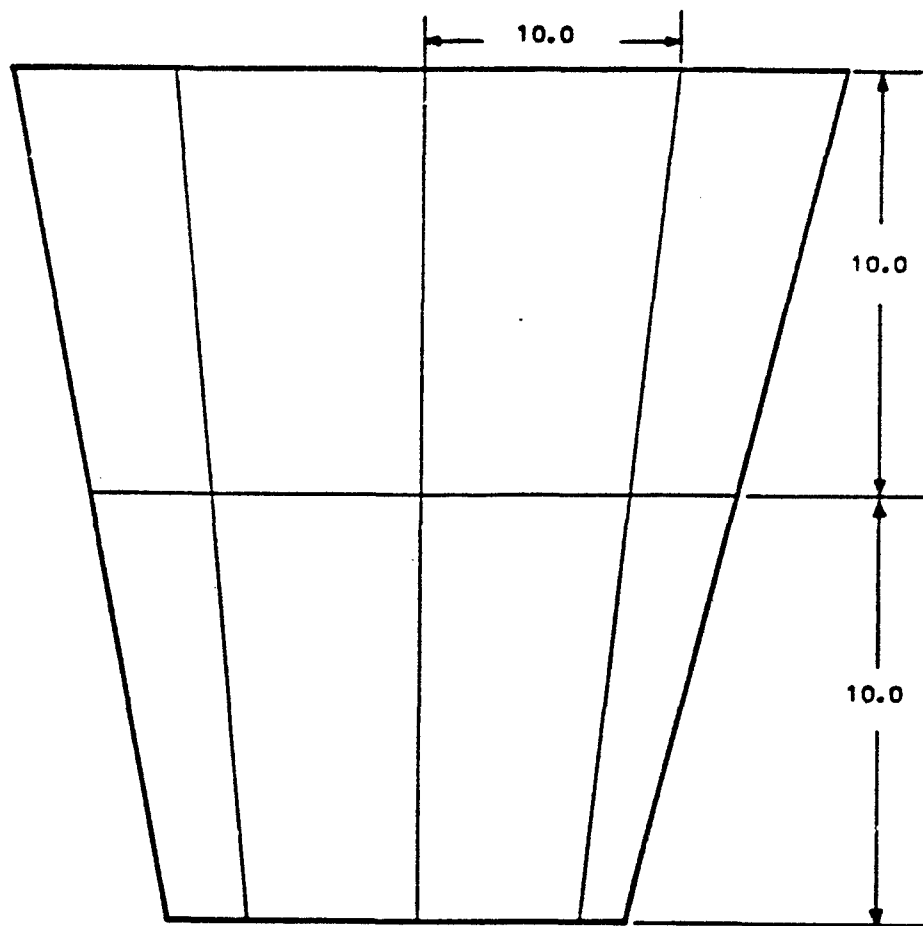
Figure VI-1

Thermal Profile of Sea-Level Cone at Expansion Ratio of 2.5:1



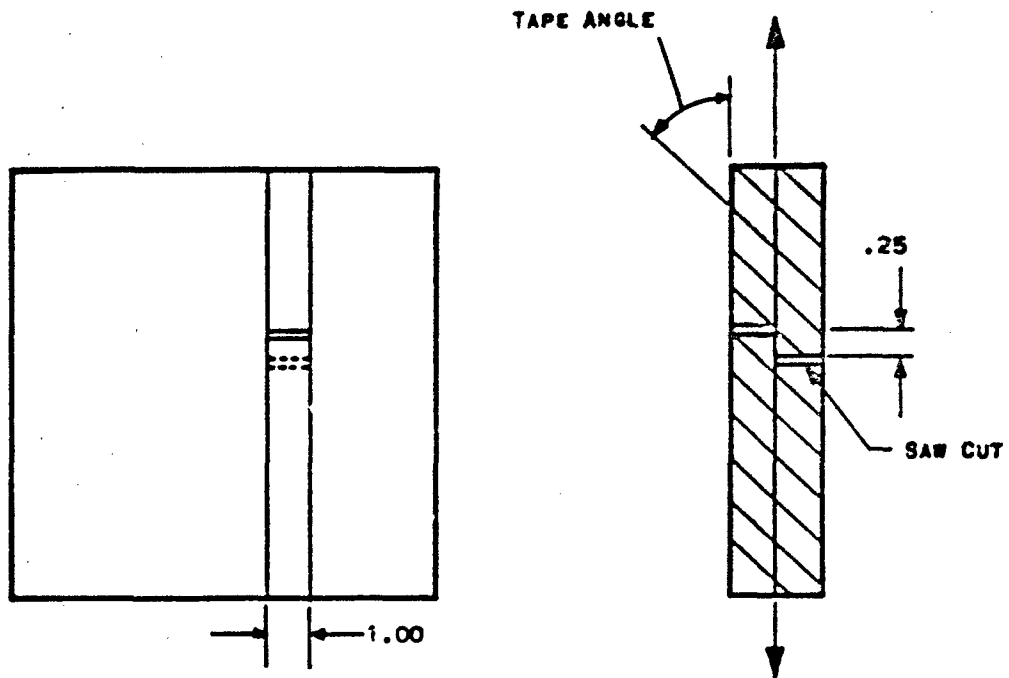
Thermal Profile of Sea-Level Cone at Expansion Ratio of 6.75:1

Figure VI-2



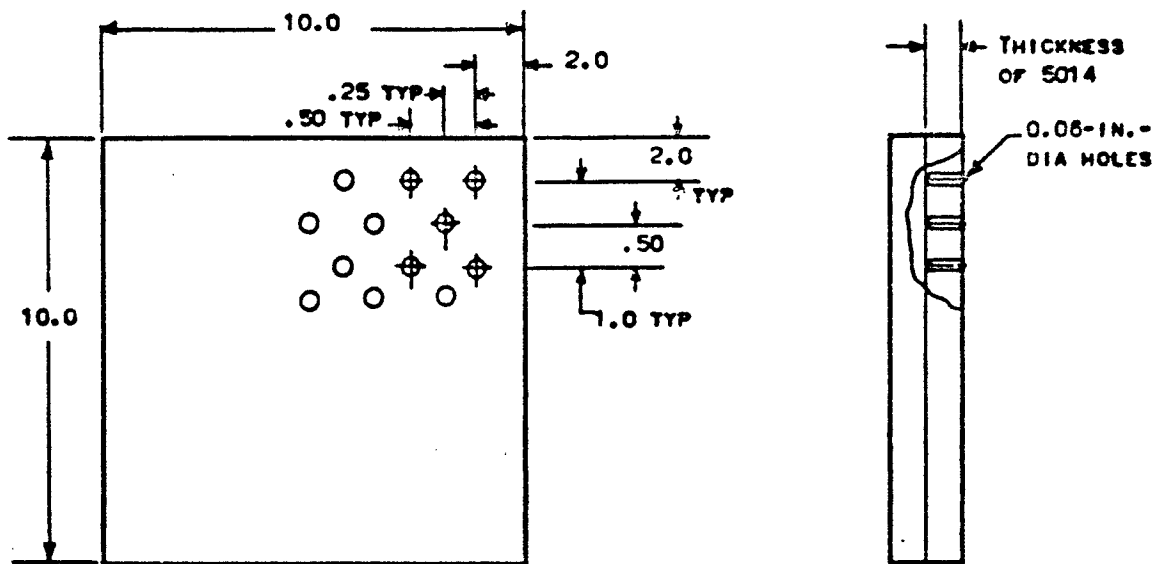
Slab Specimen from Full-Scale Cone

Figure VI-3



Shear-Test Specimens

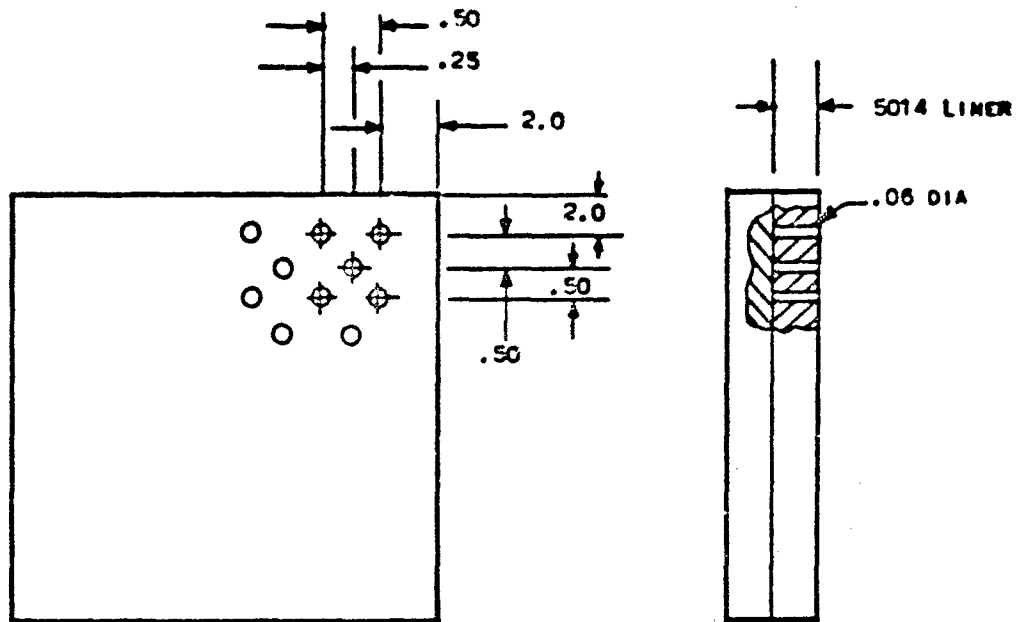
Figure VI-4



First-Hole Pattern for Slabs

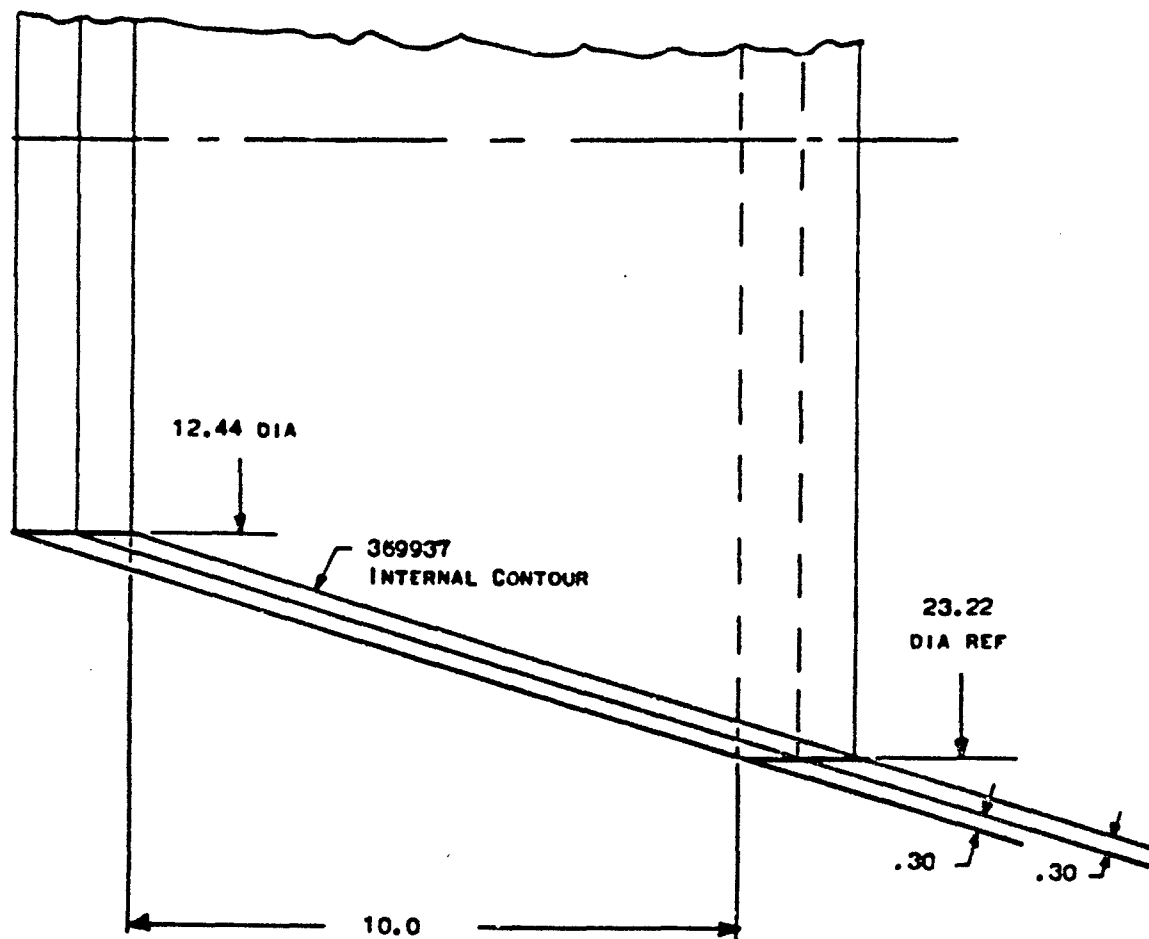
Figure VI-5





Second-Hole Pattern for Slabs

Figure VI-6



Configuration of Subscale Cones

Figure VI-7

0162-06TDR-9-Vc1 2

Comp	Specific Gravity	Material	Moisture Content	Ash Content	IBT	No. Baseline	Tensile $\times 10^3$	Flow $\times 10^3$	Flow Mod $\times 10^3$	Specimen Code
No. 2 C/M 0001 (Item No. 1)	1.43	PM 5004	32.2%	54.2%	1.82	1.11	13.8	18.0	2.03	96-1 & 2
No. 2 C/M 0002	1.79	PM 5000	34.0%	---	1.28	0.92	19.6	24.7	2.99	
No. 3 C/M 0003	1.44	PM 5004	33.0%	52.2%	2.69	1.22	16.8	19.4	1.93	01-1 & 2
No. 3 C/M 0004	1.76	PM 5000	34.4%	0	1.98	1.11	23.1	31.2	2.90	
No. 4 C/M 0005 (Item No. 2)	1.44	PM 5004	33.3	53.4%	1.98	1.13	16.8	19.4	1.93	02-1 & 2
No. 4 C/M 0006	1.80	PM 5000	32.2%	67.2%	1.40	0.98	26.2	29.3	1.04	
No. 5 C/M 0007 (Item No. 2)	1.44	PM 5004	31.0%	54.2%	1.99	1.08	16.8	19.4	1.93	99-1 & 2
No. 5 C/M 0008	1.76	PM 5000	33.2%	66.7%	1.25	0.92	27.1	31.2	2.90	
No. 6 C/M 0009 (Item No. 3)	1.43	PM 5004	32.2%	54.2%	1.82	1.11	13.8	18.0	2.03	92-1 & 2
No. 6 C/M 0010	1.77	PM 5000	34.2%	65.5%	1.29	0.93	21.7	26.6	2.78	
No. 7 C/M 0011 (Item No. 3)	1.43	PM 5004	32.2%	54.2%	1.82	1.11	13.8	18.0	2.03	94-1 & 2
No. 7 C/M 0012	1.79	PM 5000	34.0%	65.2%	1.28	0.92	19.6	24.7	2.99	

Material Data for Subscale Cones

Figure VT-8

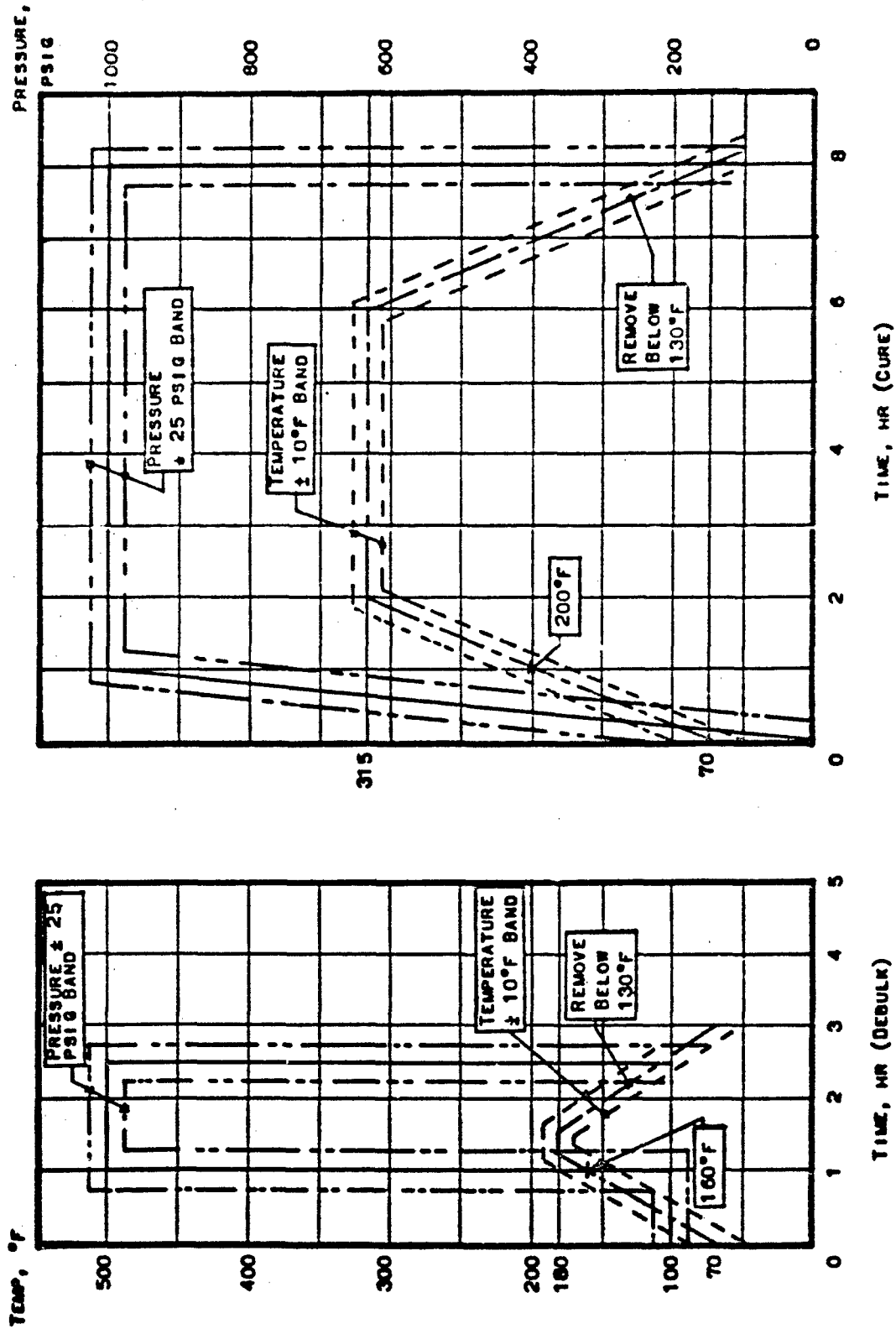
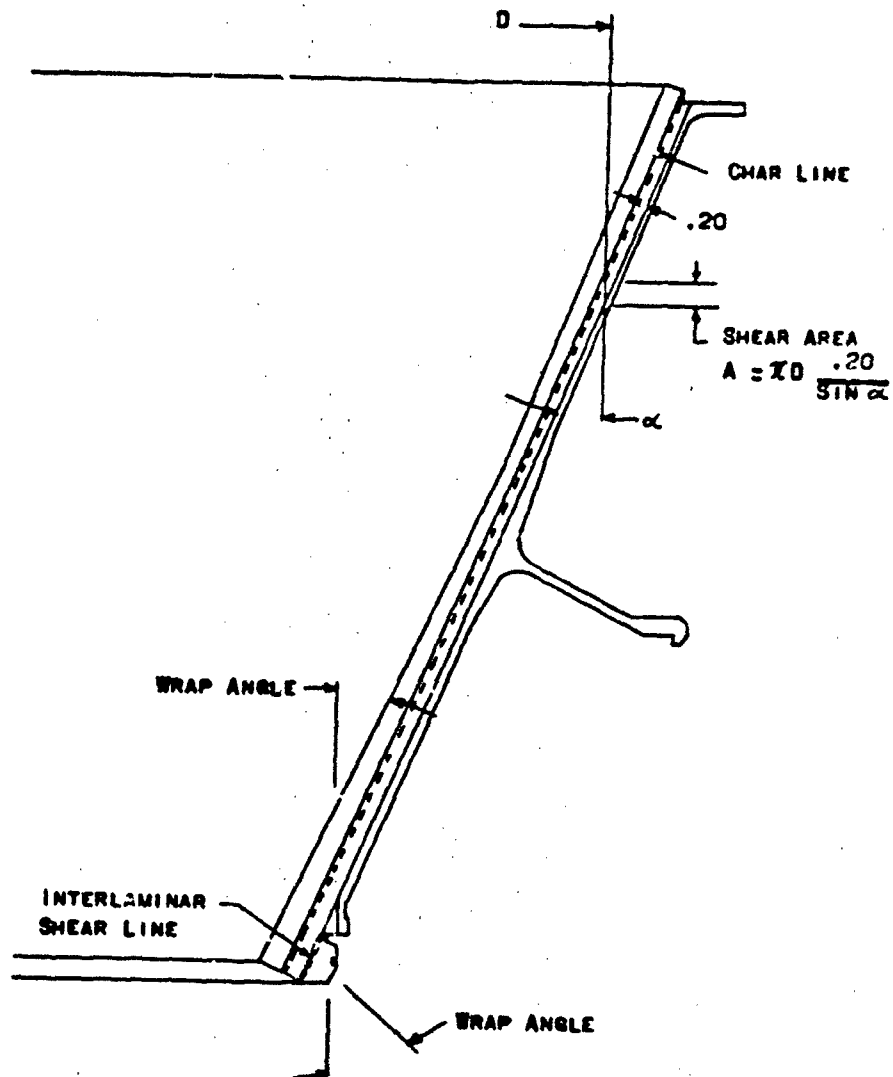


Figure VI-9

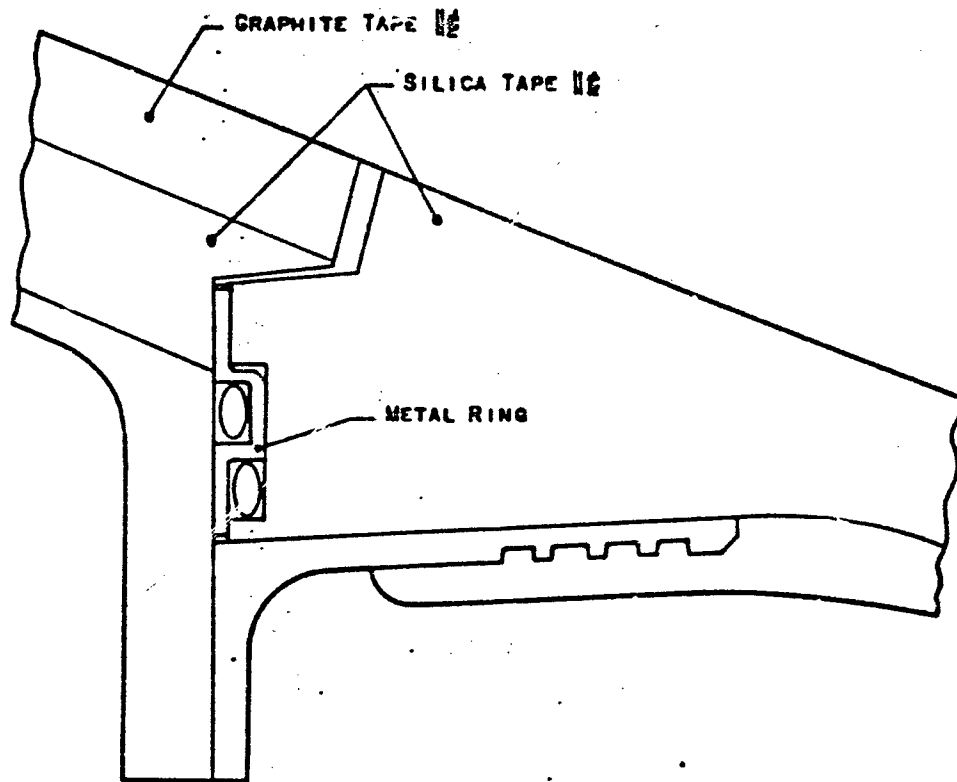
Debulk and Cure Cycles for Cones Code 92-1 and -2 and 94-1 and -2





Cross Section of Sea-Level Cone and Titanium Housing

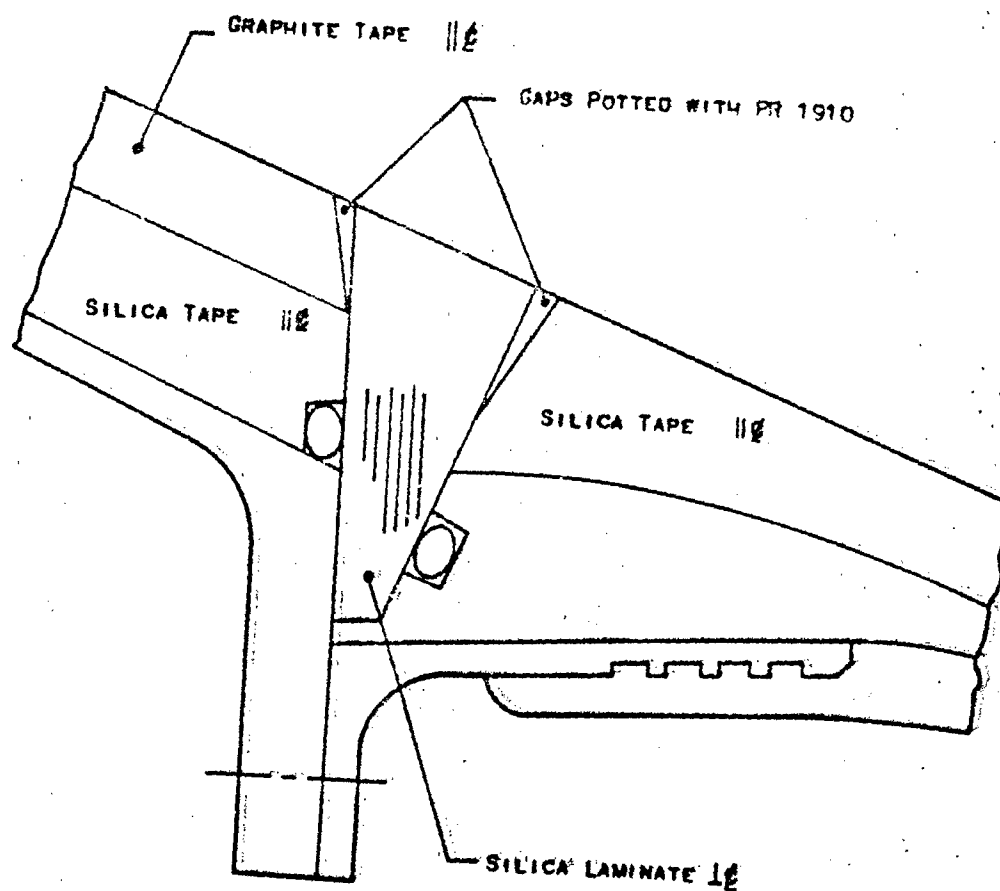
Figure VI-11



Sketch of Metal Ring for Sea-Level Cone Retention

Figure VI-12

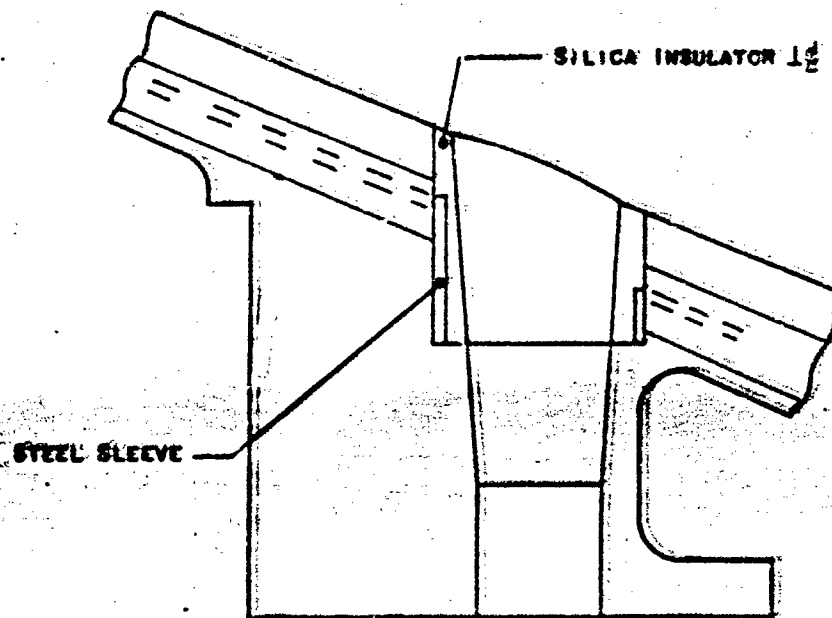
0162-06TER-9-Vol 2



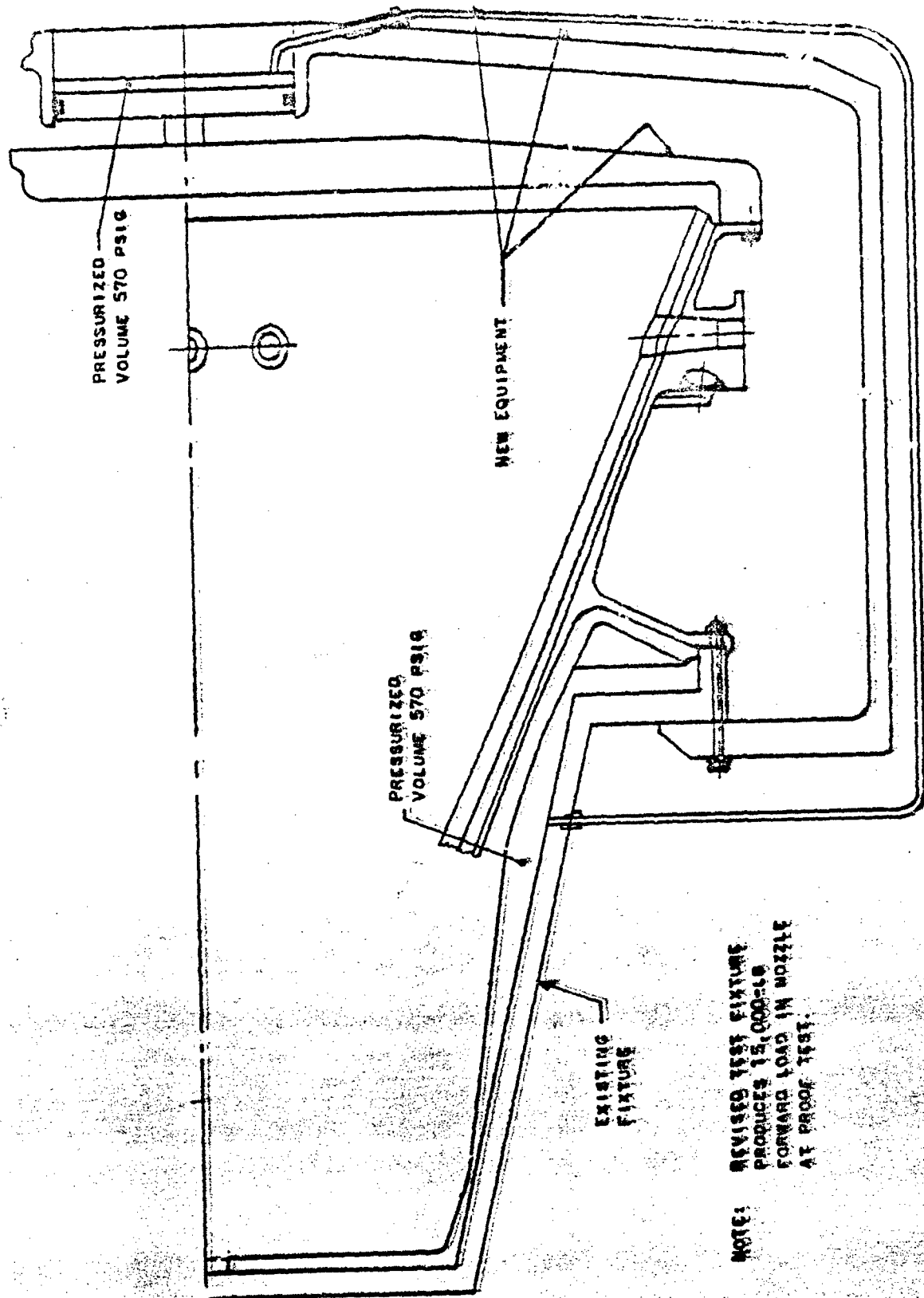
Sketch of Silica Laminate Ring for Sea-Level Cont. Retention

Figure VI-13





Sketch of Steel Sleeve for Sea-Level Cone Retention



Sketch of Revised Proof Test Fixture

NOTE: REVISED TEST FIXTURE  
PRODUCES 15,000-16  
FORWARD LOAD IN NOZZLE  
AT PROOF TEST.

Figure VC-15

Report 0162-06TDR-9-Vol 2

APPENDIX VI-A

TESTING OF SPECIMENS FROM FULL-SCALE EXT.  
CONES, RESULTS AND OBSERVATIONS

Report 0162-06TDR-9-Vol 2, Appendix VI-A

SN 2168016, Code O-1 (As-Received)

This specimen developed a distinct blister similar to the ones seen in some cones of fired Wing VI motors. The blister developed in spite of the low volatile content in both the graphite and the silica wrap.

The temperature and pressure measurements were taken at the edge of the heat affected zone on this specimen which accounts for the low pressure and temperature of 5 psi maximum and 190°F maximum.

This was the only specimen from cone SN 2168016, in which the interface line did not crack all the way to the edge of the part.

SN 2168016, Code O-2 (As-Received)

This specimen was observed to delaminate in the graphite wrap at 31 sec simultaneous with a change in temperature. No pressure was recorded at this time; therefore, the delamination must have been caused by thermal expansion. No pressure was recorded until approximately 500°F, at which temperature the resin starts breaking down.

SN 2168016 Code P-1 (Post-Cured)

This post-cured specimen did not show any improvement over the as-received specimen although the volatile content was reduced.

The pressure started increasing at approximately 225°F and probably was caused by steam from volatiles boiling. At approximately 48 sec the two wraps were observed to delaminate at the edge of the part. The pressure dropped sharply to almost zero.

SN 2168016, Code P-2 (Post-Cured)

This post-cured specimen did not show any improvement over the as-received specimen although the volatile content was reduced.

The temperature and pressure plots for the specimen were invalid.

SN 2168016, Codes 5-1, 5-2, 6-1, 6-2 (Drilled Specimens)

The average temperature and time on these specimens were 1560°F and 162 sec.

These slabs with the holes drilled through the graphite wrap showed some improvement at the interface line between the two materials. There were visible cracks at the interface, but the material was not separated as far apart as in the previous specimens. The graphite wrap in the slabs with the 1/4-in.-hole pattern was quite severely cracked between plies with one crack in each extending to the edge of the part. The silica in all these parts had small delaminations at the interface with the graphite. The parts were subjected to more heat for a longer period of time than the undrilled slabs.

Report 0162-06TDR-9-Vol 2, Appendix VI-A

SN 2168017, Code 0-1 (As-Received)

The recorder was started too late and shows a 300°F interface temperature at the start of test.

Cracks were observed to develop in the graphite during the test. At 40 sec a loud pop was heard and the pressure dropped to zero. This probably coincides with cracking of the interface from the center to the edge of the part and gas relief through this opening.

SN 2168017, Code 0-2 (As-Received)

The maximum pressure and temperature for this specimen were 26 psi and 420°F. The pressure increase started at 200°F or close to the boiling point of water.

SN 2168017, Code P-1 (Post-Cured)

The pressure increase started at approximately 225°F. Interlaminar separation between materials extending to the edge of part was observed at time of pressure drop to zero. Post-cure of the specimen decreased the volatiles and seemed to improve the appearance slightly.

SN 2168017, Code P-2 (Post-Cured)

The temperature recorder was started too late. Pressure did, however, start before breakdown temperature of the resin was reached.

SN 2168017, Codes 5-I and 6-I (Drilled Specimens)

The interface between the material of the drilled slabs cracked, but separated less than the undrilled slabs.

The maximum temperature and pressure for the two drilled specimens were 860°F at 91 sec and 1380°F at 312 sec.

SN 2168018, Code 0-1 (As-Received)

There was pressure indication at low temperature. The graphite was observed to delaminate at peak pressure.

SN 2168018, Code 0-2 (As-Received)

There was a sharp pressure increase at 210°F and a maximum pressure of 62 psi at which time delaminations occurred in the graphite wrap.

SN 2168018, Code P-1 (Post-Cured)

No pressure was developed although maximum temperature recorded was 630°F. The cracks in the graphite liner possibly developed early and relieved the pressure. This could account for the better than normal post heat condition of this slab.

Report 0162-06TDR-9-Vol 2, Appendix VI-A

SN 2168018, Code P-2 (Post-Cured)

Although treated like Code P-1 and with even lower volatile content, this slab had a pressure increase starting at 100°F with a maximum of 35 psi at 300°F.

Both charred interface shear specimens had very low shear strength.

SN 2168018, Codes 5-1, 5-2, 6-1, 6-2 (Drilled Specimens)

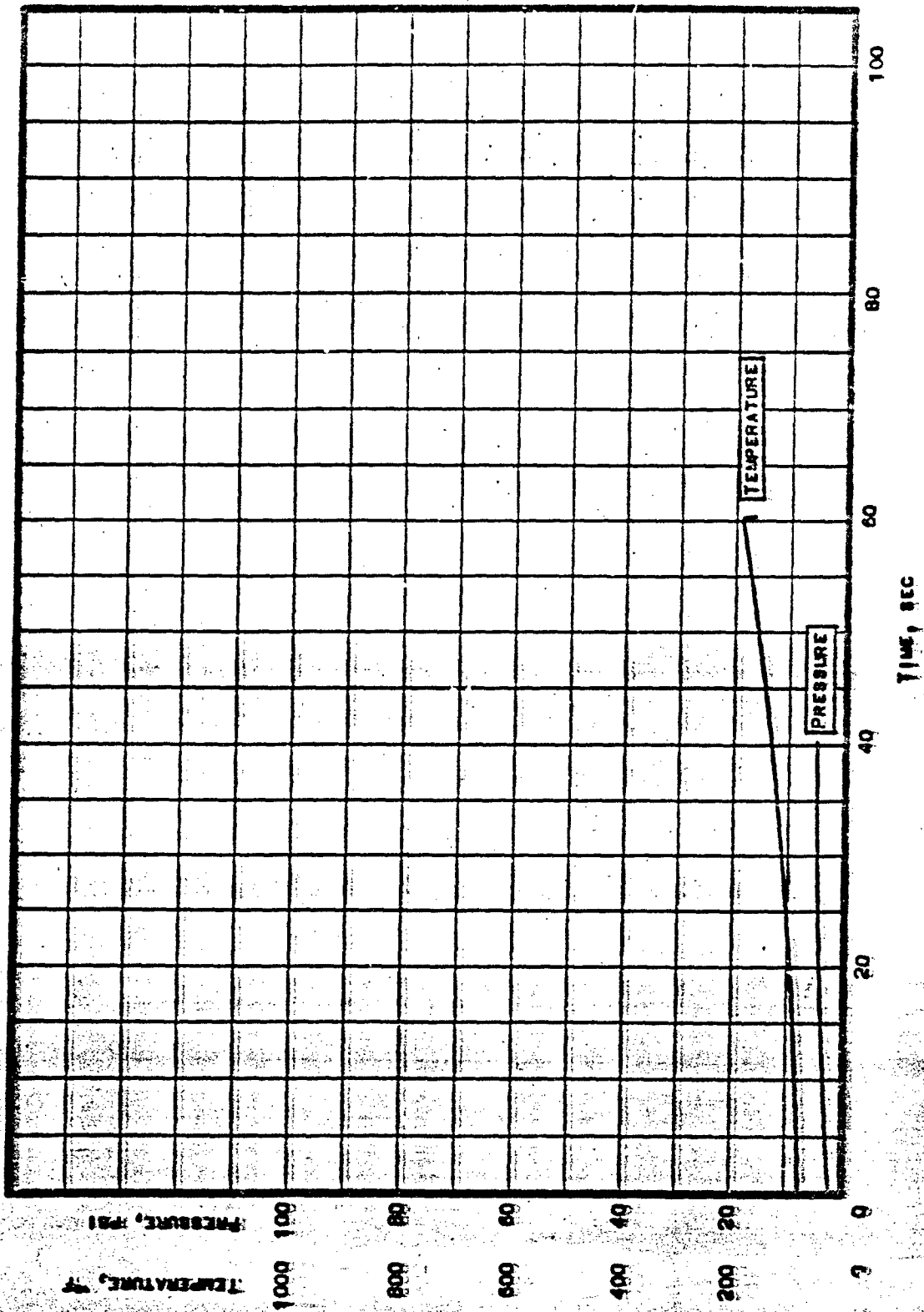
The drilled slabs, 5-1 and 5-2, with the 1/4-in.-hole pattern showed some interface delamination between the two materials in the heat-affected area, but the graphite and the silica wrap did not show any delaminations.

The drilled slabs, 6-1 and 6-2, with the 1/2 in. hole pattern had no continuous delamination between the two materials.

The average temperature and time on these specimens were 1530°F and 243 sec.

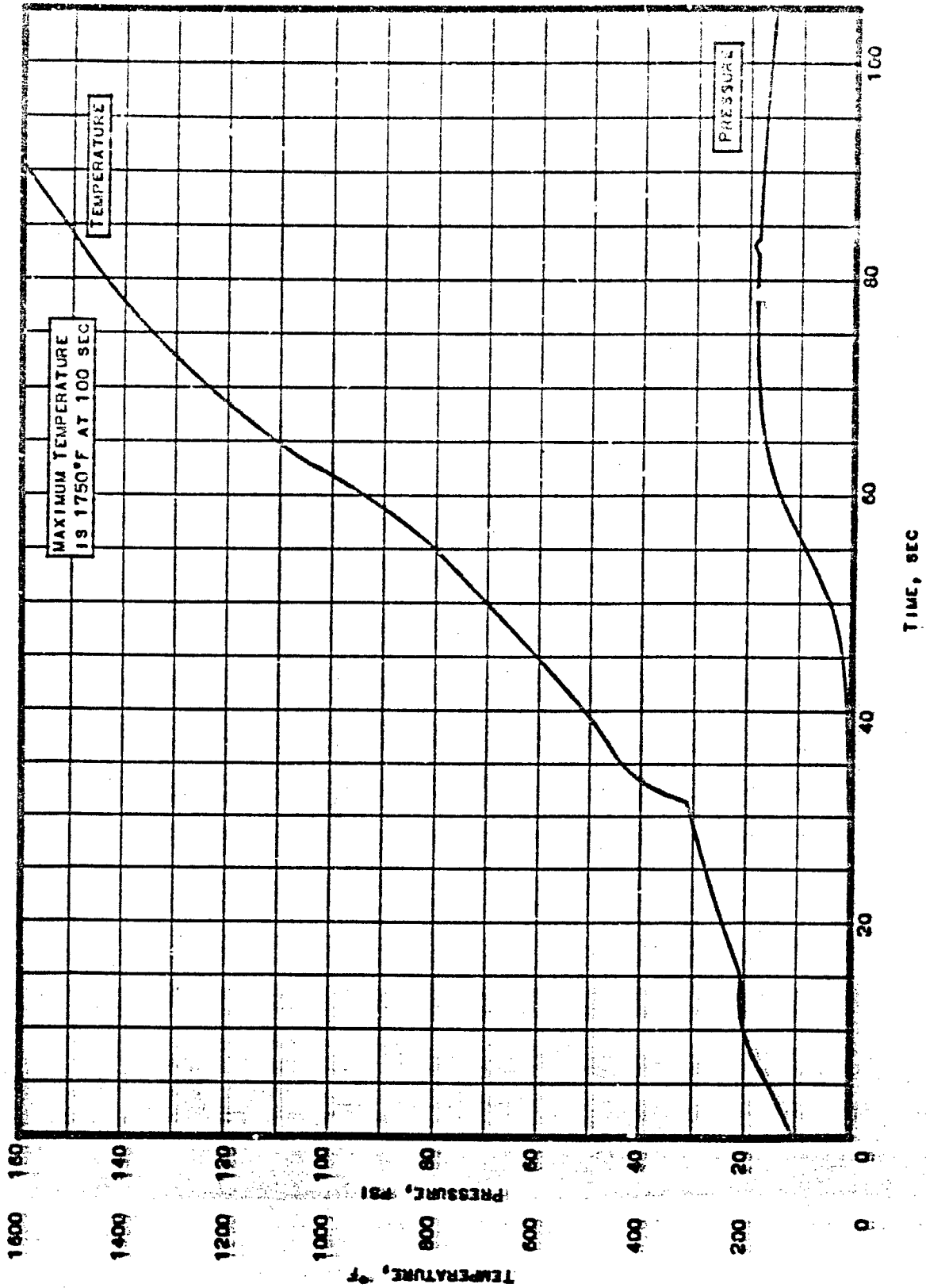
Temperature- and Pressure-vs-Time Curves

Temperature- and pressure-vs-time curves for various specimens taken from full-size cones are presented in Figures VI-A-1 through -11.



Temperature- and Pressure-vs-Time Curves for Specimen Q-1  
(As Received) from Full-Size Cone 2168016

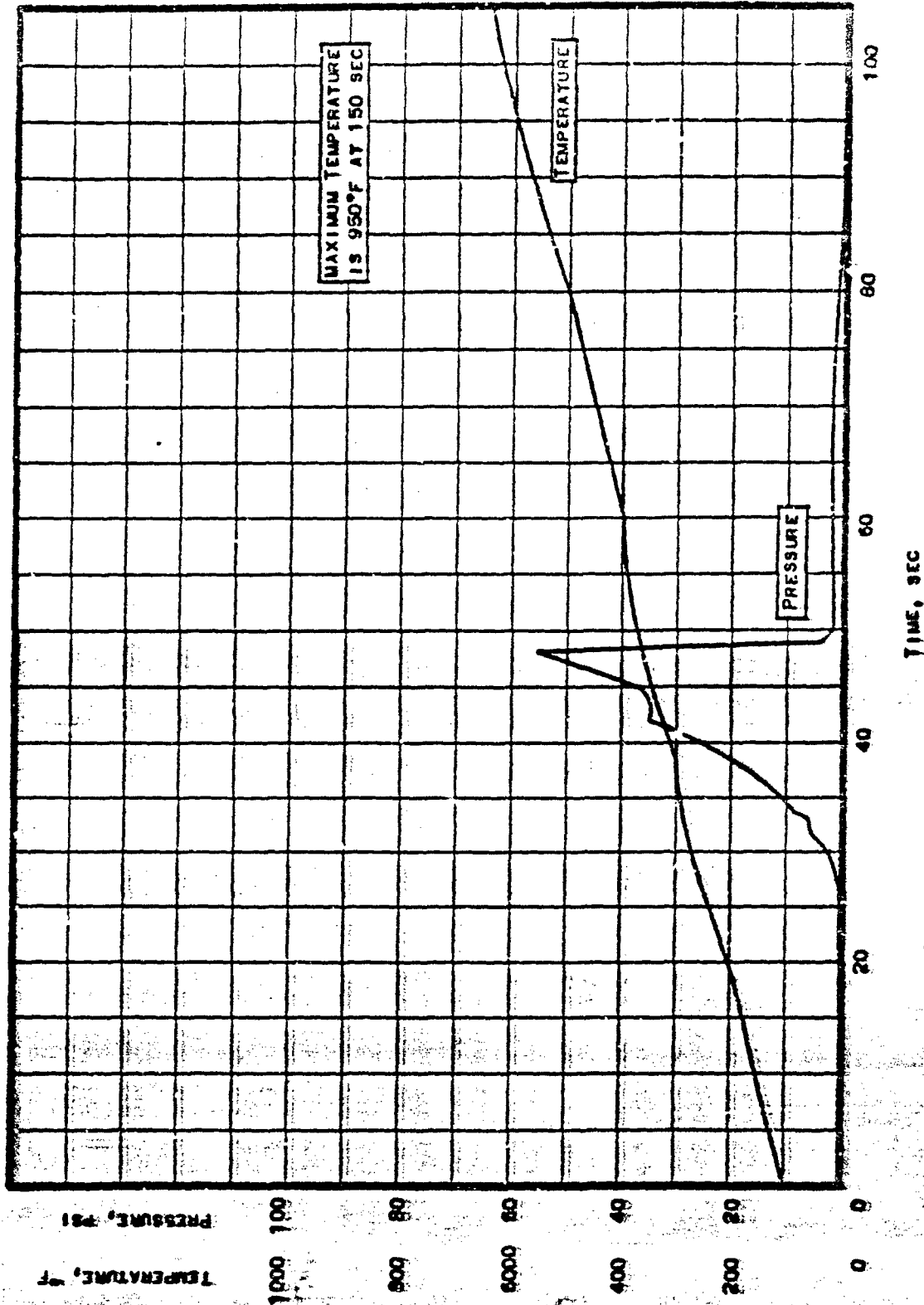
Figure VI-A-1



Temperature- and Pressure-vs-Time Curves for Specimen O-2  
(As Received) from Full-Size Cone 2168016

Figure VI-A-2





Temperature- and Pressure-vs-Time Curves for Specimen P-1  
(Post-Cured) from Full-Size Cone 2168016

Figure VI-A-3

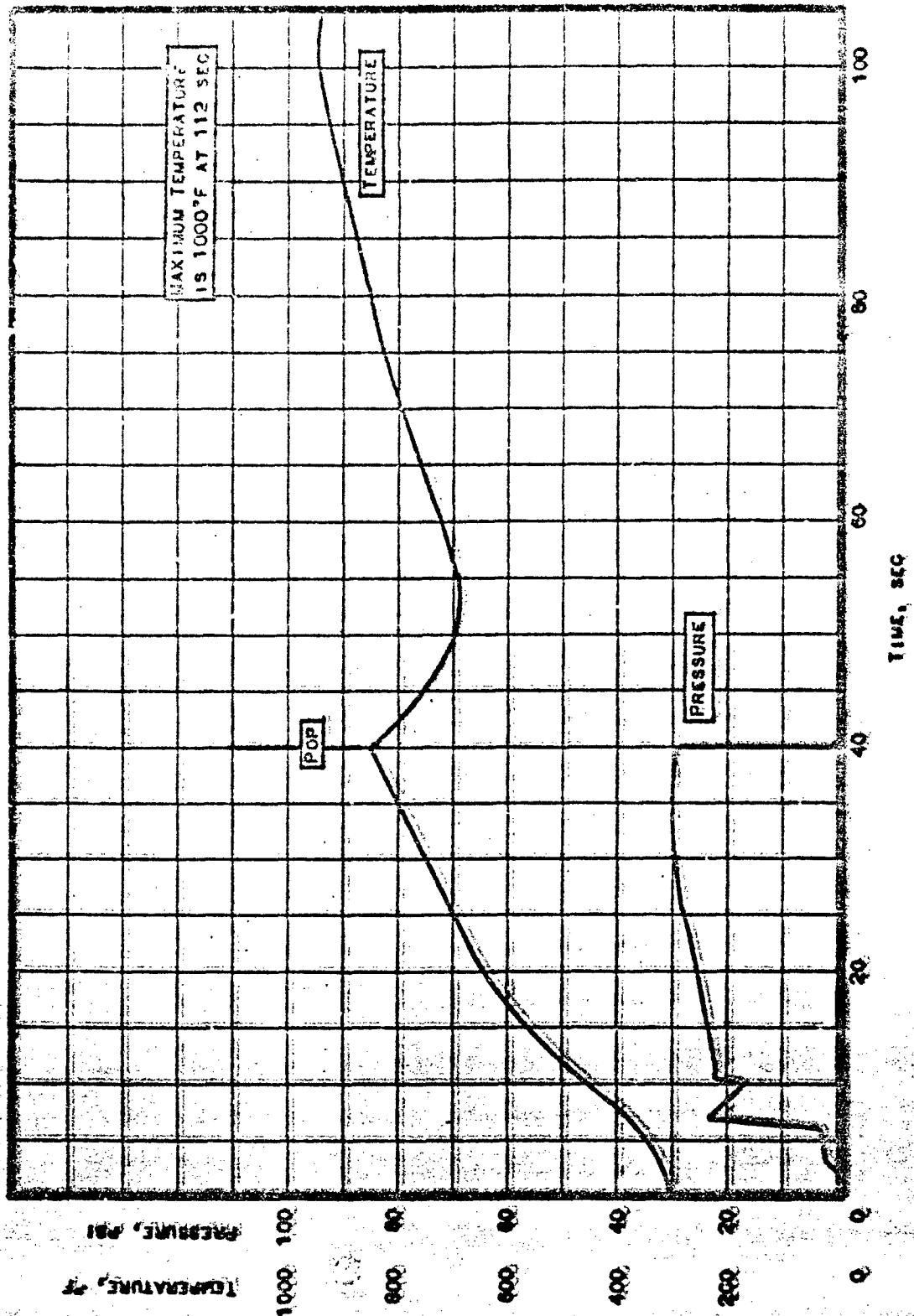
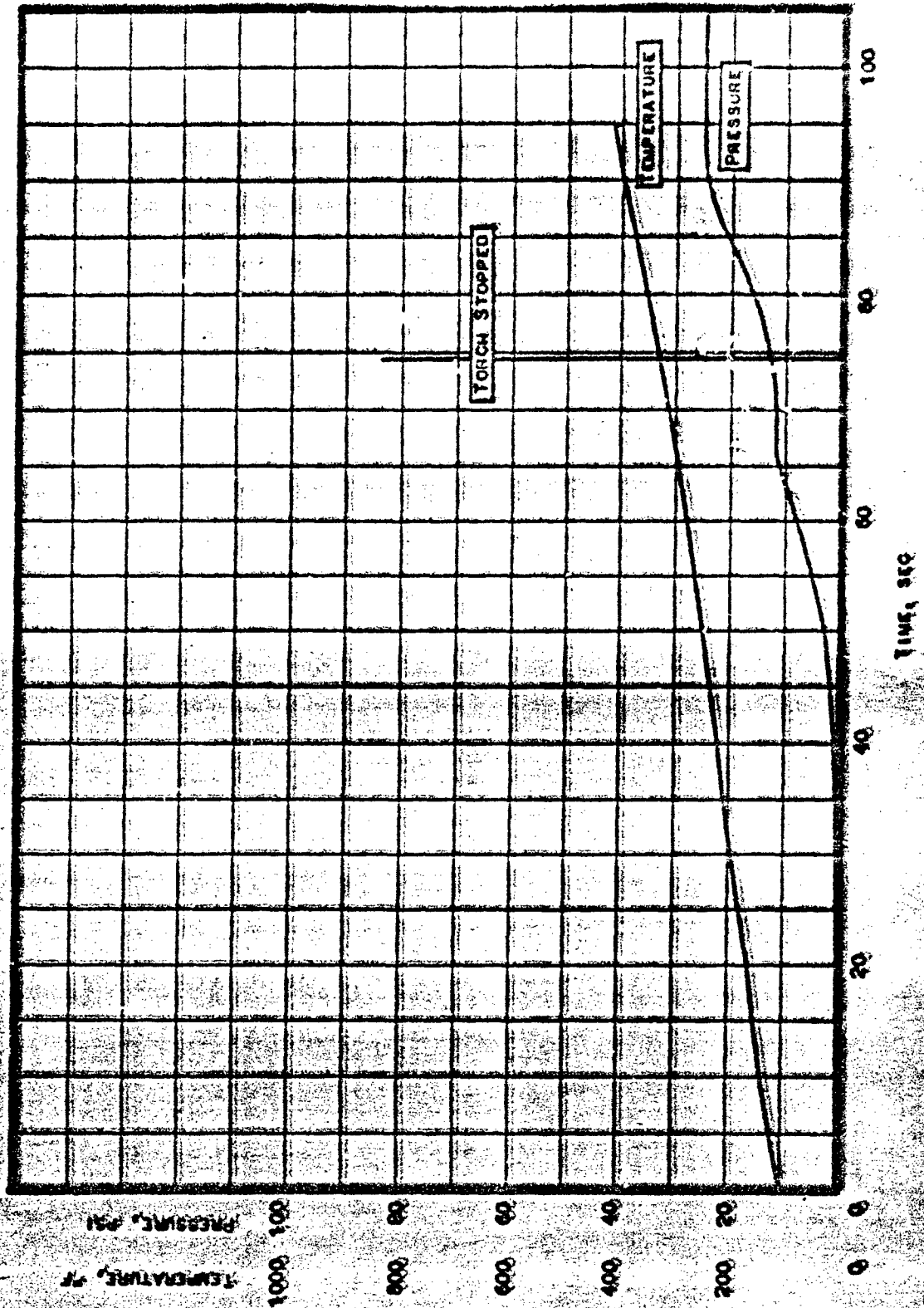


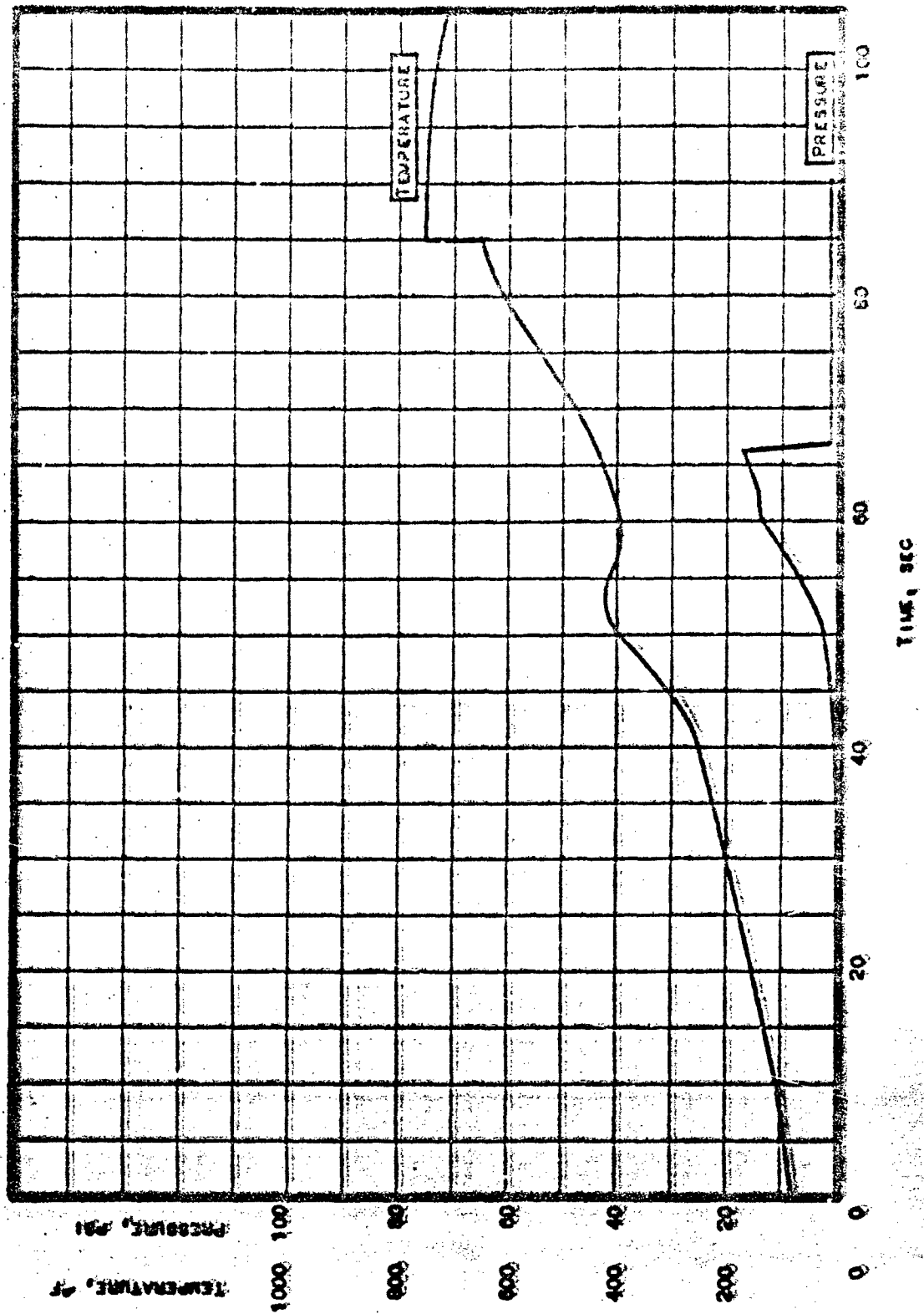
Figure VI-A-4

Temperature- and Pressure-vs-Time Curves for Specimen O-1  
(As Received) from Full-Size Cone 2168017



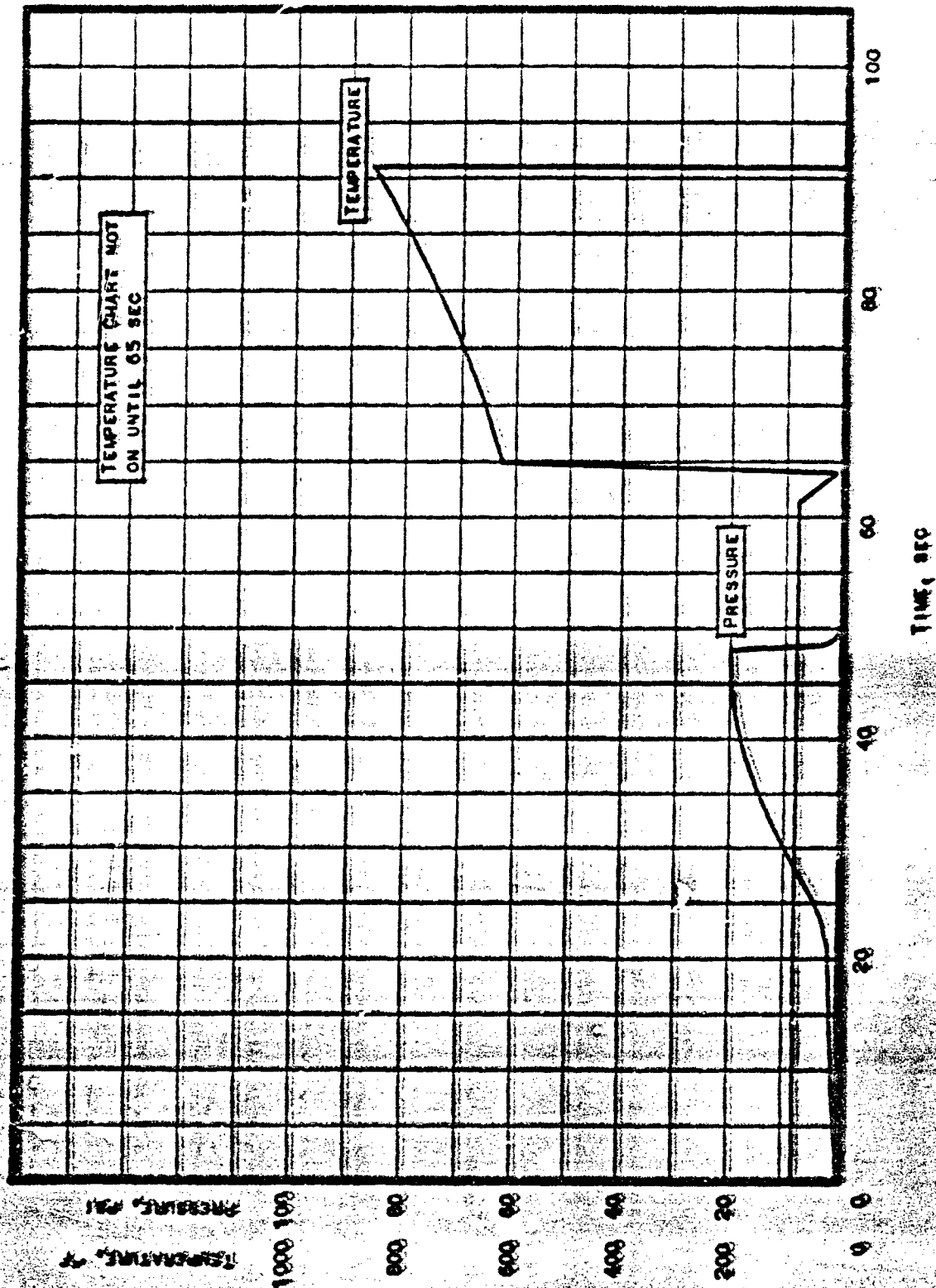
Temperature- and Pressure-vs-Time Curves for Specimen Q-2  
(As Received) from Full-Size Cone 2168017

Figure VI-A-5



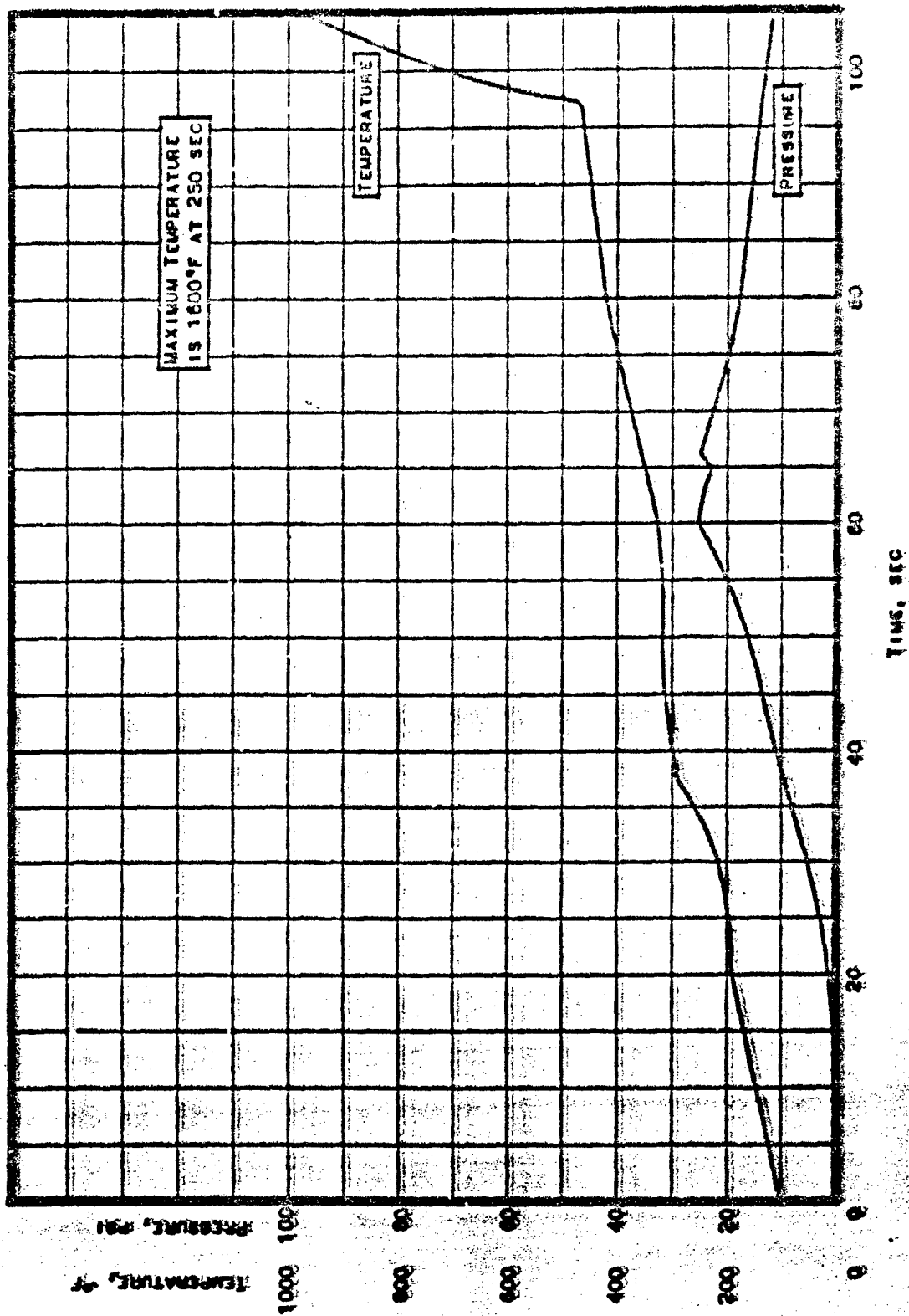
Temperature- and Pressure-vs-Time Curves for Specimen P-1  
(Post-Cured) from Full-Size Cone 2168017

Figure VI-A-6



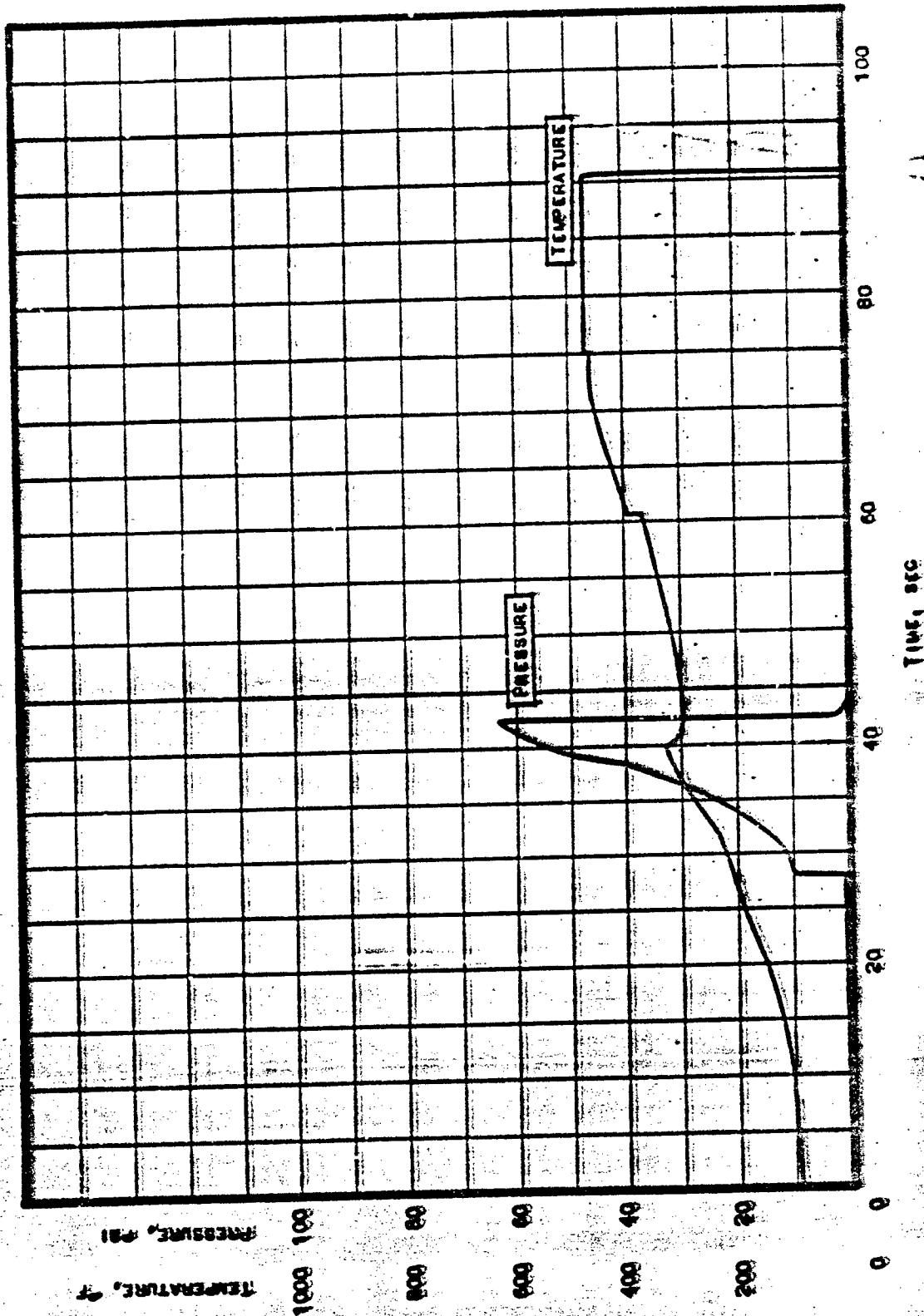
Temperature- and Pressure-vs.-Time Curves for Specimen R-2 (Post-Cured) from Full-Size Cone 2168017

Figure VI-A-7

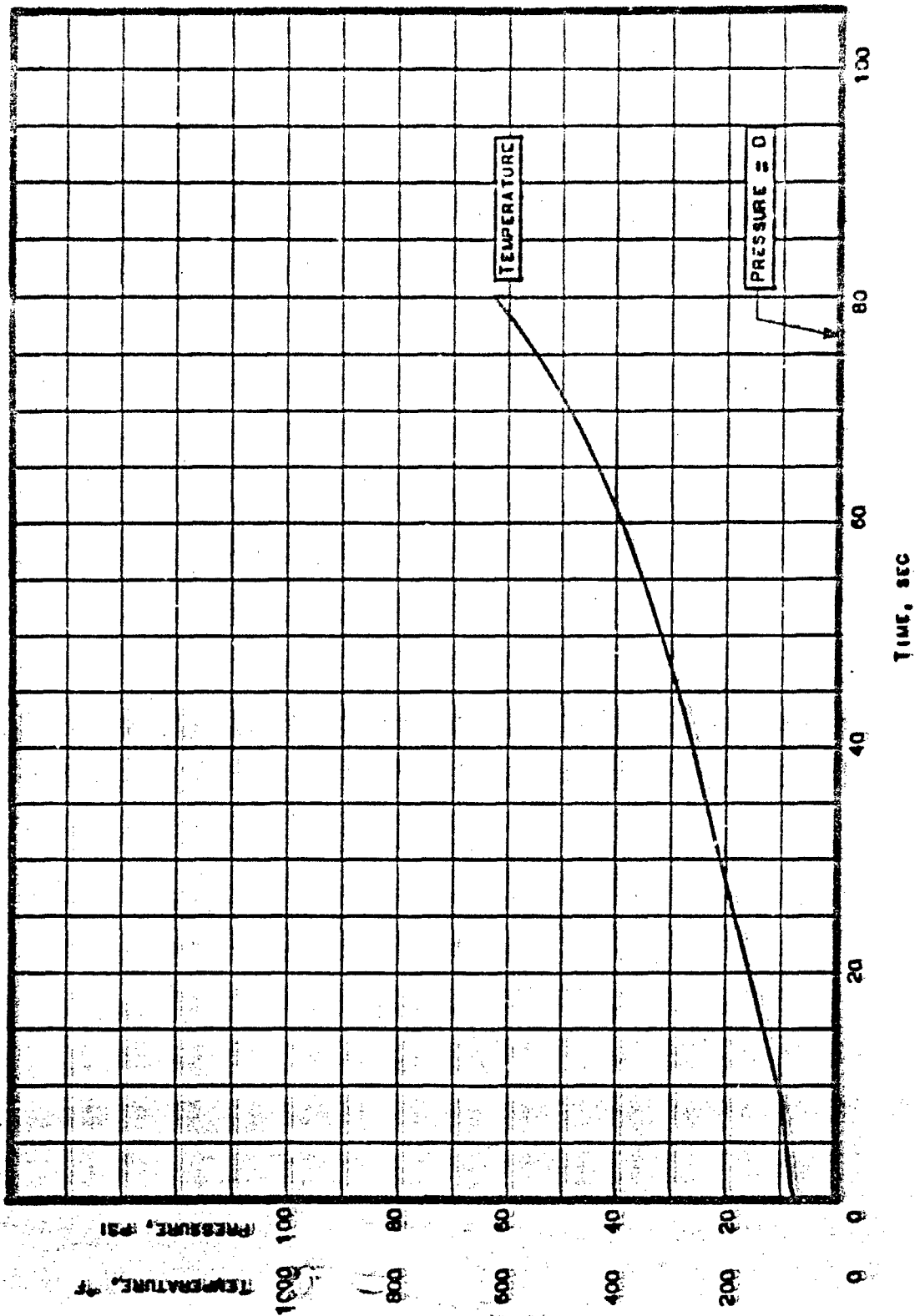


Temperature- and Pressure-vs-Time Curves for Specimen O-1  
(As Received) from Full-Size Cone 2168018

Figure VI-A-6



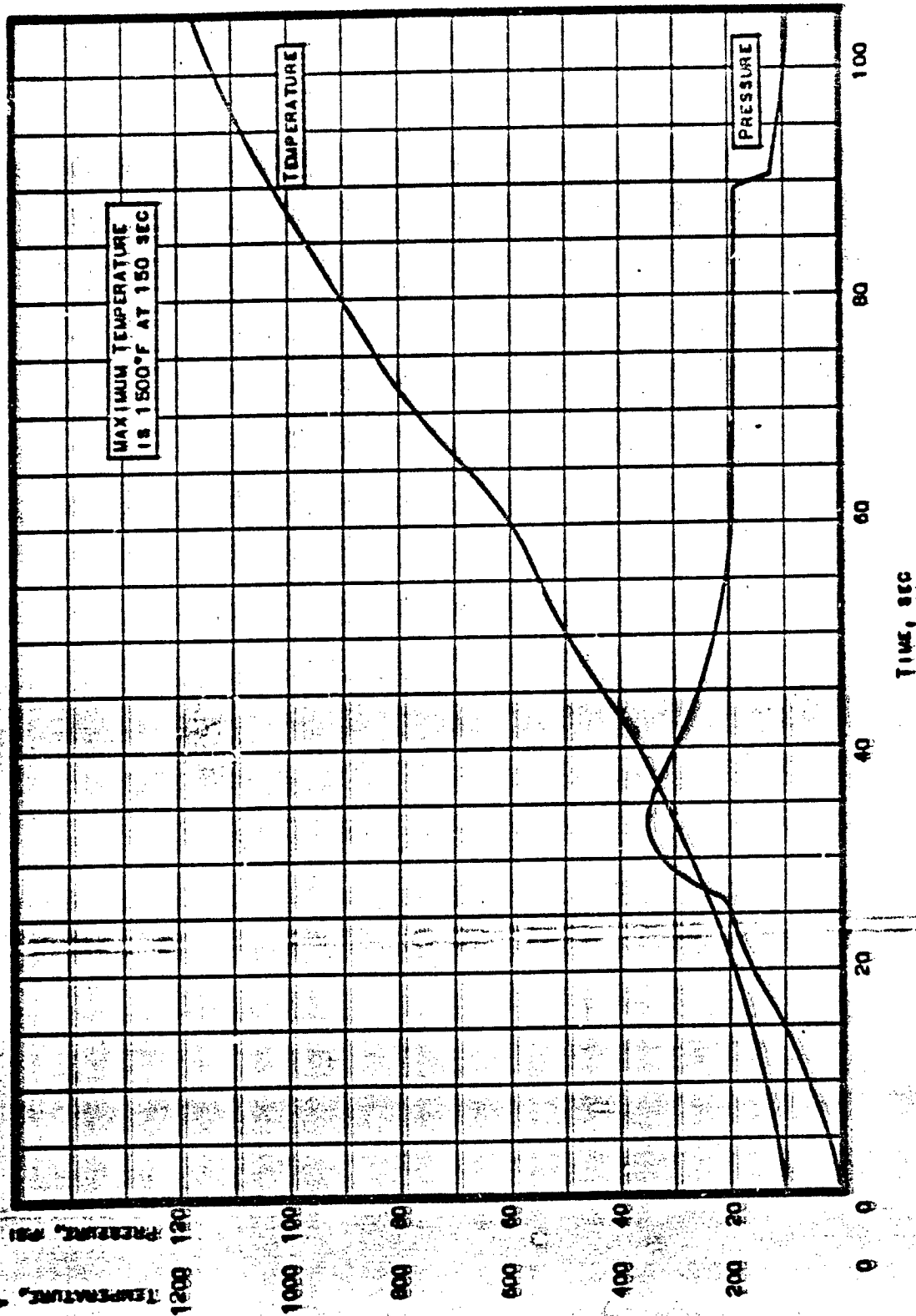
Temperature- and Pressure-vs-Time Curves for Specimen Q-2  
(As Received) from Full-Size Cone 2168018



Temperature- and Pressure-vs-Time Curves for Specimen P-1  
(Post-Cured) from Full-Size Cone 2168018

Figure VI-A-10





Temperature- and Pressure-vs-Time Curves for Specimen P-1  
(Post-Cured) from Full-Size Cone 2168018

Figure VI-A-11

Report 0162-06TTR-9-Vol C

APPENDIX VI-B

TESTING OF SPECIMENS FROM SUBSCALE  
EXIT CONES, RESULTS AND OBSERVATIONS

Report 0162-CGTOR-9-Vol 2, Appendix VI-B

Code FSC-1 (Snap Cure)

This specimen had an extremely low volatile content in both wraps. The graphite and the silica wrap separated completely at the end of the test. The bonding material used between the two wraps burned.

After the test both wraps appeared better than any other test samples with no cracks. The graphite had a hard, good char, but the silica appeared low in interlaminar strength as plies readily peeled off when the part was strained. The individual plies seemed smoother with less mechanical bond between them than in conventionally made wraps.

The uncharred interface shear specimens showed interlaminary failure in the silica wrap at low tensile values. The charred specimens separated during charring at the interface.

Code FSC-2 (Snap Cure)

The results and observations for this specimen are the same as for Code FSC-1.

Code 96-1 (Water Added)

No water penetrated into the graphite wrap and only very little was absorbed by the silica wrap. The method used did not provide sufficient force for water penetration of the material. Instead, the water was forced along the surface between the bag and the silica and out through the vacuum line.

This specimen delaminated to the edge of the part between the materials, but showed no delaminations in the silica.

Code 96-2 (Water Added)

This specimen developed a blister similar to the ones seen in cones of fired Wing VI motors. This part did not separate all the way to the edge between the materials, but showed cracks through the graphite wrap and delaminations in the silica at the interface with the graphite. Delaminations and pops were observed in the graphite wrap at peak pressure.

Code 99-1 (Low IRPI)

Popping was heard at 26 and 52 sec after the start of the test. The time of the noise from cracking did not coincide with any radical changes in temperature or pressure or with the maximum pressure of 35 psi at 46 sec.

Code 99-2 (Low IRPI)

This specimen opened up between the materials at the edge of the part at peak pressure. The temperature was abnormally low and is possibly incorrect.

Code 02-1 (Medium IRPI)

A sharp pressure-increase occurred at the boiling temperature of water; the peak pressure was 44 psi.

Code 02-2 (Medium IRPI)

The temperature pickup was faulty on this test; the maximum pressure was 23 psi.

---

Code 03-1 (High IRPI)

No pressure developed at the interface of this specimen. The part was observed to develop interlaminar cracks in the graphite wrap early in the test.

Code 03-2 (High IRPI)

A very low pressure, 6 psi, was measured. Both 03-1 and 03-2 were observed to develop interlaminar cracks in the graphite wrap early in the test. These cracks may have released pressure and thermal stresses and could be the reason for the improved postfire condition of these parts.

---

Code 92-1 (Special Debulk)

A crack was observed to develop in the graphite wrap at peak pressure, 46 psi. The volatile content was relatively high and may account for the severe delaminations at the interface between the two materials.

Code 92-2 (Special Debulk)

This specimen developed a blister similar to those of some cones from fired Wing VI motors. Delaminations were observed at peak pressure, but the gas release opening in the graphite wrap formed by the delaminations may have been insufficient to release the gas as rapidly as it was formed. This is also indicated by the slow pressure drop-off. The volatile content was very high in this cone.

---

Code 94-1 (Special Debulk)

This specimen had high volatile content and delaminated quite severely.

Code 94-2 (Special Debulk)

Three loud pops were heard before any pressure was indicated. One pop coincided with a sharp temperature increase. The popping noises, which obviously indicate either interface or interlaminar crackings of fairly solid materials, were probably caused by thermal expansion stresses. The sharp temperature increase may be caused by a shift in the thermocouple when the part cracked.

Report 0162-06TDR-9-Vol 2, Appendix VI-B

Temperature- and Pressure-vs-Time Curves

Temperature- and pressure-vs-time curves for various specimens from subscale exit cones are presented in Figures VI-B-1 through-14.

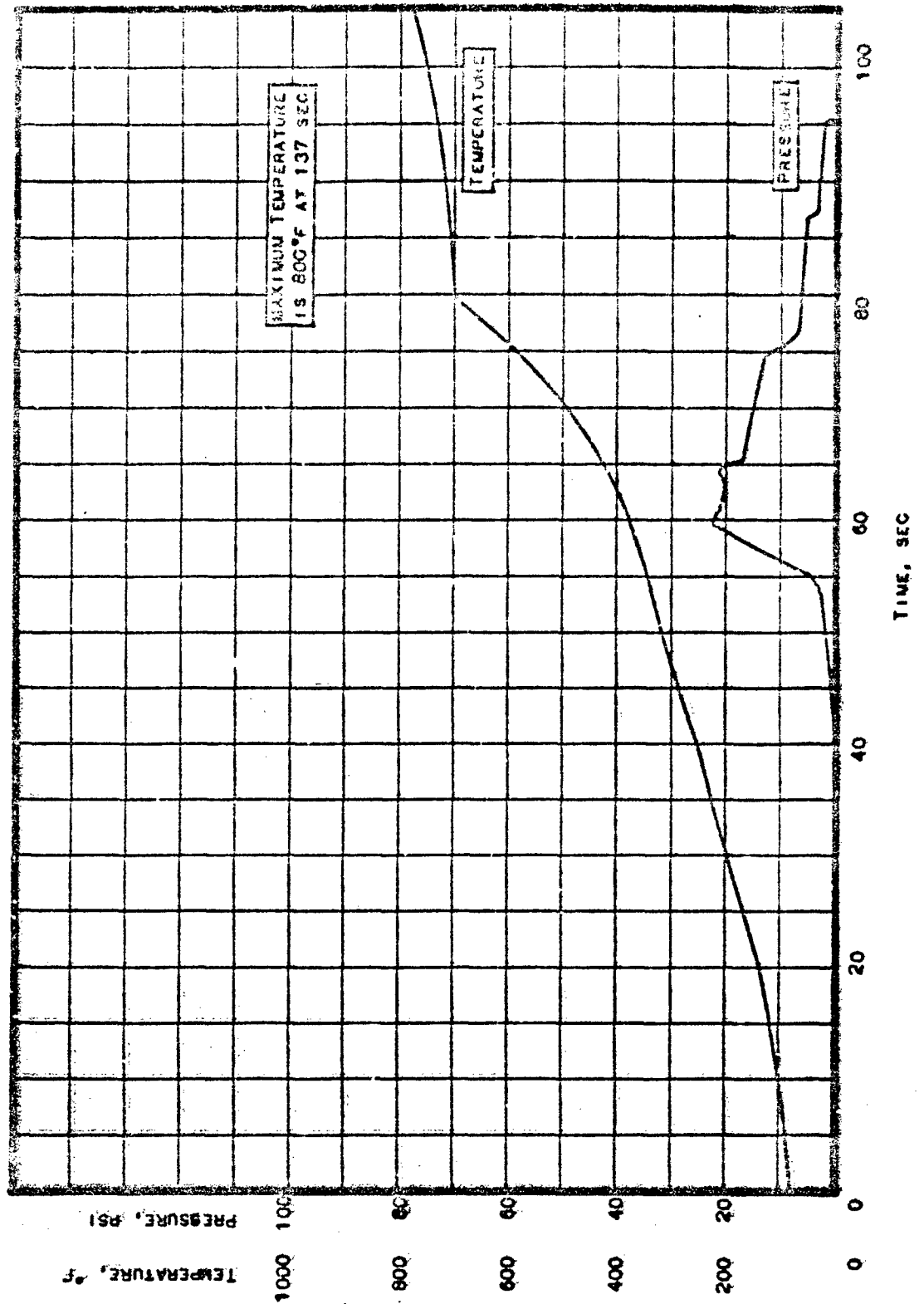


Figure VI-B-1

Temperature- and Pressure-vs-Time Curves for Specimen FSC-1 from Low-Volatile Content, Snap-Cured Subscale Cone

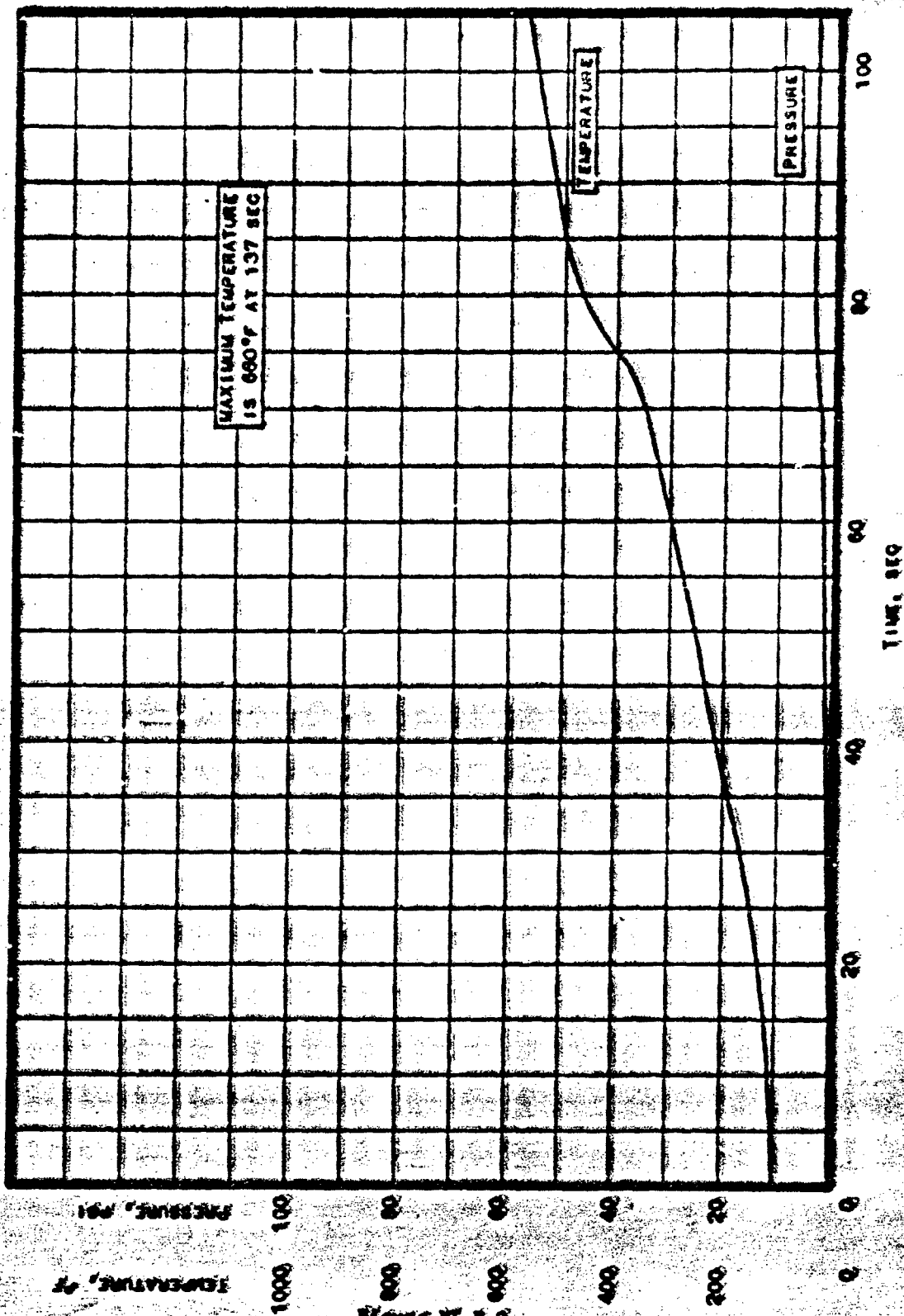


Figure VI-B-2

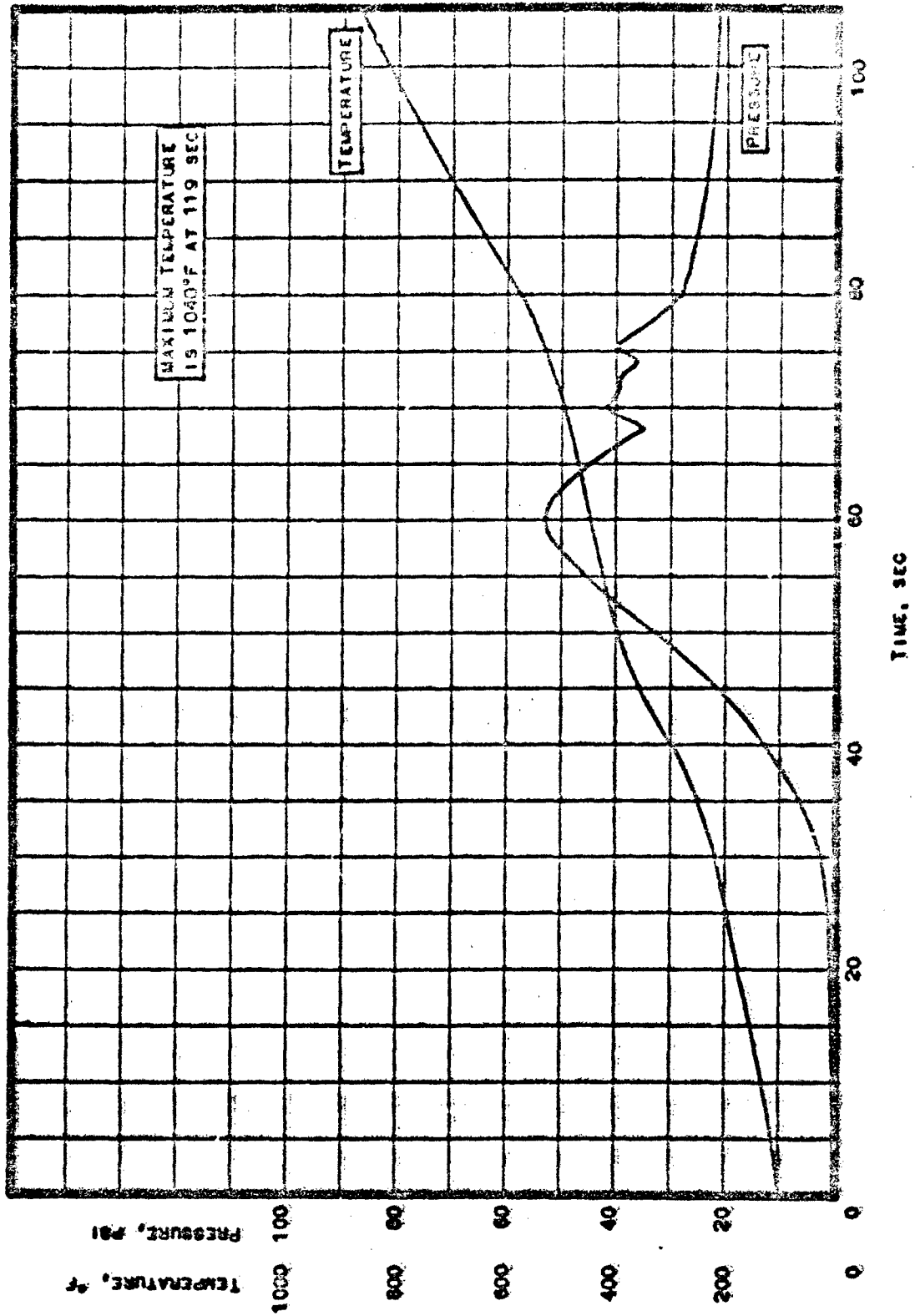
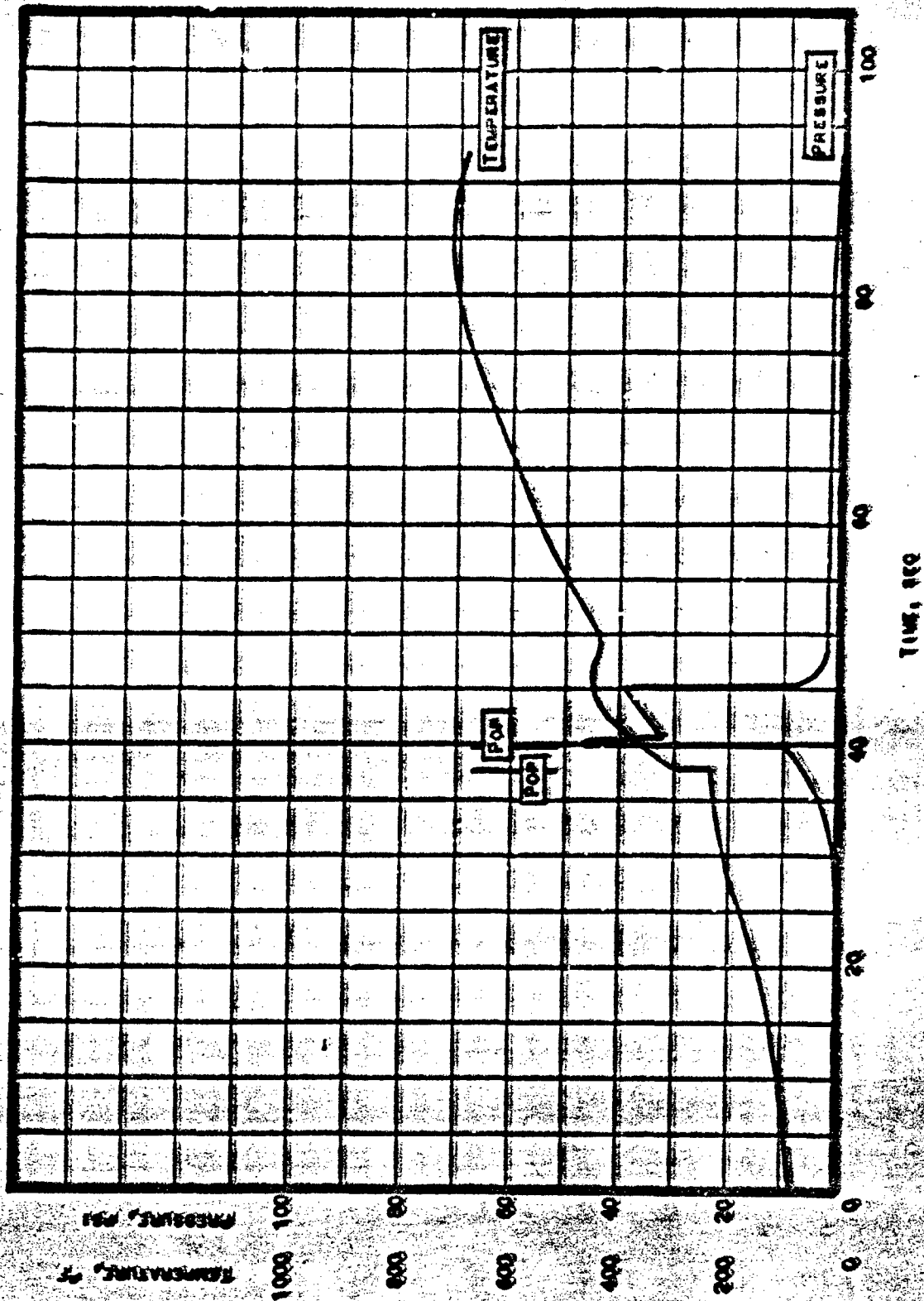


Figure VI-B-3

Temperature- and Pressure-vs-Time Curves for Specimen 96-1 from  
Subscale Cone (Water Added During Cure)





Temperature- and Pressure-vs.-Time Curves for Specimen 96-2 from Subscale Cone (Water Added During Cure)

Figure VI-B-4

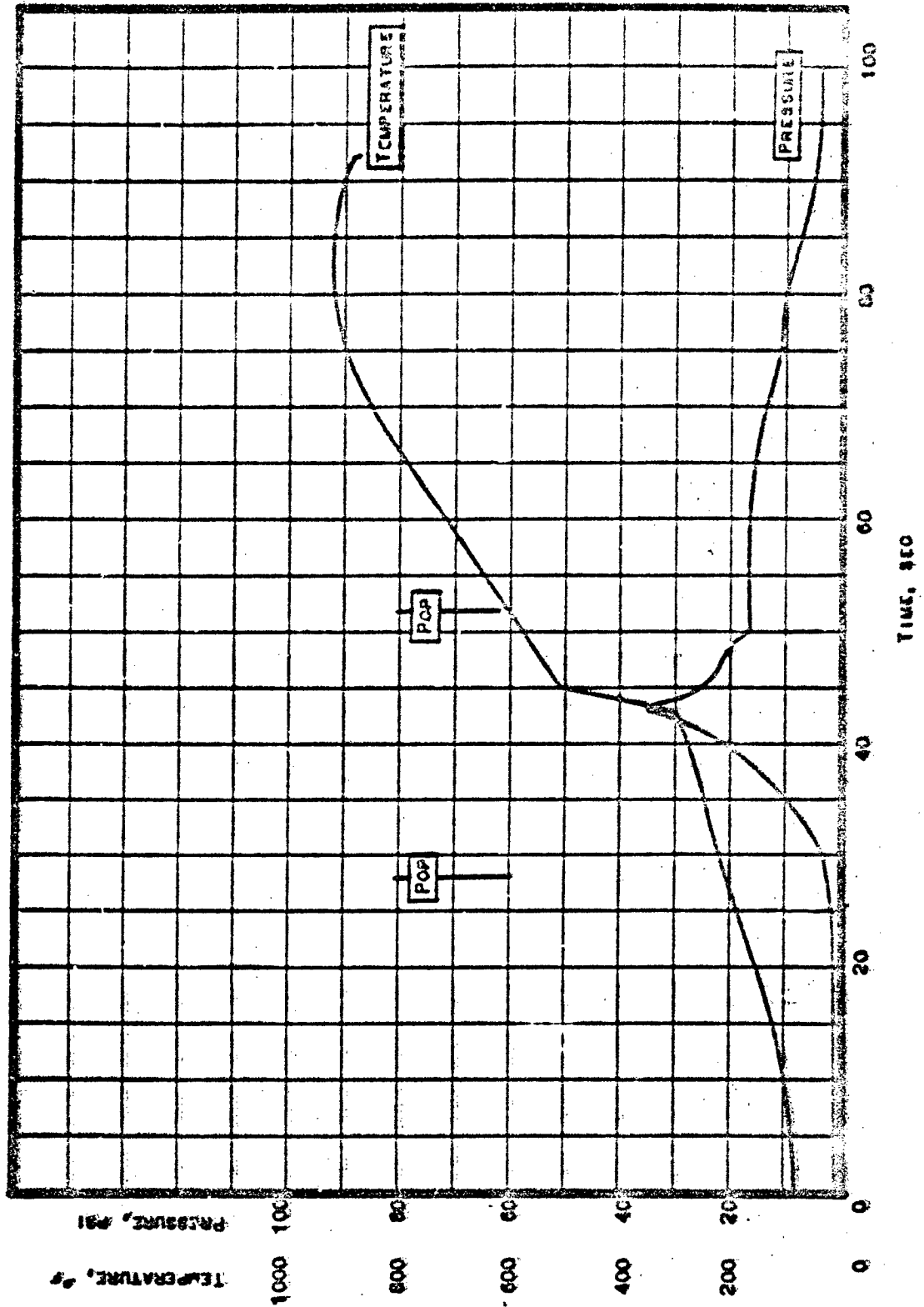
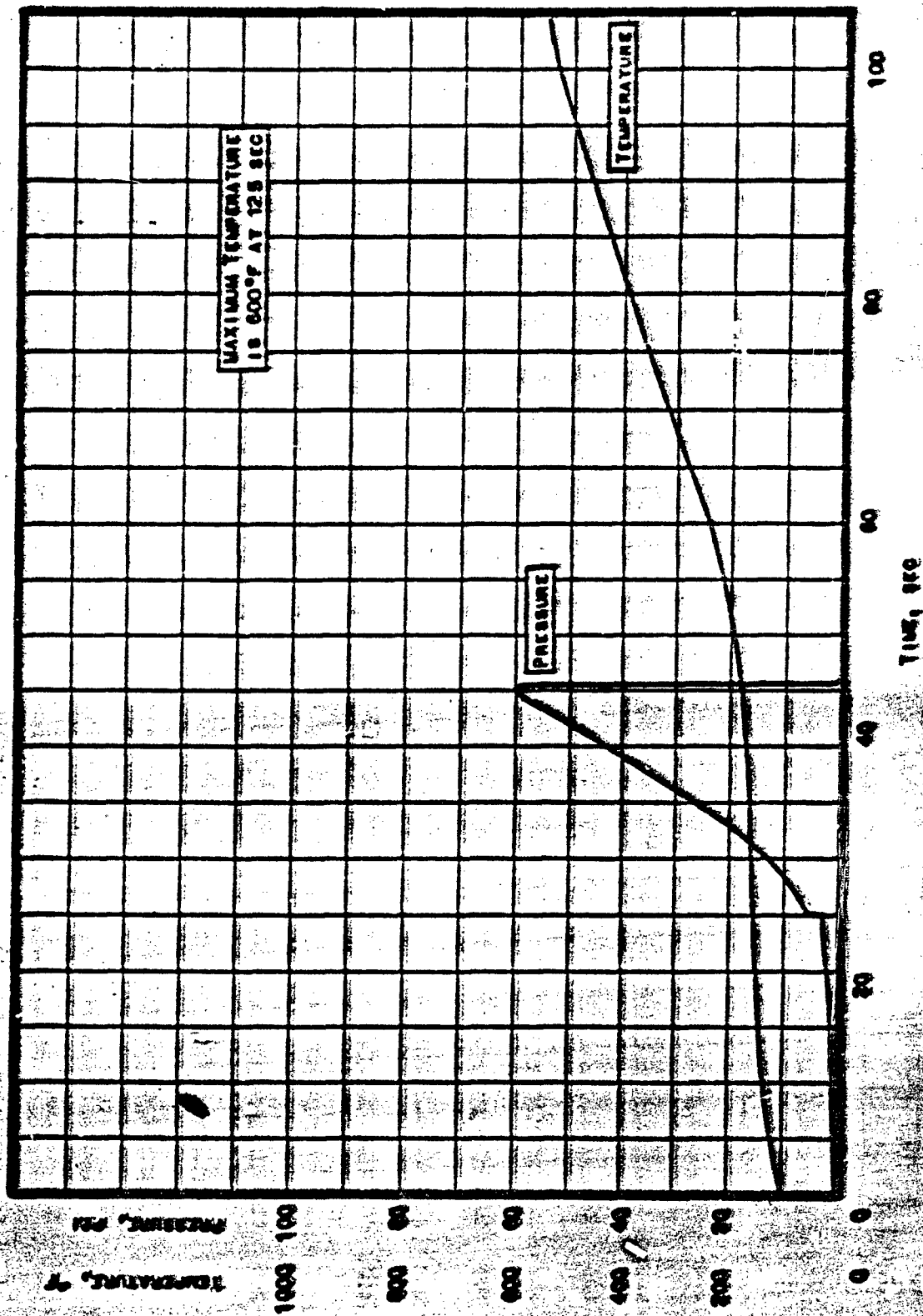


Figure VI-B-5

Temperature- and Pressure-vs-Time Curves for Specimen 99-1 from  
Low IRPI Subscale Cone



Temperature- and Pressure-vs-Time Curves for Specimen 90-2 from Low INPI Subscale Cone

Figure VI-B-6

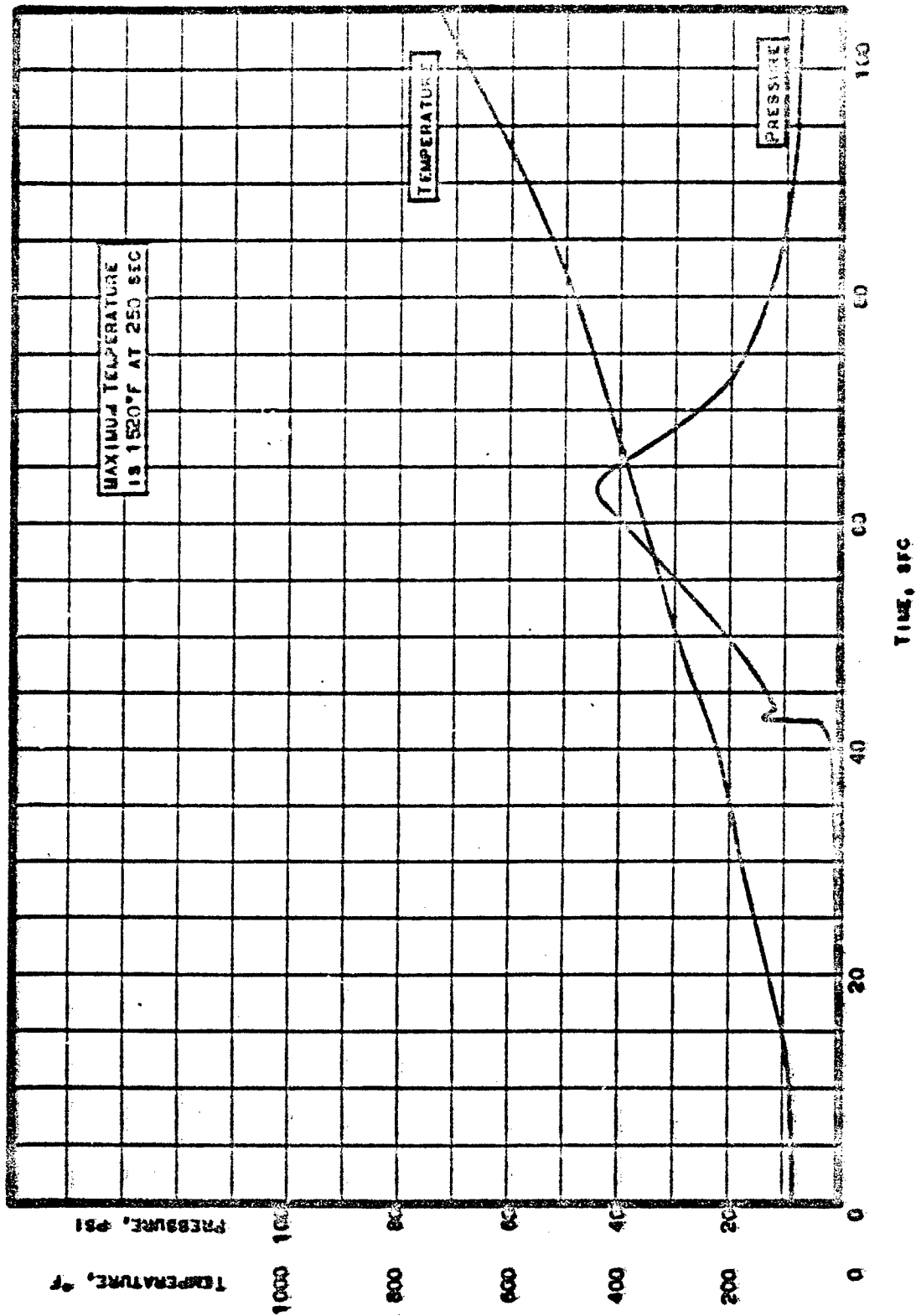


Figure VI-B-7

Temperature- and Pressure-vs-Time Curves for Specimen 02-1 from  
Medium IRPI Subscale Cone

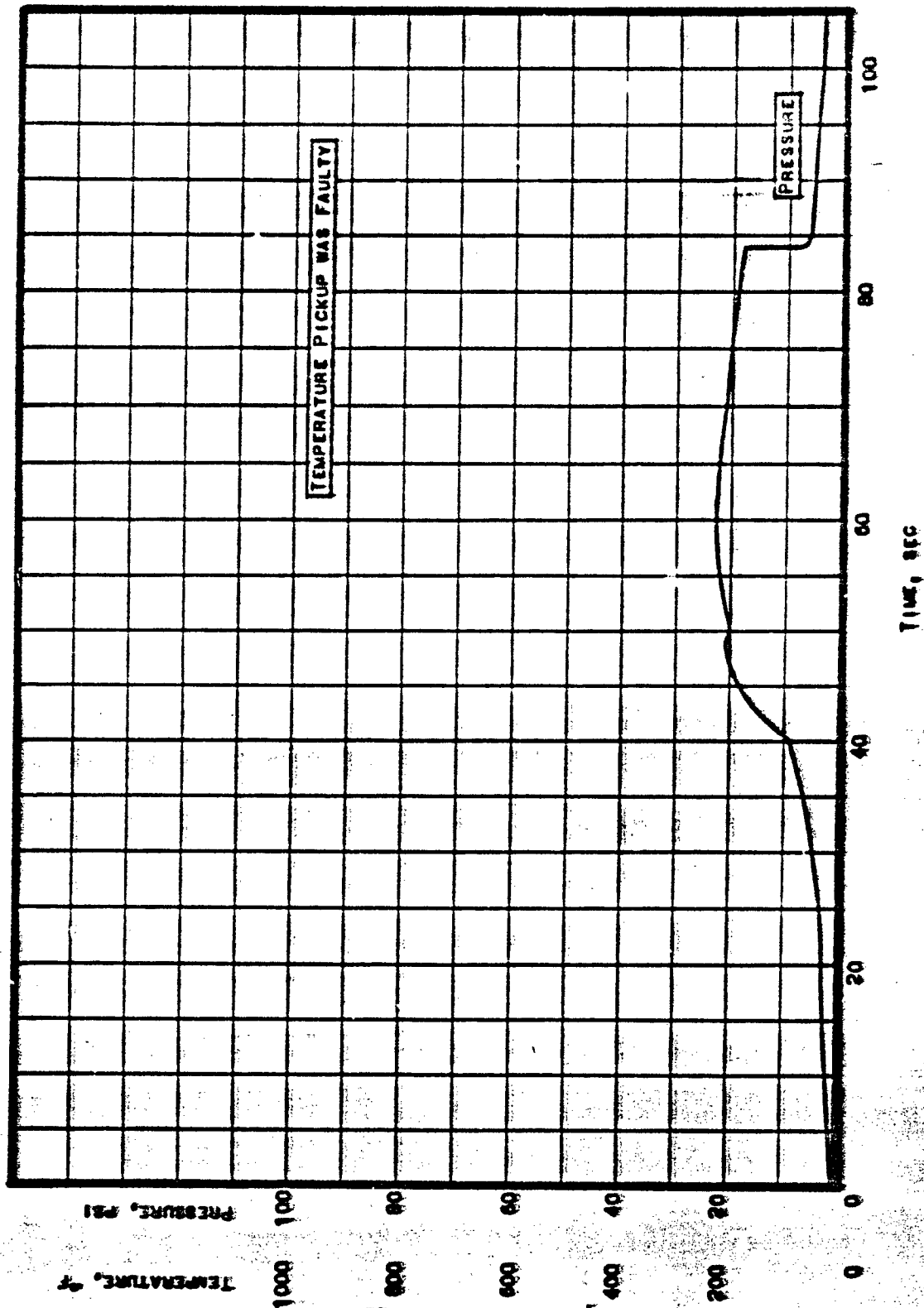


Figure VI-B-8

Temperature- and Pressure-vs-Time Curves for Specimen 02-2 from  
Medium IAPI Subscale Cone

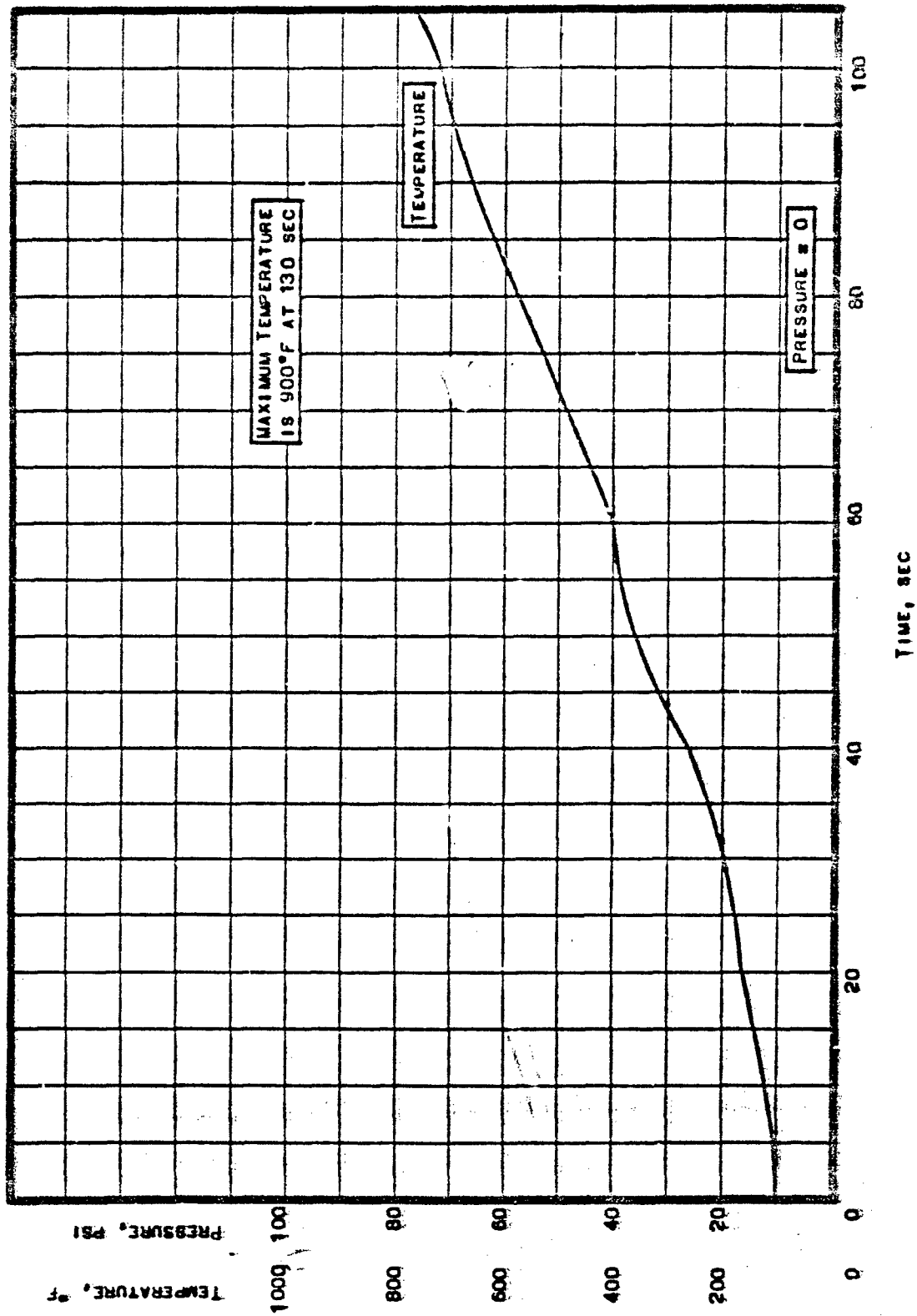
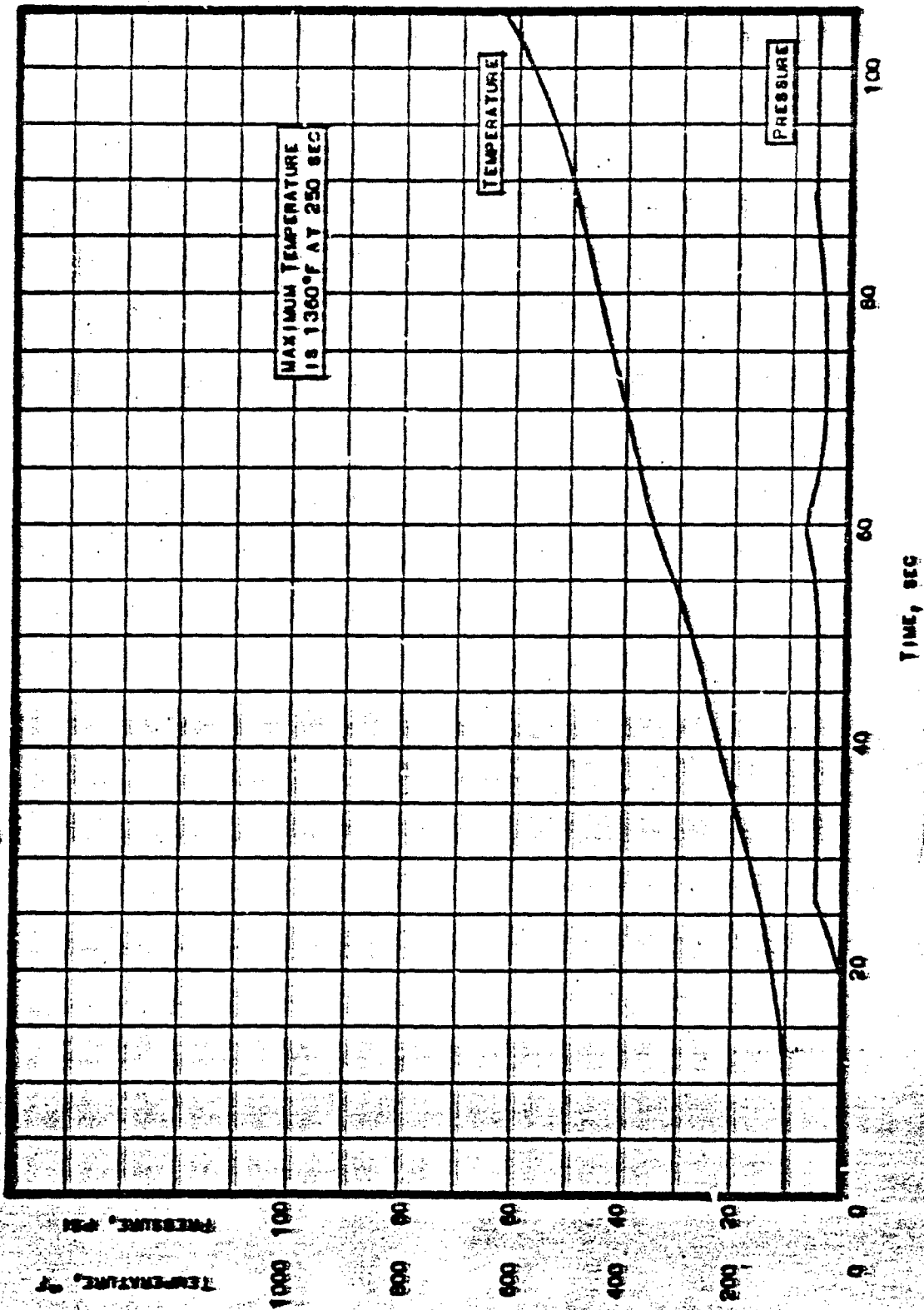


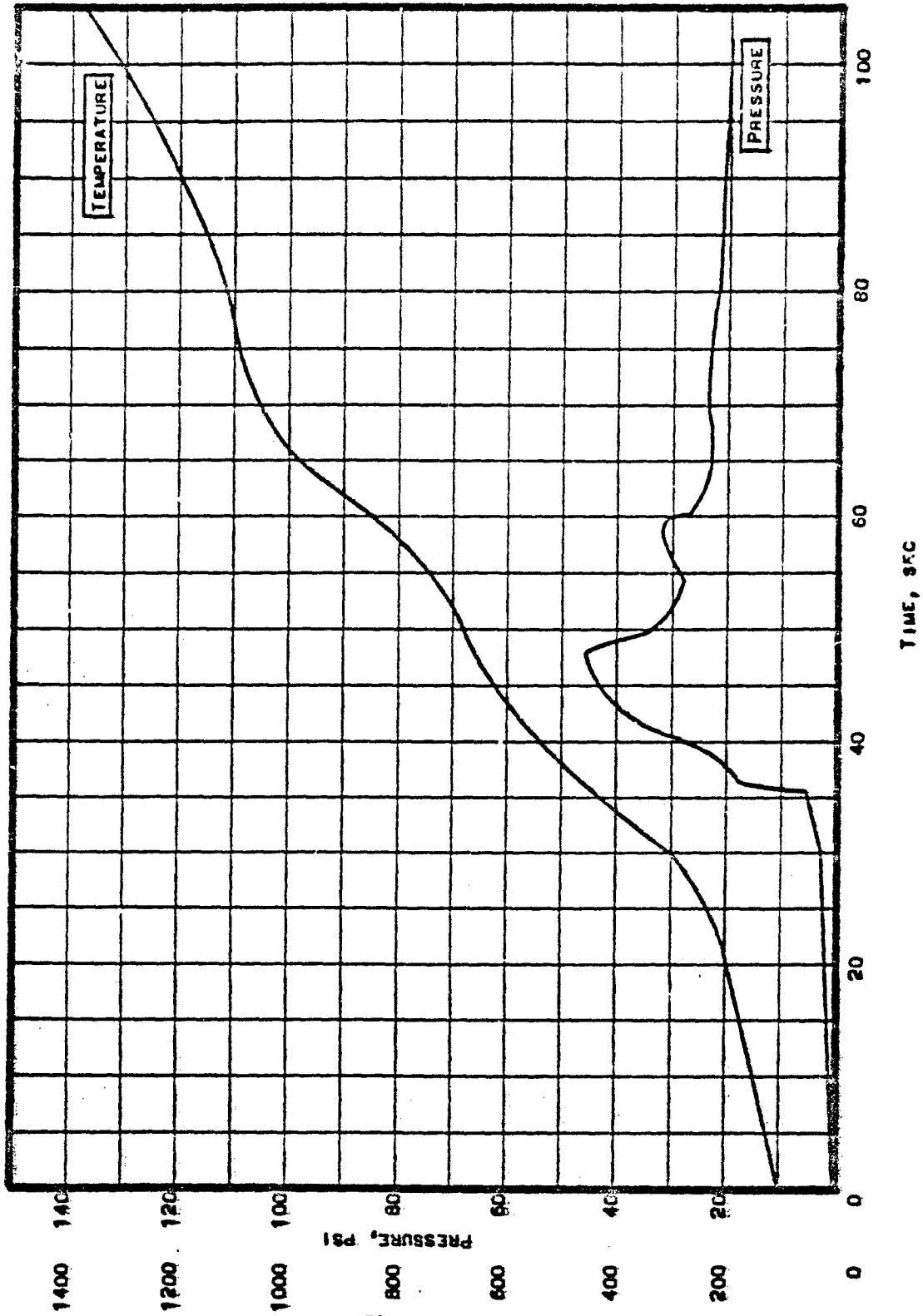
Figure VI-B-9

Temperature- and Pressure-vs-Time Curves for Specimen 03-1 from  
High IAPI Subscale Cone



Temperature- and Pressure-vs-Time Curves for Specimen 03-2 from High 1871 Subscale Cone

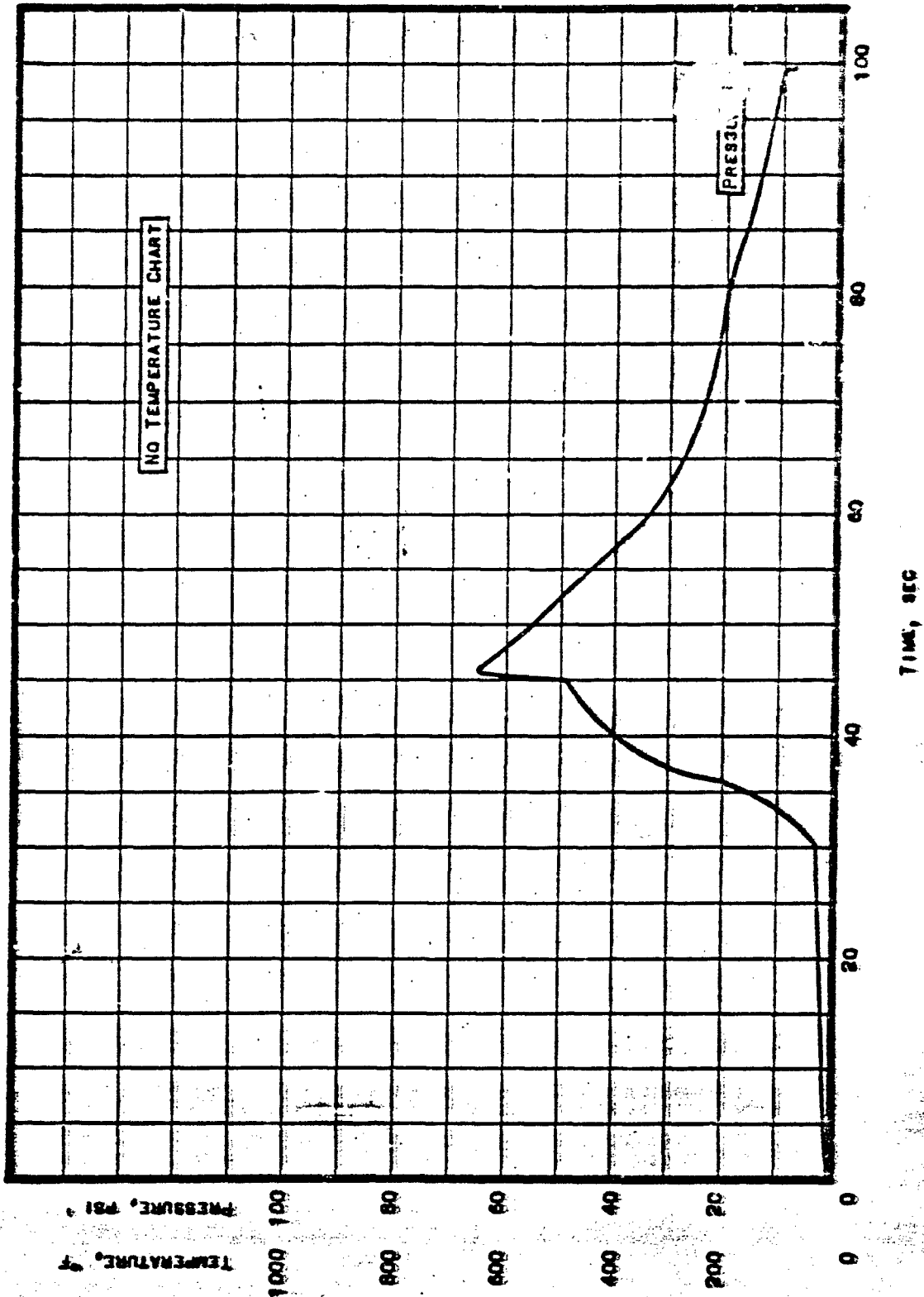
Figure VI-B-10



Temperature- and Pressure-vs-Time Curves for Specimen 92-1 from  
Special Debulk Subscale Cone

Figure VI-B-11





Temperature- and Pressure-vs-Time Curves for Specimen 92-3 from  
Special Depth Subscale Cone

Figure VI-B-12

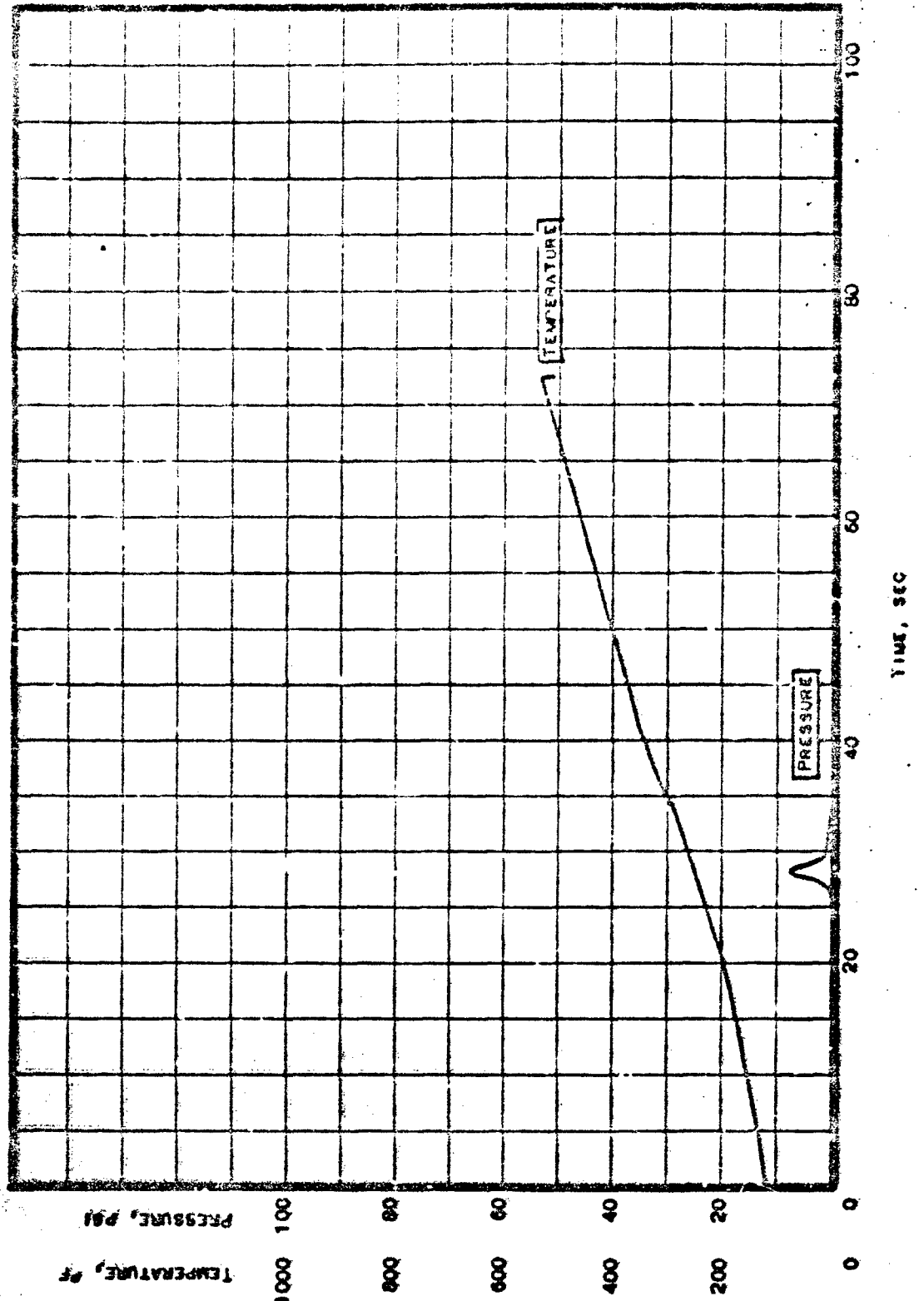
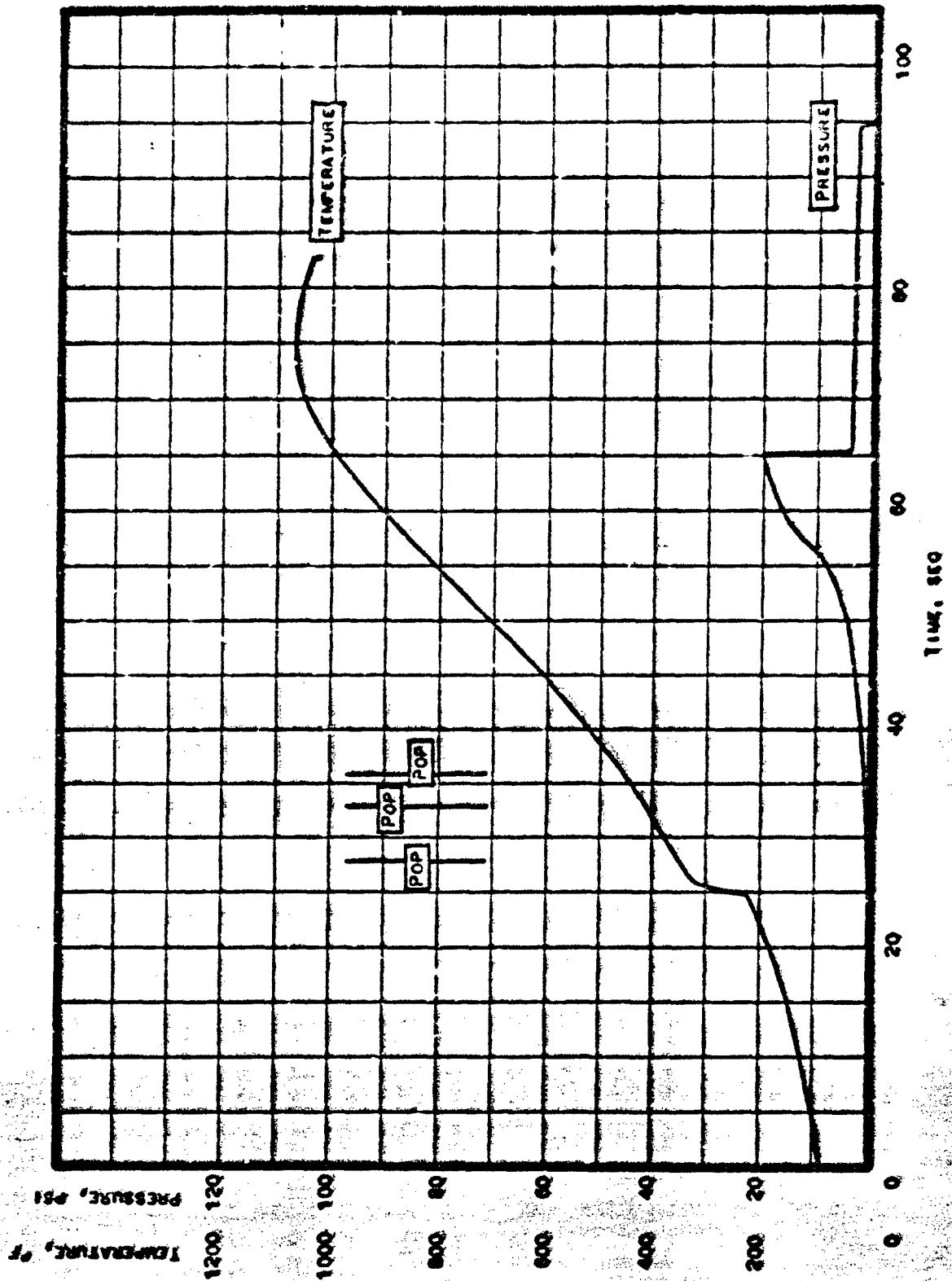


Figure VI-B-13



Temperature- and Pressure-vs-Time Curves for Specimen 94-2 from  
Special Debulk Subscale Cone

Figure VI-B-14

Report 0162-06TDR-9-Vol 2

APPENDIX VI-C

STRESS ANALYSIS OF THE WING VI MINUTEMAN  
NOZZLE SUPPORT STRUCTURE AND SEA-LEVEL EXIT CONE

FIGURE LIST

<u>Description</u>	<u>Figure</u>
7.54-in. Bond Release	
Stress Strain Curve for Epon 2216	VI-C-1
FM 5014 Meridional Stress	VI-C-2
FM 5014 Hoop Stress	VI-C-3
FM 5020 Meridional Stress	VI-C-4
FM 5020 Hoop Stress	VI-C-5
Epon 2216 Bond Normal Stress	VI-C-6
Epon 2216 Bond Shear Stress	VI-C-7
Interlaminar Shear FM 5014 - FM 5020	VI-C-8
6AL-4V Titanium Hoop Stress	VI-C-9
6AL-4V Titanium Meridional Stress	VI-C-10
System Deflection Curves	VI-C-11
6.04-in. Bond Release	
FM 5014 Meridional Stress	VI-C-12
FM 5020 Meridional Stress	VI-C-13
Sea Level Exit Cone Hoop Stress	VI-C-14
Epon 2216 Bond Shear	VI-C-15
Epon 2216 Bond Normal Stress	VI-C-16
System Deflection Curves	VI-C-17-18
System Deflection Curves for Various Proof Test Conditions	VI-C-19

Report 6162-C64DR-2-Vol 2, Appendix VI-C

The stresses and deflections of the Wing VI nozzle support structure and sea-level exit-cone liners were determined using the IEM 7094 computer program number 14063.

The program for analysis of axisymmetric structures subject to thermal and mechanical loads is based upon the finite element method which replaces the basic structure with a system of rectangular ring elements. The program is capable of handling multilayered, transversely isotropic shells with varying temperature and mechanical loading conditions.

The basic nozzle configuration was analyzed for various environmental conditions. Analyses during motor operation were conducted at ignition phase, after 1-sec of firing and at the end of the operation, and after 70 sec of firing. The proof test environment was analyzed for effects of pressurization at both 570 psi and 627 psi, along with a simulated back pressure in the sea-level exit cone. At the 570 psi proof-test environment.

The length of bond release in the vicinity of the T-joint was also investigated to determine the optimum release configuration. The analysis shows the effects of a basic 7.54-in. release length and the changes in stress at critical locations for a bond release of 6.04 in.

The 7.54-in. release length is very close to the optimum system release length as evidenced by a significant reduction in bond stress and sea-level exit-cone stress levels.

To compare the reduction in stress levels at critical locations, the basic structure was also analyzed for a fully bonded titanium, exit-cone interface.

The results of the analysis are shown in the various graphs listed in the table of figures, and in the general summary of stresses at critical points throughout the structure.

In conclusion, the analysis substantiates the structural integrity of the present configurations, with the sea-level exit cone released 7.54 in. in the vicinity of the T-joint. The stresses induced into the various components are generally well within acceptable limits.

A conservative estimate of the true bond stress was made using the assumptions that the total energy in the bond line must remain constant (see Figure VI-C-1 and page VI-C-5, and that the stress encountered must lie along the stress strain curve. It is also noted that the value of bond stress is a re-entrant stress confined within narrow limits. The actual bond stress encountered is within the allowable ultimate tensile strength and also, the total energy within the bond element is well below that allowed in the specification minimums.

The various proof-test environments were investigated in an attempt to more closely simulate actual firing environments. The various pressurized proof tests do not significantly change stresses in critical areas and it was found that the 627 psi proof-test environment was, in most areas, a reasonable approximation of actual firing conditions, with the optimum bond release of 7.54 in.

Report 0162-06TDR-9-Vol 2, Appendix VI-C

No change in the present buckling allowable or nozzle and bolted joint stresses will occur as a result of liner release. The values in the present Wing VI Minuteman stress analysis are still applicable to the structure and have not been included as a portion of this report.

Report 0162-06WDR-9-Vol 2, Appendix VI-C

The stresses and deflections of the Wing VI nozzle support structure and sea-level exit-cone liners were determined using the IEM 7094 computer program number 14063.

The program for analysis of axisymmetric structures subject to thermal and mechanical loads is based upon the finite element method which replaces the basic structure with a system of rectangular ring elements. The program is capable of handling multilayered, transversely isotropic shells with varying temperature and mechanical loading conditions.

The basic nozzle configuration was analyzed for various environmental conditions. Analyses during motor operation were conducted at ignition phase, after 1-sec of firing and at the end of the operation, and after 70 sec of firing. The proof test environment was analyzed for effects of pressurization at both 570 psi and 627 psi, along with a simulated back pressure in the sea-level exit cone. At the 570 psi proof-test environment.

The length of bond release in the vicinity of the T-joint was also investigated to determine the optimum release configuration. The analysis shows the effects of a basic 7.54-in. release length and the changes in stress at critical locations for a bond release of 6.04 in.

The 7.54-in. release length is very close to the optimum system release length as evidenced by a significant reduction in bond stress and sea-level exit-cone stress levels.

To compare the reduction in stress levels at critical locations, the basic structure was also analyzed for a fully bonded titanium, exit-cone interface.

The results of the analysis are shown in the various graphs listed in the table of figures, and in the general summary of stresses at critical points throughout the structure.

In conclusion, the analysis substantiates the structural integrity of the present configurations, with the sea-level exit cone released 7.54 in. in the vicinity of the T-joint. The stresses induced into the various components are generally well within acceptable limits.

A conservative estimate of the true bond stress was made using the assumptions that the total energy in the bond line must remain constant (see Figure VI-C-1 and page VI-C-5, and that the stress encountered must lie along the stress strain curve. It is also noted that the value of bond stress is a re-entrant stress confined within narrow limits. The actual bond stress encountered is within the allowable ultimate tensile strength and also, the total energy within the bond element is well below that allowed in the specification minimums.

The various proof-test environments were investigated in an attempt to more closely simulate actual firing environments. The various pressurized proof tests do not significantly change stresses in critical areas and it was found that the 627 psi proof-test environment was, in most areas, a reasonable approximation of actual firing conditions, with the optimum bond release of 7.54 in.



DESIGN CRITERIA

Two proof conditions exist according to Specification-AGE 32098A.

Condition I        570 psi in 1.5 sec

Condition II       627 psi and held for 1 min.

The pressurization rate for Condition I is much lower than that encountered in actual firing, 570 psi in 300 millisecc. Therefore, it will not be as critical as Condition II and only Condition II will be analyzed.

BSD Design Document 6120-8726-7C-02 requires that there shall be no evidence of excessive deformation (yielding) at the proof pressure of  $1.10 \times \text{MEOP}$  (627 psi). The document further requires a minimum ultimate factor of safety of 1.15 on the pressurized motor case chamber.

All margins of safety quoted in this report are based on actual critical environment and do not reflect the required 1.15 factor on the titanium support structure or the 1.25 factor on the remaining components. All margins of safety do exceed design requirements, stated above, as shown in the general summary of maximum stresses.

Aft Closure and Nozzle Support Structure

DN 369722 Nozzle Assembly

DN 384021 Housing, Annealed

DN 369937 Liners, Exit Cone

DN 367950 Bolt, 12 Point, NAS 626

MATERIALS

\* Aft Closure Housing - 6AL4V Titanium

$F_{tu} = 130,000$  psi minimum

$F_{ty} = 120,000$  psi minimum

Bending  $F_{bu} = 187,500$  psi


$F_{by} = 140,000$  psi

Reference Convair

Design Manual

Young's Modulus =  $16.4 \times 10^6$  psi

Elongation = 8% minimum

\* Reference Note  DN 380787 and MIL 5 Handbook

Design Criteria (cont.)

\* Liners, Exit Cone

Inner FM 5014

Outer FM 5020

FM 5014 - Graphite Tape and Phenolic Binder

$F_{tu} = 2500$  psi meridional minimum at 20 degrees

$F_{tu} = 5200$  psi hoop minimum

$F_{cu} = 11,500$  psi minimum at 20 degrees

$E_t = 1.6 \times 10^6$  psi

$E_c = 2.0 \times 10^6$  psi

FM 5020 - Silica Tape and Phenolic

$F_{tu} = 4470$  psi minimum meridional at 20 degrees

$F_{cu} = 15,900$  psi minimum meridional at 20 degrees

$E_t = 2.0 \times 10^6$  psi

$E_c = 1.8 \times 10^6$  psi

Bond

Epon 2216

$F_{tu} = 1250$  psi

$F_{su} = 1000$  psi

$E = 16,700$  psi

Inter Laminer Shear Between FM 5014 and FM 5020

$F_{su} = 1500$  psi at room temperature

$F_{su} = 200$  psi at end of firing

\* Reference U. S. Polymeric Co. Material Data Sheets and AGC Test Results

GENERAL SUMMARY OF MAXIMUM STRESSES IN THE KING VI MINUTEMAN  
PRODUCTION NOZZLE SUPPORT STRUCTURE AND SEA LEVEL EXIT CONE

Type and location of Maximum Stress	7.54 in. Bond Release		6.04 in. Bond Release		Fully Bonded 627 psi	Minimum Margin of Safety**
	627 psi Proof	1 sec Firing	End of Firing	627 psi Proof	570 psi Proof	
FM 5014 Merid Tension	1100	600	None	1500	1400	1.27
FM 5014 Merid Comp	2400	2400	220	4000	3600	High
FM 5014 Hoop Tension	700	800	None	1080	1000	High
FM 5020 Merid Comp	None	None	None	700	640	-
FM 5020 Merid Comp	3600	3000	5500	4000	-	High
FM 5020 Hoop Tension	800	800	2400	1900	1625	High
FM 5014-FM 5020 Interlaminar Shear	660	500	125	1520	1400	0.60
Epon 2216 Bond Tension	765*	625*	None	1170*	-	0.63
Epon 2216 Bond Shear	550	450	350	690	-	0.81
6Al-4V Titanium Merid Stress	62000	48000	40000	-	-	0.93
6Al-4V Titanium Hoop Stress	77000	69000	73500	64000	58500	0.56

\* Elastic Stress Adjusted to True Stress.

\*\*Margin of Safety Based on 7.54 in. Bond Release Length

CALCULATION OF TRUE BOND TENSILE STRESS

Assume that the work done by the bond must remain constant, i.e., the area under the stress-strain curve must yield a constant energy function.

$$\text{Elastic Stress} = 1225 \text{ psi}$$

$$\text{Elastic Strain} = 7.25\%$$

$$E_E = \frac{1}{2} 1225 \times 0.0725 = \underline{44.41 \text{ lb-in./in.}^3}$$

FIRST APPROXIMATION

$$\sigma_{\text{bond}} = 800 \text{ psi}$$

$$\epsilon_{\text{bond}} = 12.25\%$$

$$E_1 = 49.00 \text{ lb-in./in.}^3$$

SECOND APPROXIMATION (See Figure VI-C-1)

$$\sigma_{\text{bond}} = 750 \text{ psi}$$

$$\epsilon_{\text{bond}} = 11.25\%$$

$$E_2 = 42.19 \text{ lb-in./in.}^3$$

FINAL APPROXIMATION

$$\sigma_{\text{bond}} = 765 \text{ psi}$$

$$\epsilon_{\text{bond}} = 11.6\%$$

$$E_F = \underline{44.37 \text{ lb-in./in.}^3}$$

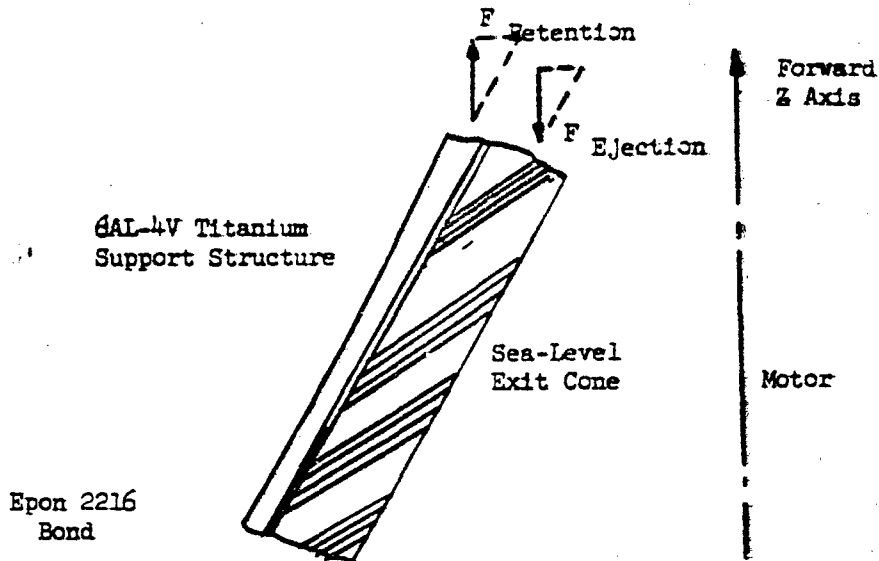
MINIMUM ENERGY PER SPECIFICATION

$$\sigma = 1250 \text{ psi} \quad \text{Minimum U.T.S.}$$

$$\epsilon = 35\% \quad (\text{Minimum percent elongation})$$

$$E_m = \underline{218.75 \text{ lb-in./in.}^3}$$

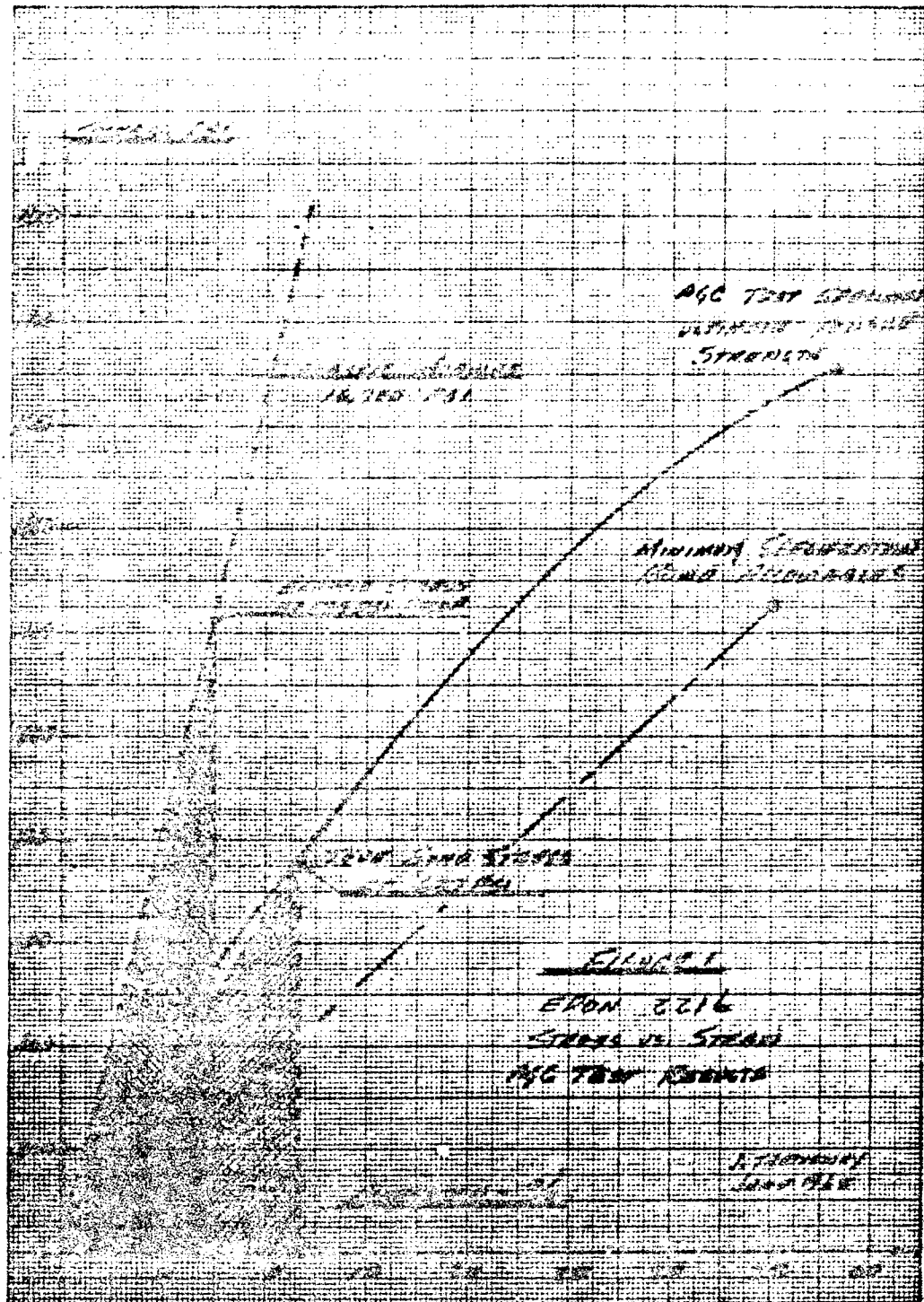
SUMMARY OF EJECTION FORCES



$\Sigma F$  in the Z Axis must equal to zero\*

At 627 psi, proof test:	$F_{\text{eject}} = 85,000 \text{ lb}$
570 psi, 1-sec firing:	$F_{\text{eject}} = 75,300 \text{ lb}$
570 psi, end of firing:	$F_{\text{eject}} = 61,130 \text{ lb}$

\* Calculation is for the 6.04-in. bond release condition.



Epon 2216 Stress vs Strain-Test Results

Figure VI-C-1

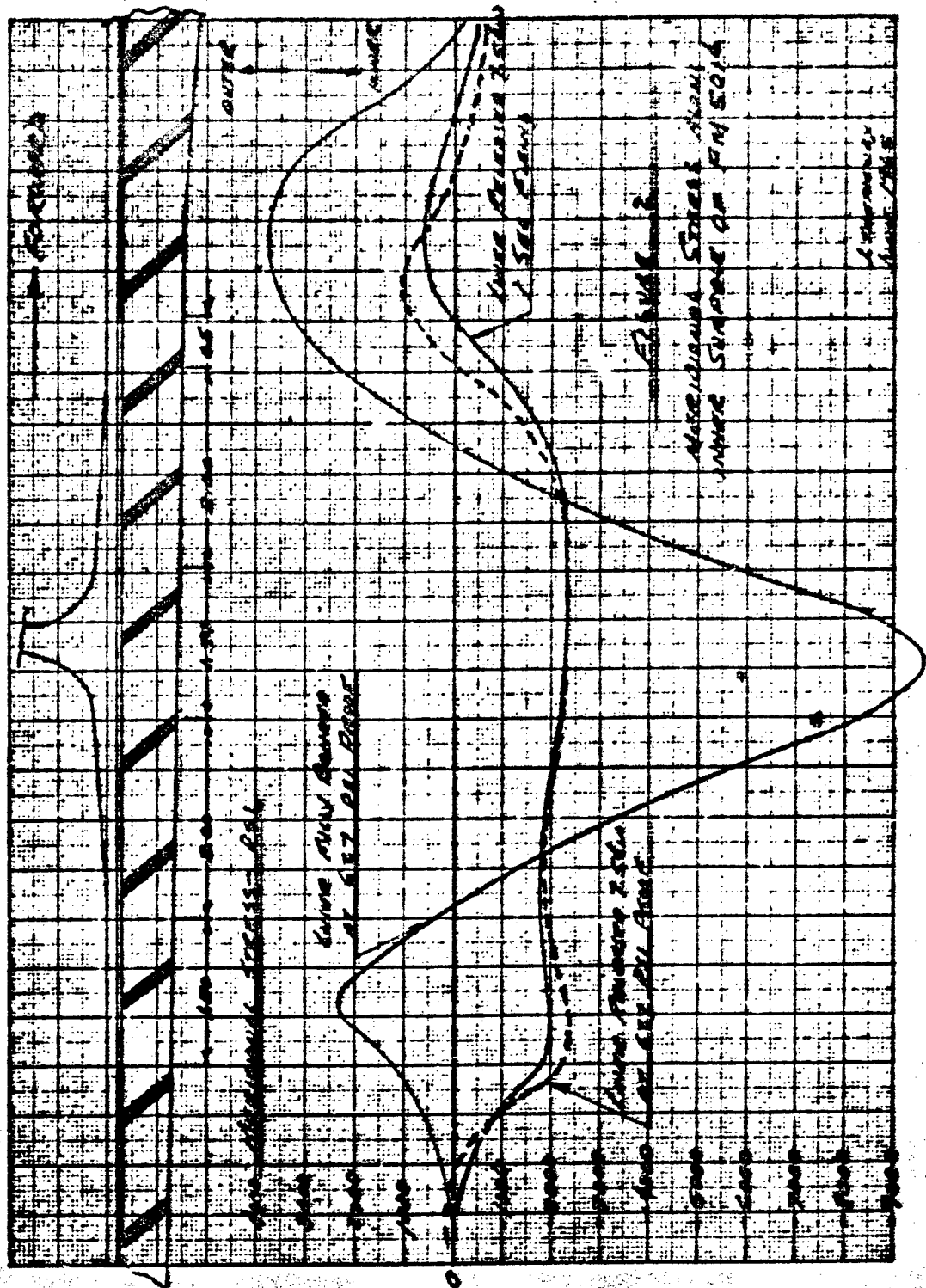


Figure VI-C-2

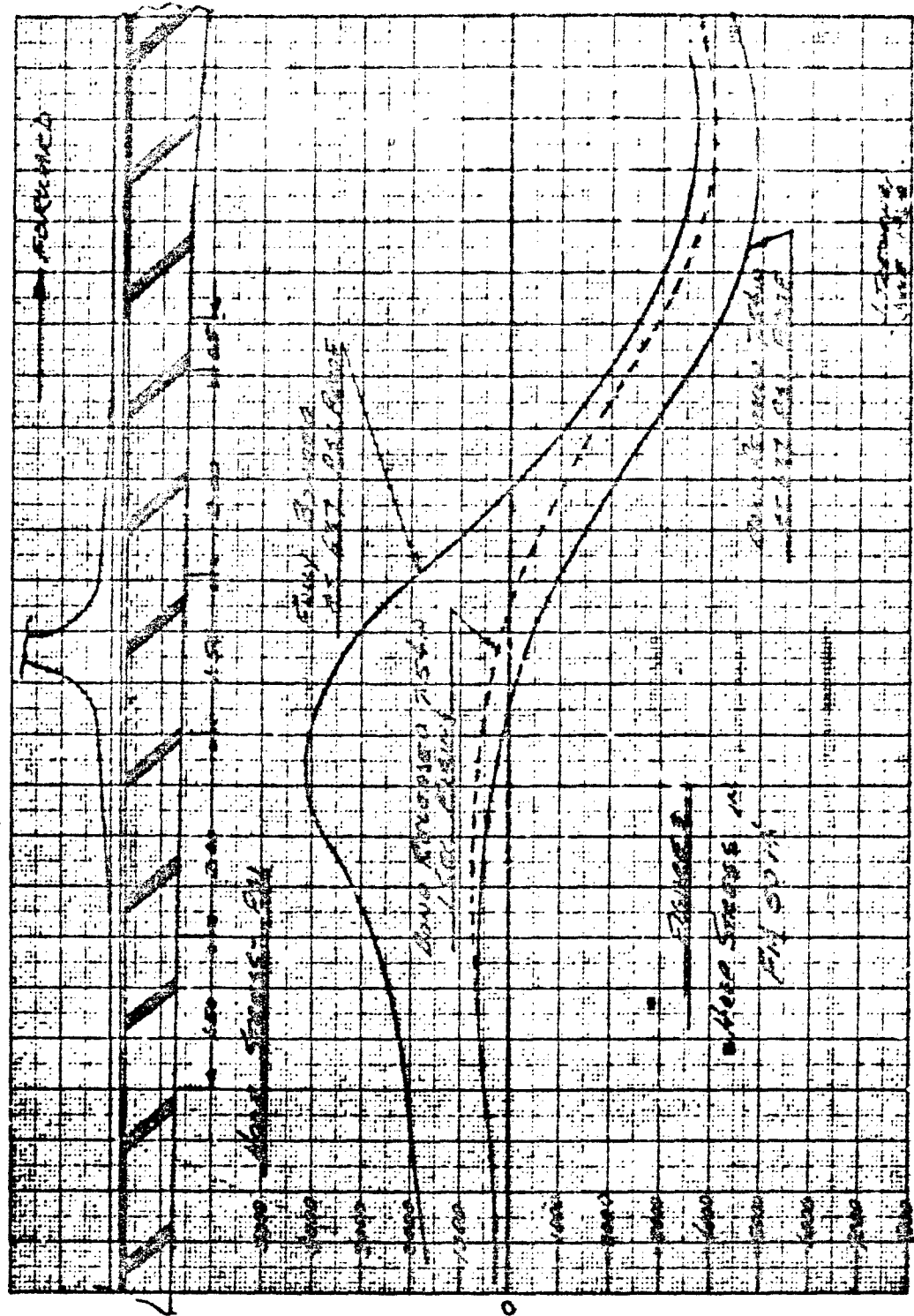
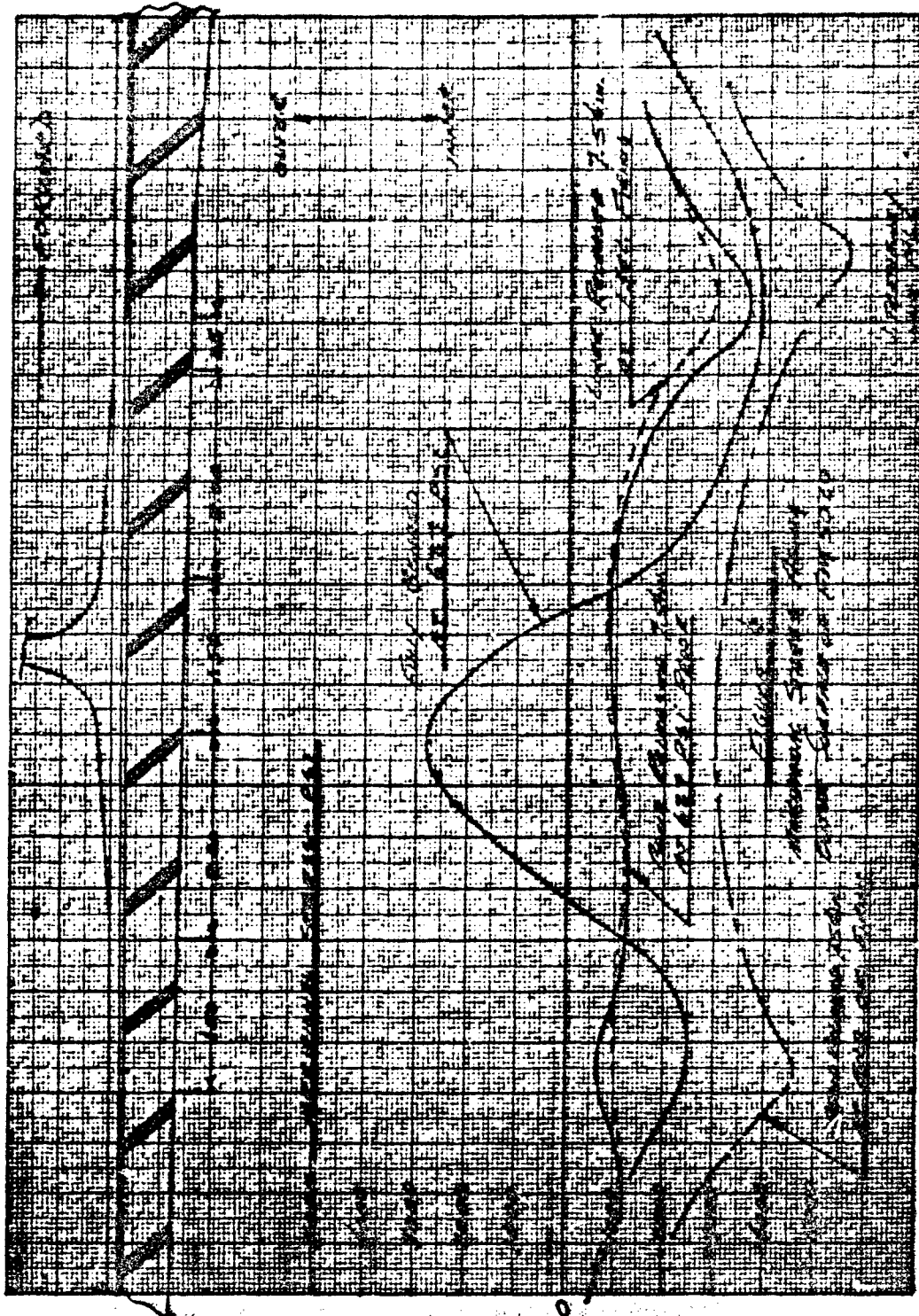


Figure VI-C-3





**Figure VI-C-4**





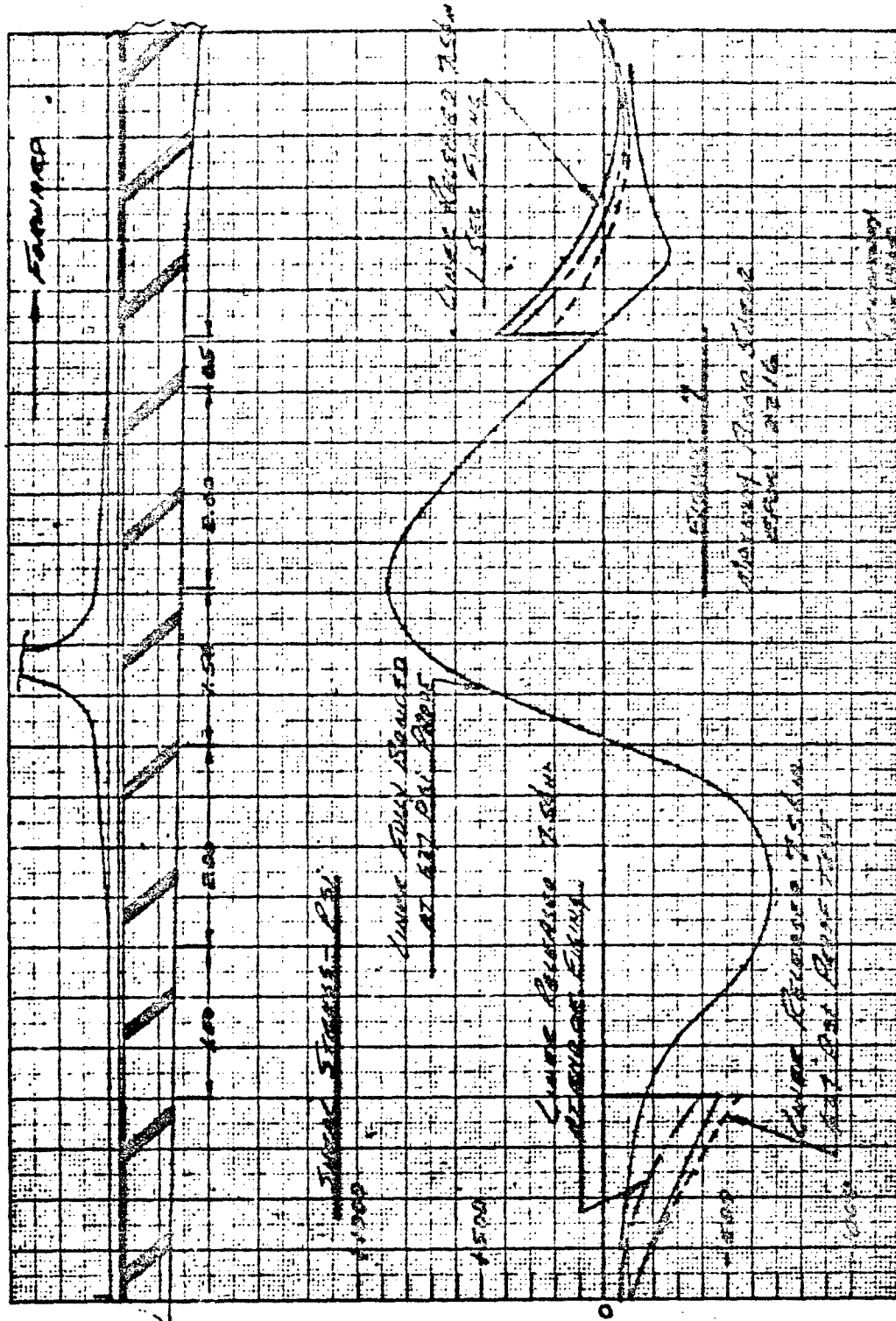
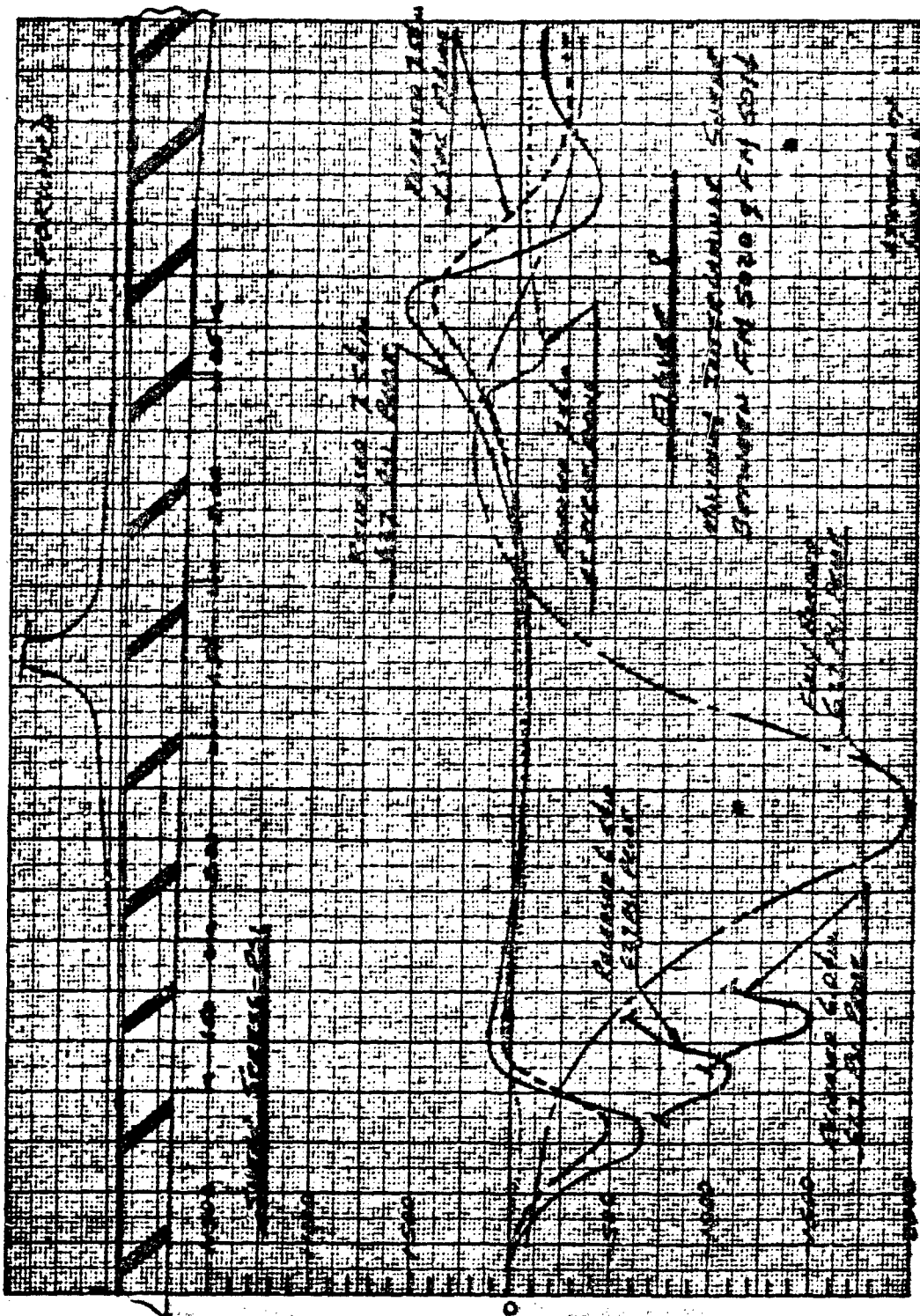


Figure VI-C-7

Maximum Bond Shear Epon 2216



Maximum Interlaminar Shear between FM 5020 and FM 5014

Figure VI-C-3

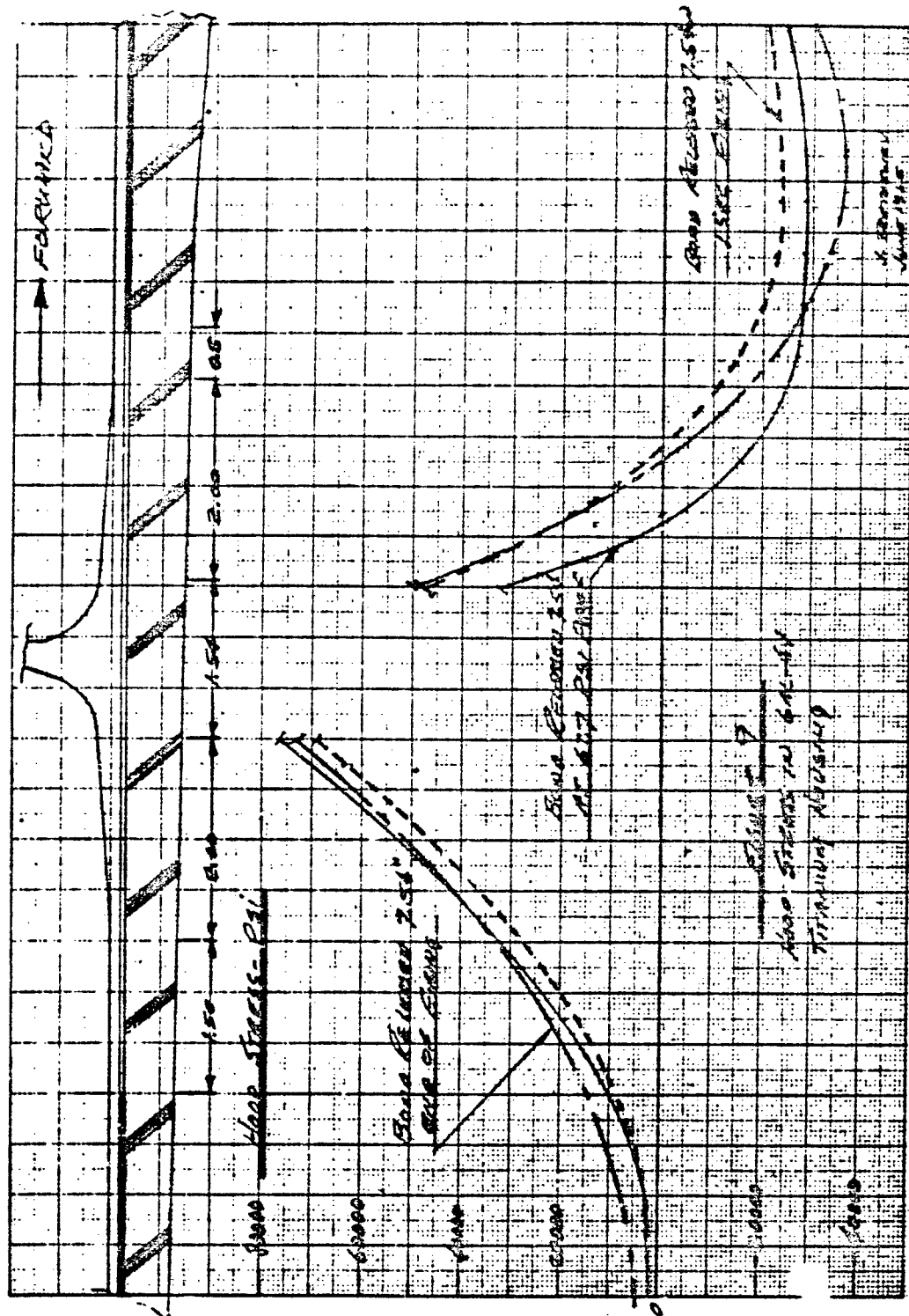


Figure VI-C-9

Hoop Stress in 6AL-4V Titanium Housing

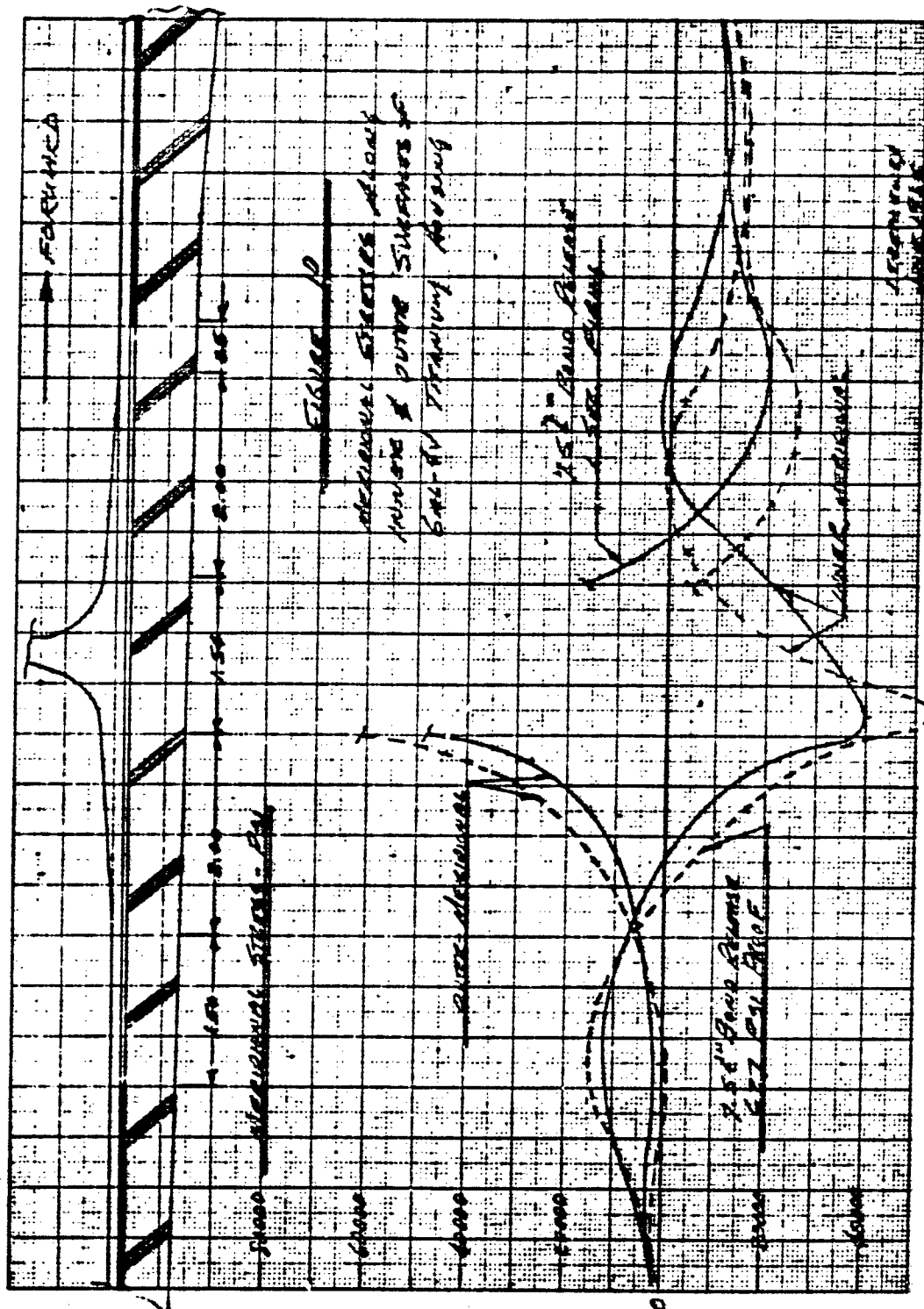
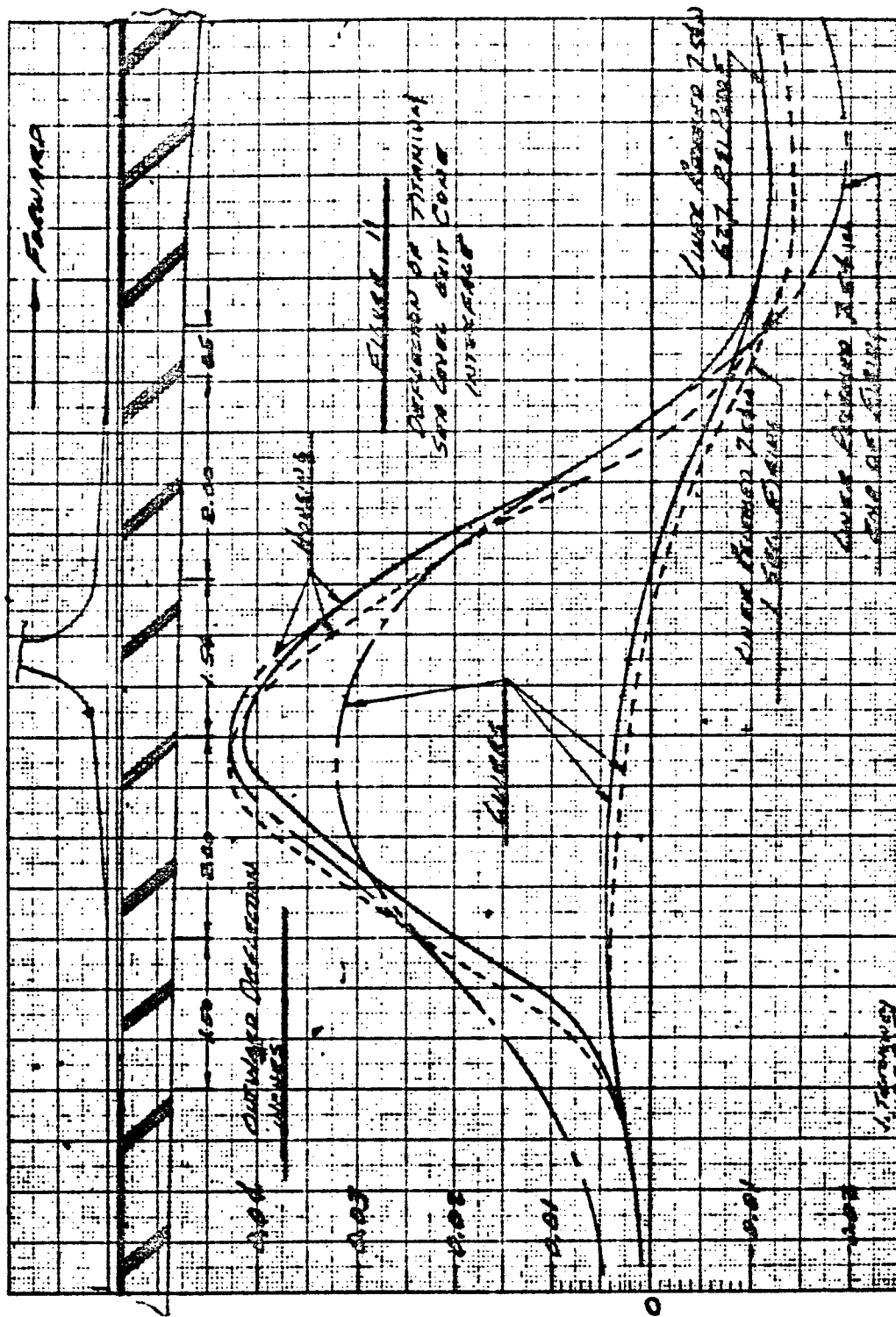


Figure VI-C-10

Meridional Stresses along Inner and Outer Surfaces of 6AL-4V





**Figure VI-C-11**

# Deflection of Titanium Sea-Level Exit Cone Interface



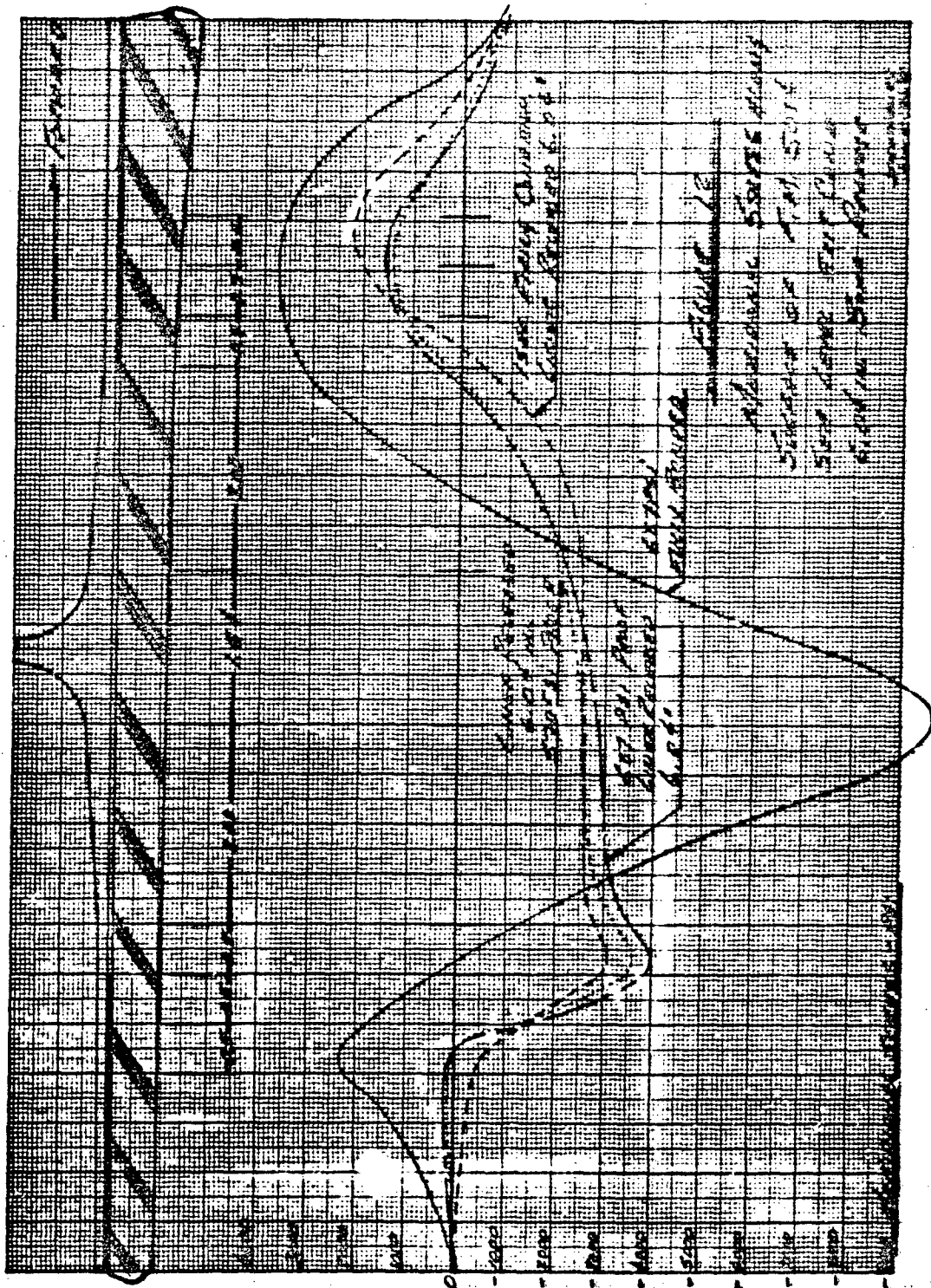


**Figure VI-C-12**

**Meridional Stress along Surface of FM 5014 Sea-Level Exit-Cone,  
6.04-in. Bond Release**

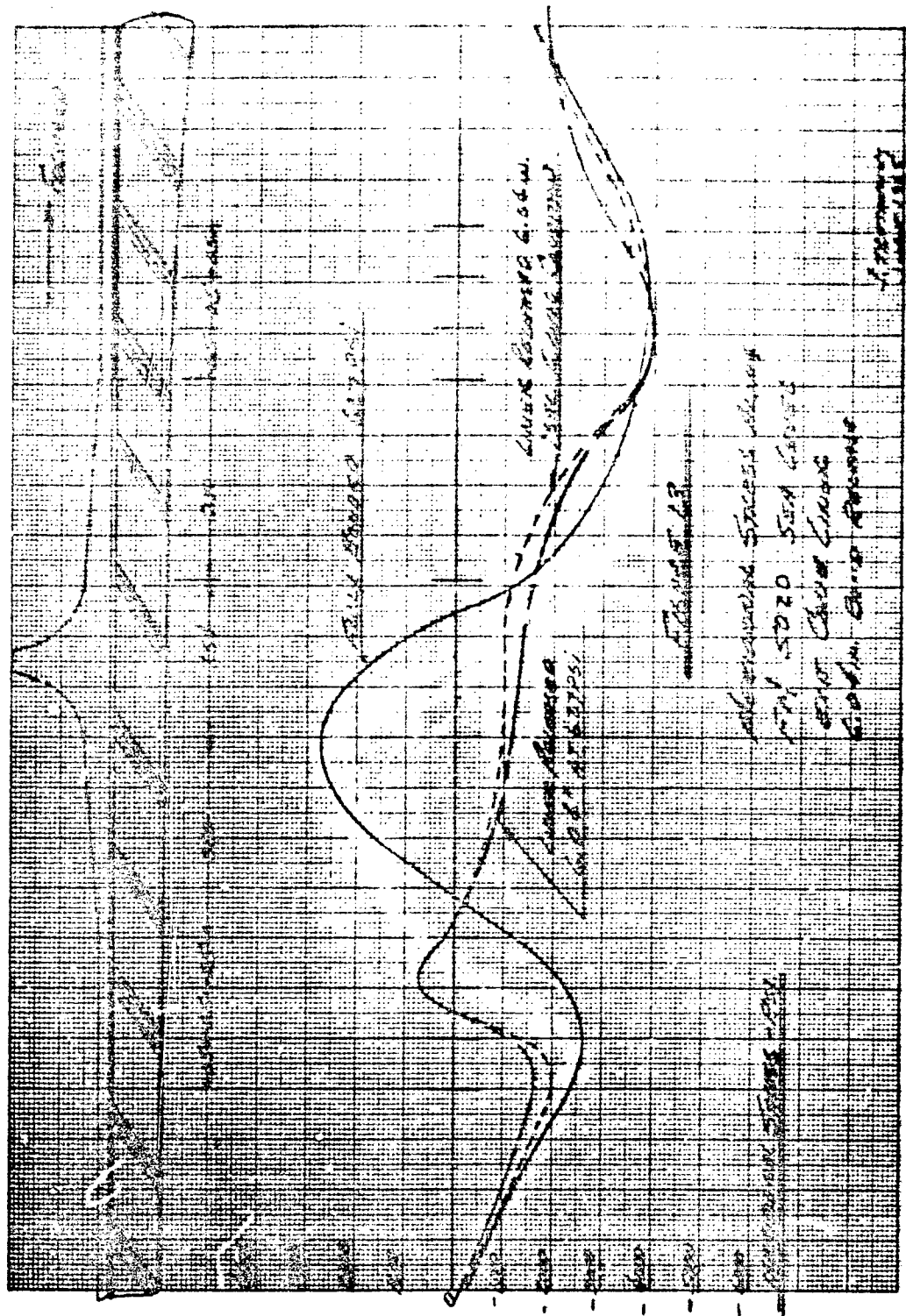
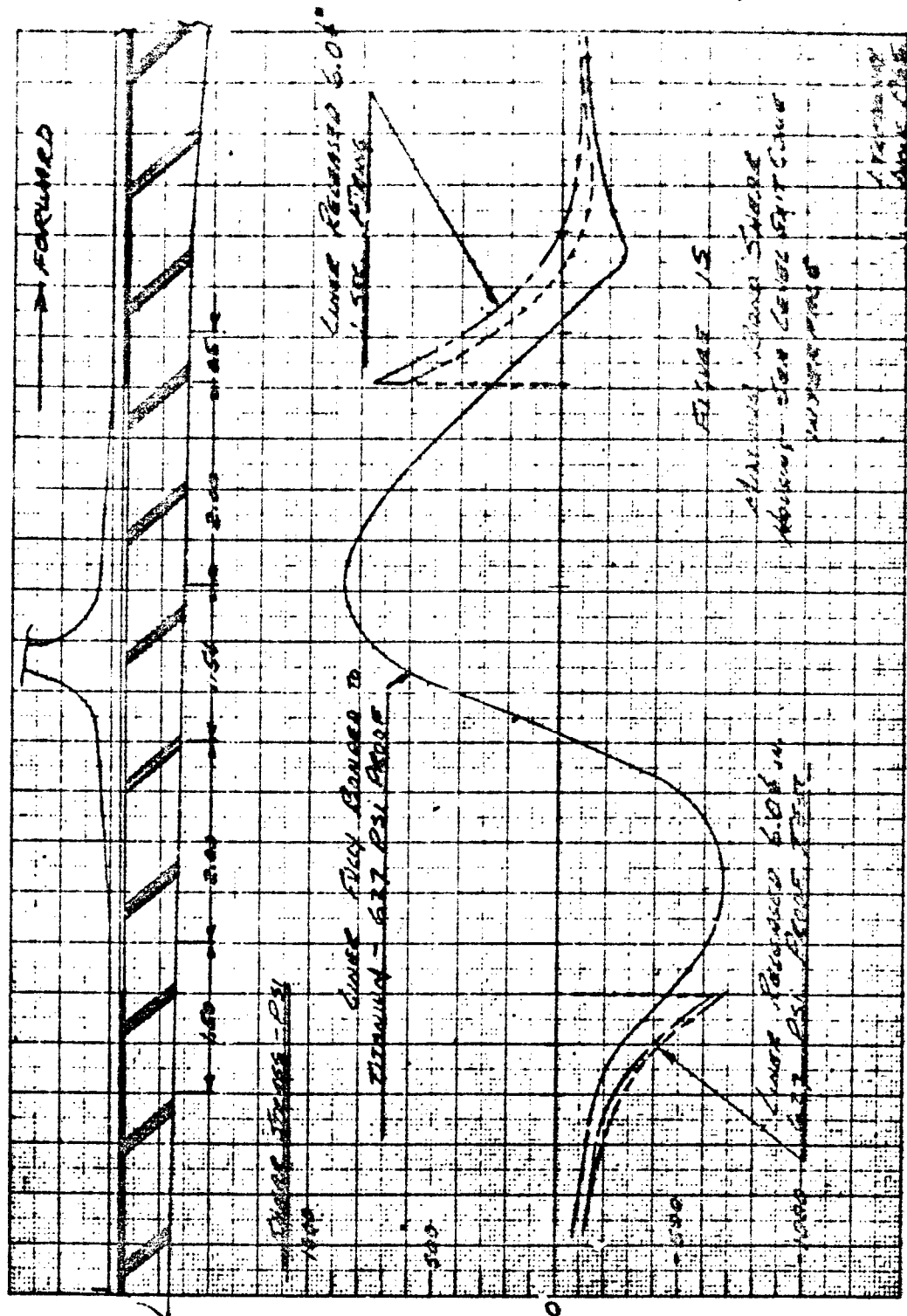


Figure VI-C-13





Maximum Bond Shear Housing--Sea Level Exit Cone Interface

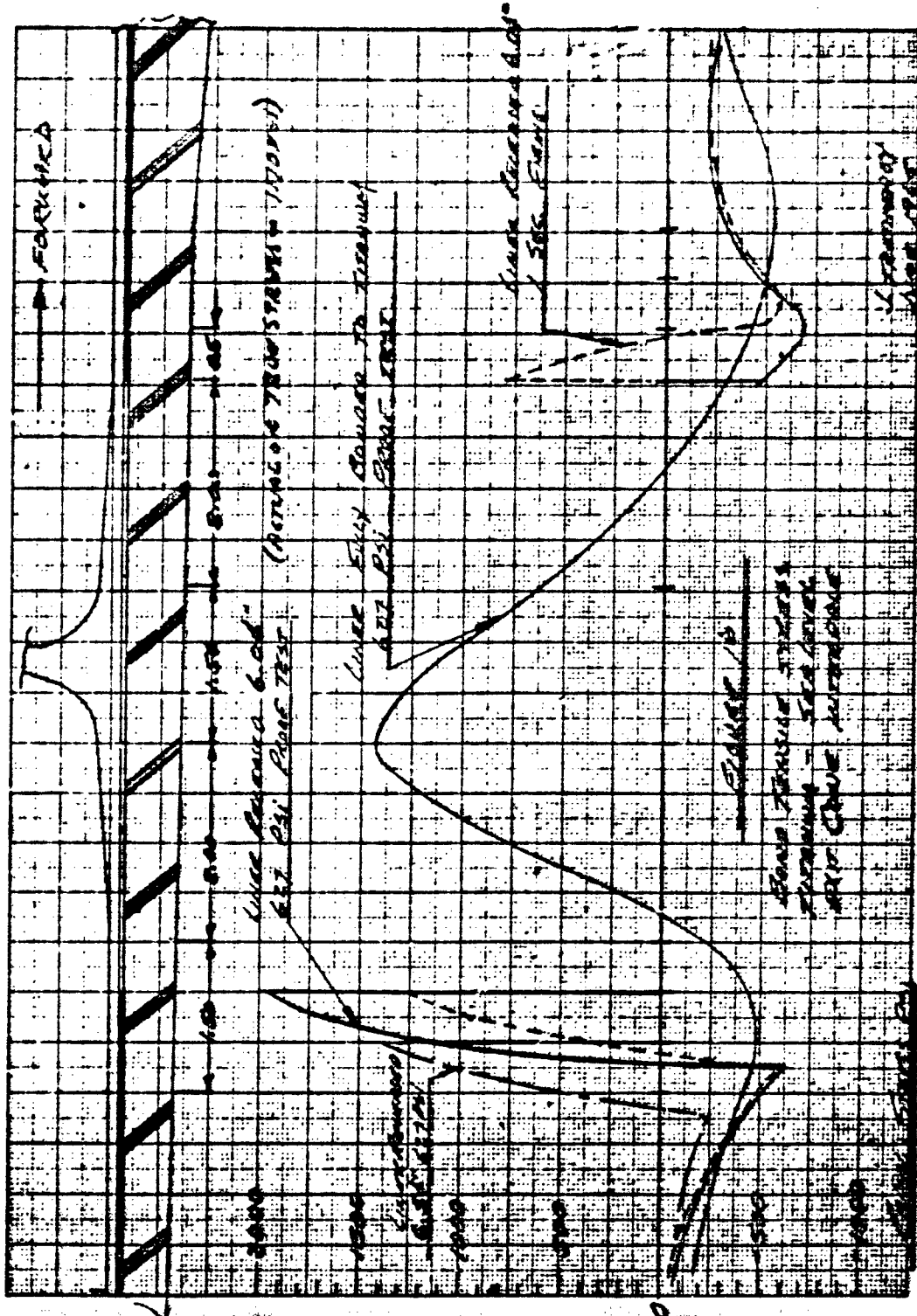
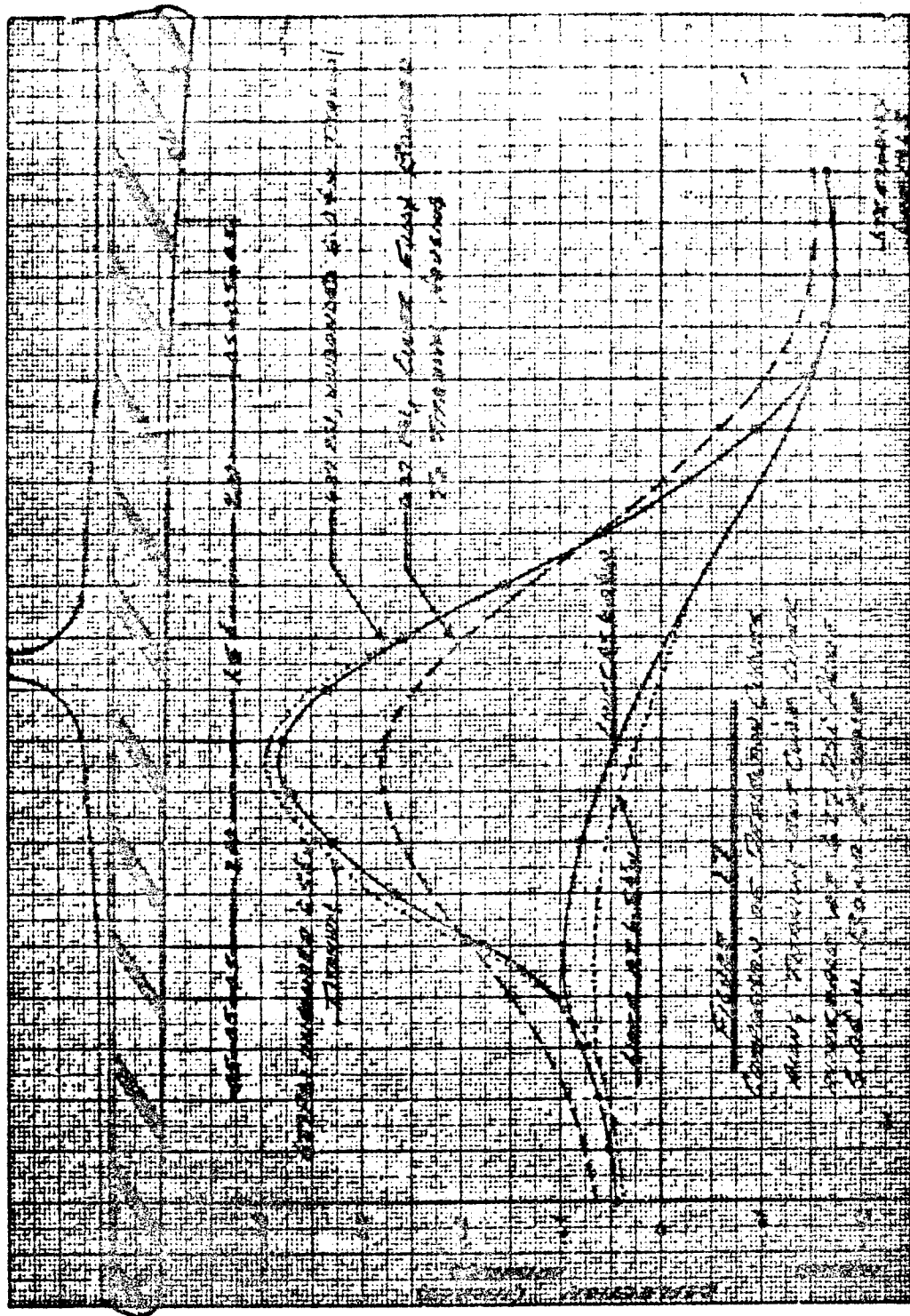


Figure VI-C-16



Comparison of Deflection Curves along Titanium--Exit-Cone  
Liner Interface at 627 psi Proof, 6.04-in. Bond Release

Figure VI-C-17



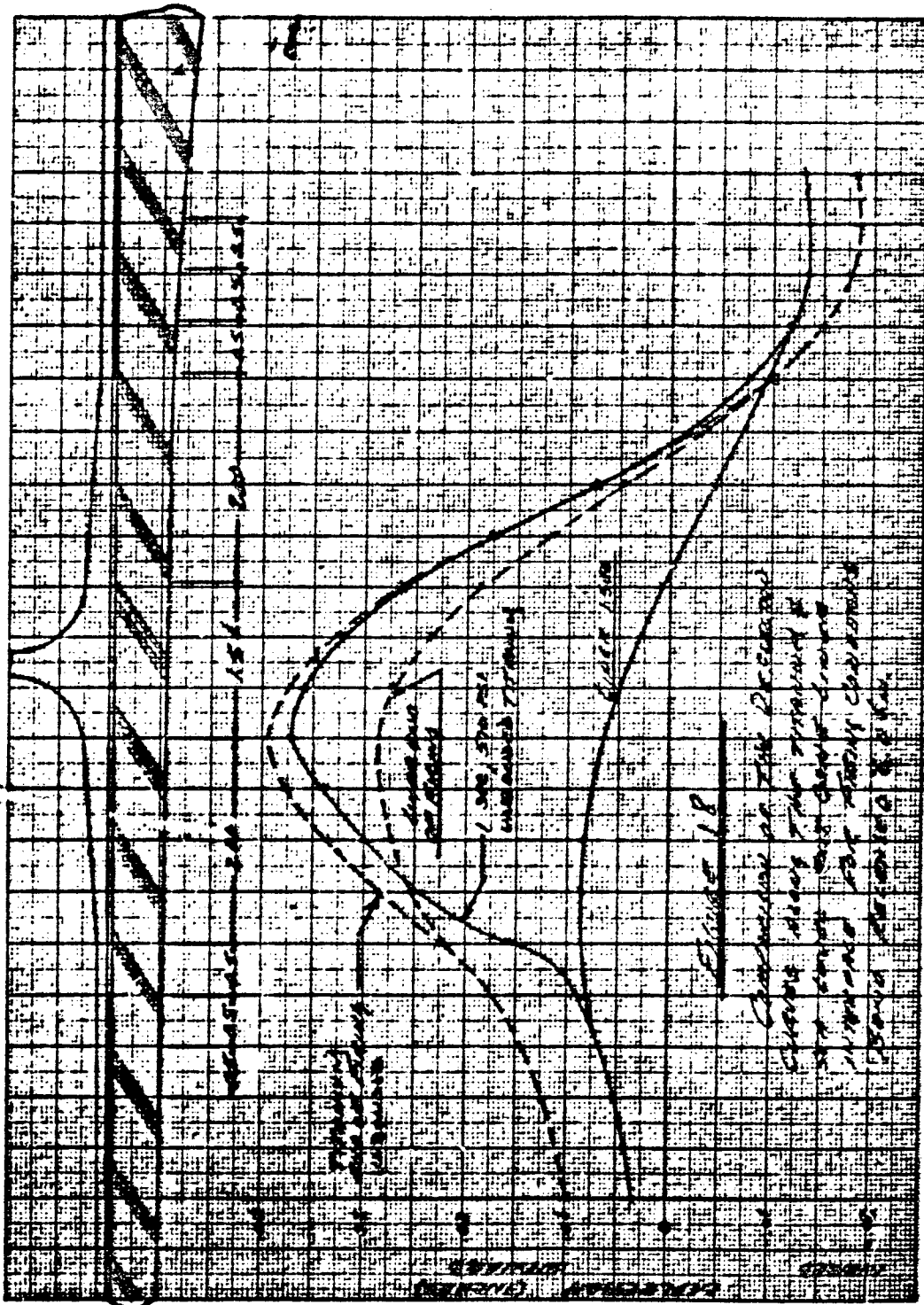
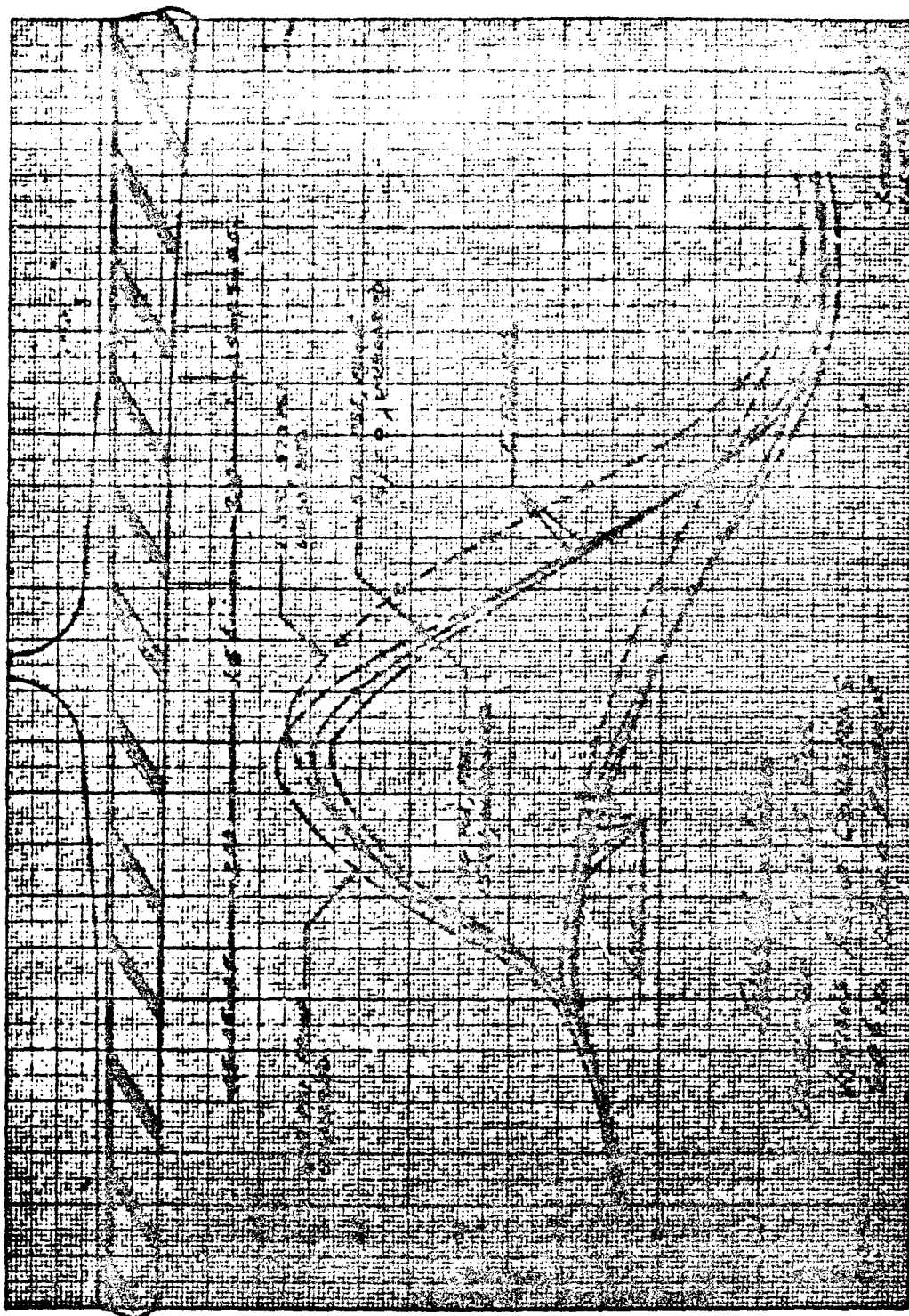


Figure VI-C-18

Comparison of the Deflection Curves along the Titanium and Sea-Level Exit-Cone Liner Interface for Firing Conditions, 6.04-in. Bond Released



### Deflection Curves for Various Proof Conditions, 6.04-in. Bond Release

Figure VI-C-19



VII.

IGNITER INITIATOR MATERIALS-AND-PERFORMANCE EVALUATION--  
PROJECT DIRECTIVE 41-020

The objective of this portion of the program was to demonstrate the performance adequacy of an igniter initiator having an unbonded, solid polyurethane-foam spacer in place of the current perforated bonded spacer.

A. TASK DESCRIPTION

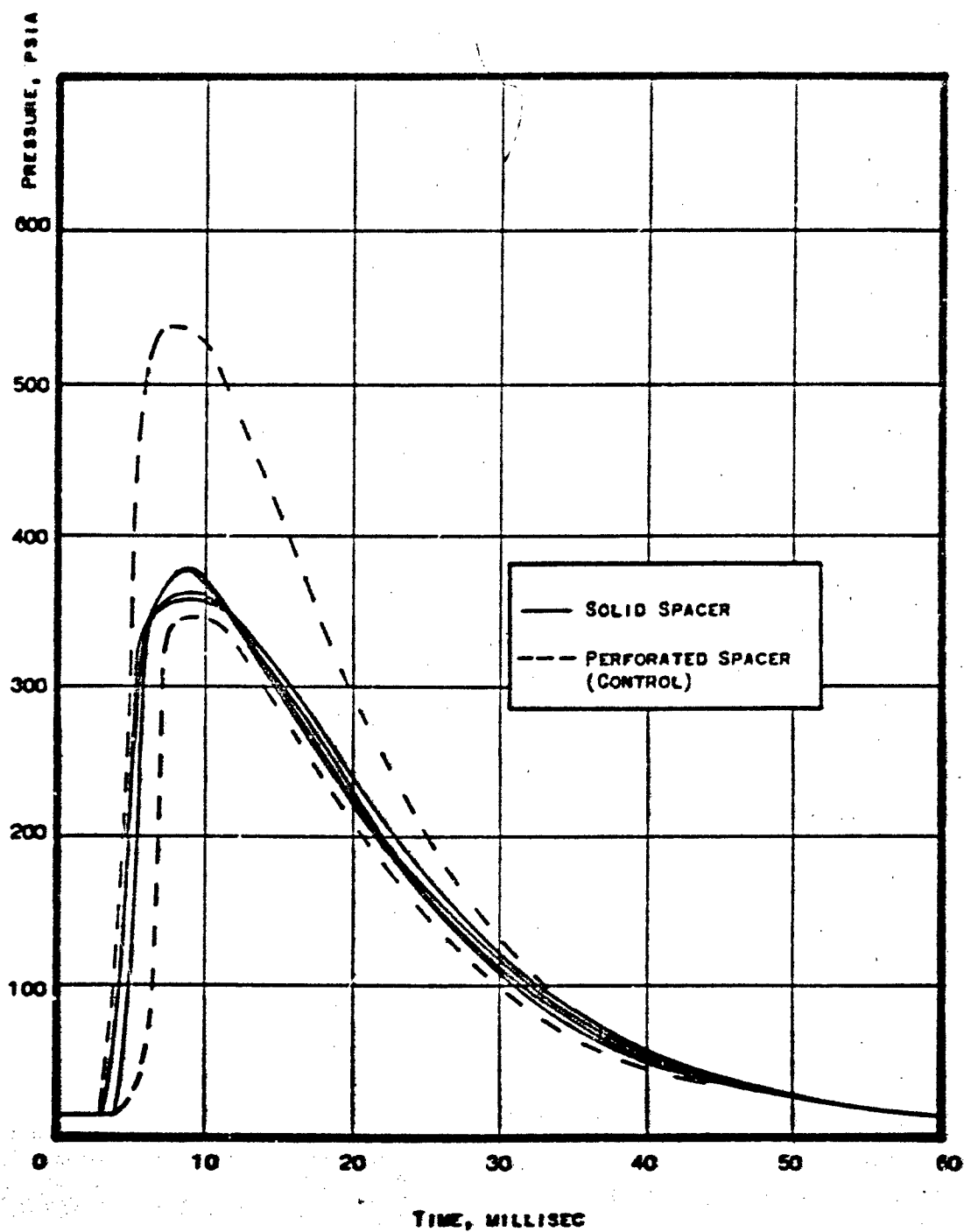
Six igniter assemblies were prepared from standard Wing VI Minuteman igniter hardware. Firing-train test fixtures were used in accordance with the requirements of Project Directive 41-020 of Report 0162-06PS-2. These six units were loaded with the standard 40-gm BPN-2A pellet initiator charge. Two initiator units were assembled with standard polyurethane-foam rings (PN 367273) for control purposes. The remaining four initiators had solid, unbonded, 2.30-in.-dia by 0.50-in.-thick AMS-3570 polyurethane-foam cushions. Each unit was serialized and coordinated with oscillograph recordings.

The initiators were fired into blank igniter chambers that were fitted with aft closures and burst discs to simulate the actual igniter configuration. The six units were fired as a lot at ambient temperature and pressure conditions. The performance of each of the six units is plotted in Figure VII-1 for comparative purposes.

B. CONCLUSIONS AND RECOMMENDATIONS

The four initiators having the solid foam cushions performed adequately and demonstrated good reproducibility. As shown in Figure VII-1, the control initiators that were equipped with the standard rings demonstrated a wide variance, or spread, in their respective performance curves. No explanation of this spread can be made at this time; however, the spread is typical of previous lot-to-lot variations in initiator performance. No indication of excessive stresses in the initiator hardware was observed during postfiring examination.

Based on the performance of the solid foam spacers, it is concluded that the objectives of the program were met. However, since the exact causes and effects of spacer degradation on normally aged and accelerated aged items are not known, additional studies are required before modification of the Wing VI igniter initiator foam spacer can be recommended.



Igniter-Initiator Pressure-vs-Time Curves

Figure VII-1

VIII.

CHARACTERIZATION OF PYROTECHNIC IGNITION PROPERTIES--  
PROJECT DIRECTIVE 41-022

A. SUMMARY

The objective of this program was to characterize the ignition properties of advanced propellants, propellant blends, and pelleted-form pyrotechnics. Of primary interest were pyrotechnics having wide temperature- and altitude-range capabilities.

Arc-image furnace testing was used to determine the time to ignition (at a constant heat flux and at variable pressures) for the propellant and propellant blends. The resultant data were then used to determine the variation in ignition properties resulting from burning rate, oxidizer ratio, and binder type for the propellant and propellant blends testing. Closed-bomb tests were used to characterize the pyrotechnic pellet output.

B. TECHNICAL DISCUSSION

1. Propellant and Propellant Blends

Various propellant samples were prepared for arc-image furnace testing in accordance with the requirements of the project directive. All propellant tests, except those for the beryllium (Be) propellant, were conducted at Hill AFB by the Material Test Section of the 2705th Airmunitions Wing; the Be propellant sample was tested at the Bermet Powder Company facilities, Saugus, California.

a. Arc-Image Furnace Testing of Minuteman Propellant

Tests at Hill AFB were made of samples of Minuteman Wing VI ANB-3066 and of one sample of Polaris A3 propellant. Variations in blending and properties of the propellants tested are shown in Figure VIII-1. The test temperature was  $72 \pm 2^\circ\text{F}$ , and testing was conducted in an inert atmosphere. The arc-image furnace heat flux was  $70 \text{ cal/cm}^2\text{-sec}$ . The general objectives of the program were met; the pertinent correlations concerning the effect of oxidizer ratio, binder type, and liquid strand burning rate (LSBR) that were determined are discussed below.

Factors affecting threshold ignition time were investigated using Aerojet computer program AS261U (one-way multiple co-variance analysis). The polybutadiene (by vendor), absolute pressure (log transformed), LSBR, and oxidizer ratio were correlated with ignition time (log transformed).

Data from this study showed different relationships with the polybutadiene from the two vendors (significant at the 0.014 level). For both vendors materials, the effect of pressure was significant at the 0.000 level. For

VIII, B, Technical Discussion (cont.)

Phillips polybutadiene, LSR and oxidizer ratio had marginal effects (significant at the 0.12 and 0.06 levels, respectively). For GT&R polybutadiene, LSR was significant at the 0.001 level but oxidizer ratio was not significant. The lack of correlation with oxidizer ratio may be a result of a very narrow range of this variable for the GT&R data.

A linear relationship of the threshold ignition time with the above variables was also investigated but this correlation was less conclusive. The effect of pressure on the threshold ignition time is shown graphically in Figure VIII-2.

Hill AFB personnel who conducted the testing misinterpreted the test requirements. Instead of testing at the requested 0, 0.15, 0.25, 0.50, 1.0, and 3.0 atmospheres, the tests were performed at 0.85, 1.0, 1.1, 1.35, 1.85, and 4.85 atmospheres; the ambient atmosphere condition at Hill (4450-ft elevation) was used for the zero atmosphere reading.

The data are still of value inasmuch as the exhaust gases from the motor igniter are capable of inducing a pressure inside the case regardless of ambient conditions. For the Wing VI second-stage motor this value is approximately 20 psia at vacuum conditions. The arc-image test results are shown in Figure VIII-3.

b. Arc-Image Furnace Testing of Be Propellant

The Be propellant (Lot G5-Be-53) was tested at Bermite Powder Company facilities. Because of the low flame temperature of the propellant (with respect to radiant energy) it was found difficult to determine time to ignition at the two lowest pressure levels (0 to 0.15 and 0.25 atmospheres). The results of the arc-image testing are shown in Figure VIII-4. (Comparison of results for the propellants tested show that at the same pressure the threshold ignition time of Be propellant is approximately double that of CTPB propellant.)

c. Expected and Observed Ignitability of ANB-3066 Propellant

Based on arc-image furnace data from Stanford Research Institute and ignition studies performed by the Aerojet Propellant Ballistics Department (4521), good correlation between the predicted (arc-image) and observed ignitability of ANB-3066 propellant for cast to RTV-60 surfaces has been demonstrated with respect to full-scale Wing VI motors. In the case of the Wing VI igniter, however, the expected difference between "cast to RTV-60" and "cut surfaces" has been the reverse between expected and observed performance, i.e., cutting or scraping the propellant surface after casting has improved the ignitability of the propellant. The reason for variation in expected and observed differences in the igniter can be attributed to:

VIII, B, Technical Discussion (cont.)

(1) Variations in oxidizer blends that produce a fuel rich propellant surface, which is more difficult to ignite.

(2) Differences in the mode of heat transfer to the propellant surface in the igniter, motor, and arc-image furnace which made correlation difficult.

(3) Lack of ignitability data at the high pressures and high heat fluxes experienced in the igniter.

2. Pelleted-Form Pyrotechnics

The closed-bomb experiment was used to determine certain ballistic properties of boron-potassium nitrate (BPN) and magnesium-tetrafluoroethylene (Mg-TFE) pellets. Parameters measured were the effective force constant ( $f$ ), the burning rate ( $r$ ), and the effective ratio of specific heats ( $\gamma'$ ). The volumetric loading density of each pellet configuration was also determined, and several heat-flux measurements were made using the vented bomb to determine the heat of explosion of both compositions.

a. Test Apparatus

The JANAF closed bomb used had an initial free volume of 47.6 in.<sup>3</sup> The BPN charges were contained in finger cots and charge ignition was provided by a Hercules S11-A2 squib and a 400-milligram, BPN-powder booster. This technique proved to be inadequate for ignition of the Mg-TFE pellets; consequently, an additional series of tests was conducted to determine the best method for containing and igniting these pellets. A glass-cloth bag with a Hercules S11-A2 squib and a 400-mg BPN powder booster was ultimately used. Pressure measurements were made at charge weights of 5, 15, and 25 gm for each pellet configuration of both the BPN and Mg-TFE compositions.

The BPN pellet configurations tested were: (1) the 2A, cylindrical shape, 0.125-in. dia by 0.188-in. long; (2) the 2D, aspirin-tablet shape, 0.250-in. dia by 0.130-in. bi-convex; (3) the 2M, cylindrical shape, 0.125-in. dia by 0.100-in. long; and (4) the 2E cylindrical with convex ends, 0.250-in. dia by 0.350-in. bi-convex. The Mg-TFE pellet configurations tested were the 3D, 3E, and 3L. The 3D and 3E had the same dimensions as the 2D and 2E, respectively, and the 3L was of aspirin-tablet shape, 0.500-in. dia by 0.250-in. bi-convex.

b. Test Procedure

Tests were made in order of descending charge weight (i.e., 25, 15, and 5 gm); two tests per charge weight were conducted. Prior to each test the bomb was purged with nitrogen gas to remove solid or gaseous residue.

VIII, B, Technical Discussion (cont.)

As determined in testing, ignition train (only) firings in the JANAF bomb pressurized the bomb to 69 psi, which was subtracted from the measured peak pressure for each test.

c. Heat-Loss Determination

To determine the heat-loss characteristics of the JANAF bomb, various charge weights of JPN propellant were burned and the peak pressure measured. From data given in the SPIA handbook, the force constant for JPN was calculated to be  $3.89 \times 10^5$  ft-lb/lb. Using this value, the heat-loss factor ( $\beta$ ) was then calculated using the following equation:

$$F_r = \frac{P_p V_c}{C(1-\beta)} \left[ 1 - \frac{c\eta}{V_c} \right]$$

where:

- $F_r$  = force constant
- $C$  = total charge weight, lbm
- $P_p$  = peak pressure, psi
- $V_c$  = chamber volume, in.<sup>3</sup>
- $\beta$  = heat-loss factor
- $\eta$  = effective co-volume

Various charge weights of JPN propellant then were fired and the fraction heat loss calculated; the results are shown graphically in Figure VIII-5.

The material used for heat-loss determination should have the same duration and peak pressure of the material to be tested. Because JPN has a slower burning rate than BPN or Mg-TFE, it was impossible to obtain similar durations and peak pressures between JPN and BPN or Mg-TFE. A relationship for correcting for the duration and charge in the determination of  $\beta$  has been established as:

$$\frac{\beta}{1-\beta} \sim \frac{(t_o)^{1/2}}{C}$$

where  $t_o$  is the total time from start of pressure rise to peak pressure, and  $C$  is the weight of the charge. It should be noted that any error involved in the value of  $\beta/(1-\beta)$  is diminished when carried over to the final calculation of the force constant.

VIII, B, Technical Discussion (cont.)

d. Test Results

The pertinent data from the BPN and Mg-TFE tests are presented in Figures VIII-6, -7, and -8.

(1) Effective Force Constant

The average effective force constant for BPN is  $9.97 \times 10^4$  ft-lb/lb and for Mg-TFE it is  $3.77 \times 10^4$  ft-lb/lb. The force constant was calculated without using a co-volume correction. At these relatively low pressures, the correction would amount to less than 1%.

(2) Burning Rate

The test data for the BPN show that the time to peak pressure varied over a relative narrow range while the peak pressure varied approximately 1000 psi. This indicates that the burning rate of BPN is nearly insensitive to pressure. The BPN burning rate vs-pressure plot is shown in Figure VIII-9. The burning rate exponent (n) is 0.11, which agrees with the manufacturer's handbook value of 0.10; the complete expression is  $r = 0.65 p^{0.10}$  in./sec. The expression derived from the test data is  $r = 0.624 p^{0.11}$  in./sec.

The Mg-TFE burning rate-vs-pressure plot is presented in Figure VIII-10. The burning rate of this material appears to be completely insensitive to pressure between 70 and 400 psi. The manufacturer's expression for burning rate between 88 and 20,000 psi is  $r = 1.04 p^{0.033}$  in./sec.

(3) Effective Ratio of Specific Heats

The heat of combustion (Q) of BPN is 1645 cal/gm. Using this value and a value of the force constant ( $F = 9.97 \times 10^4$  ft-lb/lb), the effective ratio of specific heats ( $\gamma'$ ) is calculated to be 1.043. The heat of combustion, (Q) of Mg-TFE is 1500 cal/gm. Using this value and a value of  $3.77 \times 10^4$  ft-lb/lb for the effective force constant, the  $\gamma'$  for Mg-TFE is calculated to be 1.018. These low values of  $\gamma'$  are the result of condensed material in the combustion products.

(4) Heat of Explosion

Heat-flux measurements were made in a vented chamber instrumented with two ATL gold-button calorimeters and two Taber Teledyne pressure transducers. A 17-gm charge of Mg-TFE 3L pellets and a 17-gm charge of BPN 2L pellets were burned in an igniter chamber and the combustion products vented into the instrumented chamber. Analysis of the calorimeter records gave a value for the total delivered energy (q). These data were then applied to the equation

VIII, B, Technical Discussion (cont.)

$$q = 0.0288 Q \left(\frac{R}{X}\right)^{0.2} \left(\frac{\dot{m}}{A_p}\right)^{0.8}$$

where:

$Q$  = heat of explosion, Btu/lb

$g$  = dynamic viscosity, lb/ft-sec

$\dot{m}$  = igniter mass flow, lb/sec

$A_p$  = port flow area, ft<sup>2</sup>

(5) Conclusions

Data indicate that while both BPN and Mg-TFE are nearly insensitive to pressure, the BPN would be the desirable pyrotechnic because:

(a) The effective force constant for BPN is approximately double that of Mg-TFE.

(b) The heat of explosion is higher for BPN.

(c) Mg-TFE requires closer confinements and higher flux for ignition and sustained combustion.



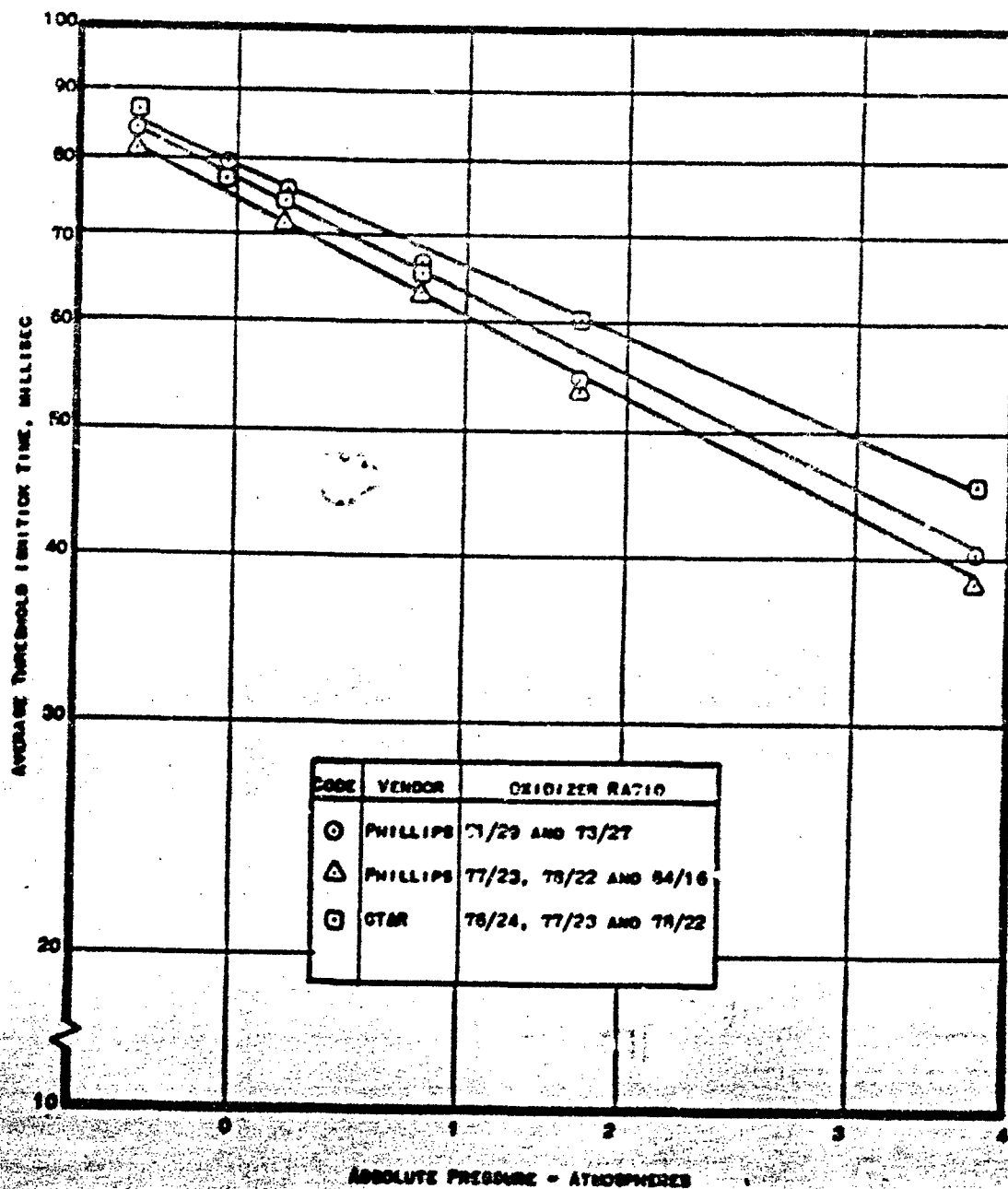
Report 0162-06TTR-9-Vol 2.

Propellant Batch	Polybutadiene Manufacturer	Oxidizer Ratio, % Ung: % HEMP	Liquid Strand Burning Rate, in./sec	Oxidizer Blend No.	Surface Condition of Sample
17-DU-70	Phillips	72:28	0.335	5165	Cut
17-DU-41	Phillips	73:27	0.320	5152	Cut
17-DU-77	Phillips	77:23	0.332	5170	Cut
17-DU-83	Phillips	84:16	0.326	5170	Cut
17-DU-74	GT&R	77:23	0.321	5152	Cut
17-DU-81	GT&R	76:24	0.326	5165	Cut
17-DU-88	GT&R	78:22	0.331	5170	Cut
ANP-2969*	--	---	---	--	Cut
FTM-003-3	Phillips	85:15	0.327	5170	Cast to RTV-60
PR-004-10	GT&R	78:22	0.316	5170	Cast to RTV-60
PR-004-67- 7-AP 6-24	GT&R	78:22	0.329	5170	Cast to RTV-60

\*For comparison purposes (Stage I Polaris A3 propellant).

Propellant Blending and Properties Variations

Figure VIII-1



Effect of Pressure on Threshold Ignition Time

Figure VIII-3

Report 0162-06TDR-9-Vol 2

<u>Propellant Batch No.</u>	<u>Sample No.</u>	<u>Test Chamber Pressure, Atmos*</u>	<u>Threshold Ignition Time, millise</u>
17-DU-70	1A	3.00	38
		1.00	54
		0.50	62
		0.25	80
		0.15	82
		0.00	85
17-DU-70	1B	Same as above	40
			55
			64
			75
			81
			87
17-DU-41	2A	Same as above	40
			56
			68
			73
			77
			84
17-DU-41	2B	Same as above	45
			54
			73
			74
			75
			79
17-DU-77	3A	Same as above	39
			45
			59
			70
			77
			78
17-DU-77	3B	Same as above	37
			49
			56
			66
			76
			85

\*Add 0.85 atmospheres to account for test procedure.

NOTE: 30 or more samples per block were tested.

Arc-Image Furnace Test Results

Figure VIII-3, Sheet 1 of 3

Report 0152-06TER-9-Vol 2

<u>Propellant Batch No.</u>	<u>Sample No.</u>	<u>Test Chamber Pressure, Atmos*</u>	<u>Threshold Ignition Time, millisec</u>
17-DU-83	4A	3.00	33
		1.00	53
		0.50	69
		0.25	74
		0.15	80
		0.00	82
17-DU-83	4B	Same as above	34
			55
			62
			73
			77
			84
17-DU-74	5A	Same as above	47
			64
			67
			81
			83
			87
17-DU-74	5B	Same as above	48
			66
			68
			79
			85
			89
17-DU-81	6A	Same as above	44
			58
			66
			73
			74
			86
17-DU-81	6B	Same as above	44
			59
			63
			72
			77
			80

\*Add 0.85 atmospheres to account for test procedure.

NOTE: 30 or more samples per block were tested.

Arc-Image Furnace Test Results

Figure VIII-3, Sheet 2 of 3

Report 0162-06TER-9-Vol 2

<u>Propellant Batch No.</u>	<u>Sample No.</u>	<u>Test Chamber Pressure, Atmos*</u>	<u>Threshold Ignition Time, millisec</u>
17-DU-88	7A	3.00	43
		1.00	62
		0.50	66
		0.25	72
		0.15	79
		0.00	85
17-DU-88	7B	Same as above	37
			53
			60
			74
			76
ANP-29C9	Polaris	Same as above	87
			31
			70
			89
			145
PR-004-64- 7-AP6-24	11	Same as above	172
			166
			59
			61
			71
PR-004-10	12	Same as above	75
			75
			76
			55
			62
FIM-003-3	13	Same as above	71
			68
			68
			88
			49
			65
			69
			72
			78
			79

\*Add 0.85 atmospheres to account for test procedure.

NOTE: 30 or more samples per block were tested.

Arc-Image Furnace Test Results

Figure VIII-3, Sheet 3 of 3

Report 0162-06TER-9-Vol 2

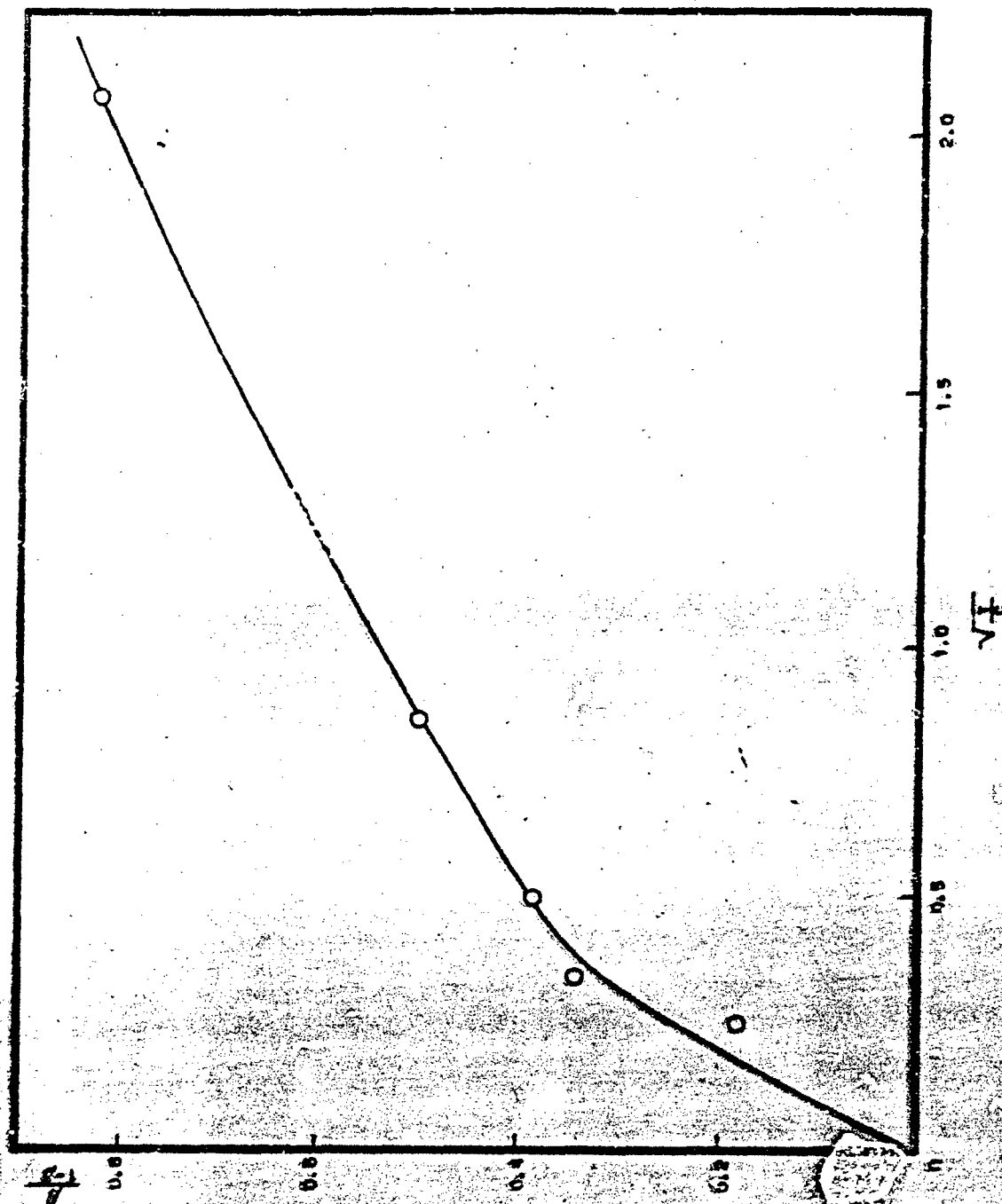
<u>Pressure, Atmospheres</u>	<u>Flux, cal/cm<sup>2</sup>-sec</u>	<u>Average Time to Ignition, millisec</u>
5	70	84.10
5	40	173.75
3	70	87.40
3	40	177.30
1	70	111.20
1	40	194.40
0.5	70	*
0.5	40	185.50**

\*No reducible traces obtained.

\*\*Large spread in data.

Beryllium Propellant Arc-Image Furnace  
Test Results

Figure VIII-4



Heat-Loss Determination, JPN Charge in JANAF Bomb

Figure VIII-5

Report 0162-06TER-9-Vol 2

Pellet Type/ Charge wt., gm	Peak Pressure, $P_p$ , psia	Time to $P_p$ , millisec	Fraction Heat Loss, $\beta$	Effective Force Constant F, x $10^4$ ft-lb/lb	Burning Rate, in./sec
2A/5	147	53.5	0.40	8.89	0.984
2A/5	132	53.5	0.40	7.98	0.984
2A/15	732	45.0	0.27	12.31	1.410
2A/15	658	47.0	0.27	10.90	1.320
2A/25	1045	46.5	0.20	9.48	1.340
2A/25	950	46.0	0.20	8.63	1.360
2D/5	160	65.0	0.41	9.84	1.000
2D/5	161	65.0	0.41	9.90	1.000
2D/15	518	62.0	0.28	8.70	1.040
2D/15	559	55.0	0.28	9.39	1.180
2D/25	928	55.0	0.22	8.64	1.180
2D/25	985	51.0	0.21	9.05	1.270
2M/5	209	40.0	0.38	12.32	1.250
2M/5	213	40.0	0.38	12.08	1.250
2M/15	630	40.0	0.26	10.29	1.250
2M/15	623	40.0	0.26	10.18	1.250
2M/25	1192	42.0	0.20	10.82	1.190
2M/25	966	31.0	0.18	8.55	1.610
2E/5	129	130.0	0.46	8.68	0.960
2E/5	206	90.0	0.43	13.11	1.390
2E/15	727	90.0	0.25	11.72	1.390
2E/15	582	85.0	0.30	10.06	1.470
2E/25	1012	85.0	0.24	9.67	1.470
2E/25	858	86.0	0.25	8.30	1.450

Ballistic Properties of BPN Ignition Pellets

Figure VIII-6



Report 0152-06TDR-9-Vol 2

Pellet Type/ Charge wt., gm	Peak Pressure, $P_p$ , psia	Time to $P_p$ , millisec	Fraction Heat Loss, $\beta$	Effective Force Constant $F$ , x $10^4$ ft-lb/lb	Burning Rate, in./sec
3E/5	95	94	0.44	6.16	1.33
3E/5	73	--	0.49	5.19	--
3E/15	244	85	0.30	4.22	1.47
3E/15	186	95	0.30	3.22	1.32
3E/25	382	105	0.26	3.75	1.19
3E/25	330	85	0.25	3.19	1.47
3L/5	73	125	0.45	4.82	1.00
3L/5	51	*	0.48	3.56	--
3L/15	226	109	0.32	4.02	1.14
3L/15	235	100	0.32	4.18	1.25
3L/25	377	100	0.27	3.74	1.25
3L/25	298	121	0.28	3.01	1.03
3D/5	81	100	0.48	5.66	1.25
3D/5	79	60	0.49	5.62	1.08
3D/15	260	70	0.31	4.55	0.93
3D/15	243	64	0.32	4.33	1.01
3D/25	386	61	0.27	3.84	1.06
3D/25	328	60	0.25	3.18	1.08

\*Uniformity of Pellet ignition questionable.

Ballistic Properties of Mg-TFE Ignition Pellets

Figure VIII-7

Report 0152-06TER-9-Vol 2

<u>Pellet Configuration</u>		<u>Loading Density, gm/cc</u>	
<u>BPN</u>	<u>Nominal Dimensions, in.</u>	<u>Unvibrated</u>	<u>Vibrated</u>
2A	0.125 dia x 0.188 long	0.984	1.043
2D	0.250 dia x 0.130 bi-convex	1.053	1.105
2M	0.125 dia x 0.100 long	1.020	1.164
2E	0.250 dia x 0.250 bi-convex	1.030	1.119

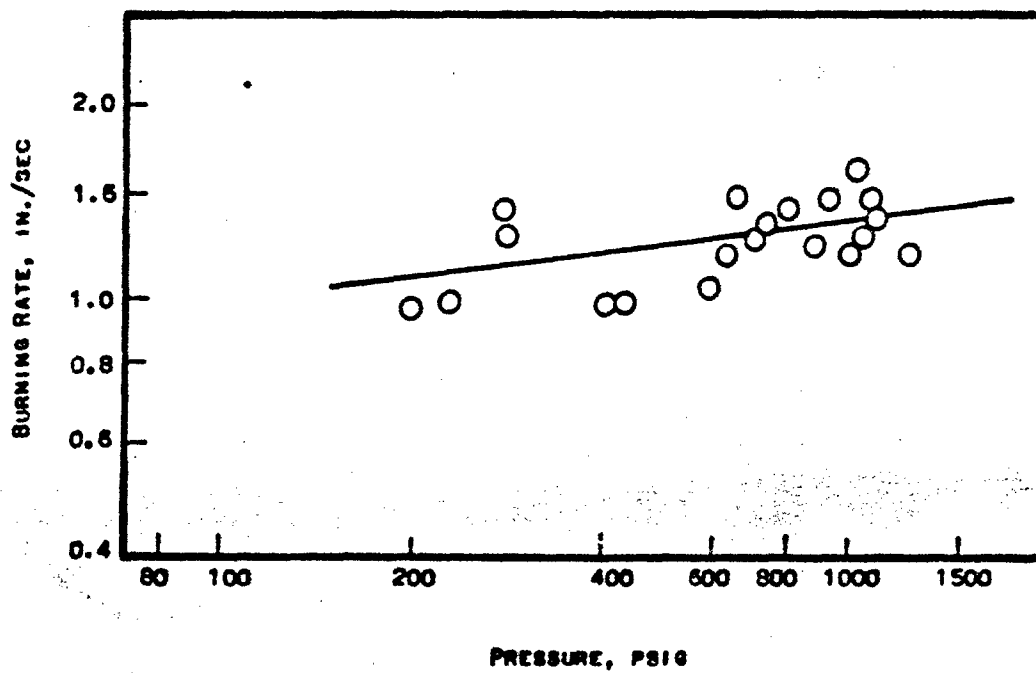
Mg-TFE

3D	0.250 dia x 0.130 bi-convex	0.995	1.115
3E	0.250 dia x 0.250 bi-convex	1.051	1.115
3L	0.50 dia x 0.250 bi-convex	0.968	1.115

\*Measurements made using graduated cylinder, 2.30-in. in dia.

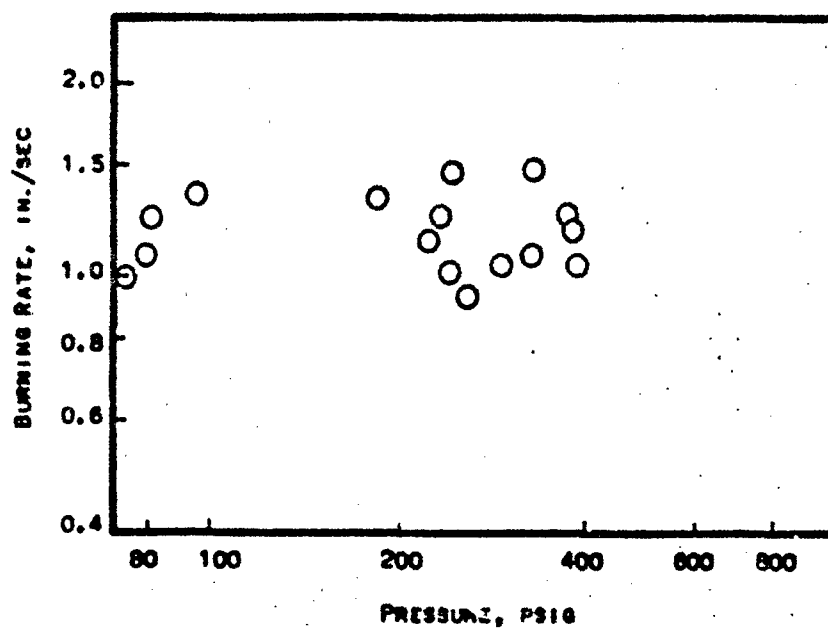
Volumetric Loading Density of BPN and Mg-TFE Ignition Pellets\*

Figure VIII-8



Burning Rate vs Pressure of BPN Ignition Pellets in JANAF  
Closed Bomb

Figure VIII-9



Burning Rate vs Pressure of Mg-TFE Ignition Pellets in JANAF  
Closed Bomb

Figure VIII-10

IX

EVALUATION OF ALTERNATIVE INSULATION MATERIALS--PROJECT DIRECTIVE 41-023

A. PROGRAM OBJECTIVE

The objective of this program was to evaluate recently developed elastomeric compounds that could provide ablation characteristics superior to those of the nitrile compounds presently used. The screening tests used to evaluate these potential materials consisted of tests to determine (1) metal-to-insulation adhesion and (2) ablation characteristics.

B. MATERIALS

The modification of Buna N polymers with various fillers was extensively studied early in the Wing VI program to achieve maximum thermal performance, commensurate with desired specific gravity and other physical properties. The conclusion was reached that the desired combination of properties (dictated by design considerations) was best achieved by the use of the NOL-type formulation. Therefore, it was decided that any investigation of new materials should be directed toward new polymers that could be tailored to conform to the performance requirements of future designs.

Results obtained from a preliminary literature search and vendors indicate that a number of prospective materials exist that could provide performances superior to those of presently used insulators. The literature search was limited to locating materials that had equal or lower density, improved thermal and aging characteristics, materials that exhibited no particular bonding or other processing problems, and which were either commercially available, or were in an advanced state of development.

Four rubber companies, General Tire and Rubber, Goodyear, Goodrich, and U. S. Rubber, known to be actively developing improved internal insulation materials, were contacted at the start of this program; each was requested to submit samples, based on polymers other than nitriles, the processing feasibility of which had at least been demonstrated in laboratory tests. Thus, the assumption was made that the determination of physical properties (hardness, tensile, and elongation) as well as processing evaluations (green building strength and molding tests) had been completed on the samples prior to submittal. Proprietary rights have been reserved on many of the materials submitted and a definition of the compounds is not available. A listing of the materials evaluated is presented in Figure IX-1.

C. TEST METHODS AND RESULTS

1. Adhesion Tests

The adhesion-test samples consisted of 1 x 8 x 0.075-in. 6Al-4V titanium strips to which the insulation material was bonded. The adhesion system used on all samples consisted of H. K. Porter 1127, Chemlok 203 metal primer, and Chemlok 220 adhesive. This system is identical to that used in the Wing VI second-stage motor.

## IX, C, Test Methods and Results (cont.)

Samples were tested in 180-degree peel according to ASTM D903. Ten individual tests were conducted of each material. The adhesion-test results are summarized in Figure IX-2. These results generally indicate that the H. K. Porter-Chemlock adhesive system is adequate for the General Tire and Rubber and Goodyear ethylene propylene polymers; however, use of the other prospective materials would require specifically designed adhesive systems.

### 2. Ablation Tests

Ablation tests were conducted in a plasma-test laboratory. The plasma generator used was a gas-vortex-stabilized design manufactured by the Thermal Dynamic Corporation. The F-80 plasma generator head was used with a power operating range of from 5 to 100 kw. The gas-stream heat flux was determined at the test-sample location prior to each run through the use of a cold-wall calorimeter.

The test samples consisted of 0.5-in.-dia dowels of the insulation material instrumented by the insertion of a 0.001-in. thermocouple through the sample at 0.060 and 0.180 in. from the exposed surface. These assemblies were then potted to a diameter of 1.0 in. with room-temperature-vulcanizing silicone rubber. The ablation tests were conducted at cold-wall heat fluxes of 27, 50, and 100 Btu/ft<sup>2</sup>-sec.

Ablation test results are summarized in Figure IX-3, which shows the ablation rate vs the heat flux, with the current Wing VI insulation material, GTER V-45, included for comparative purposes. Two ethylene propylene-based materials exhibited ablation characteristics superior to those of GTER V-45. Not as a result of this study, but based on previews of technical literature,\* the two butyl acrylics from Goodyear may provide aging advantages when used in low heat-flux environments.

### D. CONCLUSIONS

The ethylene-propylene terpolymers, as a class of insulation binders, could provide significant weight decreases in the Wing VI second-stage Minuteman motor.

In addition to having superior ablation characteristics, the adhesion of the ethylene-propylene materials to metal substrates does not appear to be a problem. In addition, a further advantage may be gained through the use of these insulation materials since ethylene-propylene costs are approximately 30% of the conventional nitrile rubbers.

This program has provided data demonstrating the significant differences in ablation characteristics of several elastomeric binders and fillers currently being developed. It is recommended that this effort be continued to maintain contact with the rubber industry toward ensuring product advancement.

\*"Engineering Elastomers," Product Engineering, January 8, 1962

"Elastomers," (A Supplement to Design News, March 31, 1965)

"Specialty Elastomers," Materials in Design Engineering, August 1965

"Polyacrylate Elastomers Attract New Interest," Chemical and Engineering News, November 18, 1963

Report 0162-06TDR-9-Vol 2

IX, D, Conclusions (cont.)

<u>Company</u>	<u>Designation</u>	<u>Polymer</u>
General Tire and Rubber	3096	Ethylene Propylene
B. F. Goodrich	570-72-55-1	Butyl Acralate/Acrylonitrile
	570-72-55-2	Butyl Acralate/Acrylonitrile
	570-72-55-3	Acrylonitrile/Polyvinyl chloride
Goodyear	M-500	Nitrile-Boric acid filled
	D-270-D458	EPR - Carbon filled
	D-270-D454	EPR - Silica filled

Prospective Insulation Materials

Figure IX-1

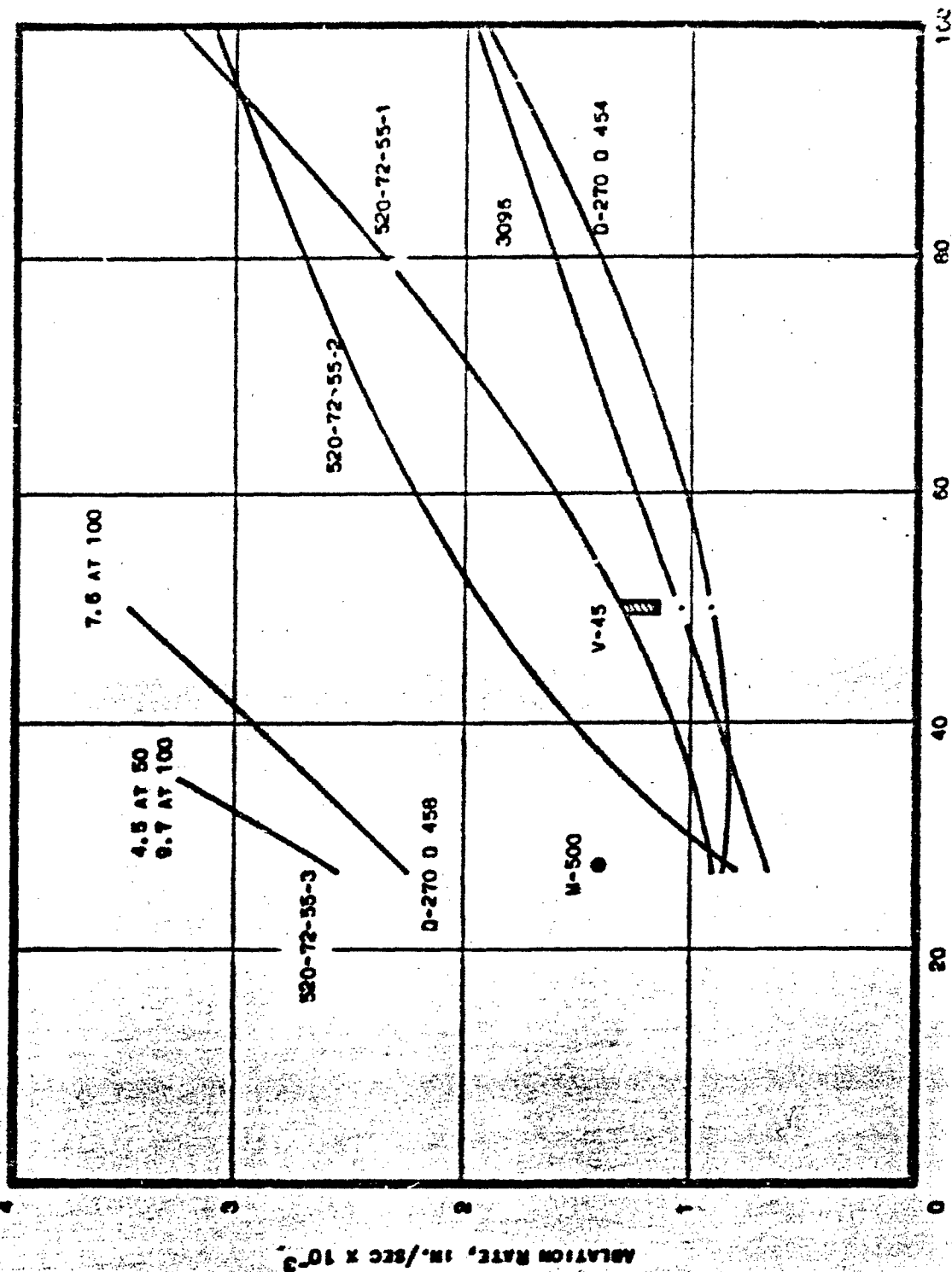
Report 0162-06TDR-9-Vol 2

<u>Material Designation</u>	<u>Average Peel, lb/in.</u>
3096	115.0
520-72-55-1	4.2
520-72-55-2	12.3
520-72-55-3	77.0
M-500	71.0
D-270-D458	44.0
D-270-D454	88.0

Metal Adhesion Test Results

Figure IX-2





Heat Flux,  $Btu/ft^2$ -sec Ablation Rate vs Cold-Wall Heat Flux

Figure IX-3

X.

ROLL-CONTROL VALVE TRANSDUCER TESTING--PROJECT DIRECTIVE 41-025

A. INTRODUCTION

The roll control valves in the Wing VI second-stage motor are subjected to several operational inspections from the time of fabrication to prelaunch checkout, using various procedures and different types of equipment. There is poor correlation between the inspection data obtained at each inspection point; Space-General, Aeronautronics, Aerojet-General-Sacramento, ETR, MAB, and launch facility. The differences in the data obtained at MAB and the launch facility were such that four valves out of a particular group of eight roll systems would be rejected for being below specification limits and an additional three valves were in the zone between acceptable and clearly rejectable. This would have been four out of eight potential flight cancellations.

The lower tolerance limit on the transducer CW output illustrates the magnitude of the problem. The nominal output is 5.00 v. The ICD minimum is 5.016 v which is 484 mv below the nominal. The observed differences from Aerojet to AVE equipment are on the order of -400 mv. Because of tolerance buildup, this would cause a high "No-Go" rate if the system were operational. The observed variation on AGE is  $\pm 170$  mv. There is also a bias from Aeronautronics equipment to AGE of approximately 140 mv which is positive or negative depending upon the type of transducers in the valve.

B. CONCLUSIONS AND RECOMMENDATIONS

The variation in transducer outputs between sites is caused by differences in equipment and conditions and not by the transducers. These differences can be either in the applied excitation or in the loading effect on the transducer output. Test results have shown that the applied excitation is not the major problem on AVE. Based on these conclusions, the following recommendations are made.

1. Data obtained from AGE can be improved by incorporating an improved and standardized calibration procedure in which a standardized simulator or dummy load is used. In this procedure the test set readout dials would first be set to a predetermined reading and with the simulator connected, the 26vac power supply would be adjusted for a test set null indication. Periodic cross checks from one site to another should also be required. Figure "A" Item 17106 has been designed as a load for the test set for use at OQAMA. It is recommended that it be revised to be used as a simulator. This change will not impair its original function. Additional quantities of this simulator would be required for each site using the AGE test set.

2. It is recommended that the revised Figure "A" Item 17106 be used at Autonetics.

3. AGE checkout equipment should be used at Aeronautronics for valve check prior to delivery. This will require three additional AGE test sets.

X, B, Conclusions and Recommendations (cont.)

4. The acceptance of valves at Aeronautronics using the AGE test set and checkout values established during Task 25 is recommended. The data and testing performed has demonstrated the capability of meeting specification and ICD requirements. The revised procedure is described in Section X,F.

If a minimum limit of 5.400 v is used at Aeronautronics, 15.6% of the Kavlico valves can be expected to be outside of the current Aerojet specification limits when tested on other AGE.

5. The computer band limits should be changed to have the computer reject on the basis of failure of both solenoids on one side, i.e., null. This would require an ICD between Aerojet and Autonetics for null only and would result in an effective loosening of the transducer adjustment. Based on preliminary data the ICD could be from 1.60 to 4.40 v.

An additional ICD would be required for the "go" limits. This value would be based on the null limits and the Autonetics band for computer resolution, variability, etc. The "go" ICD limit would be measured on Aerojet AGE only and could be 4.90 v CW and 1.10 v CCW. The corresponding Aerojet component specification values would be 5.20 and 0.90 v, respectively.

The above is based on null calculations shown in Figure X-1 and assumed Autonetics values. Additional testing in the null position would be required. These recommendations are alternatives to Item 4.

6. Aeronautronics will be directed to proof test and perform an electrical check prior to spot welding the transducer in place.

7. Elimination of the Kavlico valve from the next procurement is recommended. The Schaeffert design is more uniform. This will also ease the calibration, setting, and adjustment required between Aeronautronics equipment and AGE by permitting use of a standard procedure.

8. New AGE limits for Aeronautronics are recommended.

9. The above items, 1 through 8, would require appropriate RFP action.

C. PROGRAM

A program was established to determine characteristic patterns and variabilities of the various pieces of equipment. Objectives of the program were to:

1. Determine the source of variation in roll-control valve position transducer data.

2. Recommend changes in drawings, specifications, flight hardware, or AGE to provide acceptable performance of the position transducer system.

X, C, Program (cont.)

The program included the following:

1. Ten roll-control valves; five each with Schaevitz and Kavlico position transducers, were tested at Aeronautronics, SGC, Aerojet, HAFB, ETR and ETR MAB to begin the study. The results of these tests (Figures X-2 through -24) established that there were differences in the data obtained from each facility. To verify the differences observed in the valve test results, a dummy load was designed, built, and shipped to each facility. Similar differences were observed in the data obtained with the dummy load. This indicated a need for improving the calibration procedure for the AGE.
2. Special tests were also conducted to determine the effects of the significant variables: excitation voltage, solenoid voltage, temperature, AGE variability and repeatability, and energization time.
3. An investigation was conducted to determine differences between the AGE and the AVE from data available to Aerojet. No obvious cause for the differences could be determined from this data and a more extensive investigation will be required.
4. Calibration of the square wave was also studied. This included measurement of the Aerojet test set and an R&D P-90 unit. These tests showed a deviation in the AGE of 0.6% or less, depending on warmup time; and a deviation in the P-90 of 0.5% or less. Details of calibration of a square wave are contained in Section X, G.
5. The AGE drawings were reviewed and found to be in agreement with the ICD.
6. Eight valves which were rejected by SGC were returned to Aeronautronics to determine if the valves could be reworked. Removal of transducers that are spot welded in place was proved to be feasible.
7. Identification of all problems involving equipment that Aerojet has direct responsibility for within the scope of the task outline was accomplished.

D. ANALYSIS

Variability between voltage output readings have been relatively large for the same valve from one location to another. On the average, the largest difference in AGE equipment was 0.122 v, transducer CW output, between Aerojet Receiving Inspection and HAFB. The largest difference in individual readings was 0.160 v, CW output, between Aerojet Line 1 and HAFB. These same valves were retested at HAFB on five additional pieces of AGE and the variability increased on the average to 0.172 v for the CW position. The valves increase and decrease in output voltage in groups, indicating the variability is probably a result of personnel, test set, and temperature differences at the various locations. Generally the same valve variabilities are observed with each test system. Differences at ETR were more pronounced. The maximum

X, D, Analysis (cont.)

average difference in Kavlico units between Autonetics Lab, GTM-060, and MAB was 0.272 CW v. The largest difference in output voltages were between AGE and missile checkout equipment. These differences were in the average magnitude of 0.406 v for CW readings, between HAFB and MAB at ETR for Kavlico units and 0.318 v CW readings for Schaevitz units at the same locations.

The CCW voltage readings also varied but were not quite as much as the CW voltages. Figures X-2 and -3 are line graphs depicting the output voltages at the different locations. Figures X-4 and -5 are histograms of output voltages at the various test sites. Data from the retested valves at HAFB are not included in the histogram but are shown in Figures X-2 and -3. Figures X-6 and -7 show that the standard production valves and the special "Task 25" valves are from similar populations.

The special tests performed at different locations were used in the analysis to determine how different factors affect the overall variability. The following variables were considered ( $\bar{b}$  referenced in the figures represents average slope of the "Task 25" valves,  $\sigma$  is the standard deviation of the slopes,  $\bar{b} \pm 3\sigma$  gives the  $3\sigma$  minimum and maximum values of the slope).

1. Transducer Output, CW, versus Excitation Voltage  
(Figures X-8 and X-23)

The test data, CW readings, indicate a very good correlation between excitation voltage and transducer output voltage. Excitation tests were conducted at HAFB and ETR and both sites showed a consistent pattern between the two variables.

2. Transducer Output, CCW, versus Excitation Voltage  
(Figures X-9 and X-24)

The test data indicated that the transducers were more sensitive in the CW position ( $\bar{b} = 0.1126$  vs  $\bar{b} = 0.007$ ). The ETR data had a more positive slope than the HAFB data for 50.5 to 52.0 v and regressed more from 52.0 to 53.5 v.

3. Transducer Output, versus Excitation Voltage, CW and CCW for  
25 Production Valves, (Figures X-10 and X-11)

The results of test data for these 25 production valves were close to the results obtained for the "Task 25" valves. CW voltage readings continued to show more sensitivity to excitation changes than CCW readings.

X, D, Analysis (cont.)

4. Transducer Output Voltages, CW, Versus Solenoid Voltage  
(Figures X-12 and X-23)

The relationship between these two variables was demonstrated by using a hysteresis loop of solenoid voltages from 32 to 22 v and then from 22 to 32 v. A very slight indication of hysteresis was demonstrated. The loop did not show a consistent pattern between the valves; breaks in the curve appeared at 25, 28, and 32 v. The curves demonstrated that solenoid voltage had an effect on output voltage.

5. Transducer Output, CCW, versus Solenoid Voltage (Figure X-12  
and X-24)

The output voltage in the CCW position was similar to that of the CW position. The difference between the CW and CCW voltage outputs is largely the slopes of the regression lines. The slopes for CW outputs are all negative (output voltage decreases as solenoid voltage increased) while the slopes for CCW outputs are positive (output voltage increases as solenoid voltage increases).

6. Transducer Output, CW, versus Temperature (Figure X-13)

The relationship between temperature and CW output voltage is irregular. There is a general upward slope between the two variables but in the area of 65 to 70°F the individual readings show an inconsistent "S" curve that does not repeat for each valve. The regression slope is shown in Figure VI-13 (in the 60 to 100°F temperature range more variability is from the "S" curve than from the regression). The effects of temperatures used in other calculations use the maximum range based on the "S" curve.

7. Transducer Output, CCW, versus Temperature (Figure X-14)

The CCW output voltage were similar to the CW output voltage except the regression line for CCW voltage is negative.

8. Test Set to Test Set Variability, AGE, CW

Test set to test set variability was determined by analyzing all AGE test sets at all locations. The statistics in Figure X-15 indicate the average difference between the test sets and the standard deviation of average differences. Variability between some AGE and ETR equipment can be seen in Figure X-15. This histogram shows ETR readings to be about 0.160 v lower on Kavlico units and 0.030 v on Schaevitz units.

9. Test Set to Test Set Variability, AGE, CCW (Figure X-16)

The CCW position results were similar to CW position results. Differences in AGE and ETR equipment are about 0.200 v for Kavlico units and 0.090 v for Schaevitz units. These values are considerably higher than can be explained by just AGE equipment variability. Figure X-16 shows the histogram for the CCW voltages.

X, D, Analysis (cont.)

10. Repeatability on One Test Set, CW

These statistics are a reflection of the average difference and the variability between output voltage readings at Aerojet on test set SN 0000001 (taken under similar conditions). Figure X-15 shows the differential readings between test data taken on two dates. Greater differences were found with test set SN RCT 0061 at HAFB but the conditions were not the same as with test set SN 0000001 above (Schaevitz units at HAFB showed an average difference of 0.052 v, CW, Kavlico showed 0.059 v). The difference was partly a result of the recalibration of test set SN RCT 0061 between tests.

11. Repeatability on One Test Set, CCW

The CCW output voltage readings were similar to CW readings. Figure X-16 shows histograms of the differential voltage readings between the two Aerojet receiving dates (average differences between HAFB test set SN RCT 0061 was 0.047 and 0.032 v for Schaevitz and Kavlico, respectively).

12. Transducer Output, CW, versus Energization Time (Figures X-17 and X-23)

Generally, as energization time increases the CW output voltage increases. The average slope for the various test sites goes through zero for the  $\Delta$  output voltage at the energization time of 4 sec as theoretically expected. The energization time represents the difference between readings taken at 4 sec and readings that were taken at other times;  $\Delta$  output voltages are represented by the difference between the output readings at 4 sec and the readings taken of times other than 4 sec for each specific valve. The scatter of slopes is relatively large indicating that the repeatability of this relationship is not very good.

13. Transducer Output, CCW, versus Energization Time, CCW (Figures X-18 and X-24)

Generally, as energization time increases the CCW voltage decreases. The average slope again goes through zero for the  $\Delta$  output volts at the 4 sec energization time; however, the variability of the slope is smaller than shown for the CW volts.

14. ETR Variability on FTM 454, CW (Figure X-19)

Test data from ETR indicated a relatively large range between and within each test station. Figure X-19 shows the individual values and the time span for the various tests.

15. ETR Variability on FTM 454, CCW (Figure X-20)

Test results were similar to CW. Individual data points are shown in Figure X-20.

X, D, Analysis (cont.)

16. FTM History (Figures X-21 and X-22)

Error analysis of the position transducer considered the variables that could possibly influence output voltage. The variability for these variables were used in propagation of errors formula (Root Sum Squaring (RSS) of the standard deviations) to arrive at the total expected variability. Using this technique, the total expected variability of output voltage was computed by determining the comparable  $3\sigma$  variability of each contributing source and then taking their RSS's. The total expected  $3\sigma$ 's are as follows:

CW Output voltage  $+3\sigma = 0.276$ ,  $-3\sigma = 0.283$   
CCW Output voltage  $+3\sigma = 0.148$ ,  $-3\sigma = 0.136$

Figures X-21 and -22 show detailed analysis of the comparables  $3\sigma$ 's for each source of variation and the RSS of the CW and CCW output voltage respectively.

E. INTERIM ACTIONS TAKEN

1. Interim limits have been established for use at Aerojet with Aerojet equipment for valves which are outside of specification limits. These limits are 5.140 to 6.134 v for the CW position based on testing at 50 and 54 v. These limits will be applied only through MRB action.
2. Six Kavlico valves have been reset by Aeronautronics to meet specification limits using a revised procedure (Section X,F) which assures tighter control. The data from these valves is shown in Figure X-25 and demonstrate the feasibility of resetting.
3. Seven new valves using position transducers from Kavlico have been set by Aeronautronics to meet specification limits using revised procedures (Paragraph F) which assure tighter control. The data from these valves are shown in Figure X-26.
4. The AGE test set will be used for final buyoff at Aeronautronics to eliminate the bias between Aeronautronics and SCC.
5. Interim limits have been established for use at Aeronautronics which allows for some test set to test set variability.
6. Based on the results from Paragraphs 2 and 3 above, production valves will be reset upon receipt of contractual direction, to meet specification limits using AGE equipment.
7. The use of Kavlico transducers has been eliminated from the Buy III production programs.



X, Roll-Control Valve Transducer Testing--Project Directive 41-025 (cont.)

F. ROLL VALVE ASSEMBLY AND TEST SEQUENCE

1. Present

- a. Install and set transducers using Aeronautronics equipment. Spot weld transducers in place.
- b. Acceptance test valve at Aeronautronics (includes proof pressure and functional tests).
- c. Final electrical buyoff at Aeronautronics using Aeronautronics test set.
- d. Perform receiving inspection on valves at SOC using AGE test set.
- e. Perform receiving inspection at Aerojet using AGE test set.
- f. Perform final check at Aerojet and valves on motor, using AGE test set.
- g. Perform receiving inspection at ETR or Plant 77 using AGE test set.
- h. Perform missile check on MAB using A/N missile electronics.
- i. Perform missile check in launcher using A/N missile electronics.

2. Future

- a. Install and set transducers, using Aeronautronics equipment, to new adjusted limits. These limits are those required to give the null band limits described in Section X,B,4.
- b. Acceptance test valve at Aeronautronics (includes proof-pressure and functional tests).
- c. Recheck transducer output using Aeronautronics test set. Reset if necessary. Spot weld transducers in place.
- d. Final electrical buyoff at Aeronautronics using AGE test set.
- e. Perform receiving inspection on valves at SOC using AGE test set.
- f. Perform receiving inspection at Aerojet using AGE test set.

Report 0162-06TDR-9-Vol 2

X, F, Roll Valve Assembly and Test Sequence (cont.)

- AGE test set.
- g. Perform final check at Aerojet with valves on motor, using AGE test set.
  - h. Perform receiving inspection at ETR or Plant 77 using AGE test set.
  - i. Perform missile check in MAB using A/N missile electronics.
  - j. Perform missile check in launcher using A/N missile electronics.

G. VOLTAGE CALIBRATION OF THE SQUARE WAVE EXCITATION

During the study, the question of accuracy of the square wave excitation voltages was introduced.

The requirement for the flight hardware is that the voltage amplitude of the square wave shall be within  $\pm 4\%$  of the nominal value. The requirement on the AGE is that it be within  $\pm 1\%$  of the nominal value. Calibration of this voltage requires equipment which will measure within  $\pm 0.1\%$  preferably or within  $\pm 0.25\%$  maximum. Current techniques for measuring square wave voltages do not provide the accuracy necessary for the measurement.

Oscilloscopes are only accurate to  $\pm 3\%$  and voltage metering equipment is not designed for use with waveforms other than sine waves.

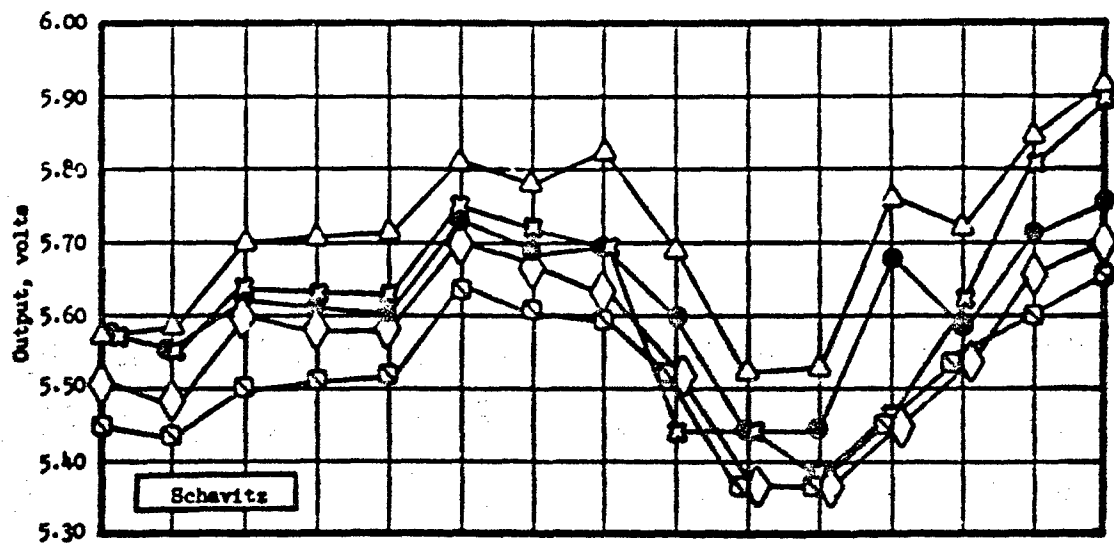
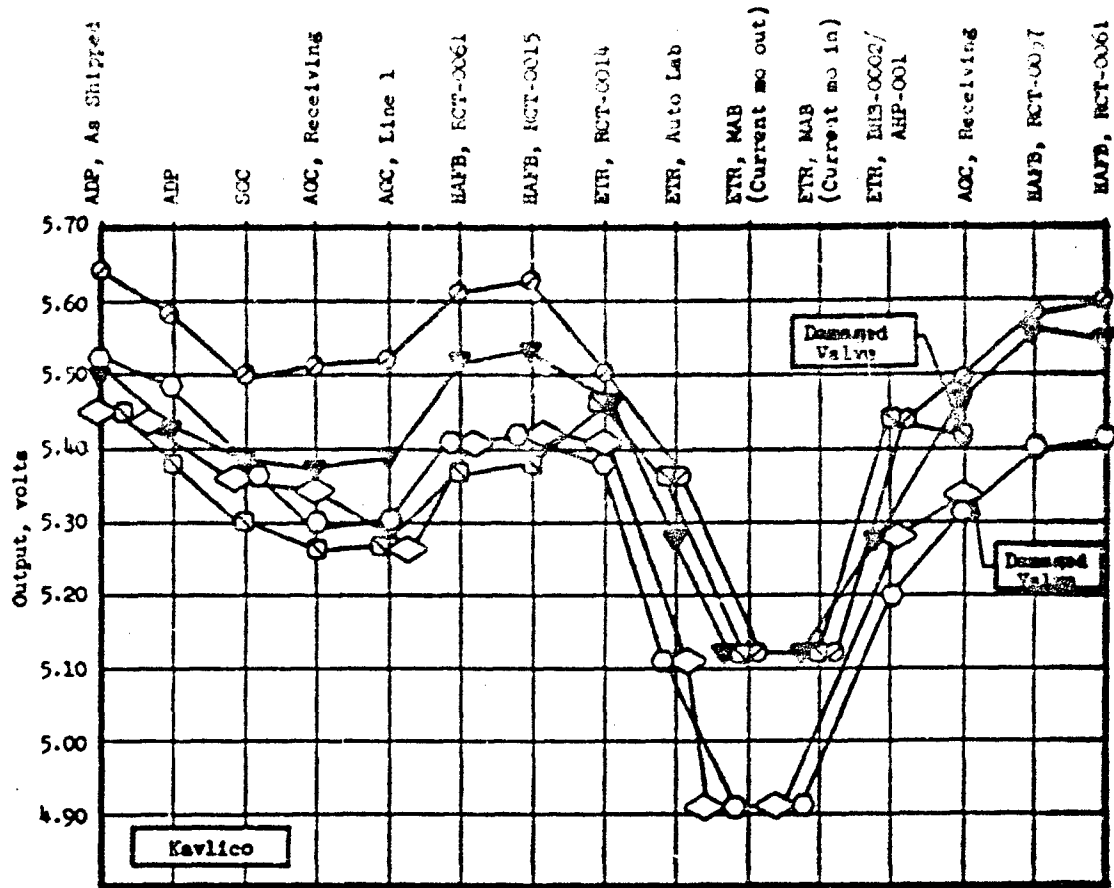
Three approaches to the problem have been considered. The recommended method is to devise a calibrated transducer simulator which can be used to calibrate the test set and the operational equipment. This method would allow calibration of the test set to overcome differences in demodulator losses and any other characteristics from one set to another. The second method is to use a John Fluke Model 803B differential voltmeter with a correction factor. The manufacturer has provided a correction factor that has not been verified locally. The third method is to use an oscilloscope in conjunction with a dc power supply. The scale of the oscilloscope can be expanded to provide the required accuracy and resolution. The wave form can then be displaced for observation and measurement by using the power supply to provide a biasing voltage.

Report 0162-06TDR-9-Vol 2

	<u>+ 3 <math>\sigma</math></u>	<u>- 3 <math>\sigma</math></u>
1. Excitation voltage	0.1251	0.1251
2. Solenoid voltage	0.063	0.083
3. Temperature	0.046	0.046
4. Age life	0.025	0.025
5. Total test set variability	0.100	0.100
Summation of individual sigmas	0.3591	0.3791
Aerojet limits (based on 40 valves)	2.00 min	4.00 min
Limit output values	1.641	4.379
Proposed ICD limits	1.6	4.4

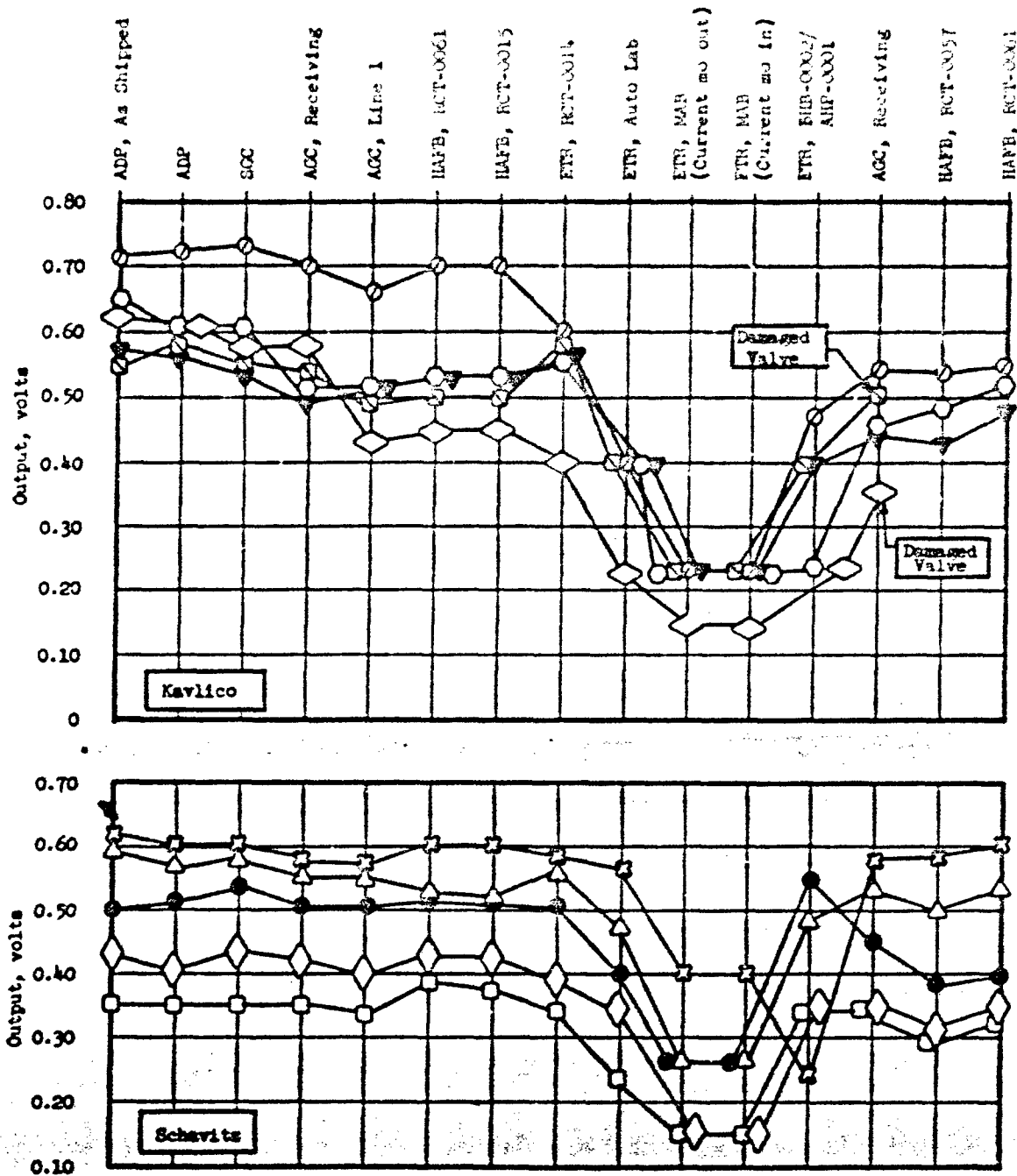
Overall Variance Analysis of Parameters  
Affecting Null Position Output

Figure X-1



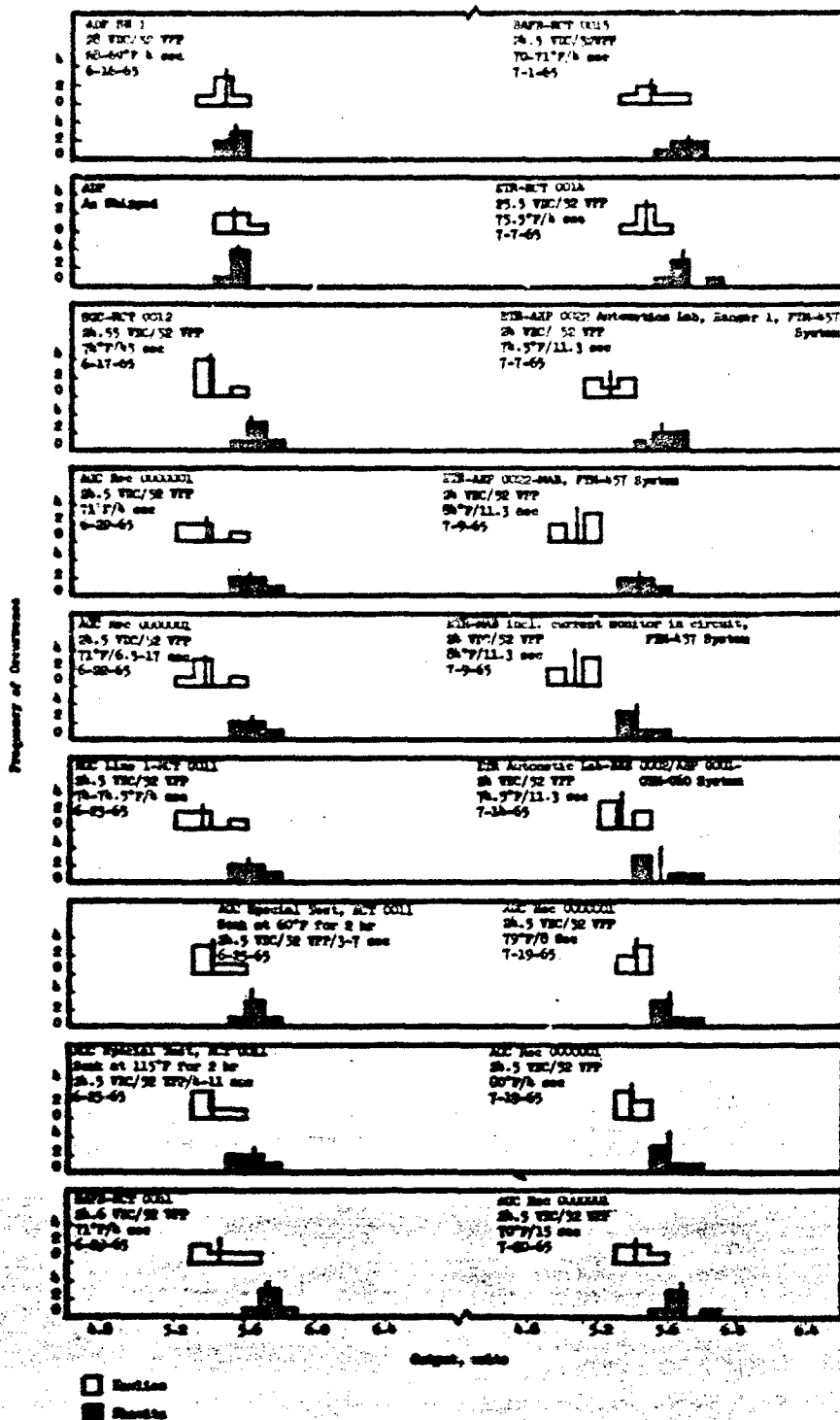
Output Voltage Readings for Task 25 Valves,  
CW Position

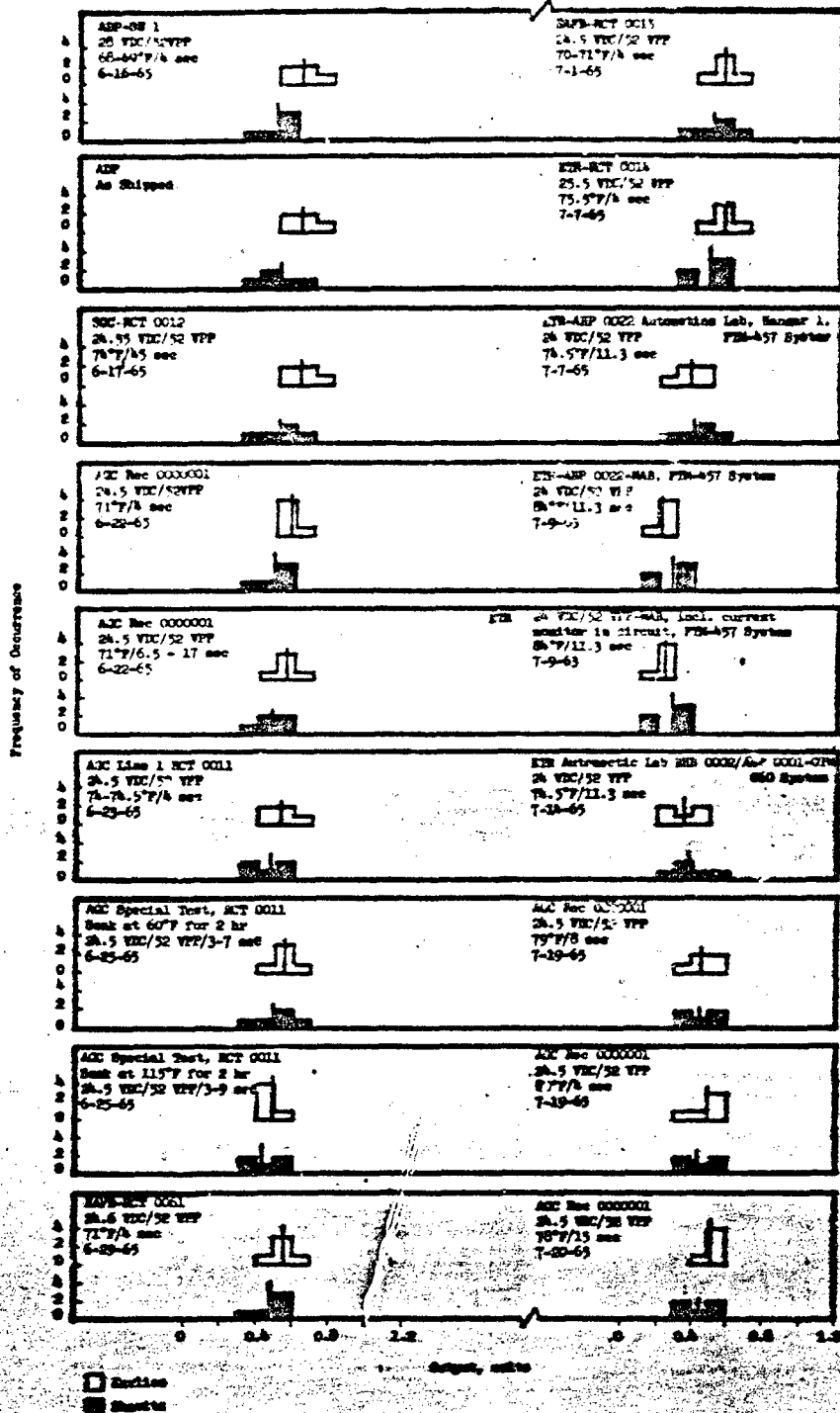
Figure X-2



Output Voltage Readings for Task 25 Valves,  
OCM Position

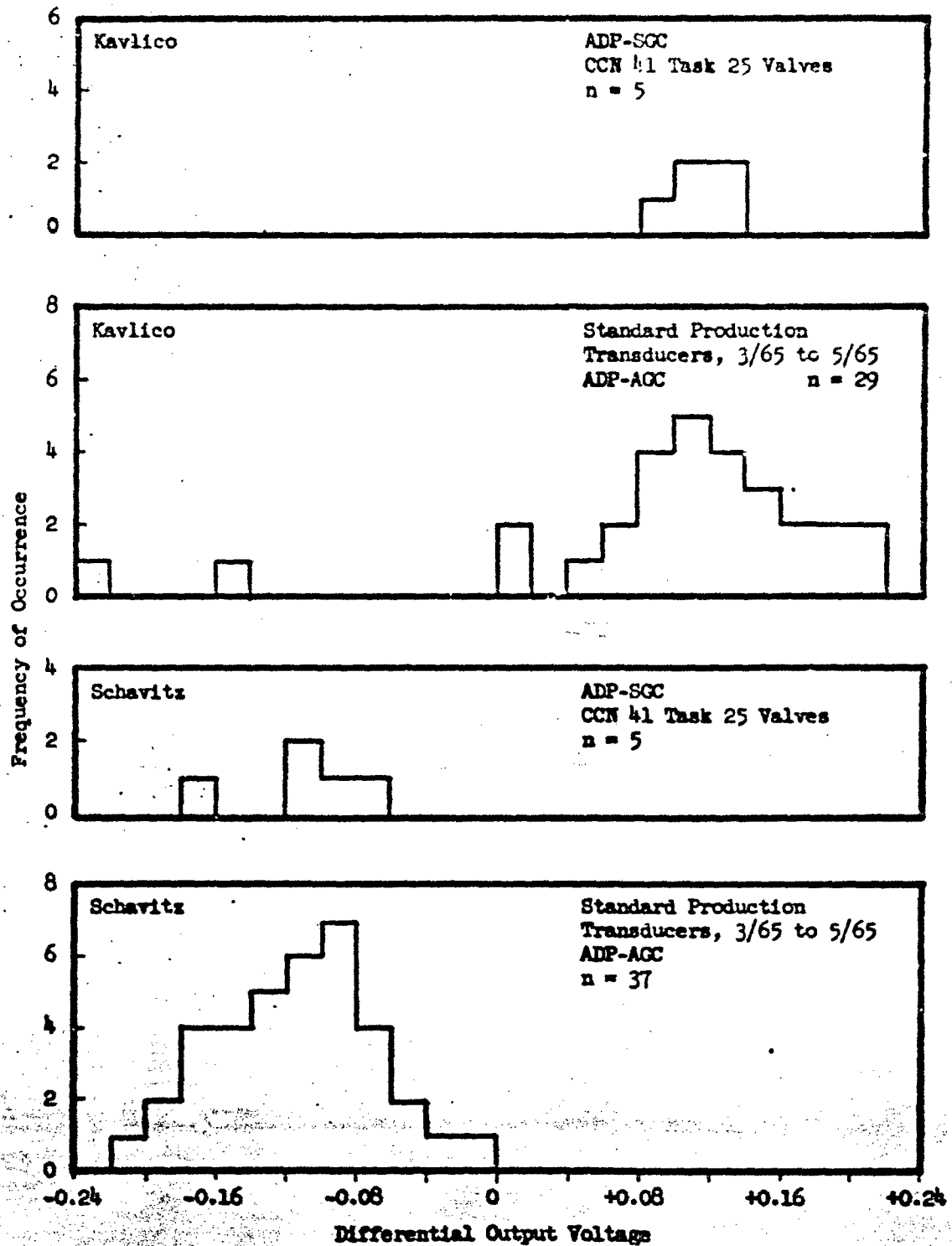
Figure X-3





Histograms of Output Voltages for Task 25 Valves,  
CCW Position

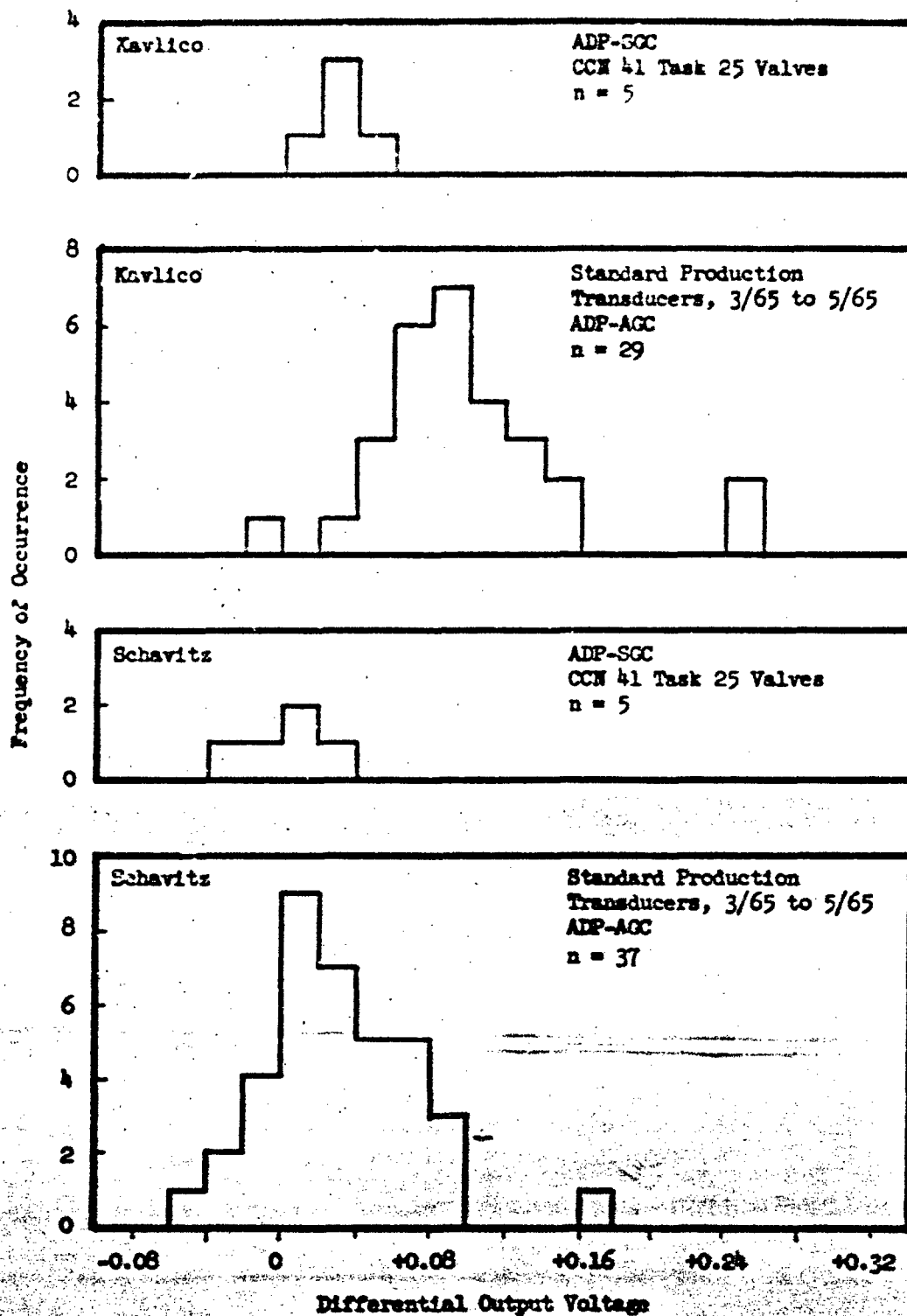
Figure X-3



Histograms of Differential Voltage Readings, RC Position Transducer, CN Position

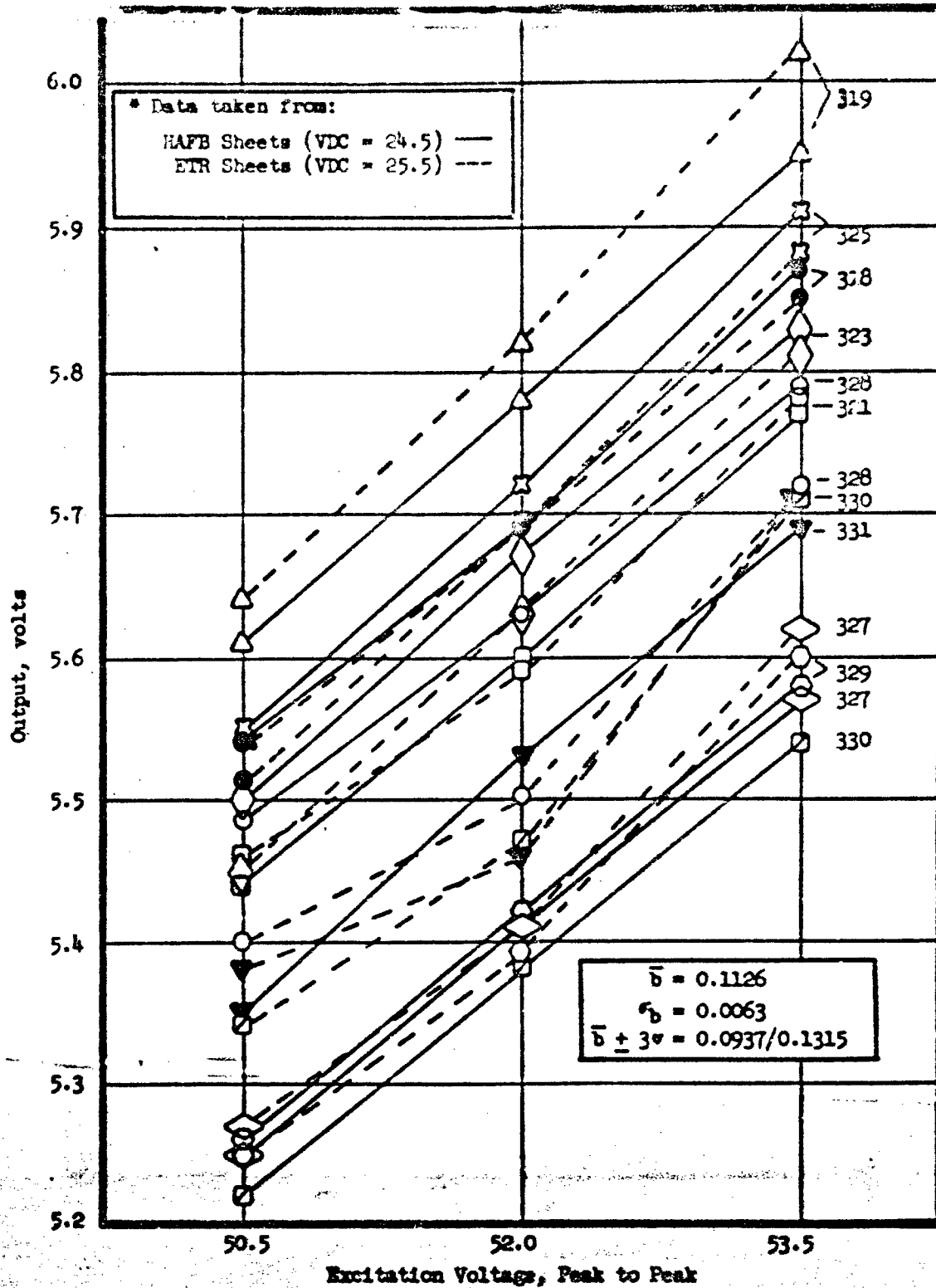
Figure X-6





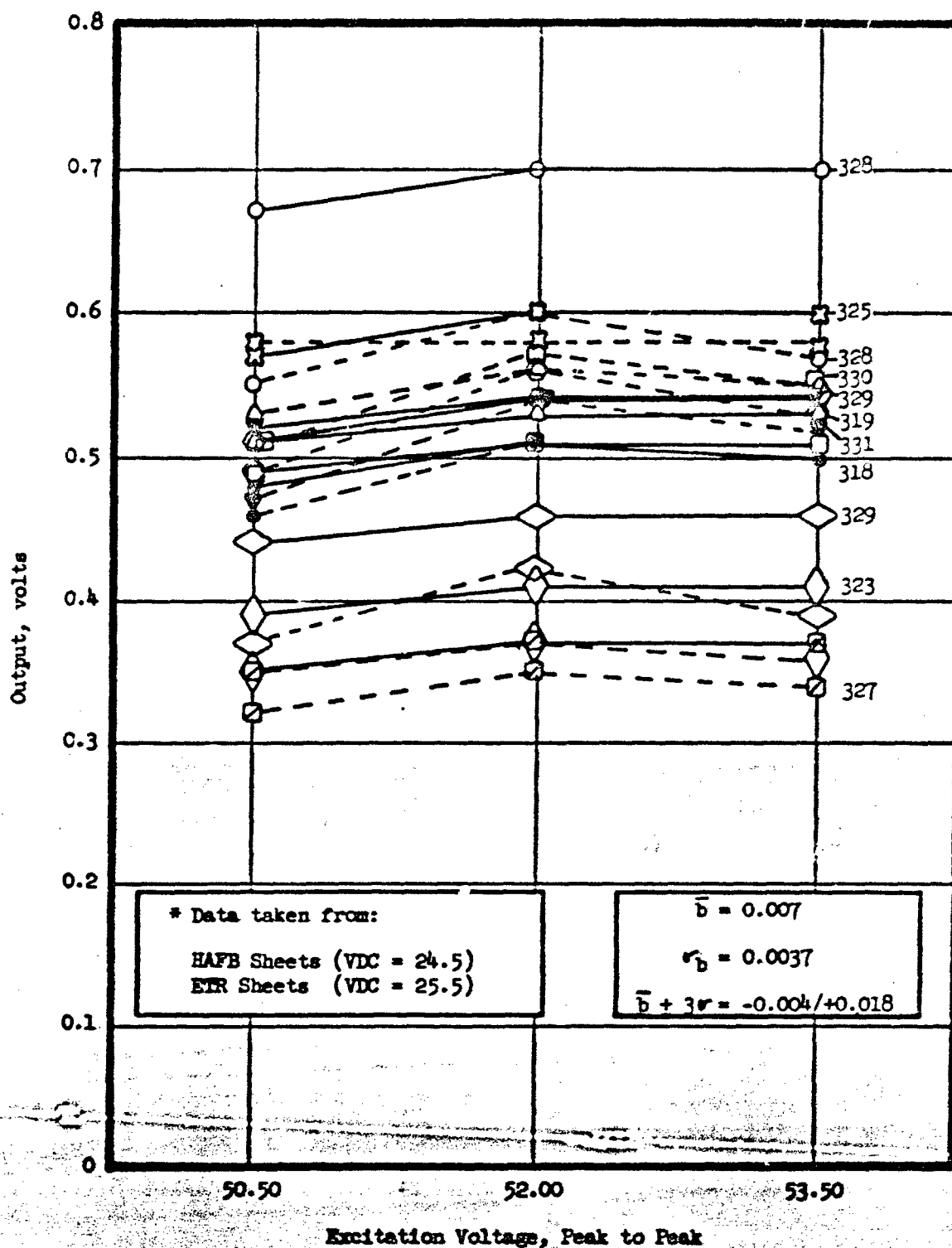
Histograms of Differential Voltage Readings, RC Position  
Transducer. CCN Position

Figure X-7



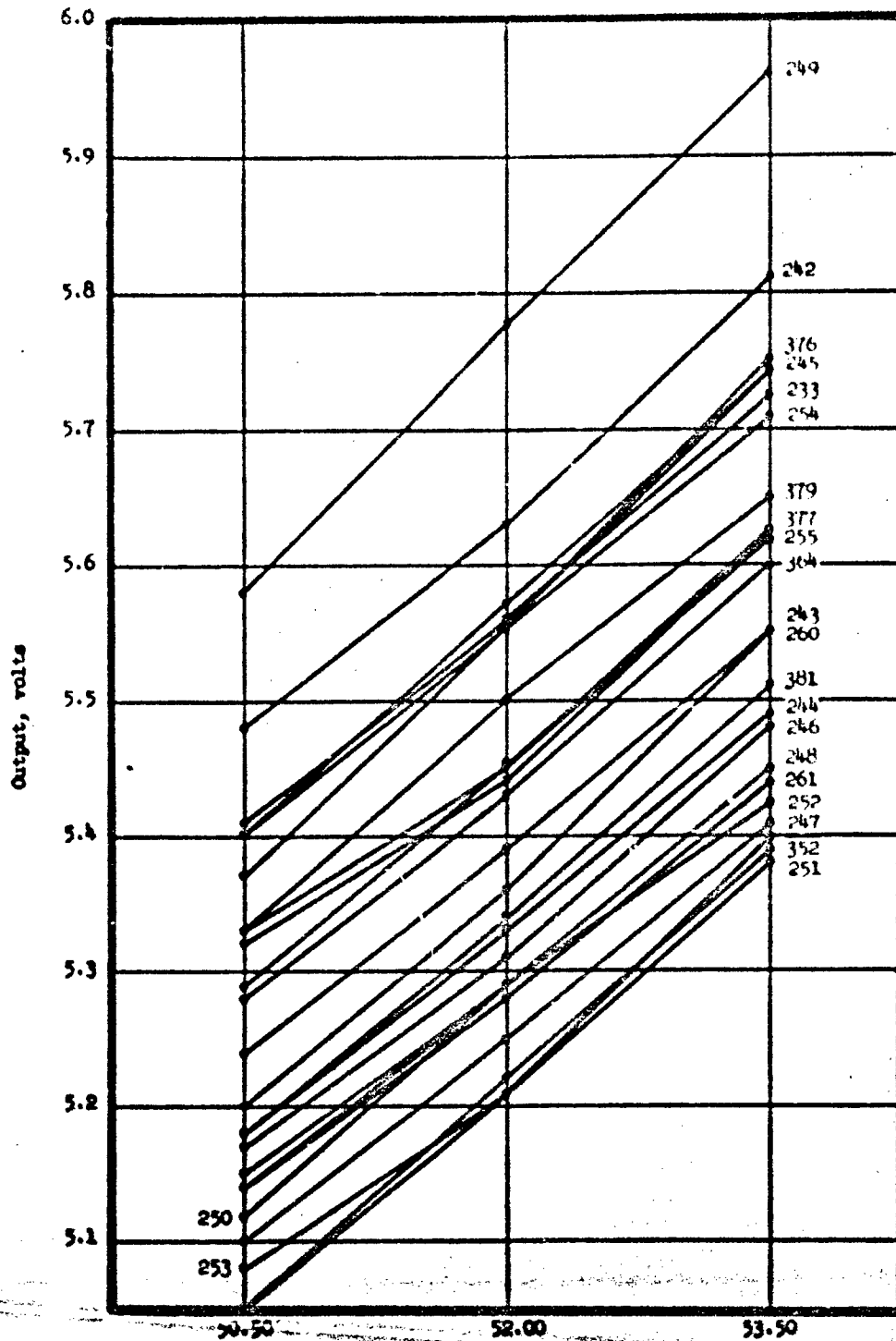
Correlation Diagram, Transducer Excitation Voltage vs Output Voltage for Task 25 Valves, CW Position

Figure X-8

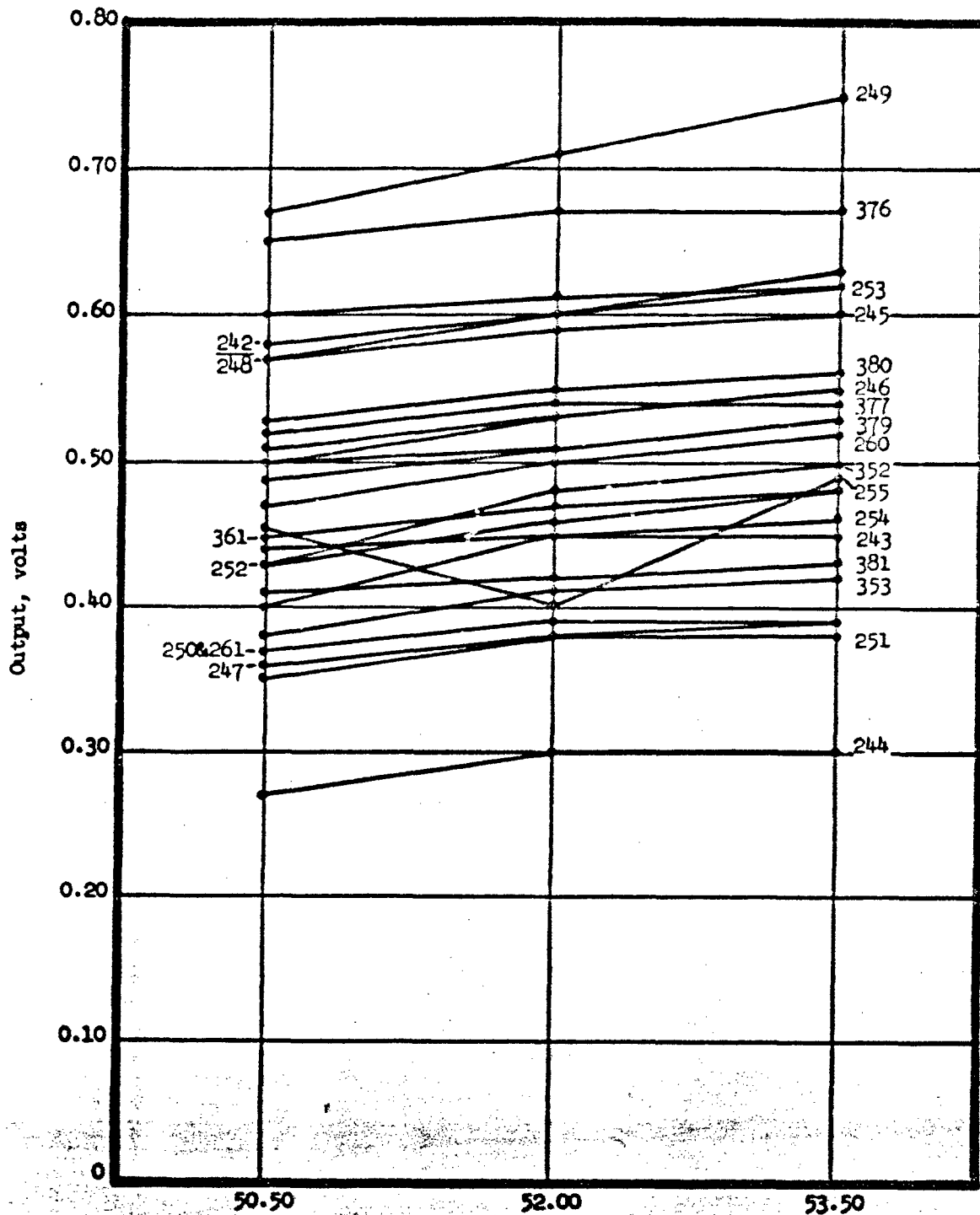


Correlation Diagram, Transducer Excitation Voltage vs Output Voltage for Task 25 Valves, CCW Position

Figure X-9

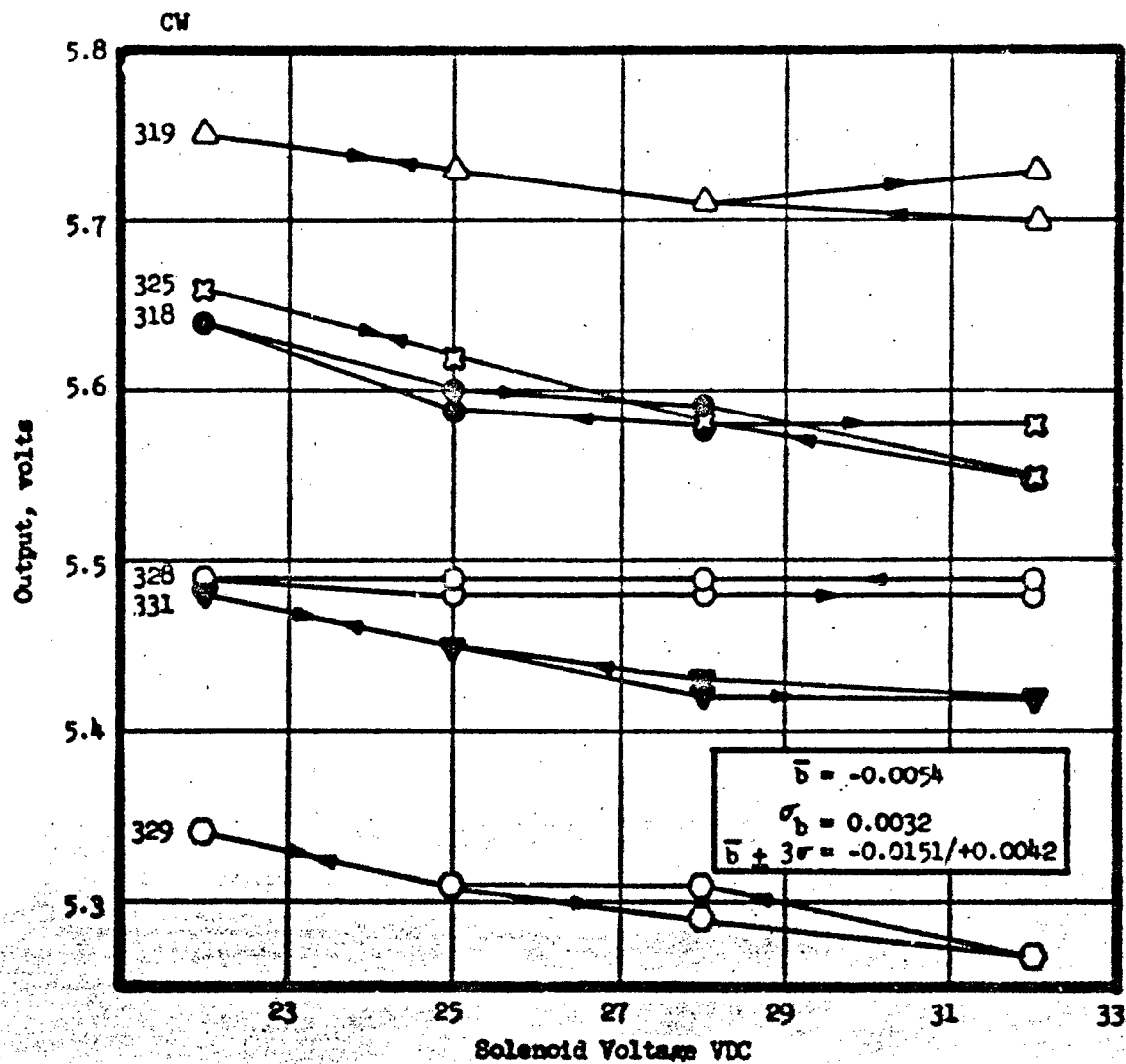
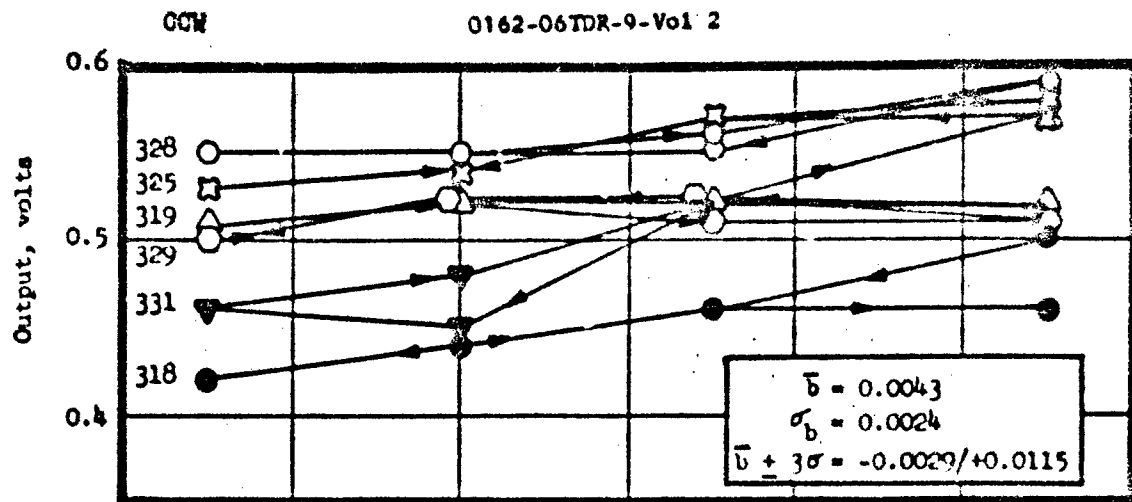


Excitation Voltage, Peak to Peak  
Correlation Diagram, Transducer Excitation Voltage vs Output  
Voltage for Production Valves, CM Position  
Figure X-10



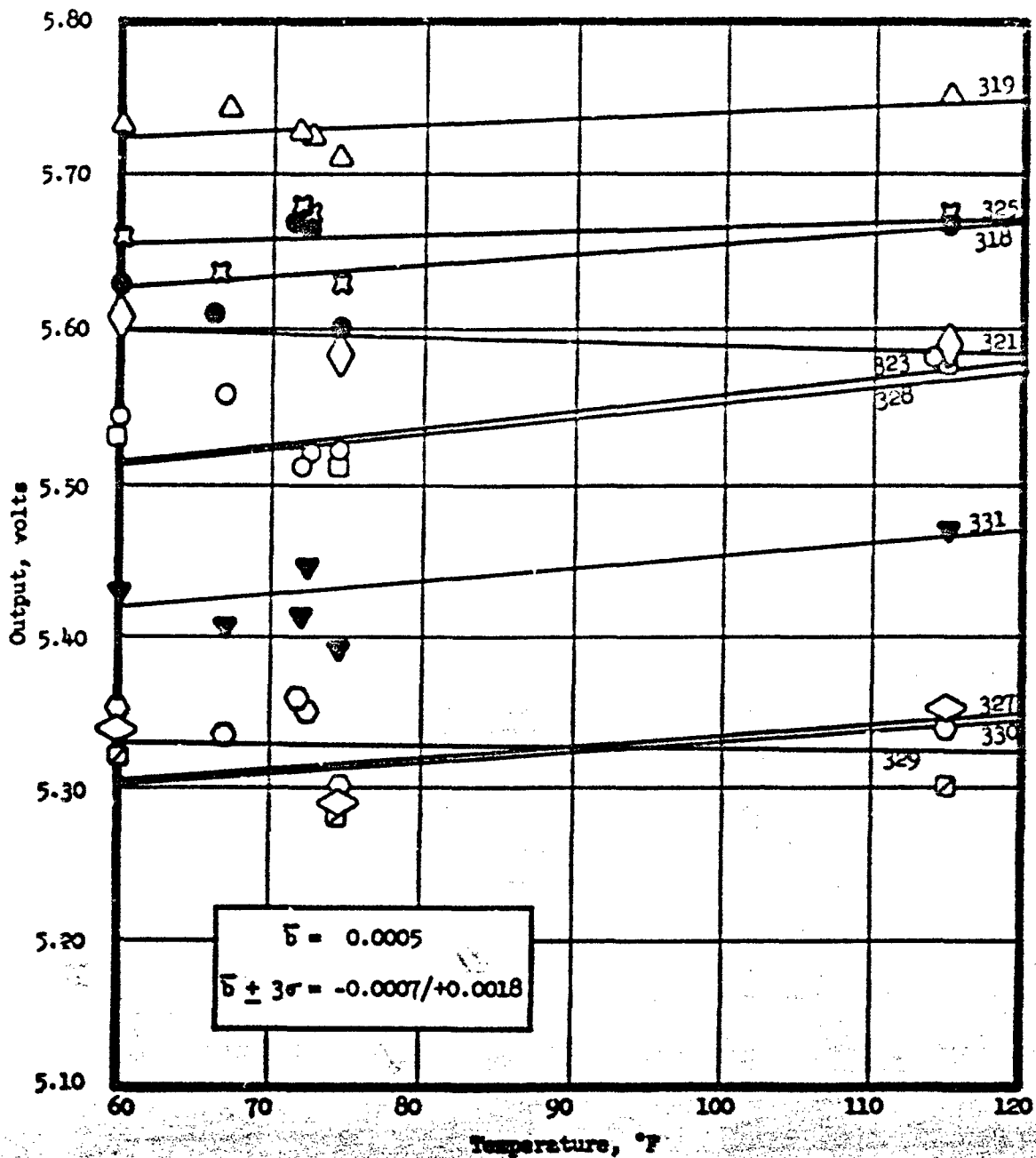
Correlation Diagram, Transducer Excitation Voltage vs. Output Voltage for Production Valves, CCW Position

Figure X-11



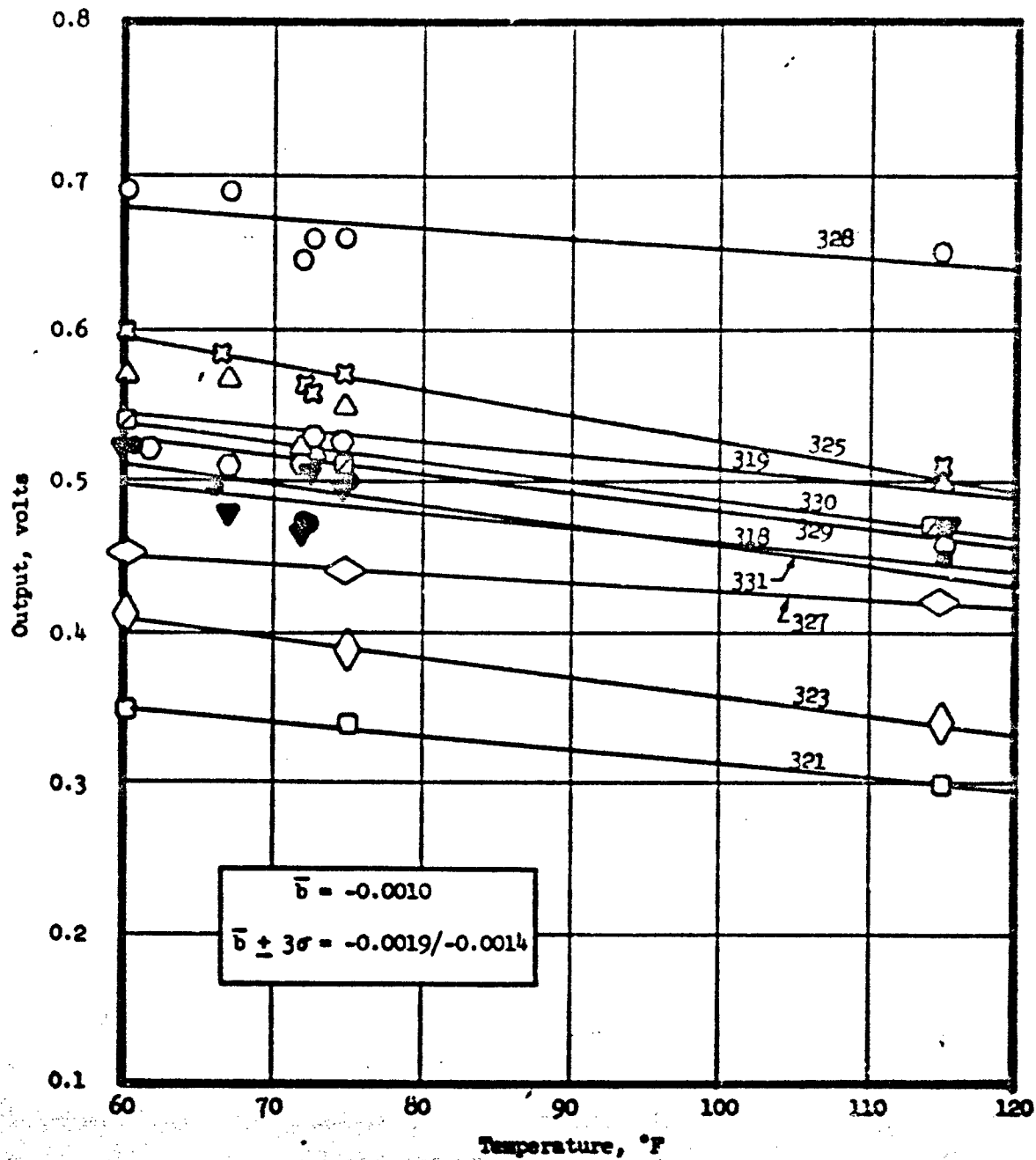
Correlation Diagram, Solenoid Voltage vs Transducer Output Voltage for Task 25 Valves

Figure X-12



Correlation Diagram, Temperature vs Output Voltage for Task 25  
Valves, CW Position

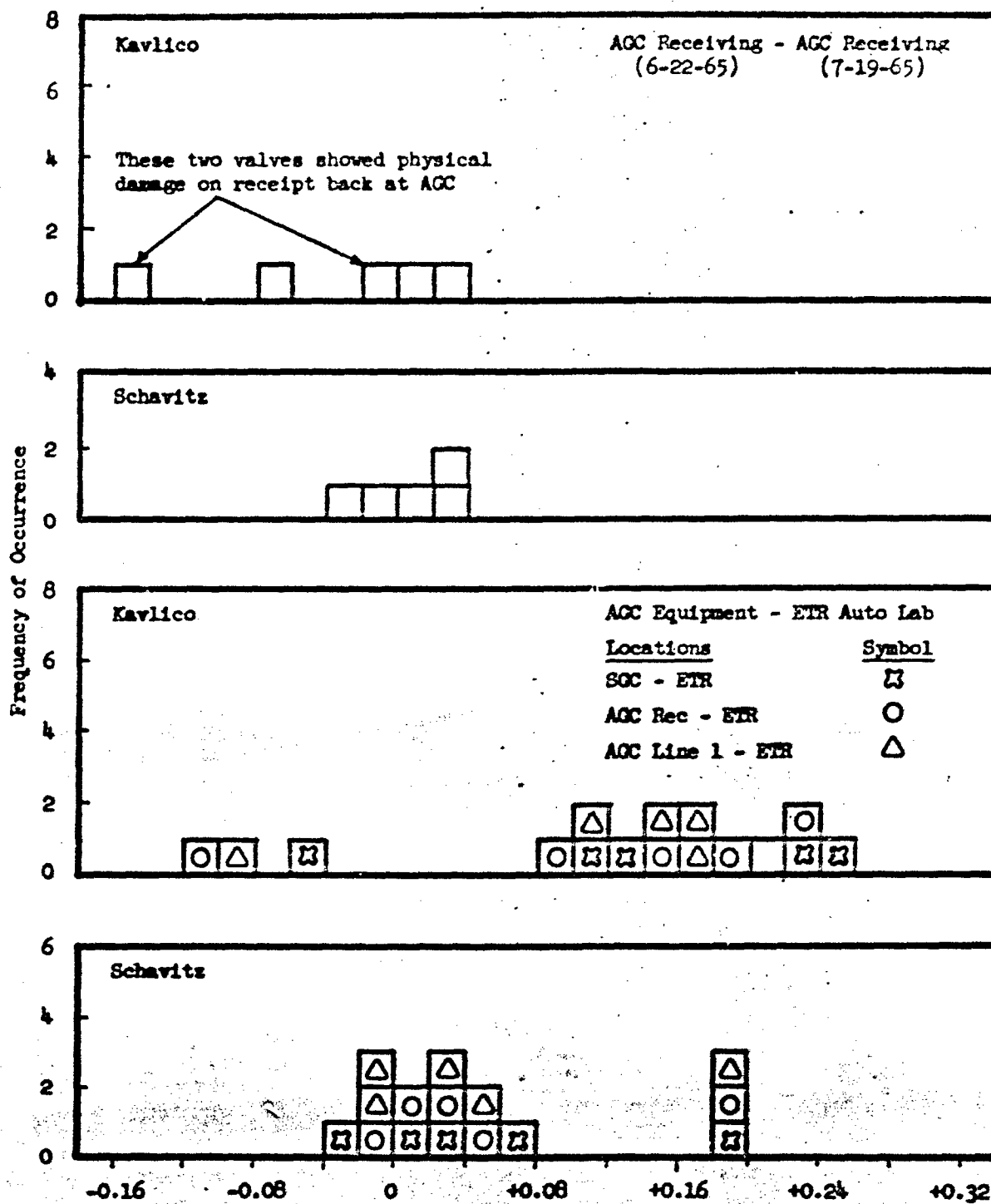
Figure X-13



Correlation Diagram, Temperature vs Output Voltage for Task 25  
Valves, OCN Position

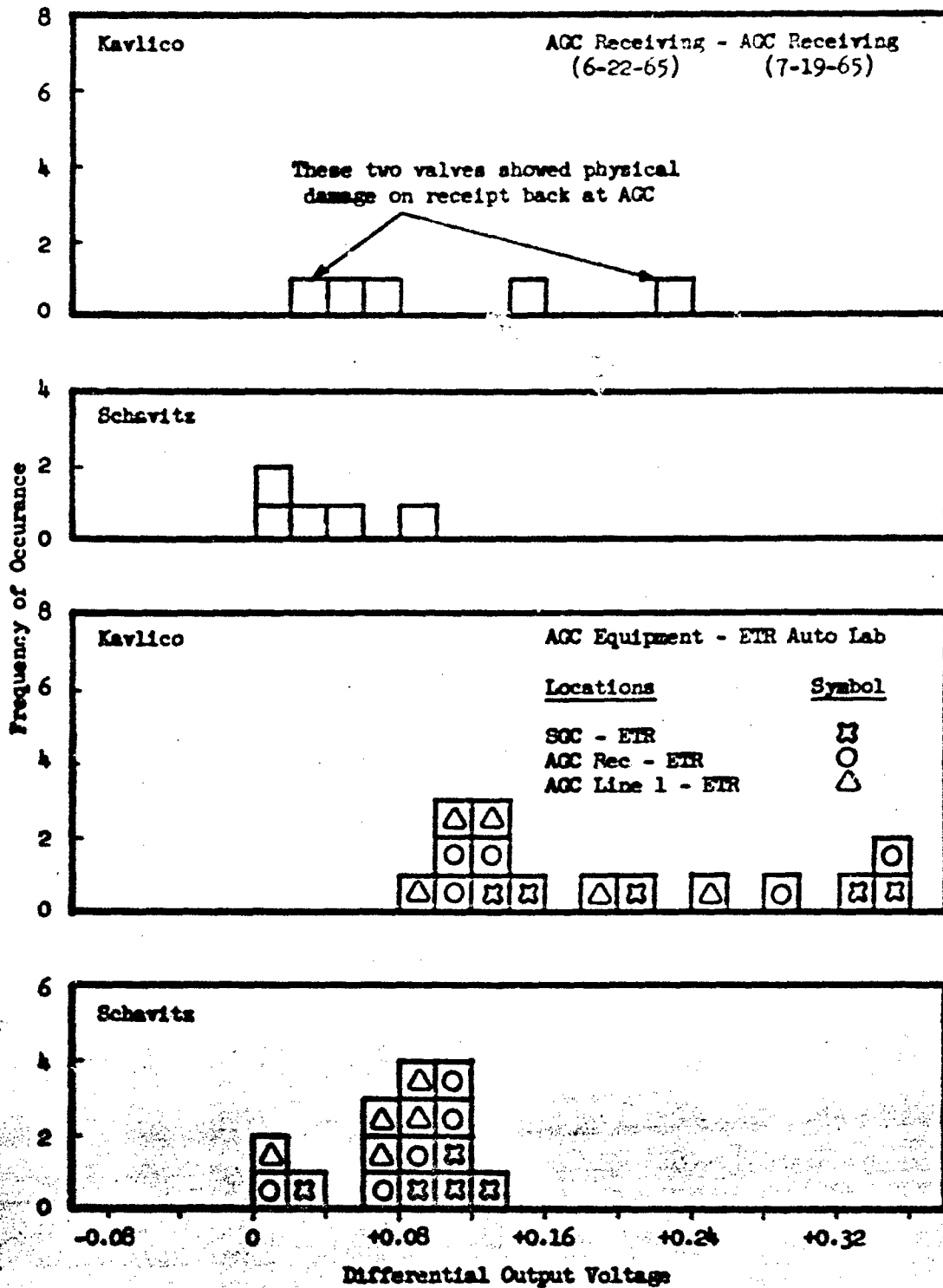
Figure X-14





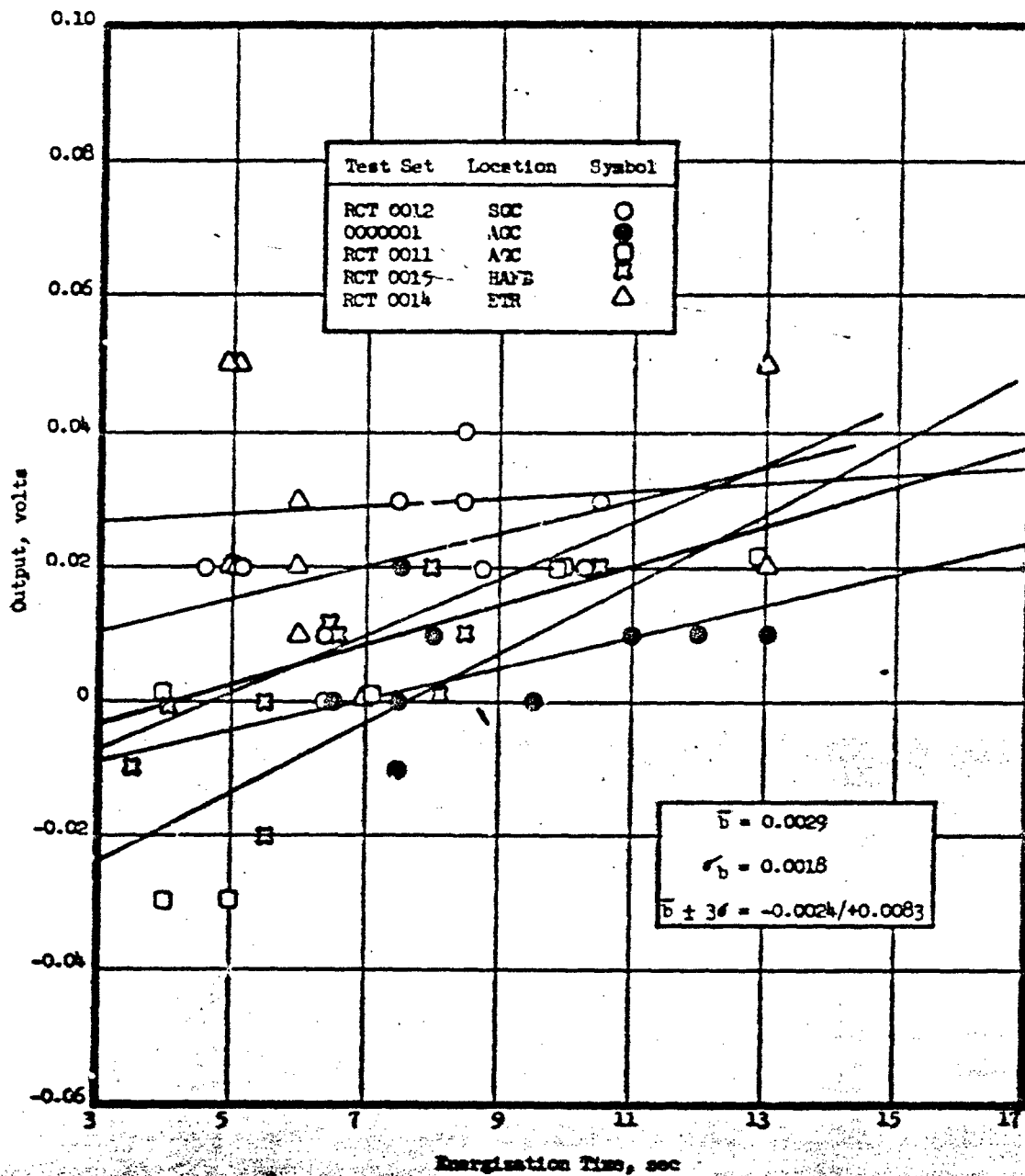
Histograms of Differential Voltage Readings between AGE and ETR  
Equipment, Task 25 Valves, CM Position

Figure X-15



Histograms of Differential Voltage Readings between AGE and ETR Equipment, Task 25 Valves, CCW Position

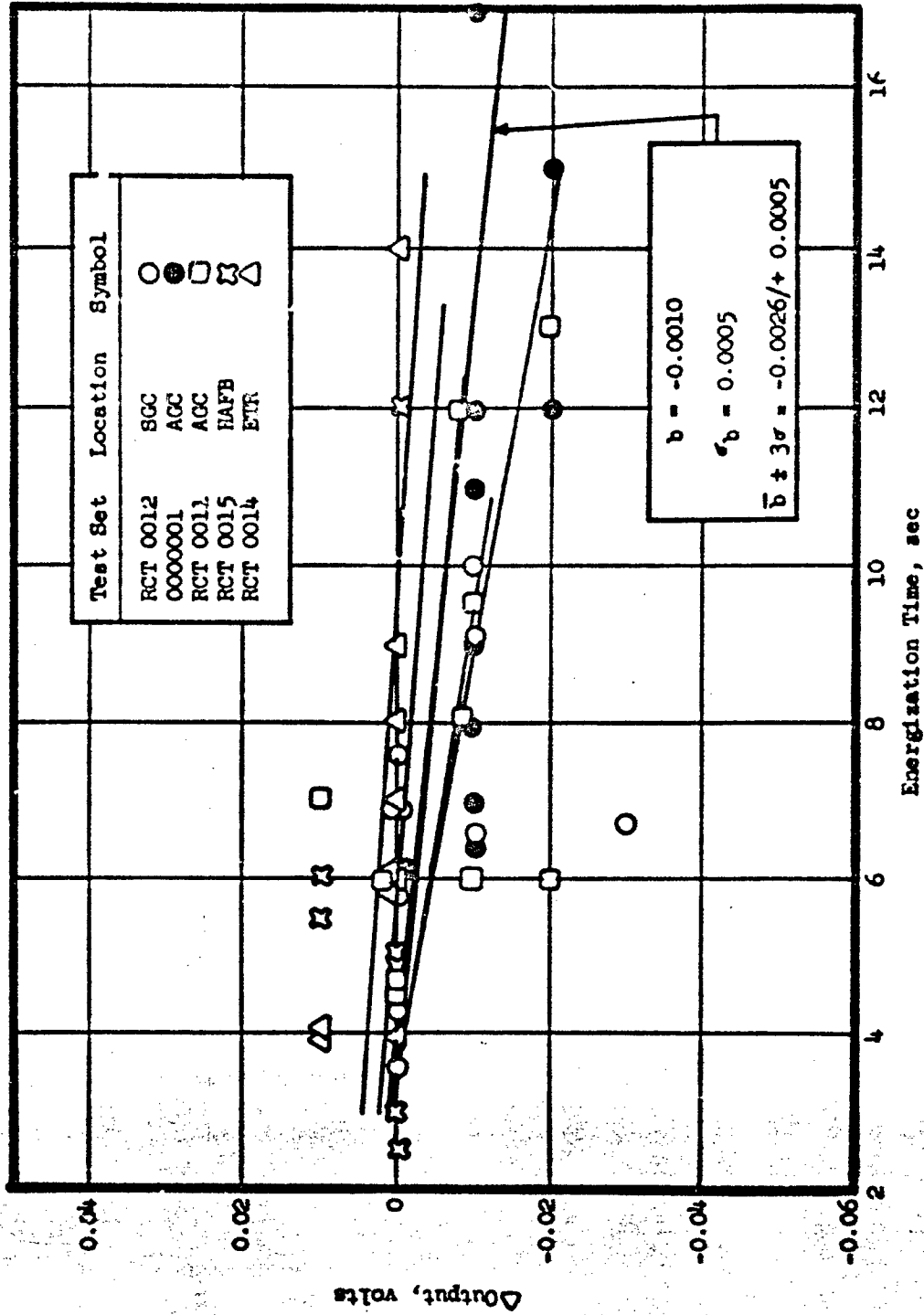
Figure X-16



\* Where four sec is used as the "control energization time"; theoretically differential output voltage at four sec should be 0. The charted points represent actual data taken between test sets.

Correlation Diagram, Differential Output Voltage vs Energization Time, Task 25 Valves, CW Position

Figure X-17



\* Where four sec is used as the "control energization time"; theoretically differential output voltage at four sec should be 0. The charted points represent actual data taken between test sets.

Correlation Diagram, Differential Output Voltage vs Energization Time, Task 25 Valves, CCW Position

Figure X-18

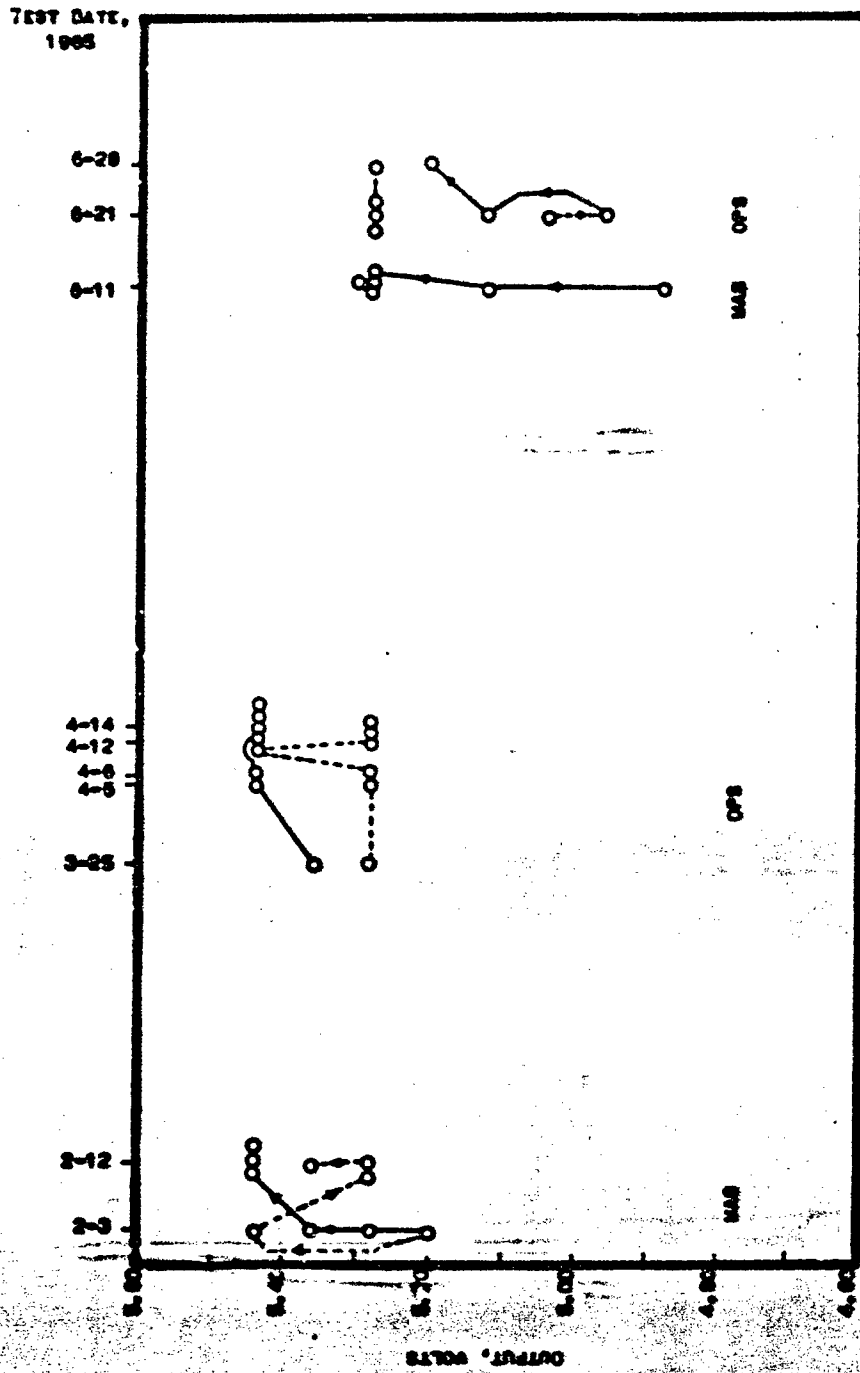


Figure X-19

RC Transducer, Output Voltage Checks at ETR on 52FDM-454, CM Position

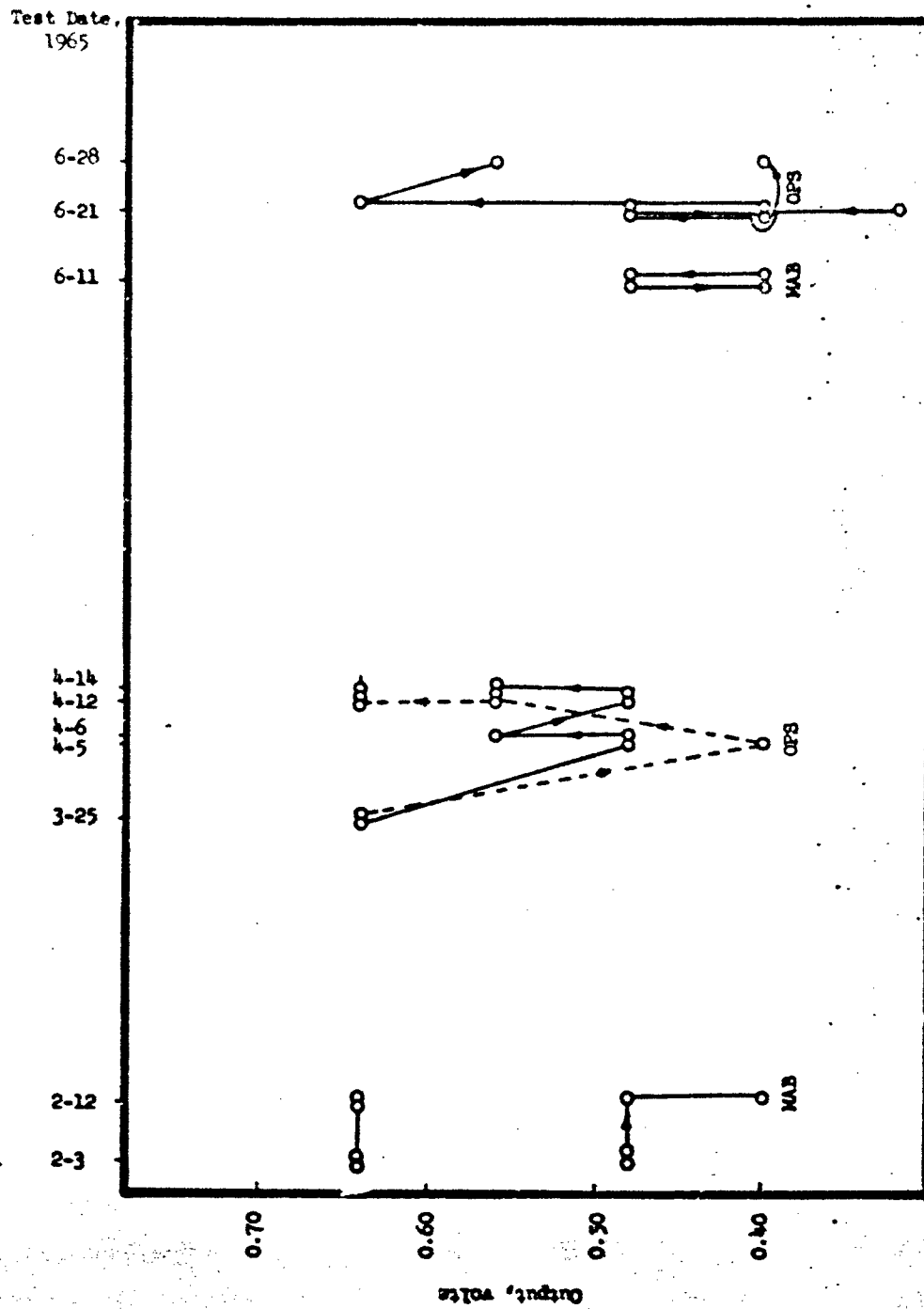


Figure X-20

# Report 0162-06TDR-9-Vol 2

Source of Variation	Comparable $3\sigma$ Variation*	
	<u>+ <math>3\sigma</math></u>	<u>- <math>3\sigma</math></u>
Excitation Voltage Variation, 50-54 volts PP $\bar{b} = 0.1126, \sigma = .0063$ (Figure X-23)	0.228	0.228
Solenoid Voltage Variation, 22-32 volts $\bar{b} = 0.0054, \sigma = 0.0032$ (Figure X-23)	0.028	0.083
Temperature Variation, 60° - 100°F $\bar{X} = 0.052, \sigma = .011$	0.042	0.042
Age Life, 3 years, estimated	0.025	0.025
Average Test Set to Test Set Readout Variation, AGC Equipment $\bar{X} = 0.0564, \sigma = .0407$	0.125	0.125
Repeatability on One Test Set $\bar{X} = 0.015, \sigma = .0157$	0.047	0.047
Energization Time, 4-17 sec $\bar{b} = 0.0029, \sigma_b = 0.0018$ (Figure 23)	0.058	0.028
RSS'd Variation	0.276	0.283

RC valves checked at Aerojet and meeting Aerojet Spec 71069 Rev C, Amend 3, could produce the following output values in the CW position under limit conditions assumed above.

AGC Spec Limits	5.360 min	6.000 max
RSS'd Variations	<u>-.283</u>	<u>+.276</u>
Limit Output Values	5.077	6.276
ICD Limits	5.016	6.300

## Statistical Difference Between Aerojet AGE (Receiving Inspection and Line 1) and Missile Equipment

Average difference	= 0.183 volts
Max observed difference	= 0.390 volts

\* For the variables utilizing regression analysis, comparable  $3\sigma$  variations are based on the variability of  $\bar{b}$  and  $\sigma_b$  when associated with CW output volts, (e.g.,  $\bar{b}$  shows an increase of 0.2252 CW volts from 52 to 54 excitation volts,  $3\sigma_b$  shows an additional increase or 0.0327 CW volts at 54 volts; these amounts are RSS'd, or  $\sqrt{(.225)^2 + (.0378)^2} = 0.228$  For variables checking out differences, comparable  $3\sigma$ 's are based on  $\sqrt{(1/2\bar{X})^2 + (3\sigma)^2}$ .

## Overall Variance Analysis of Parameters Affecting CW Output Voltages

Figure X-21

Report 0162-06TLR-9-Vol 2

Source of Variation	Comparable $3\sigma$ Variation*	
	+ $3\sigma$	- $3\sigma$
Excitation Voltage Variation, 50-54 volts PP $\bar{b} = 0.007, \sigma = 0.0037$ (Figure 24)	0.026	0.026
Solenoid Voltage Variation, 22-32 volts $\bar{b} = 0.0043, \sigma = 0.0024$ (Figure 24)	0.063	0.021
Temperature Variation, 60°-100°F $\bar{t} = 0.043, \sigma = 0.0125$	0.046	0.046
Age Life, 3 years, estimated	0.025	0.025
Average Test Set to Test Readout Variation, AGE Equipment $\bar{X} = .0230, \sigma = .0429$	0.115	0.115
Repeatability of One Test Set $\bar{X} = .018, \sigma = .0121$	0.037	0.037
Energization time, 4-17 sec $b = -0.0010, \sigma = .0005$ (Figure 24)	0.008	0.025
RSS'd Variation	0.148	0.138

RC valves checked at Aerojet and meeting Aerojet Spec 71069 Rev C, Amend 3, could produce the following output values in the CCW position under limit conditions assumed above.

AGC Spec Limits	0.250 min	0.500 max
RSS'd Variations	<u>-0.138</u>	<u>+0.148</u>
Limit Output Values	0.112	0.648
ICD Limits	0	1.090

Statistical Difference Between Aerojet AGE  
(Receiving Inspection and Line 1) and Missile Equipment

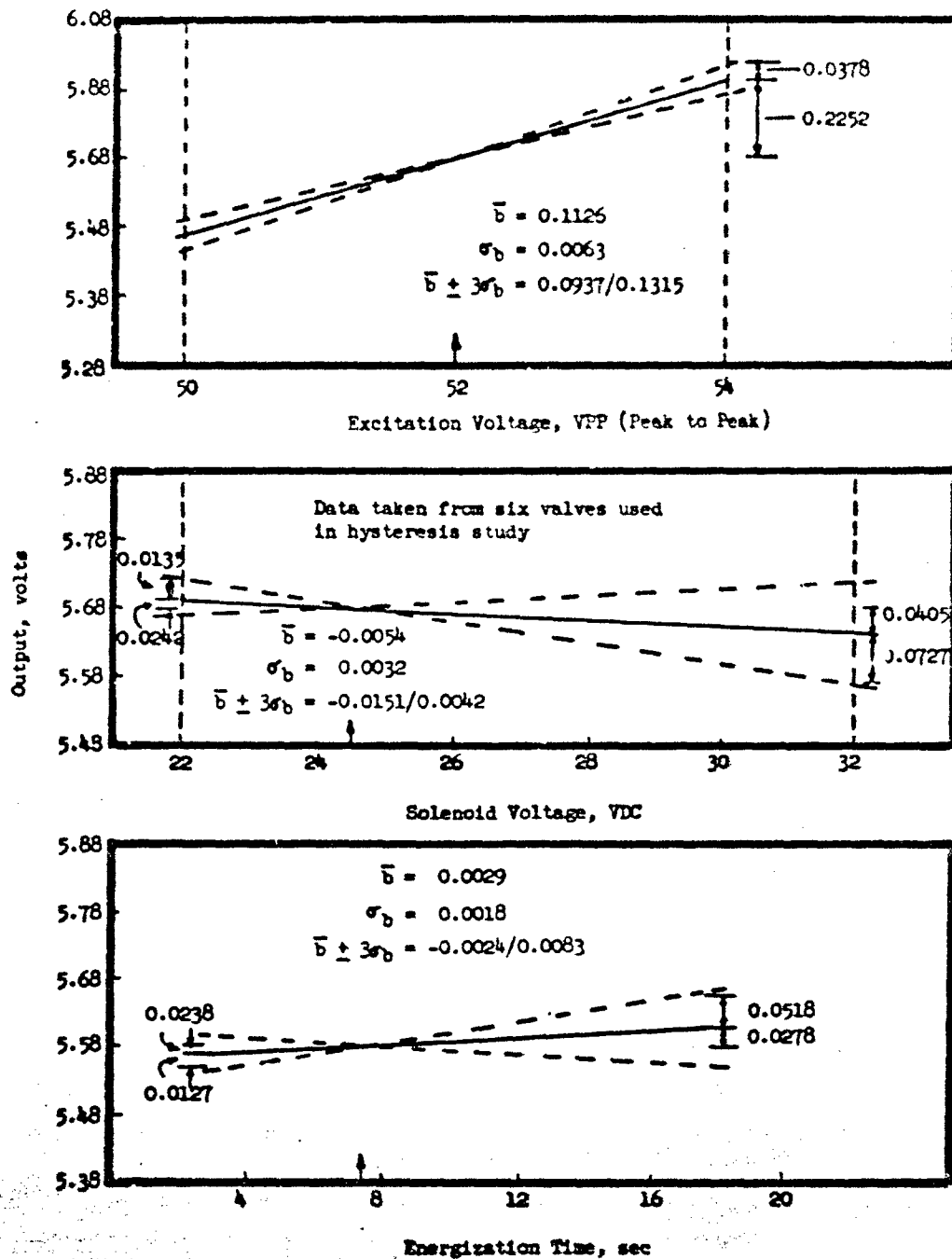
Average difference,	= 0.155
Max observed difference,	= 0.430

\* For the variables utilizing regression analysis, comparable  $3\sigma$  variations are based on the variability of  $\bar{b}$  and  $\sigma$ , when associated with CCW output volts (e.g.,  $\bar{b}$  shows an increase of 0.014 CCW volts from 52 to 54 excitation volts,  $3\sigma$  shows an additional increase of 0.022 CCW volts at 54 volts; these amounts are RSS'd or  $\sqrt{(0.014)^2 + (0.022)^2}$ . For variables checking out differences, comparable  $3\sigma$ 's are based on  $\sqrt{(1/2\bar{X})^2 + (3\sigma)^2}$ .

Overall Variance Analysis of Parameters  
Affecting CCW Output Voltages

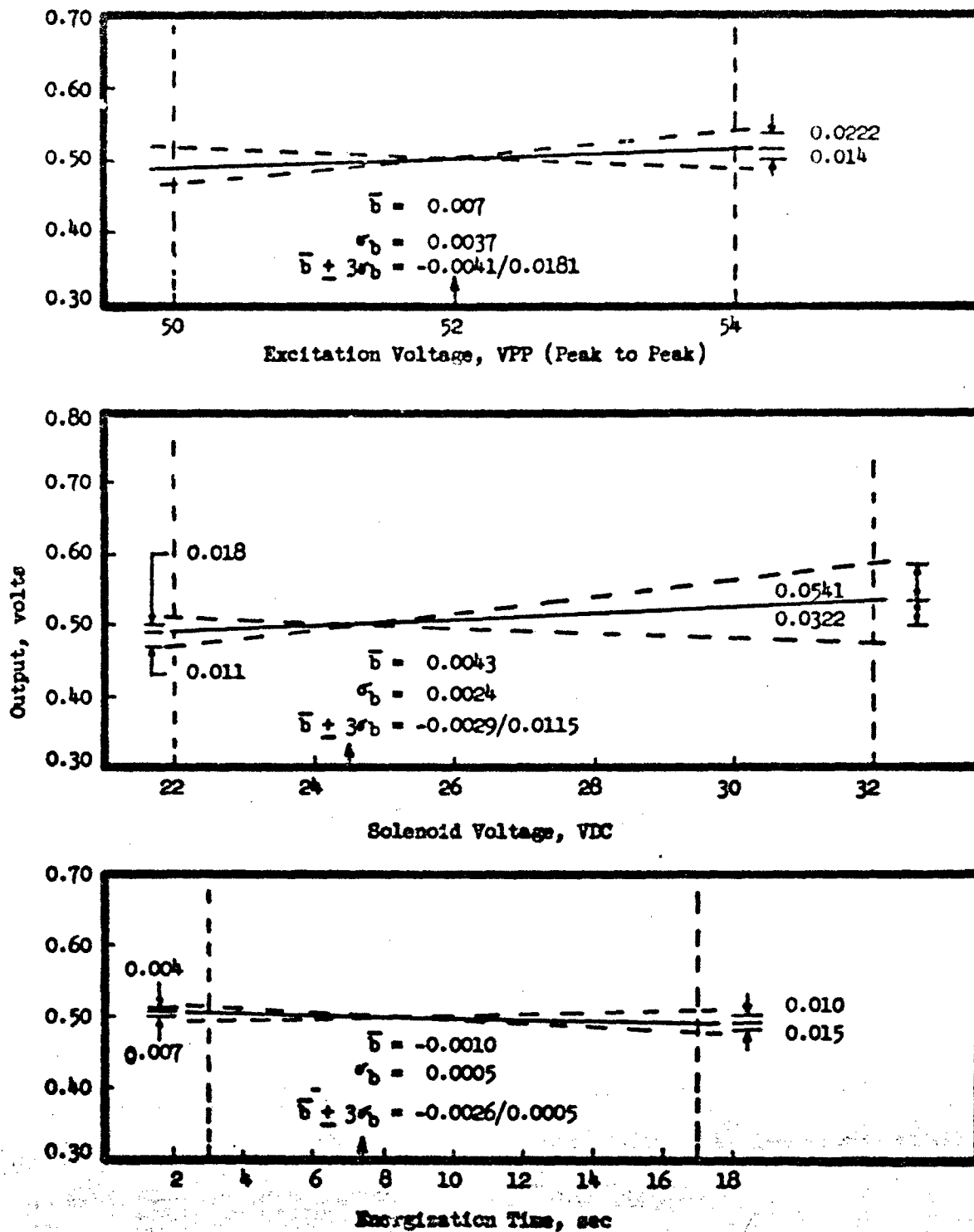
Figure X-22





Normalized Regression Line Diagram for Preliminary Normalized Output Voltages vs Excitation, Solenoid Voltage, and Energization Time, CW Position

Figure X-23



Normalized Regression Line Diagram for Preliminary Normalized Output Voltages vs Excitation, Solenoid Voltage, and Energization Time, CCW Position

Figure X-24

# Report 0162-06TIR-9-Vol 2

## Valves Before Resetting

<u>Serial Number</u>	<u>Aeroneutronics</u>	<u>Aerojet Test Set</u>
EAS 0001	CW - 5.31, CCW - 0.46	CW - 5.23, CCW - 0.49
EAS 0002	CW - 5.41, CCW - 0.55	CW - 5.32, CCW - 0.58
EAS 0003	CW - 5.45, CCW - 0.51	CW - 5.36, CCW - 0.54
EAS 0007	CW - 5.34, CCW - 0.50	CW - 5.27, CCW - 0.52
EAS 0011	CW - 5.48, CCW - 0.41	CW - 5.37, CCW - 0.43
EAS 0019	CW - 5.37, CCW - 0.36	CW - 5.28, CCW - 0.38

## Valves After Resetting

<u>Serial Number</u>	<u>Aeroneutronics</u>	<u>Aerojet Test Set</u>
EAS 0001	CW - 5.55, CCW - 0.24	CW - 5.43, CCW - 0.30
EAS 0002	CW - 5.61, CCW - 0.31	CW - 5.45, CCW - 0.37
EAS 0003	CW - 5.68, CCW - 0.33	CW - 5.55, CCW - 0.39
EAS 0007	CW - 5.65, CCW - 0.41	CW - 5.55, CCW - 0.45
EAS 0011	CW - 5.58, CCW - 0.39	CW - 5.42, CCW - 0.38
EAS 0019	CW - 5.57, CCW - 0.36	CW - 5.46, CCW - 0.36

Valve S/N 0003 did not meet requirements after first tack weld. Tack weld was broken and valve satisfactorily re-adjusted. The position transducer also required replacement.

## Recalibration Values of Six Kavlico-Equipped Valves

Figure X-25

Report 0162-06TER-9-Vol 2

<u>Serial Number</u>	<u>Aeroneutronics Test Set</u>	<u>Aerojet Test Set</u>
EAS 0110	CW - 5.60, CCW - 0.45	CW - 5.44, CCW - 0.45
EAS 0111		CW - 5.46, CCW - 0.43
EAS 0112	CW - 5.57, CCW - 0.45	CW - 5.41, CCW - 0.45
EAS 0113	CW - 5.62, CCW - 0.44	CW - 5.41, CCW - 0.44
EAS 0114	CW - 5.60, CCW - 0.39	CW - 5.41, CCW - 0.40
EAS 0115	CW - 5.56, CCW - 0.42	CW - 5.40, CCW - 0.40
EAS 0116	CW - 5.66, CCW - 0.46	CW - 5.50, CCW - 0.42

Valve S/N 0111 failed to meet leakage requirements during acceptance tests and had to be removed.

Calibration of New Kavlico-Equipped Valves

Figure X-26

END

IATE

LMED

--66